Glass Particles as an Active and CO2 Reducing Component in Future Cement

Moesgaard, Mette; Yue, Yuanzheng

Citation for published version (APA):
Moesgaard, M., & Yue, Y. (2010). *Glass Particles as an Active and CO2 Reducing Component in Future Cement* (1 ed.). Institut for Kemi, Miljø og Bioteknologi, Aalborg Universitet.

AALBORG UNIVERSITY

Ph.D. Dissertation

Glass Particles as an Active and CO$_2$ Reducing Component in Future Cement

by
Mette Moesgaard

Section of Chemistry
Department of Biotechnology, Chemistry and
Environmental Engineering
Aalborg University

Date of defense
10.12.2010

Assessment committee
Reinhard Conradt
Department of Glass and Ceramic
Composites
RWTH Aachen University, Germany
Donald E. MacPhee
Mechanics of Materials Research Group
University of Aberdeen, Scotland
Kristian Keiding
Aalborg University

Supervisor
Yuanzheng Yue
Aalborg University

Abstract

Portland cement manufacture is an energy intensive industry responsible for approximately 5% of the global anthropogenic CO_2 emission. Considerable efforts are thus being made by the industries to reduce their CO_2 emissions.

The approach taken in this study is to lower the CO_2 emissions from cement production by clinker substitution. This means that the clinker is partly substituted by supplementary cementitious materials (SCMs). This work deals with the development of innovative SCMs based on calcium aluminosilicate (CAS) glass particles produced specifically for the purpose as SCM. The objectives of this study fall into two parts:1) Optimization of the composition of the CAS glasses to reduce the CO_2 emission linked to glass production while as the same time ensuring high pozzolanic reactivity (i.e., the ability of the glasses to participate in the formation of strength giving hydration phases when mixed with the cement); 2) Study of both the physical performances of blended cements containing 30 wt% of the newly developed SCMs and the hydration behavior. In addition to the blended cements containing just one SCM, investigations are carried out on cements containing both limestone and CAS glass particles.

It is found that one tonne of the CAS glasses made from natural raw materials namely clay, limestone and sand, referred to as the so-called CLS glasses, can be produced emitting less than 60% of the CO_2 released producing one tonne of clinker. In addition, the glasses possess pozzolanic reactivity upon contact with water and $Ca(OH)_2$ forming hydration products resembling the C-S-H and the calcium aluminate hydration phases formed during Portland cement hydration.

Investigations of the composition-structure relationship of a range of three components CAS model glasses show evidence of structural heterogeneity to exist in the intermediate-range order. This is manifested as clustering of highly depolymerized regions with only limited Al present and highly polymerized regions of alternating SiO_4 and AlO_4 tetrahedra.

Examinations of physical performances of the blended cements reveal that the CLS glass makes little or no contribution to the early strength. The glass reactivity however increases over time and it makes considerable contribution to the late strength that is approaching that of pure Portland cement. Increase of the CLS glass surface area (to 629 m^2/kg) is found to have positive effect on the strength development reaching 90% of the strength of the pure cement reference at 90 days. Combining this result with that of the CO_2 emission caused by producing blended cements containing 30 wt% CLS glass, it is concluded that the CO_2 emission can be reduced with 10% for the same performance as Portland cement. This is valid when substituting the clinker with glass on a 1:1 weight basis.

When limestone and CLS glass is added to the same cement, a synergetic effect is observed for the long term strength. This is caused by a larger fraction of the limestone participating in the cementitious reactions as the content of Al_2O_3 available for reaction with limestone is increased by introducing CLS glass to the cement. For blends containing 20% CLS glass (surface area of 629 m^2/kg) and 10% limestone, the 90 days strength exceeds that of Portland cement. Using these blended cements, reductions in the CO_2 release of 20% can be achieved for the same concrete performance. The use of CLS glasses as SCMs is a good approach for significantly reducing the CO_2 emission from cement production maintaining acceptable performance of the final material.

Danish abstract

Store mængder energi forbruges til fremstilling af Portland cement. Dette gør cementindustrien ansvarlig for ca. 5% af den globale menneskeskabte CO_2-udledning. Cementindustrien gør derfor et stort stykke arbejde for at sænke sine emmisioner.

Strategien, der anvendes i dette studie, er at sænke CO_2-udledningen vha. klinkersubstitution. Det betyder, at klinkerne delvist erstattes af supplerende cementagtige materialer (SCMs), og dette studie omhandler udvikling af nyskabende SCMs baseret på calcium aluminosilikat (CAS) glaspartikler produceret specifikt til denne anvendelsen. Formålet falder i to dele. 1) Optimering af sammesætningen af CAS glasset med henblik på at reducere CO_2-udledningen forbundet med produktion af glasset samt at sikre høj pozzulanitet. Pozzulanitet refererer til glassets evne til at tage del i dannelsen af strykegivende hydratiseringsprodukter, når glasset blandes med cement; 2) Undersøgelse af de fysiske egenskaber af blandingscementer indeholdende 30wt% af de nyudviklede SCMs samt undersøgelse af hydratiserings-processen for disse cementer. Udover blandingscementer indeholdende én SCM undersøges også cementer indeholdende både fint formalet kalksten og CAS glaspartikler.

Ud fra undersøgelser af glassets karakteristika kan det konkluderes, at et ton CAS glas baseret på de naturlige råmaterialer, ler, kalksten og sand, kan fremstilles under udledning af blot 60% af den mægnde CO_2, der udledes til fremstilling af et ton klinker. Glasser baseret på disse naturlige råmaterialer referes til som CLS glas. Ydermere har glasset pozzolanegenskaber og er i stand til ved reaktion med vand og $Ca(OH)_2$ at danne hydratiseringsprodukter svarende til C-S-H og calcium aluminat hydratfaserne, som dannes ved hydratisering af Portland cement.

Studier af sammenhænge mellem komposition og struktur for en række glas i tre-komponent CAS modelsystemet udviser evidens for eksistensen af strukturel heterogenitet i ordenen i "mellem-udstrækning" (intermediate-range order). Dette kommer til udtryk som klyngedannelse af områder med høj grad af depolymerisation og kun begrænset indhold af Al samt områder med høj grad af polymerisation og vekslende tilstedeværelse af SiO_4 og AlO_4 tetraeder

Undersøgelse af de fysiske egenskaber for blandingscementerne viser at CLS glasset bidrager svagt eller slet ikke til den tidlige styrkeudvikling. Reaktiviteten af glasset øges dog over tid, og dette bidrager signifikant til den sene styrkeudvikling, som for blandingscementerne nærmer sig den for den rene Portland cement. Forøgelse af glaspartiklernes overflade har betydelig positiv effekt på styrkeudviklingen, som når 90% af styrken af den rene cement efter 90 dages hydratiserings ved et overfladeareal på 629 m^2/kg. Hvis dette resultat kombineres med CO_2-udledningen forbundet med fremstilling af blandingscementer indeholdende 30 wt% CLS glas,

kan det konkluderes, at CO_2-udledningen kan reduceres med 10% for sammen fysiske ydeevne som Portland cement. Dette er gældende for 1:1vægtbaseret substituering af klinker med glas.

For cementerne indeholdende både kalksten og CLS glas opnås en synergieffekt for den sene styrke. Det konkluderes, at baggrunden for denne er, at en større procentdel af kalkstenen tager del i de styrkegivende kemiske reaktioner, når indholdet af Al_2O_3 tilgængelig for kalkstenen til denne reaktion øges ved tilsætning af CLS glas. For blandinger indeholdende 20% CLS glass og 10% kalksten opnås 90 døgns styrker, som overstiger styrken af den rene cement. Ved anvendelse af disse cementer, kan der opnås reduktioner i CO_2-udledningen på 20% for samme 90 døgns mørtelstyrke. Alt i alt kan det konkluderes, at anvendelsen af CLS glaspartikler som SCM tilvejebringer en god mulighed for at opnår signifikante reduceringer i CO_2-udledningen forbundet med cementproduktionen, samtidig med at egenskaberne for det endelige produkt bibeholdes.

Preface

This dissertation is submitted to the Faculties of Engineering and Science, Aalborg University in partial fulfillment of the requirement for obtaining the Ph.D. degree.

The Ph.D. study is carried out at the Section of Chemistry in the Department of Biotechnology, Chemistry and Environmental Engineering at Aalborg University from August 2007 to September 2010. The study is part of the FUTURECEM project financed by the Danish National Advanced Technology Foundation. The FUTURECEM project is an interdisciplinary collaboration between Aalborg Portland A/S, GEUS (Geological Survey of Denmark and Greenland) and iNANO at University of Aarhus and Aalborg University.

Throughout the thesis the common cement chemistry abbreviations for the oxides are used when suitable. The most widely used are: $C = CaO$, $S = SiO_2$, $A = Al_2O_3$, $F = Fe_2O_3$, $H = H_2O$, $S' = SO_3$ etc. If nothing else is stated, % always refers to wt%.

Table of Contents

1 Introduction

Portland cement (PC) is an inorganic hydraulic binder mainly used as the material giving adhesion in concrete which is the most widely used construction material in the world. Large quantities of PC are thus produced worldwide. The production of PC is highly energy intensive co-producing significant amounts of CO_2. In total, the cement industry is responsible for approximately 5% of the global anthropogenic CO_2 emissions. Today much scientific work links the observed global warming to emissions of green house gasses among which CO_2 is probably the most important. Considerable effort is thus made within energy intensive industries including the cement industry to reduce their green house gas emissions (World Business Council for Sustainable Development 2009, Worrel et al. 2001, Damtoft et al. 2008).

In Denmark, Aalborg Portland is the only cement manufacturer with 2009 annual production of 1.55 million tonnes. White cement with very low Fe_2O_3 content accounts for approximately one third of the cement produced at Aalborg Portland with the remaining two thirds being grey cement referred to as ordinary Portland cement (OPC). About 2% of the total Danish CO_2 release originates from the cement production at Aalborg Portland (Aalborg Portland 2009).
Cement production is a global growth industry with 2006 production of 2.55 billion tonnes. The global demand for cement is continuously increasing, especially in developing countries, and is expected to at least double by 2050. Thus, just to maintain the status quo CO_2 emissions, the emission per ton cement must be halved. This leaves a big challenge for the cement industry (World Business Council for Sustainable Development 2009, Damtoft et al. 2008, Humphreys, Mahasenan 2002).

The present Ph.D. thesis is part of the FUTURECEM project which is an interdisciplinary collaboration between Aalborg Portland, GEUS (Geological Survey of Denmark and Greenland) and iNANO at University of Aarhus and Aalborg University. The aim of FUTURECEM is to develop "the cement of the future" by increasing the production capacity while at the same time reducing the raw materials consumption and CO_2 emission. The main focus is placed on reducing the CO_2 release by at least 30%.

1.1 Background and challenges

Cement is produced by burning the raw materials consisting of 80-85 wt% limestone, sand, clay and possibly minor constituents at temperatures of about 1450°C. Partial fusion occurs and nodules of clinker are obtained. These are mixed with a few percentages of gypsum and finely ground to produce the cement. Using the present production technology approximately 0.8 tonne of CO_2 is released on average producing one ton of cement. The majority of this CO_2 release, i.e., 500-550 kg CO_2 per tonne clinker, results from calcination of carbonates in the raw materials mix.

This is referred to as the "raw materials CO_2 release". The other significant contributor is the "fuel-derived CO_2" which in an efficient kiln accounts for 250-300 kg CO_2 per ton clinker (World Business Council for Sustainable Development 2009, Worrel et al. 2001, Damtoft et al. 2008).

Different strategies are taken within the cement industry to reduce the CO_2 release and in 2009 the World Business Council for Sustainable Development (WBCSD) pointed out the 4 most promising levers available to achieve these reductions. These are 1) improvement of the thermal and electric efficiencies, 2) use of alternative fuels, 3) clinker substitution and 4) carbon capture and storage (World Business Council for Sustainable Development 2009, Worrel et al. 2001, Damtoft et al. 2008).

1. Thermal and electrical efficiency increases gradually over time as state of the art technologies are employed in new cement plants and old plants are upgraded when economically feasible. Current state of the art is the dry manufacturing process with preheater and precalciner technology having a specific heat consumption of 3.1 GJ per tonne clinker produced. The global weighted average energy consumption is however 3.7 GJ per tonne clinker as this consumption also includes the energy used for burning wet raw materials in inefficient and long rotary kilns. The theoretical minimum energy consumption, i.e., the enthalpy of reactions, is estimated at 1.6-1.85 GJ/t. Technical reasons however makes it impossible ever to reach this value. WBCSD estimates that the global average energy consumption will be reduced to 3.2-3.3 GJ/t clinker in 2050.

2. Alternative fuels with relatively low carbon content can replace conventional fuels i.e., coal and petcoke of higher carbon content, resulting in a reduced CO_2 emission. The alternative fuels could be natural gas or biomass. Another important class of alternative fuels is waste materials which would otherwise have to be incinerated or disposed of in land-fillings, and an advantage of the cement production is that the ashes of the alternative materials most often can be integrated into the clinker product. Today the developed regions use 16% alternative fuels compared to 5% in the developing regions. In 2050 it is expected that the fraction of alternative fuel will be increased to 50% for developed regions and to 30% for the developing regions.

3. Clinker is the cement component associated with the highest energy consumption. Thus, lowering the clinker factor by partly substitution of cement with alternative materials, the so-called supplementary cementitious materials (SCMs) offers a possibility of reducing the overall CO_2 release from cement production. A requirement to the alternative materials is that they must possess hydraulic reactivity when ground and mixed with cement and gypsum to ensure similar or better cement performance, resulting in acceptable concrete performance without having to increase the content of

cement per cubic meter of concrete. Commonly used SCMs are blast furnace slag, fly ash and natural volcanic materials. The first two are regarded as industrial by-products. From a technical point of view high replacement levels are possible but other factors might create limitations. The factors of limitations could e.g. be, low regional availability and increasing prices of the SCMs, strict national cement standards as well as common practice and acceptance within the area of construction.

4. Carbon capture and storage is a new and promising technology. However until now it has not been proven on industrial scale within the cement industry. As the process name implies the CO_2 is captured from the flue gases, compressed to a liquid and transported in pipelines for permanently storage underground. Extensive research and development activities must be carried out before the technology can be used, and in addition to technical challenges limitations in regard to e.g. high process costs as well as political and public support must be overcome. It is estimated that carbon capture and storage could become commercial implemented after the year 2020.

In FUTURECEM the focus is mainly lowering the CO_2 emissions from cement production by reducing the clinker content in the cement, i.e., the 3rd WBCSD lever. The strategy of the project is to develop new and for the purpose optimized SCMs to partly substitute the clinker. In addition, these materials should be based on low-cost raw materials locally available in large quantities. This approach makes the industry independent of possibly uncertain availability of the industrial by-products traditionally used.

One of the tasks for the FUTURECEM project is to develop reactive particles from thermally modified clays. Previous work has proven these heat treated clays to be hydraulic reactive when mixed with cement and water (Ambroise, Maximilien & Pera 1994, He, Osbæck & Makovicky 1995). The present work focuses on a different approach; the development and synthesis of reactive particles from glass materials. The metastable state of the glass, i.e., the amorphous nature of the structure, is proven to provide hydraulic reactivity for certain chemical compositions (Mishulovich, Hansen 1996, Mishulovich, Hansen 2000). The main success criteria for the newly developed alternative materials are that they possess high cementitious reactivity without changing important properties e.g. water demand and setting behavior of the mortar. The preparation of the materials should be cost-efficient and involve significantly reduced CO_2 emissions compared to OPC production, and the grindability of the materials should be similar or better than that of OPC clinker.

Another part of the FUTURECEM project focuses on development of novel low energy cements. This part is concerned with development of highly reactive clinker types, i.e., clinker showing high early strength, thus being highly compatible with the alternative materials often giving rise to reduced early strength when added to cement as a partly clinker replacement. Furthermore focus has been on increasing the

content of C_3A with the aim of increasing the chemical reactivity of any limestone filler added. The last part of the project deals with development of geopolymers, i.e. alkali activated open-framework aluminosilicates. Using these systems the goal is to achieve at least 40% clinker substitution.

1.2 Objectives of the present study

The objectives of the present Ph.D. thesis are 1) development of a glassy system with a composition optimized for the use as a partial replacement material for cement clinker and 2) to test the physical performances of cement mortars containing these newly developed glass particles. The glass composition is optimized in relation to energy consumption during production and thus the CO_2 release. This is evaluated from glass characteristics such as CaO content, practical melting temperature and glass forming ability. In addition, the pozzolanity, i.e. the ability of the glass to form strength giving phases in the presence of calcium hydroxide and water at ordinary temperatures, is tested.

The physical performance of cements containing the newly developed glass particles or combinations of both glass and limestone is investigated regarding workability, setting behavior and compressive strength. The hydration behavior of these blended cement pastes are investigated using thermal analyses, X-ray diffraction (XRD), nuclear magnetic resonance (NMR) spectroscopy and scanning electron microscopy – energy dispersive X-ray spectroscopy (SEM-EDS).

1.3 Content of the thesis

The thesis is presented as a plurality including an introductory overview followed by papers written for publication. The thesis is based on the following publications. Later in the text these will be referred to by roman numerals.

I M. Moesgaard, Y. Z. Yue, Compositional dependence of fragility and glass forming ability of calcium aluminosilicate melts, *J. Non-cryst. Sol*, 355 (2009) 867-873.

II M. Moesgaard, D. Herfort, J. Skibsted, Y. Z. Yue, Calcium aluminosilicate glasses as supplementary cementitious materials, *Eur. J. Glass Sci. Technol. A.*, 51 (2010) 183-190..

III M. Moesgaard, R. Keding, J. Skibsted, Y. Z. Yue, Evidence of intermediate-range order heterogeneity in calcium aluminosilicate glasses, *Chem. Mater.*, 22 (2010) 4471-4483.

IV M. Moesgaard, D. Herfort, L. F. Kirkegaard, Y. Z. Yue, Optimal composition of calcium aluminosilicate glass particles used as supplementary cementitious materials, Proceedings of the 12th International Inorganic-Bonded Fiber Composites Conference (2010) 23-29.

V M. Moesgaard, D. Herfort, M. Steenberg, L. F. Kirkegaard, Y. Z. Yue, Physical performances of blended cements containing calcium aluminosilicate glass powder and limestone, submitted to *Cem. Concr. Res.*, 41 (2011) 359-364.

VI M. Moesgaard, D. Herfort, M. Steenberg, Y. Z. Yue, Mechanical performances of blended Portland cements containing calciumaluminosilicate glass particles, 12th International Inorganic-Bonded Fiber Composites Conference (2010) 30-38.

VII M. Moesgaard, D. Herfort, S. L. Poulsen, J. Skibsted, Y. Z. Yue, Hydration of Blended Portland Cements Containing Calcium-Aluminosilicate Glass Powder and Limestone, *J. Am. Ceram. Soc.*, 95 (2012) 403-409.

2 Blended cements

Blended cements (or composite cements) are hydraulic cements composed of Portland cement and one or more inorganic materials taking part in the hydration reactions. Blended cements have been used for many years and for various purposes. One of the initial aims was to lower the production costs of cement and concrete. Objectives such as the necessity of utilizing industrial waste or by-products and demands for concrete with special performance requirements have also promoted the development and production of blended cements (Taylor 1997, Lawrence 2007b). Energy savings and reduced CO_2 emissions have in recent years been the driving forces in the area of blended cement research (World Business Council for Sustainable Development 2009, Worrel et al. 2001, Damtoft et al. 2008, Taylor 1997, Lawrence 2007b).

In the following section, a brief introduction to the constituents of the blended cements will be given. The constituents are the ordinary Portland cement (OPC) and the conventional supplementary cementitious materials (SCMs).

2.1 Portland cement

Portland cement is the most commonly employed active hydraulic binder. The term active refers to a binder that hardens upon reaction with water without the presence of an activator such a lime. The name Portland cement dates back to a patent by Joseph Aspdin in 1824. The name is said to be chosen to call to mind Portland stone, a limestone quarried on the Isle of Portland in England and having a color resembling Portland cement. At that time Portland stone had a high reputation as a building stone due to its quality and durability (Blezard 2007).

Portland cement clinker is an intermediate product produced during cement manufacture. Typically the clinkers have a composition in the range 67% CaO, 22% SiO_2, 5% Al_2O_3, 3% Fe_2O_3 and 3% other components. Upon heating, the oxides react chemically forming primarily the four clinker minerals alite, belite, aluminate and ferrite. Alite, an impure form of C_3S ($3CaO \cdot SiO_2$), is the most abundant clinker phase constituting 50-70% of the clinker minerals. Belite constitutes 5-30% of ordinary Portland cement and is an impure form of C_2S ($2CaO \cdot SiO_2$) present in the hydraulic reactive β polymorph. The phase aluminate refers to C_3A ($3CaO \cdot Al_2O_3$) and accounts for 5-10% of the clinker phases, whereas ferrite being C_4AF (Ca_2AlFeO_5) makes up 5-15% (Taylor 1997, Lawrence 2007a).

Cement is produced by grinding the clinker with about 2-5% gypsum. Portland cement is unstable in the presence of water, resulting in chemical reactions taking place between the anhydrous clinker minerals and water yielding solid hydration products. The hydration of cement is associated with physico-mechanical changes, divided into the setting, i.e., the rather sudden loss of plasticity of the paste converting it to a solid material of limited strength, and the hardening, i.e., the development of hardness and strength of the solidified paste. As mentioned above a

few percentages of gypsum is added during grinding of the clinker. This acts as a "set regulator" to avoid flash set, i.e. setting of the mortar within a few minutes, which would otherwise occur (Nepper-Christensen 1985, Odler 2007).

The mineralogical composition of the clinker (Bogue (Taylor 1997, Lawrence 2007a)) used within this project is given in Table 2.1. A commercially available clinker with a rather high alite/belite ratio is chosen to ensure high early strength to compensate the reduced early strength expected as the clinker is partly replaced by an alternative and less reactive material (Massazza 2007, Shi, Zheng 2007). In addition, a CEM I, i.e. cement with high clinker content is chosen to isolate the effect of the glassy materials developed within this project. Cement kiln dust is for example otherwise often added to the cement. Table 2.2 gives the chemical composition of the final cement. The cement has a surface area of 575 m^2/kg determined by air permeability using the Blaine method.

Table 2.1: Mineralogical composition (wt%) of clinker.

Component	C_3S	C_2S	C_3A	C_4AF	Free lime [a]	LFS (-) [b]
Clinker	63.4	9.2	8.4	12.0	1.4	1.02

[a] The content of free lime is measured by titration in alcohol.
[b] Lime saturation factor.

Table 2.2: Chemical composition of the cement in wt% determined by XRF.

Component	SiO_2	Al_2O_3	Fe_2O_3	CaO	MgO	K_2O	Na_2O	SO_3	L.O.I. [a]
Cement	19.0	5.8	3.9	65.1	1.0	0.4	0.3	3.7	0.9

[a] Loss on ignition

2.1.1 Hydration of Portland cement

As Portland cement is a multi-component system the hydration is a rather complex process. In the following an overview is given using phase diagrams to predict the phase assemblage formed. Figure 2.1 shows the location of the Portland cement used within this work (Table 2.2) in the ternary $CaO-Al_2O_3-SiO_2$ hydrate system. The composition of PC is located in the CH ($Ca(OH)_2$), C-S-H (calcium silicate hydrate), C_3A hydrate (calcium aluminate hydrate) phase field. These phases are thus formed as equilibrium is reached upon hydration. The addition of gypsum however yields calcium aluminate hydrates present in the form of monosulfate and ettringite. The compositions of the phases are given in Table 2.3. As the system consists of six major components prior to hydration, i.e., CaO, SiO_2, Al_2O_2, SO_3, Fe_2O_3 and water, the phase rule predicts the existence of six hydration phases. This is valid for a system with constant temperature and pressure and with the composition of all phases fixed and independent from one another (Ehlers 1972). In addition to the four phases predicted from the phase diagram (CH, C-S-H, monosulfate and ettringite) iron oxide probably in the form of iron hydroxide gel and pore solution also exists.

Part of the iron oxide is also incorporated into the lattice of the AFt and AFm phases[1], i.e., phases similar to ettringite and monosulfate, respectively. These predictions are in agreement with numerous investigations on the hydration behavior of OPC (Taylor 1997, Odler 2007).

Aluminate and alite react rather fast upon contact with water and are the mineral phases responsible for the early strength of the cement. In addition to the amorphous or poorly crystalline C-S-H phase, portlandite is a product of the alite hydration also contributing considerably to the strength. If no gypsum was present the aluminate would react almost instantaneously leaving no time to work with the paste before it solidifies. Belite hydrates significantly slower and is said to give rise to the late strength. The belite hydration also gives rise to formation of portlandite, however in lower amounts than the alite hydration due to the lower CaO/SiO_2 ratio. The C-S-H phases formed from alite and belite hydration are similar (Taylor 1997, Odler 2007).
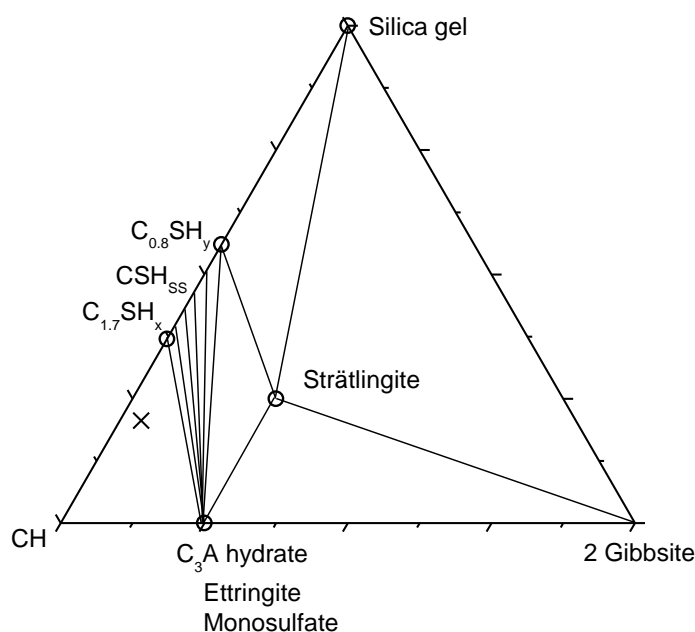
Figure 2.1: CAS (H) sub-ternary phase diagram (mol%) predicting the phase assemblage formed at steady state during hydration of Portland cement. In addition, to the phases predicted by the phase diagram iron oxide and pore solution are present in excess, i.e. plotting outside the phase diagram.

---

[1] AFm refers to Al_2O_3-Fe_2O_3-mono phases of the general formula $C_3(A,F) \cdot CX_2 \cdot yH_2O$, where X denotes different anions with the most important ones being OH^-, SO_4^{2-} and CO_3^{2-}. AFt (Al_2O_3-Fe_2O_3-tri) refers to the phases of compositions $C_3(A,F) \cdot 3CX_2 \cdot yH_2O$ (Taylor 1997).

Table 2.3: Typical chemical composition of the hydration phases formed in OPC. Minor components are expected to be incorporated into the phases e.g. small contents of Al are expected in the C-S-H gel.

Phase	Nomenclature	Chemical composition
C-S-H	$C_{1.75}SH_4$	$1.75CaO\text{-}SiO_2\text{-}4H_2O^a$
Portlandite	CH	$Ca(OH)_2$
Monosulfate	$C_3A\text{-}CS'\text{-}H_{12}$	$3CaO\text{-}Al_2O_3\text{-}CaSO_4\text{-}12H_2O$
Ettringite	$C_3A\text{-}3(CS')\text{-}H_{32}$	$3CaO\text{-}Al_2O_3\text{-}3CaSO_4\text{-}32H_2O$
Iron hydroxide	FH_3	$Fe_2O_3\text{-}3H_2O$
Pore solution	H	H_2O

[a] The CaO/SiO_2 ratio of the C-S-H phase is the average value reported in literature (Taylor 1997, Odler 2007).

2.2 Supplementary cementitious materials

The inorganic materials partly substituting the cement in blended cements are referred to as supplementary cementitious materials (SCMs). As focus has been on reusing industrial by-products, materials such as fly ash, blast furnace slag and micro silica have traditionally been used as supplementary cementitious materials (Taylor 1997, Lawrence 2007b). The use of industrial by-products is a neat approach for the cement industry as the use does not give any production related CO_2 emissions. In practice, the utilization of these traditional SCMs is as mentioned limited by their availability, transport cost and competition with other applications. Today, these materials are essentially fully utilized in Western Europe and the supply of fly ash and blast furnace slag is furthermore expected to be reduced in the future as coal fired power stations and blast furnace plants are expected to be replaced by more CO_2 efficient processes. This raises the demand for new and alternative sources of SCMs. Possible candidates are natural pozzolans of volcanic origin (Taylor 1997, Massazza 2007) and calcined clays (He, Osbæck & Makovicky 1995, Massazza 2007).

Another commonly used clinker replacement material is limestone. Limestone is often referred to as a filler material, although the effects of limestone addition on cement hydration are both physical and chemical (Taylor 1997).

The traditional SCMs (fly ash, micro silica and slag) are amorphous or at least partly amorphous silicates. It is reported for blast furnace slag that only the rapidly cooled and highly amorphous slag possesses cementitious properties. This is in contrast to the slowly cooled and crystalline slag which virtually has no hydraulic reactivity (Taylor 1997). Mishulovish & Hansen, 1996 also reports a drastic drop in the strength given properties of two vitrified mixes of molten cement kiln dust and shale upon partial crystallization. This implies the amorphous nature of a material to be of importance for the applicability as SCM. The thermodynamic instability of glasses is expected to be the origin of the hydraulic reactivity of the amorphous silicates. In the

highly alkaline environment of a cement paste (pH = 13.4-14.0) (Taylor 1997), the OH⁻ ions will attack the glassy network resulting in a depolymerization into oxyhydroxides that can take part in the formation of hydration phases.

In recent years, utilization of waste glass as a SCM has been the topic of several papers (Shi, Zheng 2007, Shayan, Xu 2006, Shi et al. 2005, Schwarz, Cam & Neithalath 2008). This has confirmed the hydraulic reactivity of waste glass when mixed with cement. Studies of this type are of particular interest in countries having no efficient glass recycling system. However, as with the other waste materials, this is a limited resource and insufficient to meet the growing SCM demand. In Denmark ≈70% of the used container glass is in addition collected and recycled making the amount of waste glass with possible use as a cement replacement very low (Hasholt, Hansen & Thørgersen 2003, Hasholt et al. 2004).

If the cement industry wants to be capable of meeting the increasing global cement demand while at the same time significantly reducing their CO_2 emission, new and alternative SCMs available in large quantities must be developed.

3 Calcium aluminosilicates in cement

The approach taken in this work is to develop and engineer a glass system with the specific aim of being used as a SCM. For that purpose the calcium aluminosilicate (CAS) glass system is selected. CAS glasses can be produced in large quantities from low cost and locally available raw materials and are in addition composed of the same oxides that also constitute OPC. Thus, depolymerization of the glass in the highly alkaline environment of the cement pore solution results in Si- and Al-oxyhydroxides similar to the species that constitute the hydration phases of OPC. Glasses of this type are thus expected to participate in the formation of strength giving hydration products hence contributing positively to the performance of the blended cement mortar and concrete.

For full scale production to be economically viable the glasses should be prepared from low cost raw materials available locally in large quantities. Hence it is chosen to base the glasses on the conventional raw materials used for cement production, i.e., clay, limestone and sand, however mixed in other proportions than within cement.

It is important if a CAS glass should provide a good SCM that the production of the glass causes reduced CO_2 emission compared to the production of OPC. Equally as important is it that the glass will participate in the hydration reactions and thereby contributing to the strength of the final concrete. Thus, to determine the optimal composition of a glass system several characteristics must be balanced. In practice this is done investigating the consumption of limestone, practical melting temperature, pozzolanity of the glass, etc.

3.1 Glasses based on pure chemicals

To simplify the understanding of the system, investigations are at first performed on a three component model system, i.e., the CaO-Al_2O_3-SiO_2 system. These are the major oxides in the natural raw materials and account for 90% of the oxides in OPC.

3.1.1 Glass characteristics

In Paper I the compositional dependence of fragility and glass forming ability (GFA) of ten CAS glasses is investigated. The glasses are divided into two series of systematic compositional changes (the eutectic series and the non-eutectic series, Figure 3.1) and are located in the vicinity of the eutectic compositions of anorthite-wollastonite-tridymite and anorthite-wollastonite-gehlenite. The glass forming ability refers to the ability of a melt to vitrify upon cooling. The critical cooling rate, i.e., the minimum cooling rate required to avoid crystallization during cooling of a melt, can be considered as a direct measure of GFA (Varshneya 1994, Shelby 2005, Ossi 2003). It is however often difficult to determine the critical cooling rate and it is of interest to use alternative methods of quantifying GFA. In Paper I it is found that

fragility, i.e., the extent of deviation from Arrhenian behavior of the viscosity-temperature relation, can be used as a measure of GFA for the CAS glasses. This is a useful evaluation method, as the fragility can rather easily be obtained from viscosity measurements.
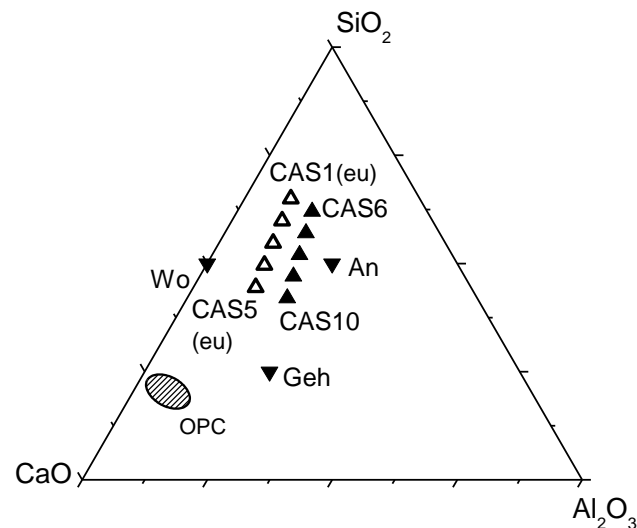
Figure 3.1: Ternary CaO-Al$_2$O$_3$-SiO$_2$ phase diagram (mol%). Upward triangles mark the glass compositions under investigation in Paper I. The open triangles represent the eutectic series, i.e. CAS1 to CAS5, with the end members being the eutectic composition of anorthite-wollastonite-tridymite and anorthite-wollastonite-gehlenite. The solid upward triangles represent the non-eutectic series, i.e. CAS6 to CAS10. The hatched area shows the compositional range of ordinary Portland cement (OPC) and the solid downward triangles state the composition of the geological phases wollastonite (Wo), anorthite (An) and gehlenite (Geh).

Melts with high GFA can be vitrified without forced cooling thus relating the glass forming ability to the fuel-derived CO$_2$ emission. Paper I concludes that the glasses in the eutectic-series in general exhibit higher GFA and that the GFA increases with increasing network polymerization. As the glasses in the eutectic series show superior GFA, the work is continued focusing on this series.

The major contributions to the CO$_2$ release during glass manufacture is the raw materials CO$_2$ release linked to calcination of limestone and the fuel-derived CO$_2$ release linked to the burning of fuel to reach the temperatures of production. This situation is similar to the cement production. Commonly used soda-lime-silica glasses for windows and containers are produced in the temperature range 1500-1600°C (Edgar et al. 2008).

The raw materials CO$_2$ release is directly related to the consumption of limestone, which is the primary source of CaO. This is valid regarding production of OPC as

well as the CAS glasses investigated in this work. Based on the composition of OPC stated in Table 2.2, the production of one ton of cement results in 516 kg of raw materials derived CO_2. In contrast, 180 kg and 300 kg CO_2 are released from the raw materials needed to produce one ton of CAS1 and CAS5, respectively. In addition to the GFA, the temperature required for melting, i.e., the practical melting temperature, affects the fuel-derived CO_2 emission for glass production. In this work, the practical melting temperature (T_{pm}) is defined as the isokom temperature corresponding to a viscosity of 10 Pa s. It is found that, T_{pm}(CAS1) = 1527°C and T_{pm}(CAS5) = 1306°C (Paper II) (Notice a different naming of the two glasses in this paper). Thus the increased content of modifying Ca^{2+} ions in CAS5 has a significant impact on the melting temperature. The determination of the practical melting temperature is described in greater detail in Paper II.

To summarize the investigations on the model system, it is found that the eutectic composition of anorthite-wollastonite-tridymite (CAS1) causes a considerable lower raw materials CO_2 emission than the eutectic composition of anorthite-wollastonite-gehlenite (CAS5), whereas the lower practical melting temperature favors the use of CAS5 compared to CAS1. Full scale production utilizing natural raw material sources will introduce a significant content of impurities e.g. alkali oxide. The presence of these impurities is expected to lead to a pronounced reduction in production temperature. Thus the reduced CaO content and superior GFA of CAS1 are considered the most important factors. This composition is chosen as the starting point for the investigations on the impure glass system.

3.1.2 Glass structure

The physical and chemical properties of glasses are determined largely by their microstructure in both short- and intermediate-range. To get a deeper understanding of the compositional dependence of the glass characteristics as described above, the composition-structure relationship of the peralkaline CAS glasses (Figure 3.1) is investigated in greater detail in Paper III. (Notice a different naming of the glasses in this paper). Especially, the clarification of intermediate-range ordering (IRO) in silicate glasses, i.e., the order extending beyond the nearest neighbors, has been of interest in recent years (Greaves, Sen 2007, Price 1996, Mauro et al. 2009a). This is also the focus point of Paper III in which the nature of the IRO is investigated by comparing the results of two different structural modeling approaches to solid-state [29]Si magic angle spinning (MAS) nuclear magnetic resonance (NMR) spectroscopy data. ^{29}Si MAS NMR is widely used for structural studies of aluminosilicates as the isotropic chemical shift (δ([29]Si)) depends on both the degree of polymerization of SiO_4 tetrahedra and the presence of Al in the second coordination sphere to Si. However, simultaneously changes in the content of both network forming Al ions and network modifying Ca ions may complicate the interpretation of single-pulse ^{29}Si MAS NMR experiments. In this work, structural modeling based on the chemical composition of the glasses allows extraction of new important information about the IRO from this type of experiments. The modeling is briefly described below with a more detailed description in Paper III.

Both structural models assume similar short-range order with Si and Al acting as network formers in the peralkaline glasses. The excess Ca ions, which are not involved in the charge balance of AlO_2 units, serve to charge balance the NBOs. Based on previous investigations on peralkaline glasses a preference of Al for fully polymerized Q^4 sites is assumed in this work (Mysen 1990, Mysen, Richet 2005, Allwardt, Lee & Stebbins 2003, Lee, Stebbins 2006). The distribution of Si(Q^n) units is then calculated by combinatorics assuming a statistical distribution. The next step is to describe the distribution of Al in the second coordination sphere of SiO_4 units, i.e., to describe the IRO.

The first modeling approach (R-IRO model) assumes that the structure beyond the nearest neighbors is of a random nature. The mole fractions of the 15 possible Si($Q^{ni}(m_iAl)$) units are thus calculated using combinatorics. This results in the prediction of 7-14 non-negligible units present within each glass (Table 3, Paper III). The number of non-negligible units increases within each glass series as a function of increasing contents of NBO and Al.

In the second modeling approach (QH-IRO model), we assume a heterogeneous IRO based on the modified random network theory by Greaves (Greaves 1985). This theory predicts clustering of NBOs within silicate glasses. For the CAS glasses, clustering of NBOs is believed to result in highly depolymerized regions containing only a minor content of Al and highly polymerized regions of alternating SiO_4 and AlO_4 tetrahedra. The second modeling approach thus predicts chemical fluctuations in the IRO. The QH-IRO model predicts the presence of 4-6 different structural Si($Q^{ni}(m_iAl)$) units for each glass (Table 4, Paper III).

To test the validity of the two IRO models, the ^{29}Si MAS NMR spectra are deconvoluted using a sum of Gaussian shaped resonances corresponding to the different types of Si($Q^{ni}(m_iAl)$) units with relative intensities equal to the molar fractions predicted by the models.

$$f(x) = \sum_{i=1}^{15} \frac{a_i}{w \cdot \sqrt{\pi/2}} exp\left[\frac{-2(x-x_{0i})^2}{w^2}\right] = \sum_{i=1}^{15} \frac{a_i}{w \cdot \sqrt{\pi/2}} exp\left[\frac{-2\left(x-\delta\left(Q^{ni}(m_iAl)\right)\right)^2}{w^2}\right] \quad (3.1)$$

Thus, the ^{29}Si NMR resonances are described as a sum of Gaussian distributions (Eq. 3.1) where a_i is the relative area for a given structural unit, i.e., the molar fraction known from the modeling, x_{0i} is the center of the resonance corresponding to the chemical shift $\delta(Q^{ni}(m_iAl))$ and w is the line width. The dependencies of chemical shift on the degree of polymerization of SiO_4 tetrahedra (n: the number of BO linked to Si) and on the incorporation of Al in the second coordination sphere (m: the number of Al) are assumed to be additive and the chemical shift for a $Q^{ni}(m_iAl)$ unit can be expressed by:

$$x_{0i} = \delta\left(Q^{ni}(m_iAl)\right) = \delta\left(Q^4(0Al)\right) + (4-n_i)A + m_iB . \quad (3.2)$$

Reasonable starting values of the four unknown parameters are used for the deconvolution and all ten resonances are deconvoluted simultaneously.

The intensity distribution predicted from the random IRO model cannot be validated from deconvolution of the ^{29}Si NMR resonances (Figure 3, Paper III). In contrast, the results of the heterogeneous IRO model provide convincing agreement between the deconvoluted and the experimental results (Figure 5, Paper III). This is a clear evidence of the existence of structural heterogeneity in the IRO. Paper III includes further discussions of these findings.

The structural heterogeneity in the IRO explains the only vague compositional dependence of melt fragility for the ten glasses despite increasing disorder in the short-range (Paper I). The increasing short-range disorder is caused by an increase in the content of both NBO and Al within each series. It is believed that the increasing ordering within the intermediate-range counterbalances the increasing disorder in the short-range thus resulting in only minor changes in fragility. Regarding the crystallization behavior of the glasses, the chemical fluctuations might constitute inhomogeneities capable of inducing heterogeneous nucleation or acting as nuclei for the crystallization process. This explains the superior stability of the glasses with lowest Al content (Paper III). Furthermore it is speculated, that the structural heterogeneity might show impact on the ability of the glasses to participate in the hydration processes of the blended cements. Structural heterogeneity will create weak points or defects in the structure. These will then act as starting points for the breakdown of the glassy network within the alkaline environment of the pore solution. A link might thus exist, with structural heterogeneity leading to enhanced pozzolanity of the glasses.

3.1.3 Effect of CaF$_2$ on melt flow and structure

A possible method of reducing the practical melting temperature of aluminosilicate melts and thus the fuel-derived CO_2 release from production is the introduction of fluorine to the melt (Hill, Wood & Thomas 1999, Zeng, Stebbins 2000, Stamboulis, Hill & Law 2004).

Adding small amounts of CaF$_2$ to the CAS melts thus makes it possible to reduce the glass production temperature while at the same time slightly reducing the use of CaCO$_3$ to obtain a given calcium content within the glass. Appendix A describes the effect of substituting 2-8 mol% of the CaO within CAS1 with CaF$_2$.

The introduction of fluorine is observed to have a pronounced effect on viscosity, reducing T_{pm} with approx. 40°C from 1527°C to 1488°C as 2 mol% CaO is substituted by CaF$_2$. By ^{19}F MAS NMR the fluorine is proven to break down the network connectivity by incorporation into Al-F-Ca(n) and F-Ca(n) species with n representing the number of Ca coordinated with the fluorine. By the formation of Al-F-Ca(n) units, bridging oxygen is replaced by non-bridging fluorines, thus reducing the network connectivity.

3.2 Glasses based on natural minerals

As the eutectic composition of anorthite-wollastonite-tridymite, i.e., CAS1 (or $C_{26}A_9S_{65}$ in Paper II and III), was concluded to be the most optimal three component composition, this composition is targeted using the natural minerals as raw materials. These are all available in large quantities in Denmark, and the compositions are given in Table 2 in Paper II. The relative content of Al_2O_3 in the clay is rather close to that in CAS1. Hence, it is possible to obtain the target composition by mixing the raw materials only in the following proportions by weight: 63% clay, 31% limestone and 6% sand. This results in the composition of CLS_{1N} stated in Table 3.1. The nomenclature refers to the three raw materials and the subscript indicates the aimed molar content of Na_2O. The use of natural minerals introduces ≈10% minor components or impurities mainly as alkali oxides, MgO and Fe_2O_3. CLS_{5N} and CLS_{9N}, containing 5 and 9 mol% Na_2O, respectively, are produced to investigate the effect of adding additional alkali oxide. In industrial-scale production, extra alkali oxide can be introduced by recycling dust collected from the cement kiln or from albite or granite high in alkali oxide (syenite and alkali granite), or directly as Na_2SO_4. Paper II and Paper IV are concerned with the characterization of the glasses.

Table 3.1: Oxide compositions (mol%) for the three CLS glasses. The composition of CAS1 is given for comparison. The compositions are determined by wet chemical analyses.

	CAS1	CLS_{1N}	CLS_{5N}	CLS_{9N}
SiO_2	64.9	59.1	56.1	53.9
Al_2O_3	9.3	8.2	7.9	7.7
Fe_2O_3	-	3.0	2.9	2.8
CaO	25.8	22.1	21.2	21.3
MgO	-	4.2	3.9	3.9
K_2O	-	1.7	2.0	1.6
Na_2O	-	1.2	5.4	8.2
SO_3	-	<0.1	0.2	0.2
TiO_2	-	0.5	0.5	0.5

3.2.1 Glass characteristics

The limestone content of the CLS glasses is comparable to that of CAS1, and the production of these results in ≈175 kg CO_2 released from limestone calcination per tonne glass produced. In addition to the raw materials CO_2 release the carbonate content also affects the fuel-derived CO_2 release as the calcination process is endothermic. From differential scanning calorimetric measurements on raw material batches of CAS1 and CLS_{9N}, the enthalpy of calcination is found to be ≈650 kJ/kg and ≈325 kJ/kg, respectively. For comparison the enthalpy of calcination of the production of PC clinker is ≈2100 kJ/kg (Taylor 1997).

The introduction of impurities to the glass system has a pronounced effect on the viscosity temperature relation (Figure 2, Paper II), with the viscosity being significantly reduced in the entire temperature range shifting from CAS1 to CLS_{1N}.

Upon introduction of additional alkali oxide the viscosity decreases even further. This is reflected in the values of T_{pm} (Table 3.2), that decreases with almost 200°C shifting from the pure chemical system (CAS1) to the natural raw materials (CLS$_{1N}$). The glasses based on natural minerals can thus be produced at temperatures in the range 1300-1350°C. This is significantly reduced compared to the production temperature of OPC.

The fragility of the melts (m) is derived from the description of the viscosity-temperature (η,T) relation using the MYEGA equation (Mauro et al. 2009b)

$$log\eta = log\eta_\infty + (12 + log\eta_\infty)\frac{T_g}{T}exp\left[\left(\frac{m}{12-log\eta_\infty} - 1\right)\left(\frac{T_g}{T} - 1\right)\right] \qquad (3.3)$$

where η_∞ is the infinite temperature viscosity and T_g is the glass transition temperature. The introduction of 10% minor components reduces the fragility thus increasing the glass forming ability of the melts. Similar values of m are obtained for the CLS glasses with varying Na_2O content.

Table 3.2: Characteristic temperatures and fragility indices (m) for CAS1 and the CLS glasses.

	T_{pm} (°C) [a]	T_g (°C) [b]	m (-) [b]	Degree of pozzolanic reactivity [c]
CAS1	1527	781.6 ± 0.6	49.6 ± 0.4	12
CLS$_{1N}$	1346	688.6 ± 1.4	43.2 ± 1.2	14
CLS$_{5N}$	1329	654.3 ± 0.9	44.0 ± 0.8	16
CLS$_{9N}$	1285	629.7 ± 0.8	43.7 ± 0.7	22

[a] The practical melting temperature (T_{pm}) is given as the isokom temperature at $\eta = 10$ Pa s. The uncertainty associated with T_{pm} is estimated to be $\pm$ 3-4%.

[b] T_g and m are obtained from the fit of the viscosity-temperature data using the MYEGA equation.

[c] Determined as mass loss of glass during reaction with $Ca(OH)_2$. From repeated measurement on CLS$_{9N}$ the uncertainty associated with the mass losses is estimated to be $\pm$ 5-10%.

To increase the ability of the glass to take part in the hydration reactions it must be crushed and ground to obtain a large surface area. As significant amounts of energy are also consumed during the crushing and grinding, the grindability of the glasses is also considered. In Paper III it is evaluated indirectly measuring the Vickers hardness (H_v) as well as the fracture tendency at a given load. Combining the results of H_v and fracture tendency, CLS$_{9N}$ is found to have the best grindability with the lowest H_v (of the CLS glasses) and the largest fracture tendency. Thus, particle formation is expected to require the smallest energy consumption for this composition. Grinding of CLS$_{1N}$ and CLS$_{9N}$ in a porcelain mill confirms that particles of cement fineness are more easily obtained for CLS$_{9N}$ than for CLS$_{1N}$. The duration of the grinding process of CLS$_{9N}$ can be reduced by 6% compared to CLS$_{1N}$.

In addition, Figure 3.2 compares the grindability of clinker with that of CLS$_{9N}$. The materials are ground in a porcelain mill using steel bodies and associated values of

surface area and duration of the grinding are found. The two materials follow the same trend until a surface area of approximately 400 m^2/kg. After this point the CLS$_{9N}$ glass shows superior grindability. Particles of the fineness of the cement used in this project, i.e., 575 m^2/kg, are thus more easily obtained with CLS$_{9N}$ particles compared to the cement clinker.
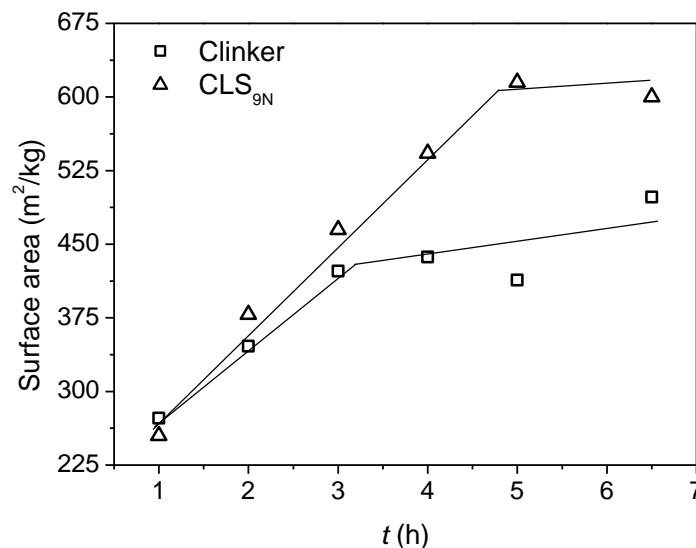

Figure 3.2: Surface area as function of grinding time for clinker and CLS$_{9N}$ glass illustrated as the surface area vs. time of grinding in a porcelain mill. The surface area is measured by air permeability using the Blaine method. The solid lines should be regarded as guides for the eye.

3.2.2 Pozzolanity

The SCMs are often less reactive than Portland cement, and a partial substitution of OPC with SCM will thus reduce the compressive strength compared to the pure cement (Massazza 2007, Shi, Zheng 2007). To ensure acceptable performance of the final mortar or concrete without being forced to increase the content of the blended cement per cubic meter of concrete, it is of importance to minimize the reduction in compressive strength. This is possible if the SCM exhibits pozzolanity and thus contributes to the strength giving reactions taking place during hydration.

The pozzolanity of the glasses is tested as the reactivity of glass particles in a saturated Ca(OH)$_2$ solution. The alkalinity of the Ca(OH)$_2$ solution resembles the pore solution of cement paste and mortar. The degree of pozzolanity is quantified as the fraction of glass that has reacted with Ca(OH)$_2$ and water after 7 days at 40°C (Table 3.2). This is determined as the mass loss of glass. The pozzolanity increases as minor components are introduced to the glass system from the natural minerals and it further increases upon introduction of additional alkali oxide.

^{27}Al and ^{29}Si MAS NMR spectroscopy investigations are performed on CAS1 and CLS$_{9N}$ to further examine the pozzolanic reactions between the calcium

aluminosilicate glasses and $Ca(OH)_2$. The idea is to test if hydration phases are formed resembling the ones formed during hydration of OPC.

During OPC hydration the main hydration product is the C-S-H phase (Section 2.1.1). As this is formed the isolated SiO_4 tetrahedra (Q^0 units) of alite and belite react with water and polymerize into dimers and chains of SiO_4 tetrahedra, i.e. Q^1 and Q^2 units, that constitute the C-S-H phase (Taylor 1997, Odler 2007). During hydration the Al ions are mainly incorporated into crystalline aluminate hydration products. The hydration of the aluminate phases can be followed by the gradual conversion of tetrahedrally coordinated AlO_4 in the anhydrous cement into octahedrally coordinated AlO_6 sites present in the calcium aluminate hydrates (Taylor 1997, Odler 2007, Richardson 1999, Andersen, Jakobsen & Skibsted 2003).

The ^{29}Si MAS NMR spectra of CAS1 and CLS_{9N} before and after the pozzolanity test (Figure 3, Paper II) exhibit broad resonances in the range from -75 ppm to -115 ppm, reflecting the amorphous nature of the glasses including different Q^n units. Subtraction of the spectra before and after the reactivity test reveals sub-spectra which only include resonances from the hydration products. For both glasses these difference spectra show resonances in the range -75 to -90 ppm assigned to Si in Q^1 and Q^2 units. This indicates the formation of a chain-like silicate structure during the reaction with $Ca(OH)_2$ and water.

In ^{27}Al MAS NMR, resonances in the range 55 to 80 ppm are expected for AlO_4 units whereas AlO_6 octahedra result in resonances with chemical shifts from -15 to 20 ppm (Merzbacher et al. 1990, Muller et al. 1981). The ^{27}Al MAS NMR spectrum of CAS1 (Figure 4, Paper II) includes a broad resonance corresponding to Al in tetrahedral coordination. In addition to tetrahedrally coordinated Al the ^{27}Al MAS NMR spectrum of CLS_{9N} (Figure 4, Paper II) reveals that a small fraction of the Al is present in octahedral coordination for this sample. The corresponding spectra of the glasses after the pozzolanic reactivity test reflect that a hydration product including octahedrally coordinated Al in a more ordered phase has formed.

The glasses are thus concluded to be pozzolanic active forming hydration products similar to the phases formed during hydration of OPC. These NMR investigations are described in greater detail in Paper II.

3.3 Summary

It is demonstrated that calcium aluminosilicate glasses can be produced at reasonable conditions, i.e. relatively low production temperature and without artificial cooling to avoid crystallization, employing the natural deposits of clay, limestone and sand as raw materials. Addition of extra alkali oxide or minor contents of CaF_2 further reduces the energy consumption required for production. Furthermore the calcium aluminosilicates are pozzolanic active and are thus expected to participate in the strength given reactions during hydration of blended cements containing the glasses.

4 Blended cements containing glasses

The reactivity test of aqueous glass-Ca(OH)$_2$ mixtures proved that the CAS glasses are pozzolanic active. This is valid for the glasses based both on pure chemicals and on impure natural minerals (the CLS glasses), however with the latter possessing the greatest reactivity. These glasses are thus expected to contribute positively to the strength of blended cements by chemical means, i.e., the glass is expected to take part in formation of strength giving hydration phases.

The effect on physical performance of adding CAS glass to Portland cement is more directly investigated by preparing blended cement pastes and mortars analyzing these by suitable methods. In the present work, blended cements containing 30 wt% clinker replacements are prepared. Mortar specimens are used to test workability and mechanical performance and paste samples are used to further investigate the hydration behavior of the blended cements.

The investigations of glass characteristics (section 3.2.1, Paper II) showed that the introduction of additional Na$_2$O to CLS$_{9N}$ as compared to CLS$_{1N}$ (obtained by directly mixing the natural minerals) has a positive impact both on the energy consumption during production and on the degree of pozzolanity. In addition CLS$_{9N}$ also showed improved grindability compared to CLS$_{1N}$. This implies CLS$_{9N}$ particles to be the best candidate as a suitable SCM. On the other hand, high contents of alkalis in the cement pore solution might cause alkali-silica reactions to occur in concretes exposed to moisture. In these reactions, hydroxide ions in the pore solution react with reactive silica from the aggregates forming a gel that can take up water. The water-taking effect causes volume changes that might lead to crack formation in the concrete (Taylor 1997, Lawrence 2007a). Hence it is of importance that the alkalis of SCMs rich in alkali oxide are incorporated into the hydration phases instead of being dissolved in the pore solution. Mortars containing both CLS$_{1N}$ and CLS$_{9N}$ are prepared.

4.1 Physical performances

The suitability of the CAS glasses as an alternative to the conventional SCMs is tested comparing the physical performance of mortars containing CAS glass particles to that of mortars containing fly ash. The effects of particle surface area as well as cooling conditions during production of the CAS glasses are also investigated. This is the topic of Paper V and VI. The experimental methods used to test the physical performance are described in these papers.

Table 4.1 lists the different SCMs tested. CLS$_{9N}$ is ground to two different surface areas and the melt of this composition is in addition spun into fibers using the cascade spinning process (Širok, Blagojević & Bullen 2008). The fibers are produced by Rockwool International A/S, Hedehusene, Denmark and are subsequently ground to the same fineness as one of the CLS$_{9N}$ samples. The effect of the fast cooling is elaborated in section 4.1.1. The fly ash is a low-CaO ash with approx. 5 wt% CaO

(composition given in Table 1, Paper V) and it is included in the investigations to represent a traditional SCM. The inert filler is coarse quartz particles. Aplite, a crystalline material consisting primarily of quartz and alkali feldspar, is also tested to elaborate the difference between crystalline and amorphous materials.

Table 4.1: Size characteristics of the SCMs under investigation.

SCM	CLS_{1N}	CLS_{9N}	$CLS_{9N\ fine}$	$CLS_{9N\ fiber}$	Fly ash	Inert filler	Aplite
Surface area (m^2/kg)[a]	338	371	629	619	330	n/a	422
D_{50} (μm)[b]	16.2	14.4	6.0	6.2	20.1	$D_{max} < 90$ μm	16.9

[a] Determined by air permeability using the Blaine method
[b] 50% fractile determined by laser diffraction

4.1.1 Excess energy stored in the glass

The CAS glasses are produced by cooling the glass melt fast enough to avoid crystallization. The degree of disorder in the glass depends on the cooling rate. The faster the cooling rate the higher the temperature at which the structure is frozen-in, and the higher the degree of disorder and thus the stored excess energy of the final glass. An increasing structural deviation from equilibrium will yield a less stable glass expected to demonstrate a higher degree of reactivity within the blended cement. To test this hypothesis, two glasses with different degrees of stored excess energy are produced employing different cooling rates.

High cooling rates can be achieved by drawing thin fibers from the glass melt. In this work, discontinuous fibers with diameters of 3-15 μm are produced from the CLS_{9N} melt using the cascade spinning process as mentioned above. This yields cooling rates of about 10^6 K/s. In contrast, the normally cooled glasses, which are cast onto a graphite plate is cooled at about 10^3 K/s. The cooling rates are calculated using the procedure reported in (Yue, von der Ohe & Jensen 2004).

The excess energy stored in the glass can be determined from the heat capacity curves of the first and second upscan obtained by differential scanning calorimetry (Yue, Christiansen & Jensen 2002). Normal heating and cooling rates of 10°C/min must be employed for both scans. Figure 4.1 depicts the heat capacity curves for $CLS_{9N\ fiber}$. The first upscan (C_{p1}) reflects the thermal history of the glass, e.g. the cooling rate used during preparation of the glass, whereas the second upscan (C_{p2}) reflects the thermal history of the glass cooled at 10°C/min. The difference between C_{p2} and C_{p1} equals the enthalpy release. Fast cooling during production results in a large amount of enthalpy stored in the glass. The total enthalpy release during the entire heating process is found as the integral of $C_{p2} - C_{p1}$, i.e., the area between the two curves. This equals the total excess energy (ΔE_{tot}) stored within the glass (Yue, Christiansen & Jensen 2002). As comparison, the heat capacity curves of the normally cooled CLS_{9N} glass are illustrated in Figure 4.2. It is found that, $\Delta E_{tot}(CLS_{9N}) = 7.1$ J g^{-1} and $\Delta E_{tot}(CLS_{9N\ fiber}) = 84.4$ J g^{-1}. Thus, the increased cooling rate of fiber production has a significant impact on the excess energy stored in the glass and hence on the stability of the glass.
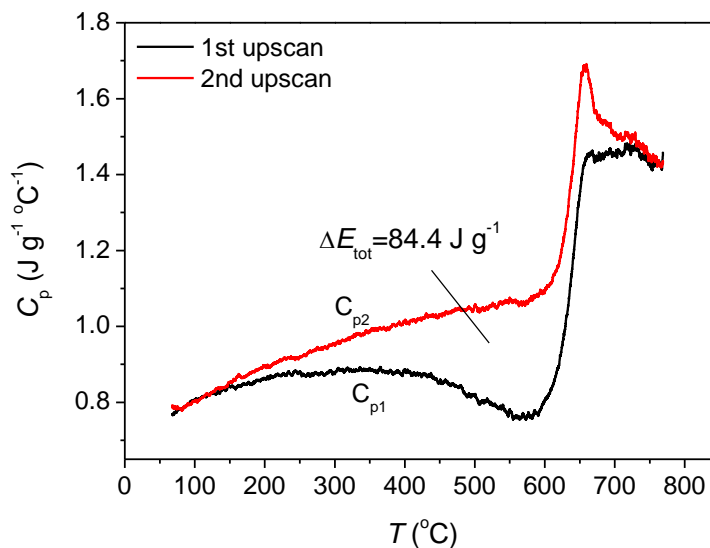
Figure 4.1: Heat capacity curves of the rapidly cooled CLS$_{9N}$ fibers. Cooling and heating rates of 10°C/min are employed for both scans. The total excess energy stored within the glass (ΔE_{tot}) is found as the area between the two curves.
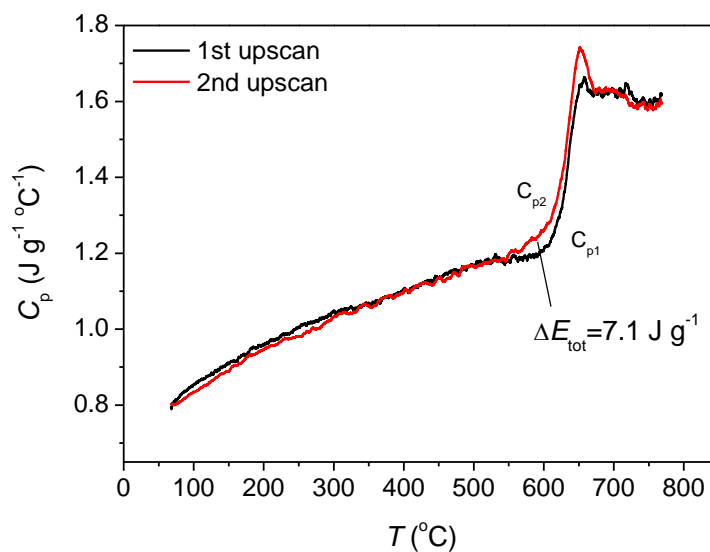
Figure 4.2: Heat capacity curves of the normally cooled CLS$_{9N}$ glass. Cooling and heating rates of 10°C/min are employed for both scans. The total excess energy stored within the glass (ΔE_{tot}) is found as the area between the two curves.

4.1.2 Workability

The workability of concrete or mortar refers to the ease of mixing, transporting, placing and compacting it to a uniform material (Taylor 1997). In this work the workability is measured at a constant water to cement ratio. For all the SCMs tested

(Table 4.1), standard mortar workability is slightly improved with increased slump on the flow table of 2-8 % compared to the pure cement mortar. This is a major advantage compared to calcined clay based SCMs also investigated in the FUTURECEM project, as these significantly reduce the workability requiring additional water or addition of superplasticizer (He, Osbæck & Makovicky 1995, FUTURECEM Unpublished data).

4.1.3 Setting behavior

The physio-mechanical changes taking place during cement hydration is as mentioned in section 2.1 divided into setting and hardening. The setting refers to the loss of plasticity of the fresh mortar as it is converted into a solid material, and the hardening is the development of hardness and strength of the solidified mortar (Nepper-Christensen 1985, Odler 2007).

The initial part of the hydration is associated with evolution of heat. The setting behavior and the initial strength development can thus be characterized by measuring the rate of heat evolution during the first hours of hydration. The heat evolution of all the blended cement mortars follows the expected pattern (Figure 1, Paper V). Immediately after mixing of cement, sand and water, a rather fast evolution of heat is observed. This is the effect of wetting the solid materials and partial dissolution of their surfaces. Formation of small quantities of the hydration products are expected during this period. A decrease in the heat evolution due to the existence of an induction period is followed by the main exothermic peak. During this period, the actual formation of hydration phases occurs and the cement paste sets (Odler 2007). The heat of hydration of all the blended cements is lower than that of the pure cement, indicating that the clinker is replaced by a less reactive material (Figure 1, Paper V).

To make the effect of the SCM more clear the heat evolution is normalized by the Portland cement fraction in the blend. This is done in Figure 4.3. CLS_{1N} and CLS_{9N} show similar behavior and only CLS_{9N} is included in the figure. Although all SCMs are concluded to be less reactive than OPC both fly ash and aplite contributes to the early hydration. For these samples the heat evolution accelerates faster than for the reference in the beginning of the second heat release and the height of the main peak is in addition slightly increased. The reason for this is believed to be that the SCM particles act as nucleation sites for the early alite hydration. This has been reported previously with various finely ground SCMs (Hjort, Skibsted & Jakobsen 1988, Krøyer et al. 2003). On the other hand, the glass does not appear to make any contribution to the early hydration having heat development patterns resembling the inert material. The reduced intensity of the main peak compared to the pure cement mortar even suggests that the presence of 30 wt% glass retards the early hydration of the cement.
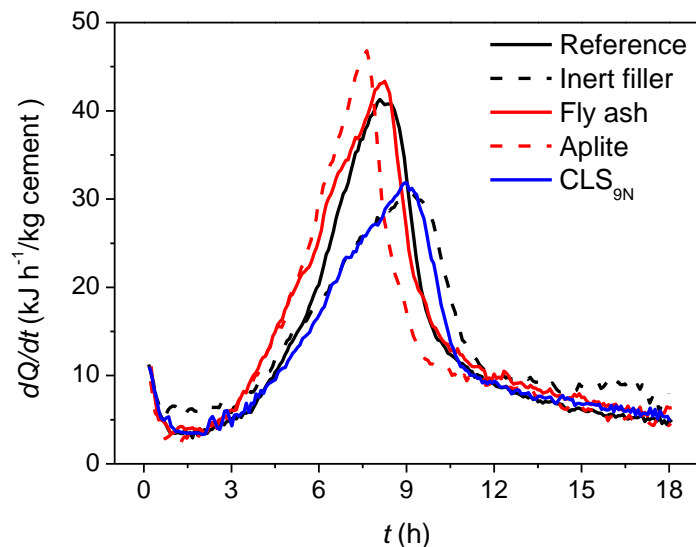
Figure 4.3: Setting behavior measured as the rate of heat evolution normalized by the fraction of Portland cement within the blended cement. The heat evolution (dQ/dt) is plotted as a function of the hydration time (t).

Figure 4.4 shows the effect on setting behavior of increasing the surface area of the glass particles and of increasing the excess energy stored in the glass. Surprisingly the increase of surface area does not show an impact on the main heat release. In contrast, the rapidly cooling significantly increases the intensity of the main peak approaching the size of the pure cement peak. Thus, increasing the structural disorder and hence the ease of bond breaking within the glassy particles increases the participation of the glass in the initial hydration.

Based on six repeated measurements on OPC paste samples, estimates of the uncertainty associated with the semi-adiabatic measurements can be deduced. From this it is found that the onset and offset temperatures of the second heat release can be given with an accuracy of approximately ± 10%, whereas the total heat release within the first 18 hours can be given an accuracy of ± 5%. This is assumed to be valid with all measurements.
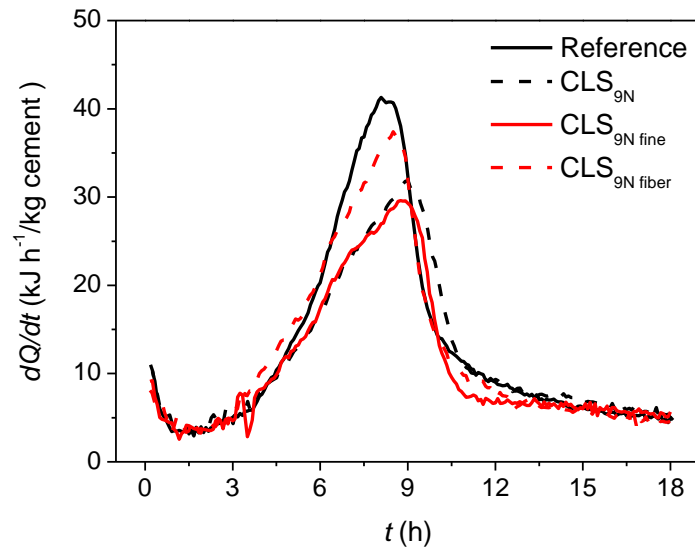
Figure 4.4: Setting behavior measured as the rate of heat evolution normalized by the fraction of Portland cement within the blended cement. The heat evolution (dQ/dt) is plotted as a function of the hydration time (t).

4.1.4 Compressive strength

The compressive strength (hereafter referred to as strength) is the most important material parameter used to characterize cement-based products. Figure 4.5 compares the strength development up to 90 days normalized by the strength of the pure cement mortar (σ/σ_{rel}) of the blended cements containing the various SCMs. CLS_{1N} and CLS_{9N} show comparable behavior (Figure 2, Paper V) and only CLS_{9N} is included in this figure. The pozzolanic reactivity of the CLS glass and fly ash is apparent, as the strength of the mortars containing these materials is significantly higher than that of the mortar containing quartz. For CLS and fly ash the relative strength reaches approximately 75% at 90 days compared to 55% for the quartz containing mortar. The pozzolanic reactions of the CAS glasses and fly ash are however limited at early stages of hydration ($\sigma/\sigma_{rel} \approx 50\%$ after 1 day of hydration) but increases over time. The superior behavior of the fly ash containing cement found during the first 18 hours hydration (Figure 4.3) is not reflected in the compressive strength measurements. Here similar strength development patterns are observed for the three SCMs (CLS_{1N}, CLS_{9N}, fly ash). The aplite containing cement exhibits a strength development pattern in between the CLS glasses and the inert filler. The early strength of the aplite cement is significantly increased as compared to the quartz containing cement. Again this is expected to be due to the aplite particles acting as seeds for the early alite hydration. A constant relative strength of 60% is reached after 28 days for the aplite containing cement compared to 55% for the inert filler. The blended cements containing fly ash and CLS glass do not reach a constant relative strength after 28 days. In contrast the strength increases steadily up to 90 days.
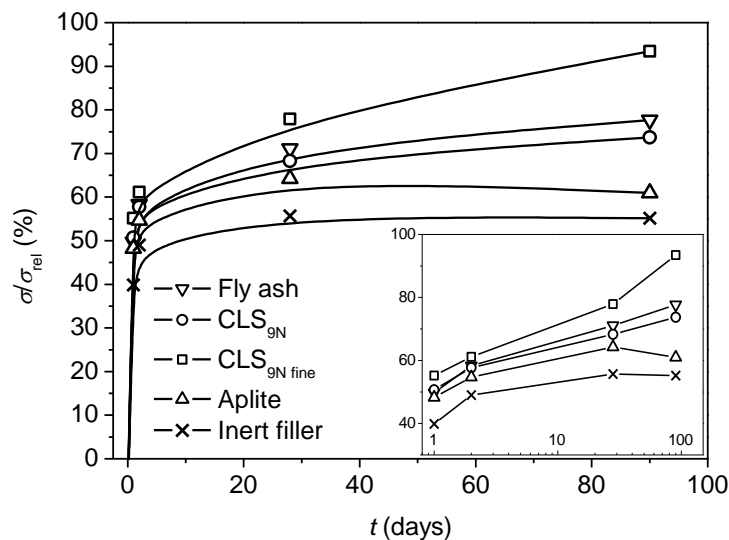
Figure 4.5: Strength development of blended cement mortars containing different SCMs. The strength is given relative to the strength of pure Portland cement mortar (σ/σ_{rel}) as a function of hydration time (t). The inset shows the strength development on a logarithmic time scale.

From repeated measurements on the reference samples, the uncertainty associated with the strength measurements is found to be in the range of ± 5-10%. This is believed to be a good indication of the uncertainty associated with all measurements. Figure 4.5 also shows the effect of grinding the glass to a higher surface area. As expected, this results in a significant acceleration of strength development reaching above 90% of the pure cement strength after 90 days of hydration. At durations longer than examined in the heat evolvement measurements (i.e., 18 hours) the surface area thus seems to be a limiting factor for the reactivity of the coarse glass particles. Contrary to this, the blended cement mortar containing the fast cooled fibers only shows slightly higher 90 day strength than that of the mortar containing normally cooled glass (Figure 3, Paper V). Despite the significant impact on setting behavior of the degree of structural disorder, the effect on compressive strength is limited.

Cements are often classified in terms of the 28 days mortar strength, and three different classes are found in the European Cement Standard, i.e., 32.5, 42.5 and 52.5. The names refer to the minimum strength (in MPa) achieved after 28 days of hydrations following the measurement procedure of the European Standard EN 196-1. The compressive strength obtained within this work for the mortars containing pure OPC corresponds to 65.9 ± 0.8 M Pa following the measurement procedure of EN 196-1. The strength of the mortars containing pure OPC is thus larger than the minimum requirement. This allows cements of relatively reduced strength to be used

for certain applications. The blended cements containing both the coarse and the fine CLS$_{9N}$ glass particles fulfill the strength requirements to the class 32.5 and 42.5 cements.

4.1.5 Summary

From the investigations of workability, setting behavior and compressive strength of mortar specimens, the performance of blends containing either CLS$_{1N}$ or CLS$_{9N}$ cannot be distinguished. The CLS glasses are found not to contribute to the setting and initial hydration of the mortars, whereas the contribution to strength development is significant. The strength development of CLS glass containing mortars is comparable to that of mortars containing fly ash.

An increase of the structural disorder within the glass reduces the restraint of the initial setting (within the first 18 hours of hydration) otherwise observed for the glass containing blends. On the other hand an increased particle surface area significantly increases the compressive strength of the mortar. In general, the CLS glass particles can be concluded to provide a promising alternative SCM with acceptable mortar workability and compressive strength.

4.2 Hydration behavior

The hydration behavior of the CLS glass containing cement blends is investigated in greater detail using paste samples. It is of interest to determine how the introduction of 30 wt% glass of higher SiO$_2$ and Al$_2$O$_3$ content affects the formation of hydration phases. The glass particles with the largest surface area are chosen for this examination. The physical performances evaluated as the strength are for this sample found to be significantly improved compared to the coarse CLS$_{9N}$ particles, implying that it reacts to a greater extent. Paper VII is concerned with the hydration behavior of these paste samples describing the experimental conditions for the paste preparation, the ^{29}Si MAS NMR and XRD investigations, and the thermal analyses.

4.2.1 Identity of hydration phases formed after 90 days of hydration

In addition to the six main components of OPC namely CaO, SiO$_2$, Al$_2$O$_3$, SO$_3$, Fe$_2$O$_3$ and H$_2$O, the 30% CLS$_{9N}$ blended cement contains significant contents of alkali oxide with 2.0 wt% Na$_2$O$_{eq}$ compared to 0.5 wt% Na$_2$O$_{eq}$ for OPC (composition given in Table 2.2). Another SCM relatively high in alkali is fly ash normally containing up to 5 wt% Na$_2$O$_{eq}$ compared to 9 wt% in CLS$_{9N}$. For fly ash containing cements the capacity of the C-S-H phase to incorporate alkalis is observed to increase as the content of acidic oxides, i.e. SiO$_2$ and Al$_2$O$_3$, increases (Chunxiang, Hongding & Xianghui 1994, Duchesne, Bérubé 1994). It is of interest to determine whether a similar incorporation takes place within the CLS$_{9N}$ containing cement pastes.

From the ^{29}Si MAS NMR spectroscopic investigations described in Paper VII it is concluded that approximately 50% of the glass (CLS$_{9N\ fine}$) has reacted chemically within 90 days of hydration. In addition, Paper VII reach the conclusion that the cement is almost fully hydrated within 90 days as only traces of the clinker minerals alite and belite are found. This results in a reactive mix of composition given in Figure 4.6 (referred to as the CLS$_{9N}$ reactive mix). The position of the mix is displaced towards higher Al$_2$O$_3$ and SiO$_2$ contents compared to OPC. The CLS$_{9N}$ reactive mix is however still positioned within the same phase field as OPC with expected formation of CH, C-S-H, ettringite, monosulfate as well as iron oxide and pore solution (Section 2.1.1).
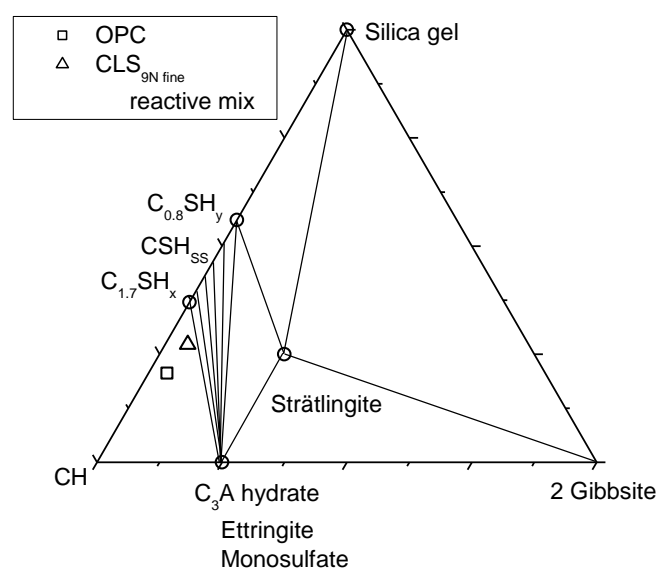

Figure 4.6: CAS (H) sub-ternary phase diagram (mol%) showing the location of the reactive CLS$_{9N\ fine}$–cement mix and that of ordinary Portland cement (OPC) and the hydration phases expected to be formed. In addition, to the phases predicted by the phase diagram, iron oxide and pore solution are present in excess, i.e. plotting outside the phase diagram.

By XRD the following phases are identified in the OPC paste hydrated for 90 days: CH, C-S-H (Ca$_{1.5}$SiO$_3$·5H$_2$O), monosulfate and ettringite. Probably due to a low content, no iron oxide is detected (Figure 1 and Table 4, Paper VII). This is in agreement with the phase assemblage predicted from Figure 4.6. In addition to the phases identified for the OPC cement, Na-C-S-H (Na$_2$CaSiO$_6$·2H$_2$O) is indentified in the CLS$_{9N}$ reactive mix. As a C-S-H phase of such low C/S ratio, i.e., C/S = 1, is not expected to co-exist with free CH (Figure 4.6), this is believed to be an artefact formed from precipitation from the pore solution during sample preparation. In OPC the majority of the alkalis are dissolved in the pore solution however with minor contents bound into the solid hydration phases mainly the C-S-H phase. The capacity of the C-S-H phase to incorporate alkalis increases as the content of acidic oxides,

i.e. SiO_2 and Al_2O_3, increases. Its capacity to bind alkali is thus very limited at C/S = 1.75 as expected for OPC. It however increases significantly for C/S ratios below 1.5 (Chunxiang, Hongding & Xianghui 1994, Duchesne, Bérubé 1994, Hong, Glasser 1999). The ability of the C-S-H phase formed within the CLS_{9N} blended cement to take up alkalis is thus expected to be limited. Hence, it requires additional experiments, e.g. test of alkali content in pore solution or expansion of mortar bars, to draw any final conclusions on the risk of expansion due to alkali-silica reactions.

Identification of hydration phases by SEM-EDS

The hydrated phases are additionally examined by scanning electron microscopy − energy dispersive spectroscopy (SEM-EDS) using a Zeiss 1540 XB focused ion beam, EDS, EBDS at Nanolab, Aalborg University, Denmark. For the SEM examinations of cement pastes a backscatter detector is used to maximize the contrast from compositional differences. In such images the brightest areas correspond to the unreacted clinker phases, CH is observed as darker areas than the unreacted clinker but brighter than the other hydration products, whereas the pores will appear black (Taylor 1997). For SEM-EDS analyses the pastes are after 90 days of hydration cast in epoxy, ground, polished and stored in a dessicator until the measurements are performed. Using EDS the chemical composition of individual spots can be determined. To make such investigations, it is important to examine areas large enough to represent the entire sample but at the same time of a sufficiently high magnification to distinguish the different phases. In this work, a magnification of 1800 is used and EDS data are collected from three images from various locations within the sample. The measurement depth is dependent on the acceleration voltage used during the measurement. High voltages result in large measurement depths. To obtain good separation of the phases a low acceleration voltage and thus energy must be employed during the measurement. It is however also of importance to use a sufficiently high energy to excite all relevant components. In this work, the EDS measurements are performed at 15keV. This gives a measurement depth of approximately 1.5 μm. The EDS data are collected performing a spectral imaging of the entire sample including all elements. The entire image is scanned for one element, before scanning for the next. This might introduce a small drifting of the image resulting in a reduced separation of the phases. A total of ≈1200 spots (400 from each image) are analyzed for each sample. The data interpretation are made plotting the atomic percentages of the elements of interest relative to the atomic percentage of Ca, e.g. as Al/Ca vs. Si/Ca (atom%). The combination of relatively large excitation energy (15keV) as well as some drifting of the image during data collection resulted in a poor separation of the various phases. Several trends can however still be found from the SEM-EDS analyses.

Figure 4.7 shows a plot of Al/Ca ratios against Si/Ca ratios of the OPC sample. Most of the analyzed data points cluster around the line representing mixtures of CH and C-S-H but also reveals the presence of C_3A hydrate containing spots. A similar plot for the $CLS_{9N\ fine}$ containing cement paste is shown in Figure 4.8. A significant

amount of the spot analyses again cluster around the line representing CH and C-S-H mixtures. In addition, a tendency of a higher fraction of spots high in SiO_2 and Al_2O_3 although still with compositions close to the C-S-H phase is found. This suggests the possibility that additional SiO_2 and Al_2O_3 are incorporated in the C-S-H phase. Furthermore a significantly larger fraction of spots clustering around the line towards C_3A is observed for this sample compared to OPC. This is in agreement with the changed composition of the CLS_{9N} reactive mix. In this sample spots of rather high Al/Ca and Si/Ca ratios are present. These fall around a line from the composition of C-S-H towards that of the unreacted CLS_{9N} glass, indicating significant amounts of unreacted glass left. Plots of S/Ca ratios vs. Al/Ca ratios indicate that the C_3A hydrate is primarily monosulfate (Appendix B, Figures B.1 and B.2). This corresponds to previous results on OPC pastes (Taylor 1997, Odler 2007, Nielsen, Herfort & Geiker 2005). There is however a clear indication that the CLS_{9N} containing cement has higher monosulfate content than the pure OPC. As additional SO_3 is not introduced, this is in agreement with the higher fraction of points clustering around the line towards C_3A hydrates for the glass containing sample.

Thus in general the conclusions drawn from the SEM-EDS analyses agree with the phases identified by XRD. Figure 4.9 illustrates one of the three SEM images on which the results of Figure 4.8 are based. The angular and rather bright areas, four of which are marked by circles, are the unreacted glass embedded in a matrix of hydration phases.
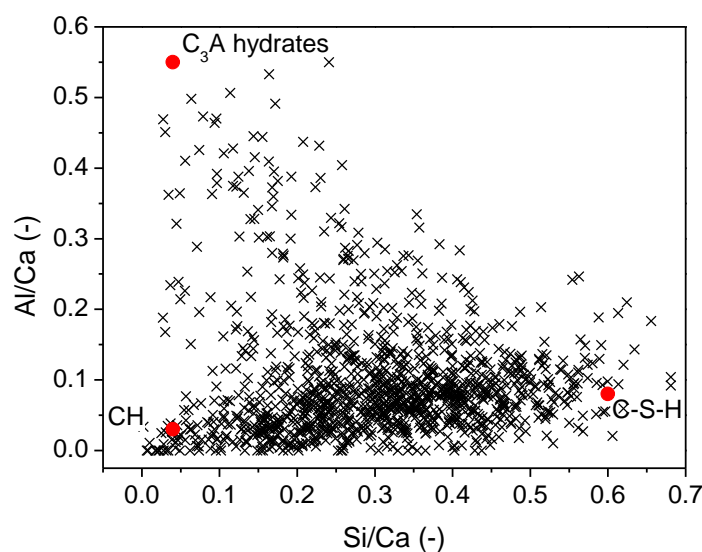

Figure 4.7: Al/Ca ratios as a function of Si/Ca atomic ratios for EDS spot analyses based on spectral imaging of an OPC paste hydrated 90 days. The atomic ratios of the hydration phases are adapted from (Odler 2007).
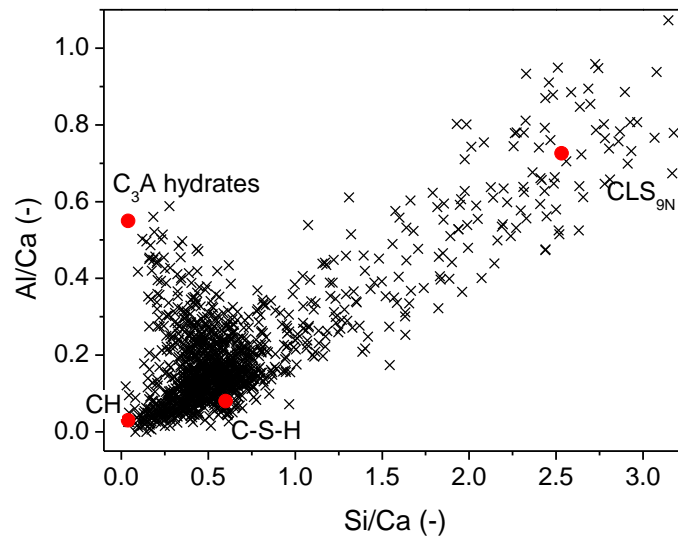
Figure 4.8: : Al/Ca ratios as a function of Si/Ca atomic ratios for EDS spot analyses based on spectral imaging on a blended cement paste containing 30 wt% CLS9N fine and hydrated 90 days. The atomic ratios of the hydration phases of OPC are adapted from (Odler 2007). CLS9N marked on the plot corresponds to the composition of anhydrous glass.
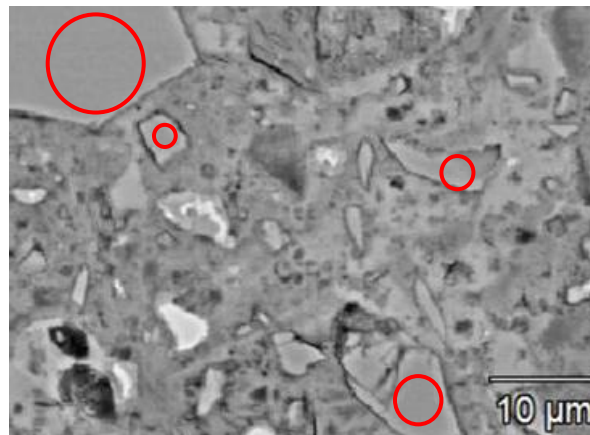
Figure 4.9: Backscattered SEM image of the CLS9N fine blended cement paste hydrated for 90 days. The angular and rather bright areas, four of which are marked by circles, are the unreacted glass embedded in a matrix of hydration phases.

4.2.2 Portlandite content

The Portlandite content within the cement pastes hydrated 90 days is determined in Paper VII by means of thermal analyses from the mass loss in the temperature range 440-540°C (Figure 3, Paper VII). The CLS_{9N} cement paste is found to have a significantly lower CH content (12 wt%) than the pure cement (19 wt%). This is due to the dilution of clinker in the blended cement but also due to the CH consumption

during the pozzolanic reaction to form C-S-H with a higher Ca/Si ratio than that of CLS$_{9N}$.

SEM-EDS analyses of the blended cement paste containing CLS$_{9N\ fine}$ after 28 days of reaction (Figures B.3, B.4 and B.5 in Appendix B) suggest a larger content of CH present, at this earlier state of hydration. As the pozzolanic reaction is most pronounced at the later stage of hydration, this can explain the larger amount of CH containing spots after 28 days of hydration compared to 90 days.

4.2.3 Reactivity of anhydrous clinker minerals and glass

The reaction of alite, belite and glass as a function of hydration time is in Paper VII determined by deconvolution of ^{29}Si MAS NMR resonances corresponding to different durations of hydration. Figure 4 in Paper VII shows the degree of hydration of alite and belite against time whereas Figure 5 in Paper VII illustrates that of CLS$_{9N}$. As expected alite reacts fast during the first days of hydration. The blended cement shows an accelerated alite hydration compared to the pure cement. As mentioned, this is previously reported for cements containing finely ground SCMs (Hjort, Skibsted & Jakobsen 1988, Krøyer et al. 2003) but could not be observed for the glass measuring the heat evolvement during the first 18 hours of hydration (section 4.1.3). After 90 days hydration comparable degrees of alite reactivity (above 90%) are however observed for the reference and the blended cement. Significant belite reactivity is not observed until after 4 days of hydration, with the final reactivity of the blended cement being 65%. In contrast, the belite reactivity reaches 75% for the OPC paste. This is in agreement with the slightly reduced 90 days strength observed for the CLS$_{9N\ fine}$ cement compared to the pure cement.

As expected the glass makes little or no contribution to early hydration, and significant glass reactivity is not observed until about 7 days of hydration. After 90 days, the degree of glass hydration is approximately 50%. As explained in Paper VII this determination is however associated with larger uncertainty than the alite and belite quantifications.

A recent ^{29}Si NMR study of blended cements containing OPC and 30 wt% natural pozzolan or fly ash used the same procedure as used in this work to determine the reactivity of the SCMs (Poulsen, Jakobsen & Skibsted 2009). Both SCMs have surface areas comparable to the fine CLS glass particles used in this work. In the study by (Poulsen, Jakobsen & Skibsted 2009), fly ash was found to have a reactivity of approximately 20% after 90 days hydration, whereas a slightly larger reactivity of approximately 25% is reported for the natural pozzolan. Despite the uncertainties associated with the glass quantification, the CLS$_{9N}$ reactivity can be concluded to be larger than that of both fly ash and natural pozzolan. This increased reactivity of the glass compared to fly ash is however not reflected in the strength measurements in this work. In this work, similar 90 day strengths are observed for the cements containing CLS$_{9N}$ glass particles and fly ash (Section 4.1.4). It should however be noticed that these strength measurements are made using SCM of significantly lower surface area than the SCMs used in the pastes investigated with ^{29}Si NMR.

4.3 Summary

The examination of physical performance of the various blended cements suggests the CLS glass particles to be a suitable alternative to the traditional SCMs. Particle surface area has great impact on the strength development whereas the different alkali contents of the two CLS glasses do not show any difference regarding mortar workability, setting behavior or compressive strength. Adding 30% CLS_{9N} with a surface area of 629 m^2/kg gives a 90 days strength of 90% compared to OPC.

Significant glass reactivity is observed after 7 days of hydration with approximately 50% of the glass reacting in 90 days. This is expected to increase for longer durations of hydration. Similar hydration phases as formed for OPC are identified for the CLS_{9N} containing cement.

5 Synergetic effect between limestone and glass in blended cements

In addition to blended cements containing one SCM, the effect of combining two SCMs in the same cement is examined in this chapter. For these investigations blended cement mortars are prepared containing combinations of the pozzolans stated in Table 4.1 and limestone (surface area 1288 m^2/kg). Thus limestone and one additional SCM are added. A clinker replacement level of 30 wt% is again used for all samples, whereas different ratios between the pozzolan and limestone are employed. Investigations are performed both regarding the physical performance of mortars and as a more detailed study of the hydration behavior of pastes.

5.1 Limestone as a supplementary cementitious material

By volume limestone is today probably the most commonly used clinker replacement material (Taylor 1997, Vuk et al. 2001, Tsivilis et al. 2003, Tsivilis et al. 1999, Zelic et al. 1999, Ramachandran 1988). The softness of limestone causes its considerable fineness when interground with cement. This accounts for the improved physical properties of Portland limestone cement (Taylor 1997, Vuk et al. 2001, Tsivilis et al. 1999). In addition, limestone is observed to participate in the hydration reactions reacting chemically with available alumina to form the so-called CO_2-AFm phase often referred to as the monocarbonate phase. The quantity of limestone reacting is however limited and reported to be in the range from a few percent to about 10% depending among other things on the C_3A content of the cement (Taylor 1997, Zelic et al. 1999, Ramachandran 1988, Klemm, Adams 1990).

The reaction sequence of C_3A for Portland limestone cement is reported to be similar to that of OPC. The fast C_3A hydration kinetics and the high gypsum solubility ensure rapid ettringite formation. As the sulfate is depleted and C_3A continues to react, the ettringite is continuously converted into the monosulfoaluminate phase (monosulfate). The calcium carbonate dissolves slowly and then reacts with any monosulfate to form an AFm carboaluminate (monocarbonate) phase. This is a more stable phase than the monosulfate due to its lower solubility. At low carbonate contents, hemicarbonate is in addition observed (Ramachandran 1988, Klemm, Adams 1990, Péra, Husson & Guilhot 1999, Ramachandran, Chun-mei 1986).

5.2 Physical performances

As for the blended cements containing just one SCM the physical performance of the mortars containing both limestone and a pozzolan is tested in terms of the workability, setting behavior and mechanical performance. For each of the SCMs in Table 4.1 four mortar samples with varying ratios between the pozzolan (*P*) (including the inert filler) and limestone (*L*) are prepared. *P*/(*P*+*L*) ratios of 0, 0.33,

0.67 and 1 are used. Paper V and VI deal with these investigations describing the experimental conditions.

5.2.1 Workability

Limestone addition does not affect the measured mortar slump on the flow table, and the workability of mortars containing two SCMs is similar to that of the mortars containing just one. The workability is thus slightly improved compared to OPC and neither additional water nor superplasticizers are required to obtain an acceptable mortar flow.

5.2.2 Setting behavior

The setting behavior of the limestone containing mortar blends relative to the content of cement is seen in Figure 5.1. This type of plot reveals an accelerated early hydration with the intensity of the main peak being larger for the Portland limestone cement than for the pure cement. This behavior is reported previously, with the small limestone particles expected to act as seeds for the initial C-S-H formation (Klemm, Adams 1990, Péra, Husson & Guilhot 1999, Ramachandran, Chun-mei 1986). A similar behavior is observed for the mortars containing fly ash and aplite (section 4.1.3). The mortars containing two SCMs exhibit a setting behavior in between that of the two boundary blends, i.e., the mortars containing only one of the SCMs. This is illustrated in Figure 5.1 using $CLS_{9N\ fine}$ as an example. A similar plot not accounting for the different cement fractions within the samples is seen in Figure 4 in Paper V.
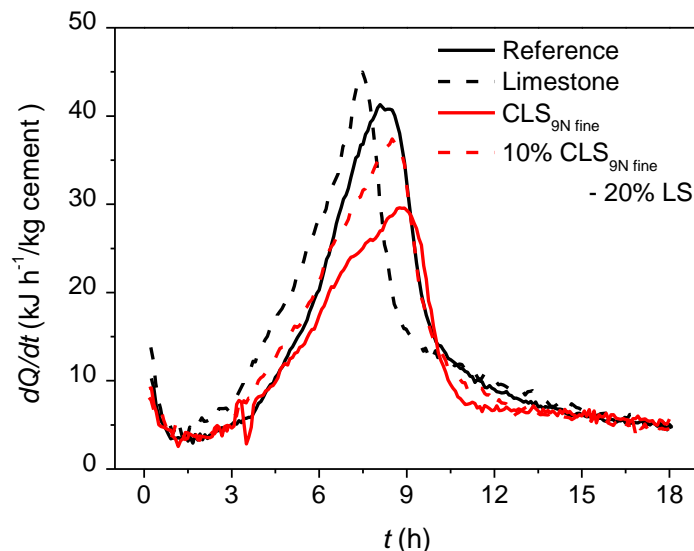

Figure 5.1: Setting behavior measured as the rate of heat evolution referred to the fraction of Portland cement within the blended cement. The heat evolution (dQ/dt) is plotted as a function of the time of hydration (t). LS is an abbreviation of limestone, with $20LS-10CLS_{9N\ fine}$ representing the blended cement containing 20 wt% limestone and 10 wt% $CLS_{9N\ fine}$.

5.2.3 Compressive strength

The early compressive strength of the blends containing two SCMs reflects the setting behavior just described. The blends containing limestone as the sole SCM, i.e., blends with $P/(P+L) = 0$, show 1 and 2 days strengths larger than the blends containing only the pozzolans of Table 4.1. The 1 and 2 days strength of the Portland limestone cements are 10-15% points larger than for the pozzolan cements. Considering the inert filler the difference is 20-25% points. An intermediate strength is found for the samples with $P/(P+L) = 0.33$ and 0.67 (Figure 5.2).
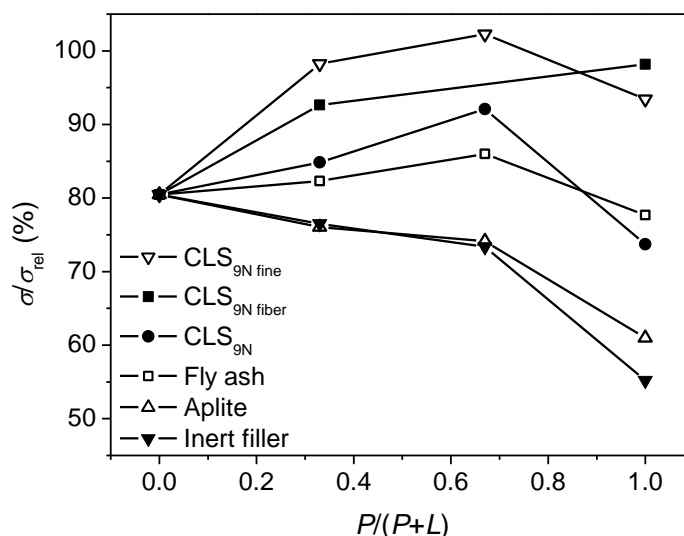

Figure 5.2: Relative compressive strength (σ/σ_{rel}) of the mortars containing different SCMs as a function of $P/(P+L)$. P is the content of pozzolan (including the inert filler) and L is the content of limestone in wt%. The solid lines are guides for the eye.

After 90 days of hydration the behavior is markedly changed for the mortars containing pozzolans participating in the strength giving reactions and, a synergy effect is found between the limestone and the pozzolan. Thus, the samples containing both limestone and pozzolan exhibit significantly higher strengths than would be predicted from the individual contributions of each constituent. This means that a synergetic effect is observed between limestone and the pozzolan. According to Figure 5.2 this is valid both for the fly ash and the two CLS_{9N} samples of various surface areas. CLS_{1N} containing mortars exhibit the same trend (Figure 5, Paper V). For $CLS_{9N\ fine}$ the compressive strength of the sample containing 20 wt% of the glass and 10 wt% limestone even exceeds that of the pure cement reference, i.e., $\sigma/\sigma_{rel} > 100\%$. Due to a limited amount of fiber sample, it has not been possible to obtain a data point at $P/(P+L) = 0.67$ for that sample. A tendency towards the synergetic behavior being larger for the CLS particles than for fly ash containing blends is observed from Figure 5.2. The origin of this synergetic effect is investigated in greater detail in section 5.3.

In contrast, this synergetic effect where the strength of the samples containing two SCMs exceeds that of the blends containing only one SCM is not observed for the aplite and inert filler containing blends.

5.2.4 Summary

The mortars based on blended cements containing both CLS glass particles and limestone exhibit acceptable workability, setting behavior and early compressive strength compared to pure cement. Regarding the late compressive strength a synergetic effect is observed between the limestone and the pozzolan with strengths exceeding that predicted from blends containing just one of the constituent. For the CLS glass of high surface area (629 m^2/kg) the 90 days strength of the blend containing 20% glass and 10% limestone even exceeds that of the pure cement reference. Blended cements containing mixes of CAS glass and limestone thus provides a qualified alternative to the traditional SCMs regarding mortar workability and compressive strength.

5.3 Hydration behavior

To clarify the origin of the synergetic behavior observed between the CLS glass particles and limestone within blended cements containing both materials, the hydration behavior is investigated in greater detail by means of paste samples. As for the examination of paste containing just one SCM, only pastes based on $CLS_{9N\ fine}$ are prepared. Pastes with $P/(P+L)$ ratios of 0, 0.33 and 1 are examined. Here the sample with $P/(P+L) = 1$ corresponds to the sample investigated in the previous chapter (section 4.2). Investigations by means of ^{29}Si MAS NMR spectroscopy, XRD and thermal analyses including the experimental conditions are described in Paper VII.

5.3.1 Identity of hydration phases formed after 90 days of hydration

As for the cements containing just one SCM the cement in the pastes under investigation in this chapter are according to Paper VII concluded to be almost fully reacted after 90 days of hydration. The glass reactivity is estimated to be 50%. The reactivity of cement components (alite and belite) and that of the glass is determined from deconvolution of ^{29}Si MAS NMR spectroscopic resonances in Paper VII. The fraction of limestone participating in the hydration reactions is in Paper VII quantified from thermo gravimetric analyses. For the blended cement containing limestone as the sole SCM it is ≈9%, whereas it for the cement containing both limestone and $CLS_{9N\ fine}$ ($P/(P+L) = 0.33$) is ≈16%.

Based on these results the location of the reactive mixes participating in the formation of hydration phases is plotted in the CAS (H) sub-ternary phase diagram (Figure 5.3). The composition of the Portland limestone cement is due to the low limestone reactivity just slightly shifted towards a higher CH content as compared to OPC. For comparison the figure also contains the compositional location of the

reactive mix of the blended cement containing 30% $CLS_{9N\ fine}$. The reactive mix of the blended cement containing 10% $CLS_{9N\ fine}$ and 20% limestone is also positioned within the same phase field as OPC with expected formation of CH, C-S-H, C_3A hydrates, iron oxide and pore solution.
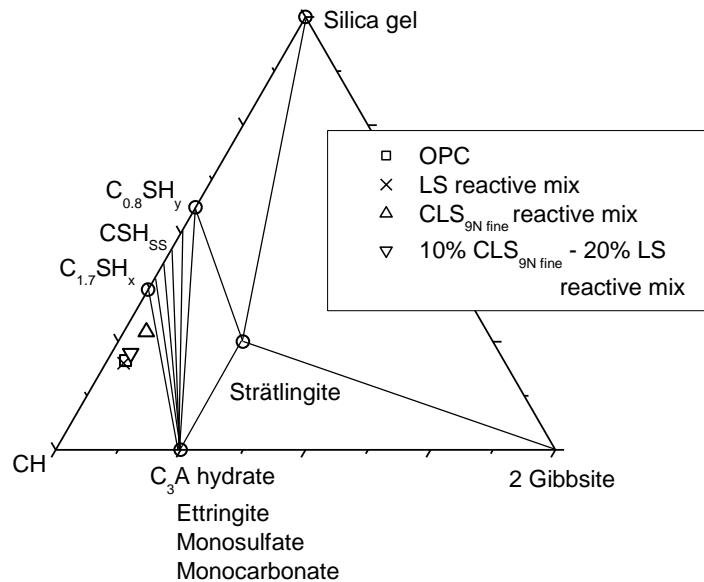
Figure 5.3: CAS (H) sub-ternary phase diagram (mol%) showing the location of the reactive mixes of the blended cements containing either 30 wt% limestone (LS), 30 wt% $CLS_{9N\ fine}$ or a combination of both (10% $CLS_{9N\ fine}$ and 20% LS). In addition, the location of OPC is shown in the diagram. Besides the phases predicted by the phase diagram, iron oxide and pore solution are present in excess, i.e. plotting outside the phase diagram.
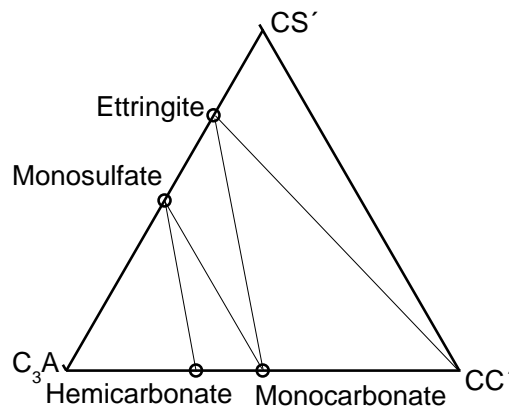
Figure 5.4: Ternary subsystem C_3A-CS'-CC' in limestone containing Portland cement system. S´ = SO$_3$ and C´ = CO$_2$.

The introduction of an additional component in the limestone containing cements namely CO_2 is expected to give an additional equilibrium hydration phase. As indicated on Figure 5.3 the C_3A hydrate forms a sub-system with $CaSO_4$ and $CaCO_3$. This subsystem is illustrated in Figure 5.4 with ettringite, monosulfate, hemicarbonate $(C_3A-\frac{1}{2}CC´-\frac{1}{2}CH-H_{12})$[2] and monocarbonate $(C_3A-CC´-H_{12})$ as possible binary solid hydration phases.

Table 5.1 gives the hydration phases identified by means of XRD in the two limestone containing cements after 90 days hydration. In addition to the phases formed in OPC, monocarbonate and calcite are identified for the blended cement containing 30% limestone. The XRD pattern (Figure 1, Paper VII) reveals large amounts of unreacted calcite to be present. This is in correspondence with the low degree of reactivity, i.e. $\approx$9%, determined by thermal analyses. The simultaneous existence of monosulfate (however in small amounts) and calcite suggest that equilibrium is not reached after the 90 days of hydration (Figure 5.4). For the blended cement containing both limestone and glass the CO_2 is again incorporated into a monocarbonate phase. Large amounts of unreacted calcite are identified in agreement with the reactivity of $\approx$16% determined by thermal analyses. No monosulfate is indentified for this sample but a carbonate containing magnesium aluminate hydrate (hydrotalcite) is identified in small amounts.

Table 5.1: Solid hydration phases identified by means of XRD after 90 days of hydration.

Hydrate phases	30% limestone	20% limestone, 10% CLS_{9N} fine
Portlandite	X	X
C-S-H	X	X
Monosulfate	X	
Ettringite	X	X
Monocarbonate	X	X
Calcite	X	X
Hydrotalcite[a]		X

[a] $Mg_6Al_2(CO_3)(OH)_{16}\cdot4H_2O$
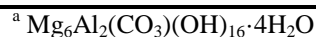
Identification of hydration phases by SEM-EDS

Figures 5.5 and 5.6 show the Al/Ca ratios as function of the Si/Ca ratios for approx. 1200 SEM-EDS spot analyses on each of the two limestone containing pastes. Most of the analysed data cluster around the line representing mixtures of $CH/CaCO_3$ and C-S-H. It should be noticed that CH and $CaCO_3$ cannot be distinguished in this type of plot. A comparison of the figure with those of the pastes not containing limestone (Figures 4.7 and 4.8) shows as expected a higher fraction of spots in the $CH/CaCO_3$ rich region.

---

[2] C´denotes CO_2

For the paste containing both limestone and CLS$_{9N}$, data points are also observed on a line towards the composition of unreacted glass suggesting this to be present in the sample. The rather low glass content in this sample compared to the sample containing CLS$_{9N}$ as the only SCM is reflected by the significantly lower abundance of points in this area compared to Figure 4.8.

Plots of S/Ca ratios as function of Al/Ca ratios indicate that less monosulfate and more ettringite are present in the samples containing limestone (Appendix B, Figure B.6 and B.7) than in OPC and the sample containing 30 wt% glass (Figure B.1 and B.2, Appendix B). This is in agreement with the expected conversion of monosulfate to monocarbonate, which also releases sulfate for formation of additional ettringite.
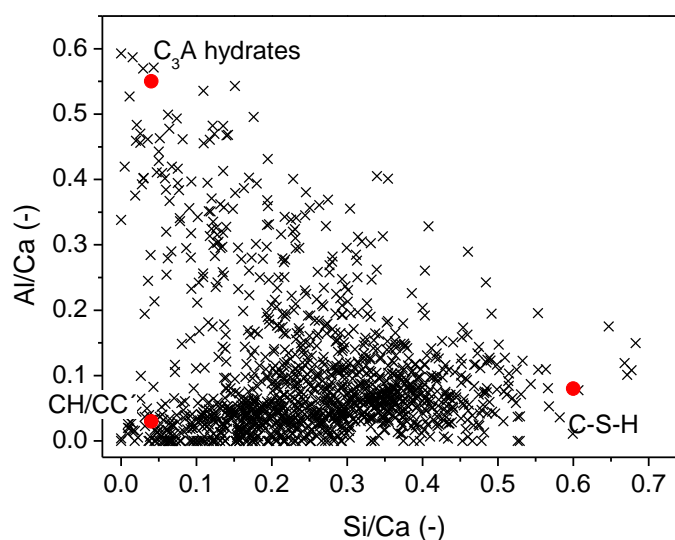

Figure 5.5: Al/Ca ratios as a function of Si/Ca atomic ratios for EDS spot analyses based on spectral imaging of a Portland limestone cement paste containing 30 wt% LS and hydrated 90 days. The atomic ratios of the hydration phases of OPC are adapted from (Odler 2007).
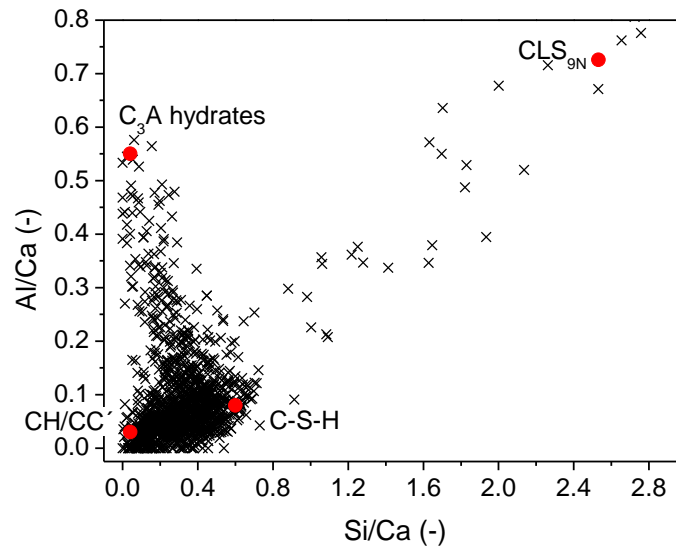
Figure 5.6: Al/Ca ratios as a function of Si/Ca atomic ratios for EDS spot analyses based on spectral imaging of a blended cement paste containing 20 wt% LS and 10 wt% CLS$_{9N\ fine}$ and hydrated 90 days. The atomic ratios of the hydration phases of OPC are adapted from (Odler 2007). CLS$_{9N}$ marks the composition of the unhydrated CLS$_{9N}$ glass.

5.3.2   Reactivity of anhydrous clinker minerals and glass

The consumption of alite and belite as a function of time is for the blended cement containing limestone as the only SCM and for that containing both limestone and CLS$_{9N}$ similar to that described in section 4.2.3 for the 30% CLS$_{9N}$ blended cement. The final belite consumption is however larger with a reactivity of 80% after 90 days of hydration as compared to 65% for the 30% CLS$_{9N}$ cement (Figure 6, Paper VII). No significant differences are observed in the course of glass consumption for the two CLS$_{9N}$ containing blended cements during the first 28 days of hydration. A tendency towards the glass of the mix containing both glass and limestone reaching a lower degree of reactivity after 90 days compared to the sample containing only glass is however found. This difference is believed to be due to the rather difficult task of deconvoluting the glass part of the ^{29}Si NMR resonances. The uncertainty associated with quantification of remaining glass is largest for long durations of hydration, as these samples contain the smallest quantities of glass (Figure 7, Paper VII). The 90 day reactivity of the glass is for both glass containing samples approximated to be 50%.

5.3.3 Synergetic effect

Based on the results presented in the previous sections, the following conclusions can be drawn regarding the origin of the synergetic effect observed for the blended cements containing both limestone and CLS_{9N}.

The fraction of limestone participating in the formation of hydration phases is increased from 9 to 16% as the limestone is combined with CLS_{9N} in the same blended cement. A larger fraction of the limestone is thus reacting chemically in the cements containing both limestone and glass. Hence, it is possible to exploit the combined effect of limestone both as a physical filler and as a chemically reacting pozzolan to a greater extent when CLS_{9N} particles are also present in the blended cement.

As explained in section 5.1 the $CaCO_3$ is slowly dissolved in the pore solution reacting with any monosulfate formed. This results in the formation of a C_3A-$C\bar{C}$-12H phase, i.e., monocarbonate. As $CaCO_3$ is present in large excess for these investigations, the formation of monocarbonate is primarily depended on the C_3A content. The Al_2O_3 content is increased as CLS_{9N} is mixed with the cement predicting a larger amount of C_3A to be formed (Figure 5.3). Assuming 50% reactivity of the glass, the Al_2O_3 content is increased with approximately 0.3 g per 100 g blended cement for the cement containing 10% glass and 20% limestone compared to the sample containing only 30% limestone. This is in correspondence with the increased limestone reactivity corresponding to ≈ 0.45 g per 100 g blended cement ($M(CaCO_3)$ = 100 g/mol $M(Al_2O_3)$ = 102 g/mol). Thus it seems reasonable to expect the increased Al_2O_3 content to be the reason for the observed synergy effect. Figure 5.2 furthermore reveals the 90 days compressive strength to be largest for the blended cement containing 20% glass compared to that containing only 10%. This is in agreement with the higher Al_2O_3 content of the reactive mixture of this sample. The same explanation is valid for the cements containing both limestone and fly ash. Based on the 90 days strength measurements (Figure 5.2) the synergy effect of the fly ash containing cement is found to be less than for the CLS containing cement despite the significantly larger Al_2O_3 content in fly ash (≈ 25 wt%) compared to the CLS glass (≈ 12 wt%). Considering the reduced reactivity of fly ash found by ^{29}Si NMR (Poulsen, Jakobsen & Skibsted 2009) the Al_2O_3 available for formation of hydration phases is reduced for the fly ash containing cement compared to the CLS glass containing cement. No synergetic effect is observed for the samples containing both limestone and aplite otherwise having an Al_2O_3 content of ≈ 10 wt%. The crystallinity of aplite makes the Al_2O_3 unavailable for pozzolanic reactions.

In addition, the conversion of monosulfate to monocarbonate releases sulfates resulting in the formation of more ettringite. This is also expected to contribute to lower porosity and higher strength.

Any incorporation of Al dissolved from the glass into the C-S-H phase will reduce the content of Al_2O_3 available for formation of monocarbonate phase. Incorporation of Al in the C-S-H phase will require absorption of alkali ions for maintaining charge neutrality. This results in an expected increase of the capacity of the C-S-H to incorporate alkali.

5.4 Summary

The introduction of both limestone and CLS_{9N} glass to the same blended cement results in a synergy effect with late strengths larger than expected from the results of the cements containing just one SCM. The increased Al_2O_3 content of the CLS containing cement compared to those not containing glass is expected to cause a larger fraction of the limestone to react chemically forming strength giving hydration phases. In this way, the combined effect of limestone as a physical filler and the pozzolanic effect of both the limestone and the CLS glass can be exploited to a greater extent.

Late strength even exceeding that of OPC is observed for the blended cement containing 20% CLS_{9N} fine and 10% limestone. Workability and early strength development of the cements containing both limestone and CLS glass is similar to the behavior of the blends containing just glass.

6 CO$_2$ reduction using blended cements

The previous two chapters dealt with the hydration behavior and physical performance of blended cements containing the newly developed calcium aluminosilicate based SCMs. Based on these investigations the CLS glasses are concluded to be a qualified alternative to the traditional SCMs. Equally as important is it to be able to significantly reduce the CO$_2$ emission from cement production by partly substituting the clinker with the CLS glass particles. Using the present production technology 800 kg CO$_2$ is on average released producing one tonne cement. The majority of this, i.e. 500-550 kg CO$_2$ per tonne clinker, is released directly from the CaCO$_3$ sources accounting for 80-85 wt% of the raw materials. The other major contributor is the burning of mainly fossil fuels to reach the temperatures of production. This accounts for 250-300 kg CO$_2$ per tonne clinker. In addition, minor CO$_2$ contributions are introduced from transport and from the use of electricity e.g. to run the mills used to grind the clinker. These account each for less than 5% of the total CO$_2$ release (World Business Council for Sustainable Development 2009, Worrel et al. 2001, Damtoft et al. 2008).

Similar to the production of cement, glass making is a highly energy intensive process taking place at elevated temperatures. Normally, the production of glass involves five main processes; mixing, melting, forming, annealing, and finishing. The major energy consumption takes place during melting within the glass furnace (Edgar et al. 2008, Sardeshpande, Gaitonde & Banerjee 2007). In the initial part of this work the composition of the glass has been optimized to reduce this energy consumption e.g. by ensuring the possibilities of working at a relatively low production temperature and achieving a glass by air cooling instead for quenching in water. In addition, the use of CAS glass as SCMs sets no requirements to homogeneity, shaping, release of stresses in the glass, etc. The processes of forming, annealing and finishing can thus be cut down compared to normal glass production of e.g. flat glasses for windows or container glasses. Importantly, the residence time within the furnace can also be significantly reduced compared to production of these materials (Beerkens 2004). Similar to cement production, CaO is introduced to the CAS glasses using limestone as the raw materials source. Hence, raw materials CO$_2$ release due to calcinations of carbonates must also be considered for the glass production.

6.1 CO$_2$ release from fuels

Soda-lime-silica glass is by far the most commonly used glass e.g. for windows and glass containers and is normally produced at 1500-1600°C. An efficient continuously operated glass melting tank producing up to several hundreds of tons of glass per day at these temperatures has a specific energy consumption of 4 GJ per ton glass produced (Edgar et al. 2008, Sardeshpande, Gaitonde & Banerjee 2007). From investigations of glass characteristics (section 3.2.1) it is found that the CAS glasses

based on natural mineral sources (the CLS glasses) can be produced at 1300-1350°C corresponding to a temperature reduction of ≈15% compared to production of normal soda-lime-silica glass.

Normally, the heat of reactions accounts for no more than 25% of the total energy consumption during glass melting. For the CLS glasses, the heat of reactions is made up of contributions from two processes, i.e. the calcinations of limestone and the melting. In Paper II the enthalpy of calcination is for CLS_{9N} found to be 325 kJ/kg of glass whereas the melting enthalpy is estimated to ≈500 kJ/kg. This corresponds to approx. 20% of the total energy requirement for the production process. For comparison the enthalpy of formation of one kg of Portland clinker is approximately 1750 kJ, with the endothermic calcinations of limestone dominating this overall enthalpy (Taylor 1997).

Two of the major energy requirements during glass manufacture are the heat carried by the glass and flue gas, respectively. A large fraction of this energy can however be recovered and reused in the process e.g. to preheat the combustion air. Another important energy consumption process is the losses through walls and openings. This heat cannot be recovered and depends to a large extend on the operating temperature of the furnace (Sardeshpande, Gaitonde & Banerjee 2007, Conradt 2007, Conradt 2000). Using the method of Paper II it is estimated that the wall losses can be reduced with more than 40% reducing the operating temperature of the furnace from 1550°C to 1300°C. Assuming that the wall losses account for 15% of the total energy consumption of the furnace this reduces the specific energy consumption to ≈3.7 GJ/ton. According to section 1.1 this is equal to the global weighted average energy consumption for clinker production. Converting this to CO_2 equivalents assuming natural gas as the energy source for glass production, results in a CO_2 release of 250 kg per ton glass produced. Assuming coal as the energy source with 15% of alternative fuels not giving rise to any CO_2 emission, the result is a total CO_2 release of 290 kg per ton glass. This is in agreement with the size of the fuel-derived CO_2 release expected for cement production.

Comparing the fuel-derived CO_2 release of the blended cements containing CLS glasses to that of cements containing conventional clinker replacements materials such as fly ash and limestone, it is important to notice that the use of these conventional materials does not cause any fuel-derived CO_2 emission linked to cement production. Figure 6.1 shows the fuel-derived CO_2 release from the production of blended cements containing either 30 wt% CLS glass or 30 wt% fly ash or limestone. Equal fuel-derived CO_2 releases of 275 kg per ton materials produced is used for production of both CLS glasses and OPC.
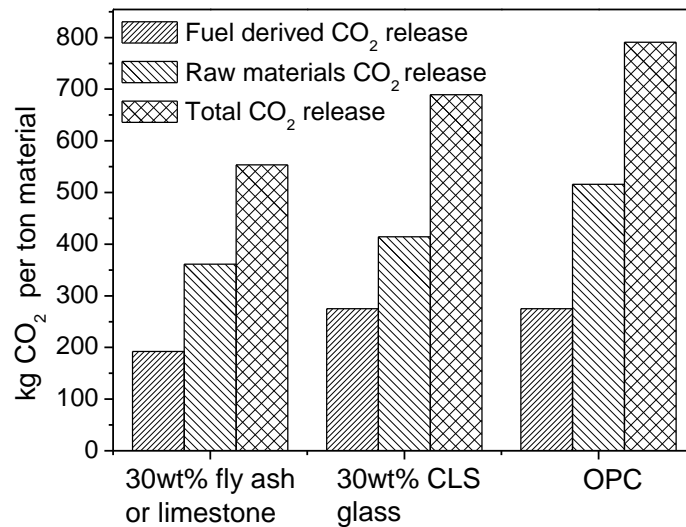
Figure 6.1: CO_2 release from production of blended cement containing 30 wt% alternative materials, i.e., either fly ahs/limestone or CLS glass. In addition, the figure gives the CO_2 release of ordinary Portland cement (OPC) manufacture.

The grindability of cement clinker and the CLS_{9N} glass is furthermore compared in section 3.2.1. Here it is concluded that to obtain particles of cement fineness (575 m^2/kg of the cement used in this project) less energy is required grinding the glass compared to the cement. The energy requirement and thus CO_2 release linked with grinding is thus less for the glass compared to the cement.

6.2 CO_2 release from raw materials

Limestone constitutes approximately one third of the raw materials for production of the CLS glasses. This results in the release of 175 kg CO_2 per ton glass directly from calcinations of the raw materials. This is significantly reduced compared to the production of OPC that gives rise to the release of 516 kg CO_2 per ton cement of the composition stated in Table 2.2. As the conventional SCMs as fly ash are industrial by-products no raw materials CO_2 release is linked to the cement industry using these materials. The situation is similar using limestone as a partial clinker replacement material as this is mixed with the cement subsequent to the burning process. Figure 6.1 compares the raw materials CO_2 release of blended cements containing either 30 wt% CLS glass or 30 wt% fly ash, limestone etc. with that of OPC. The raw materials CO_2 release is significantly reduced for both blended cements relative to OPC. ≈360 kg CO_2 is release per ton blended cement containing limestone or fly ash whereas ≈415 kg CO_2 is released per ton using CLS glass as SCM.

Figure 6.1 shows in addition the total CO_2 release for the three types of cements. 30% less CO_2 is emitted adding 30 wt% of the conventional waste material SCMs or limestone compared to the production of OPC. On the other hand, the use of the newly developed CLS glass particles results in a reduction of the CO_2 release of 13% compared to the pure cement.

6.3 CO$_2$ release relative to cement performance

A more meaningful measure of the CO$_2$ release of the blended cements is the CO$_2$ release relative to the performance of the material. A plot illustrating this is shown in Figure 6.2. Here the total CO$_2$ release as described above (m_{CO2} in kg) is normalized by the 90 days compressive strength of the given cement (σ in M Pa). Figure 6.2 compares m_{CO2}/σ for the different blended cements relative to that of pure cement as a function of the *P/(P+L)* ratio. If $(m_{CO2}/\sigma)_{rel} < 1$ the CO$_2$ per mechanical performance is reduced for the blended cement compared to the pure cement. From the figure it is concluded that if CLS$_{9N}$ is used as the only SCM it must be ground to a rather large surface area in order to obtain reductions in the CO$_2$ emission without having to increase the cement fraction per cubic meter of the concrete or mortar. Grinding the CLS$_{9N}$ glass particles to a surface area of 629 m^2/kg it is possible to reduce the CO$_2$ release with almost 10% for the same 90 days strength. Combining both limestone and CLS$_{9N}$ in the same cement, reductions in CO$_2$ emission of up to slightly above 20% can be reached. Regarding the CO$_2$ release from production, the CLS glasses provides a promising alternative to the limited sources of traditional SCMs.

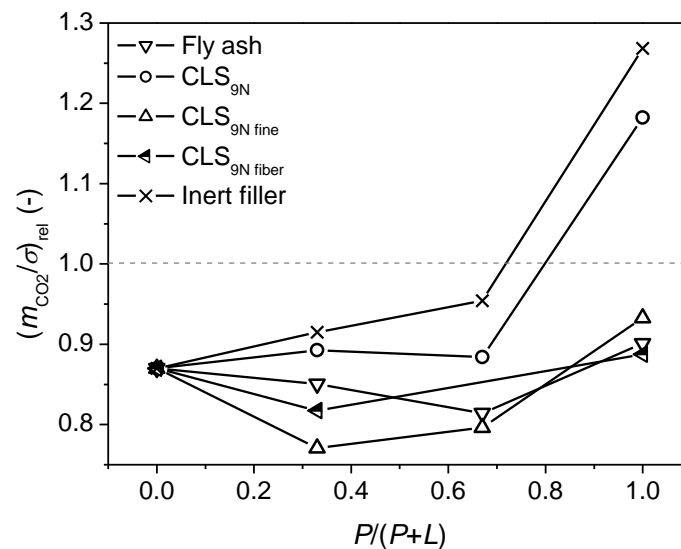**Figure 6.2: Relative raw materials CO$_2$ emission $(m_{CO2}/\sigma)_{rel}$ as a function of *P/(P+L)*. $(m_{CO2}/\sigma)_{rel}$ < 1 indicates blended cements with a reduced CO$_2$ emission relative to the mechanical performance compared to pure cement. This limit is indicated by the dashed grey line.**

7 General discussion and perspectives

According to the World Business Council for Sustainable Development 2009, clinker substitution is a potential method for reducing the massive quantities of CO_2 released from manufacture of cement. This requires the availability of large amounts of SCMs. Traditionally, industrial by-products such as fly ash, blast furnace slag and micro silica have been used for this purpose. This is a good solution, as it in addition to lowering the clinker content solves the problem of getting rid of significant amounts of waste materials. The availability of these materials is however limited and as mentioned in section 2.2 they are today almost fully utilized in Western Europe. Furthermore, the supply of such waste materials is expected to be reduced in the future. This sets up challenges for the cement industry if it wants to be able to meet the increasing future demand for cement while at the same time reduce its CO_2 emission.

For a new material to be a qualified SCM it must meet several types of criteria, some of which are listed here:

1) It should possess cementitious reactivity when mixed with the cement without altering important properties such as increasing the water demand. This is important to ensure acceptable performance of the final mortar or concrete.
2) To avoid facing the same challenge as for the traditional materials it must be available in large quantities.
3) The use of this material should result in a significant reduction of the CO_2 release linked to cement production.
4) The manufacture of blended cement containing the new SCM should be economically viable.

In this work, calcium aluminosilicate (CAS) based glass particles of compositions stated in Table 3.1 are investigated for use as SCMs. In this approach the glasses referred to as CLS glasses are produced particularly for the use as SCM. Regarding the first requirement, the addition of 30 wt% of the newly developed CLS glasses to an OPC mix slightly increases the workability of the fresh mortar. The water demand is thus not increased. This is an advantage compared to the calcined clay based SCMs tested in another part of the FUTURECEM project. Reduced early strengths are observed using the CLS glasses, whereas the blended cements show 28 and 90 days strengths approaching the strength of OPC.

To meet the second requirement it is chosen to produce the glasses using raw materials available locally and in large quantities. Similar raw materials as used for conventional PC manufacture is used for production of the glasses.

The composition of the glasses is furthermore optimized to reduce the CO_2 emission from production. Optimizations are made in regard to both the raw materials CO_2

release and the fuel-derived CO_2 release. It is estimated that the glasses can be produced emitting approximately 40% less CO_2 compared to OPC production.

Regarding the economical viability of producing the blended cements several factors, which are beyond the scope of this work, must be considered.These include a balance between the costs of establishing and maintaining facilities for glass production and the cost savings from emitting less CO_2 and thus spending less CO_2 quotas. This might leave the cement industry with the opportunity of disposing of unused CO_2 quotas. As a first step to ensure an economically reasonable production of the blended cements, it is as part of this work chosen to use low cost and locally available raw materials for glass production.

As mentioned in section 4.1.4, similar strength development patterns are found for the blended cements containing either 30 wt% CLS glass or 30 wt% fly ash (surface area of ≈350 m^2/kg). These two SCMs are however different when comparing the CO_2 releases. As fly ash and the other conventional SCMs are industrial by-products, they can directly be used in the cement industry, and hence, do not cause additional CO_2 release like CLS glasses, production of which releases CO_2. Due to the insufficient resources of these waste products, however, we have to think about an alternative way to obtain SCMs, e.g., by producing SCMs although this causes a production related CO_2 emission. Nevertheless, the overall CO_2 emission will be reduced by using the CLS based SCMs.

Another clinker replacement material not causing any production related CO_2 release is limestone. When using limestone for this purpose it is directly added into the clinker without calcination. Addition of 30 wt% limestone to the OPC results in 90 days strength reaching 80% of the pure cement strength. This is due to the combined effect of the very fine limestone particles (1288 m^2/kg) acting as physical filler and the ≈9% of the limestone taking part in the formation of hydration phases. Limestone is thus a promising clinker replacement material. It is cheap and available in large quantities near the cement producing facilities.

Generally during glass production of e.g. soda-lime-silica glass, cullet is added during the melting process to reduce the energy consumption. For instance the use of cullet significantly reduces the duration of the fining process required to obtain a homogenous glass melt. As the homogeneity is not of great concern for the positive performances of glass when mixing with cement, the addition of cullet is not considered for the production of the glasses used in this project. Instead any available waste glass, i.e., container glass, window glasses or inorganic residues from incineration of glass fiber reinforced composite materials, could be mixed with the glass after production, e.g., during the grinding process. Following this approach no energy is spent on re-melting the cullet. Dependent on the type and amount of waste glass, compositional adjustments could be made during production of the CAS glass varying the proportions of the mineral raw materials. Normal soda-lime-silica glass is not considered as the basic composition for the SCM glasses, as this in general

have a very low Al_2O_3 and rather high alkali oxide contents. Available Al_2O_3 turned out to have significant impact on the synergy effect found between the CLS glasses and limestone.

In addition to the blended cements containing one SCM, cements combining both the CLS glass particles and limestone are examined in this work. For these blended cements, a synergy effect with late strengths exceeding the ones predicted from the cements containing just one of the alternative materials is observed. This effect is caused by the relatively high Al_2O_3 content of the glass, which results in an increase of the limestone fraction reacting chemically and thus contributes to the formation of strength giving hydration products. As the addition of limestone does not result in any production related CO_2 release linked to cement production, the addition of both limestone and CLS glass to the same cement significantly reduced the final CO_2 release. Combining limestone and finely ground CLS glass in the same cement reduction in the CO_2 emission slightly above 20% can be reached for the same 90 days strength as the OPC. To elaborate the understanding of the synergy effect between limestone and pozzolans containing available Al_2O_3 in larger contents than found in the cement, additional examinations of hydration behavior should be performed. For that purpose calcium aluminosilicate glasses with systematic variations of the Al_2O_3 content should be produced, mixed with limestone, cement and water and analyzed e.g. by means of thermal analyses after various durations of the hydration process. The hydration period could beneficially be extended beyond 90 days.

An interesting observation during investigation of the performance of the blended cement mortars is the effect of increasing the surface area of the glass particles in comparison to an increasing structural disorder and hence enthalpy of the glass. On a short time scale, observable from measurements of the evolution of heat during the first 18 hours of hydration, an increasing deviation from equilibrium conditions is found to enhance the reactivity of the glass whereas an increased surface area does not show any impact (Figure 4.4). On a longer time scale, evaluated by means of compressive strength, the situation is opposite (Figure 4.5). This gives indications of the reaction mechanism. In general, the glasses show little reactivity during the first 4 days of hydration (Paper VII). Hence, the surface area and thus the number of sites available for dissolution of the glass do not impose a limiting factor on the glass reactivity. Decreased glass stability with a structure further from equilibrium conditions on the other hand eases the breakage of bonds during the initial reactions thus increasing the reactivity of the fast cooled glass particles. As the OH^- concentration in the pore solution increases as a function of time (Gartner, Tang & Weiss 1985, Thomas, Double 1981), the reduced stability of the glass becomes of minor importance. And as the glass starts to participate more in the hydration reactions with significant amounts of glass being depolymerized, the number of available sites for reaction at the surface starts to have an impact on reactivity. ^{29}Si NMR investigations of paste samples containing glass of different surface areas and

with varying degrees of structural disorder could be made to elucidate these mechanisms further.

In addition to the properties of the blended cements investigated in this work, the long term characteristics and durability of concrete based on the blended cements are also of great importance. Characteristics such as chloride penetration and corrosion of reinforcement material as well as susceptibility to sulfate attack should be investigated before final conclusions on the usage of the calcium aluminosilicate glass based SMCs can be drawn. Generally, the addition of SCMs to cement decreases the permeability possibly due to the consumption of portlandite to form additional C-S-H. Low permeability will reduce the inward diffusion of chloride and sulfate which in turn might reduce the risk of deleterious reactions caused by these ions (Taylor 1997). If this is also the case for blended cements containing the CLS glasses will however have to be examined experimentally.

As mentioned in chapter 4, high contents of alkali in the pore solution might cause alkali-silica reactions to occur in concrete exposed to moisture. As CLS_{9N} is relatively rich in alkali it is of importance to establish whether or not there is an increased risk of expansion and crack formation in the concrete due to alkali-silica reactions. This could be established by determining the content of alkali in pore solution. This might however not be straightforward as the measurement must be made after relativity long hydration to ensure significant reactivity of the glass. This will complicate the collection of pore solution from prisms as the content hereof diminishes over time. Mortar bar expansion tests could also be performed as this is a more direct method to determine the degree of expansion.

Prior to use of the CAS based SCMs in larger scale concrete production, experiments must be made regarding large scale production of the glass. This includes design of the furnace and optimization in order to reduce the energy consumption during production. It is of importance to examine possibilities for the casting process to ensure sufficiently fast cooling conditions to avoid crystallization. Within this work, two portions of glass melts of approximately 8 kg each have been made using a 5 liter silicon carbide/graphite crucible. For these glass preparations the melt was casted tilting the crucible thus pouring the melt unto a steel plate. The melt was spread on the plate by hand using long steel tools. This casting method provided sufficiently fast cooling to avoid crystallization of the melt. The glass produced in this test will be used to investigate the formulation and mixing of concrete using blended cements containing 30 wt% of the glass. The preliminary results indicate that concrete mixes can be made without changing the precipices used for the OPC based concrete. This is also an important characteristic of the CLS glasses.

8 Conclusions

The aim of the present study is the development of innovative supplementary cementitious materials based on calcium aluminosilicate glasses. The incentive to produce such materials specifically for the use as SCM is that the availability of the traditional by-product based SCMs such as fly ash and blast furnace slag is insufficient to meet the future requirements from the cement industry. This is especially a problem in regions like Western Europe.
The objective of this work has been: 1) to design a glassy system with a composition optimized for the use as SCM, and 2) to examine the physical performance of cement mortars as well as hydration behavior of pastes containing these newly developed glass particles.

The glass composition has been optimized regarding three main requirements:

- To ensure a future economical viable production and to avoid the problem of insufficient availability of the SCMs, the glass should be based on low cost raw materials available locally in large quantities. Hence it is chosen to base the glass on the conventional raw materials used for cement production, i.e., clay, limestone and sand, however mixed in proportions different from cement.
- The production of the glass should give rise to a significantly reduced CO_2 emission compared to the production of Portland cement. The glass composition is thus adjusted to ensure both low raw materials CO_2 emission and low fuel-derived CO_2 emission. The amount of CO_2 released from raw materials in directly linked to the CaO content of the glass, as the CaO is provided by addition of limestone. For the CLS glasses ≈175 kg of CO_2 is released per tonne glass produced. This account for around one third of the 516 kg of CO_2 released producing one tonne of the OPC used in this work. Acceptable fuel-derived CO_2 release can be ensured by adjusting the composition to obtain a relatively low practical melting temperature thus allowing for the use of a correspondingly low furnace operating temperature. The CLS glasses can be produced at 1300-1350°C which is significantly lower than the production temperature for OPC (≈1450°C) as well as for common soda-lime-silica glass products (1500-1600°C). In addition, all glass melts studied in this work exhibit rather high glass forming ability thus allowing for the melts to be vitrified without forced cooling. This also contributes to maintaining the fuel-derived CO_2 at a minimum. Combining these investigations, it is estimated that the glass can be produced with comparable or slightly reduced fuel-derived CO_2 in relation to the production of cement. Using 275 kg CO_2 per tonne material as an estimate of the fuel-derived CO_2 release from production of both clinker and glass, the total CO_2

release from production of both materials can be calculated. As expected the production of cement clinker releases approximately 800 kg of CO_2 per tonne, whereas the production of CLS glass in contrast results in the release of approximately 450 kg CO_2 per tonne. The glass can thus be produced under conditions causing significantly lower CO_2 emissions than the cement.

Measurement of surface area as a function of grinding time in a porcelain mill have shown that the clinker and CLS_{9N} glass possess comparable grindability to a surface area of approximately 450 m^2/kg. At surface areas larger than this, the glass show superior grindability in comparison to the clinker. Approximately 5% of the CO_2 release for cement production is due to the use of electricity, e.g. to run the mills used to grind the clinker.

- For the glass to be a useful SCM it must in addition contribute to the formation of strength giving hydration phases as it is mixed with cement. The glass should thus possess pozzolanity to ensure similar or better cement performance, resulting in acceptable concrete performance without having to increase the content of cement per cubic meter of concrete.
  This is at first tested as the reactivity of the glass in a saturated $Ca(OH)_2$ solution. ^{29}Si and ^{27}Al MAS NMR spectroscopy is used to investigate any products formed from these reactions. It is found that dimers and chains of SiO_4 units are formed during reaction with $Ca(OH)_2$ and water, and that a phase containing AlO_6 units possessing a higher degree of order than in the original glass is also formed. These phases resemble the C-S-H phase and the calcium aluminate hydrates formed during OPC hydraion. The calcium aluminosilicate based glass particles are thus pozzolanically active. The degree of pozzolanity is found to increase as minor components are introduced from the natural raw materials and further as additional Na_2O is introduced to the CLS_{5N} and CLS_{9N} glasses.

From investigations of these properties, the CLS glasses show promising potential as SCMs both in regard to both reduction of the CO_2 emission and ensuring acceptable performance of mortars and concretes.
To get a deeper understanding of how compositional changes affect the glass properties via alteration of the glass structure, the composition-structure relationship of the ten three component CAS glasses is investigated is section 3.1.2. Structural heterogeneity is found in the intermediate-range order with clustering of highly depolymerized regions of low Al content and highly polymerized regions of alternating SiO_4 and AlO_4 tetrahedra.

The next step of the work has been more direct investigations of the performance of blended cements containing the CLS glasses. For these investigations blended cements containing 30 wt% clinker replacements have been prepared. The physical performances of mortars are tested in relation to workability, setting behavior and

compressive strength after various durations of hydration. These investigations demonstrate:

- Standard mortar workability is slightly improved for the blended cements compared to OPC.
- The glass does not contribute to early hydration measured as the heat evolvement during the first 18 hours of hydration. These measurements indicate a slightly increased duration until the onset of setting for the blended cements.
- From measurement of strength the pozzolanic reactivity of the CLS glasses is limited at early stages of hydration but increases over time. At 90 days hydration the strength reaches 75% of the OPC for blended containing CLS_{9N} with a surface area of 371 m^2/kg. This increases to above 90% as the surface area of the glass is increased to 629 m^2/kg. In general, the strength development is similar to that of blended cements containing fly ash.
- A synergetic effect is observed at long durations of hydration for blended cement containing both limestone and CLS glass. For these blends strengths are higher than predicted from the individual contributions of each constituent for the cases of 28 and 90 days hydration. This is due to a larger fraction of the limestone participating in formation of the strength giving monocarbonate phase as the content of Al_2O_3 available for reaction with limestone is increased by the presence of CLS glass. For blended cements containing 20% $CLS_{9N\ fine}$ and 10% limestone the 90 days strength even exceeds that of OPC.
- From investigations of hydration behavior by means of ^{29}Si MAS NMR spectroscopy and XRD the glass is found to be incorporated in hydration phases similar to the once formed during hydration of OPC.

From the investigations of physical performances of the mortars containing blended cements with 30 wt% clinker substitution it is confirmed that the CLS glasses are a qualified candidate as a SCM. This is due to the fact that the usage of blended cement results in acceptable mortar performance as the clinker is substituted with glass on a 1:1 weight basis.

To get a measure of the CO_2 release relative to the performance of the blended cements, the CO_2 release of the given blended cement has been normalized with the 90 day strength. If the CAS based glasses are used as the sole SCM it must be ground to a rather large surface area in order to obtain reduction in the CO_2 release without increasing the content of cement per cubic meter of concrete. With a surface area of 629 m^2/kg the CO_2 emission can be reduced by 10% for the same performance as OPC. Combing limestone and CLS glass particles in the same cement, 20% reductions can be achieved.

Thus, the use of CLS glasses as SCMs is a good approach for significantly reducing the CO_2 emission from cement production. To reach the FUTURECEM aim of reducing the CO_2 release with at least 30%, the use of CAS based SCMs must

however be combined with other approaches to reduce the CO_2. This could e.g. be a combination of the CLS glasses with clinkers optimized to show high compatibility with the CLS based SCMs.

9 List of references

Aalborg Portland 2009, *Årsrapport 2009, Aalborg Portland,* Aalborg Portland, Cementir Holding, Aalborg, Denmark.

Allwardt, J.R., Lee, S.K. & Stebbins, J.F. 2003, "Bonding preferences of non-bridging O atoms: Evidence from O-17 MAS and 3QMAS NMR on calcium aluminate and low-silica Ca-aluminosilicate glasses", *American Mineralogist,* vol. 88, pp. 949-954.

Ambroise, J., Maximilien, S. & Pera, J. 1994, "Properties of Metakaolin Blended Cements", *Advances in Cement Based Materials,* vol. 1, pp. 161-168.

Andersen, M.D., Jakobsen, H.J. & Skibsted, J. 2003, "Incorporation of aluminum in the calcium silicate hydrate (C-S-H) of hydrated Portland cements: A high-field ^{27}Al and ^{29}Si MAS NMR investigation", *Inorganic Chemistry,* vol. 42, pp. 2280-2287.

Beerkens, R. 2004, "Modular Melting - Industrial Glassmelting Process Analysis", *American Ceramic Society Bulletin,* vol. 83, no. 4, pp. 28-32.

Blezard, R.G. 2007, "The History of Calcareous Cements" in *Lea's Chemistry of Cement and Concrete*, ed. P.C. Hewlett, Fourth edn, Elsevier, Oxford, UK, pp. 1-23.

Chunxiang, Q., Hongding, G. & Xianghui, L.M., T. 1994, "Meachnism of mineral admixture supressing alkali-silica reaction: Part II. Retardtion of the transport of Na, K and OH ions in the pore solution structure caused by acidic action of mineral admixture particles in matrix", *Cement and Concrete Research,* vol. 24, pp. 1327-1334.

Conradt, R. 2007, "Production efficiency, environmental sustainability, and glass quality - a thermodynamic optimisation of three conflicting objectives", *Glass Technology-European Journal of Glass Science and Technology Part A,* vol. 48, no. 5, pp. 235-241.

Conradt, R. 2000, "A generic approach to the relation between pull rate and energy consumption of glass furnaces", *Glastechnische Berichte-Glass Science and Technology,* vol. 73, pp. 252-261.

Damtoft, J.S., Lukasik, J., Herfort, D., Sorrentino, D. & Gartner, E.M. 2008, "Sustainable development and climate change initiatives", *Cement and Concrete Research,* vol. 38, pp. 115-127.

Duchesne, J. & Bérubé, M.A. 1994, "The effectiveness of supplementary cementing materials in supressing expansion due to ASR: Another look at the reaction mechanisms part 2: Pore solution chemistry", *Cement and Concrete Research,* vol. 24, pp. 221-230.

Edgar, R., Holcroft, C., Pudner, M. & Hardcastle, G. 2008, *UK Glass Manufacture - 2008 A Mass Balance Study,* 1st edn, GTS specialist knowledge in glass, Envirowise - sustainable practices, sustainable profits, UK.

Ehlers, E.G. 1972, *The Interpretation of Geological Phase Diagrams,* first edn, W. H. Freeman and Company, USA.

FUTURECEM Unpublished data.

Gartner, E.M., Tang, F.J. & Weiss, S.J. 1985, "Saturation factors for calciumhydroxide and calciumsulfates in fresh Portland cement pastes", *Journal of American Ceramic Society,* vol. 68, no. 667, pp. 673-J. Am. Ceram. Soc.

Greaves, G.N. 1985, "EXAFS and the structure of glass", *Journal of non-crystalline solids,* vol. 71, pp. 203-217.

Greaves, G.N. & Sen, S. 2007, "Inorganic glasses, glass-forming liquids and amorphizing solids", *Advances in Physics,* vol. 56, no. 1, pp. 1-166.

Hasholt, M.T., Hansen, H. & Thørgersen, F. 2003, *Metoder til genanvendelse af farvede glasskår til produktion af tegl og beton til vejbygning - del 1: Litteraturstudium, Miljøprojekt Nr. 819 2003,* Miljøstyrelsen, Denmark.

Hasholt, M.T., Mathiesen, D., Hansen, H. & Thørgersen, F. 2004, *Metoder til genanvendelse af farvede glasskår til produktion af tegl og beton til vejbygning - del 2: Pilotforsøg, Miljøprojekt Nr. 889 2004,* Miljøstyrelsen, Denmark.

He, C., Osbæck, B. & Makovicky, E. 1995, "Pozzolanic reactions of six principal clay minerals: Activation, reactivity assessments and technological effects", *Cement and Concrete Research,* vol. 25, no. 1691, pp. 1702.

Hill, R., Wood, D. & Thomas, M. 1999, "Trimethylsilylation analysis of the silicate structure of fluoro-alumino-silicate glasses and the structural role of fluorine", *Journal of Materials Science,* vol. 34, pp. 1767-1774.

Hjort, J., Skibsted, J. & Jakobsen, H.J. 1988, "29Si MAS NMR studies of Portland cement components and the effects of microsilica on the hydration reaction", *Cement and Concrete Research,* vol. 18, pp. 789-798.

Hong, S.Y. & Glasser, F.P. 1999, "Alkali binding in cement pastes Part I. The C-S-H phase", *Cement and Concrete Research,* vol. 29, pp. 1893-1903.

Humphreys, K. & Mahasenan, M. 2002, *Toward a sustainable cement industry. Sub-study 8: climate change,* An Independent Study Commissioned to Battelle by World Business Council for Sustainable Development.

Klemm, W.A. & Adams, L.D. 1990, "An investigation of the formation of carboaluminates" in *Carbonate Additions to Cement, ASTM STP 1064*, eds. P. Klieger & R.D. Hooton, 1st edn, American Society for Testing and Materials, Philadelphia, USA, pp. 60-72.

Krøyer, H., Lindgreen, H., Jakobsen, H.J. & Skibsted, J. 2003, "Hydration of Portland cement in the presence of clay minerals studied by 29Si and 27Al MAS NMR spectroscopy", *Advances in Cement Research,* vol. 15, pp. 103-112.

Lawrence, C.D. 2007a, "The Constitution and Specification of Portland Cements" in *Lea's Chemistry of Cement and Concrete*, ed. P.C. Hewlett, fourth edn, Elsevier, Oxford, UK, pp. 131-193.

Lawrence, C.D. 2007b, "The Production of Low-Energy Cements" in *Lea's chemistry of cement adn concrete*, ed. P.C. Hewlett, 4th edn, Elsevier, Oxford, pp. 421-470.

Lee, S.K. & Stebbins, J.F. 2006, "Disorder and the extent of polymerization in calcium silicate and aluminosilicate glasses: O-17 NMR results and quantum chemical molecular orbital calculations", *Geochimica et Cosmochimica Acta,* vol. 70, pp. 4275-4286.

Massazza, F. 2007, "Pozzolana and Pozzolanic Cements" in *Lea's chemistry of cement and concrete*, ed. P.C. Hewlett, 4th edn, Elsevier, Oxford, pp. 471-635.

Mauro, J.C., Uzun, S.S., Bras, W. & Sen, S. 2009a, "Nonmonotonic Evolution of Density Fluctuations during Glass Relaxation", *Physical Review Letters,* vol. 102, pp. 15506.

Mauro, J.C., Yue, Y.Z., Ellison, A.J., Gupta, P.K. & Allan, D.C. 2009b, "Viscosity of glass-forming liquids", *Proceedings of the national academy of sciences,* vol. 106, pp. 19780-19784.

Merzbacher, C.I., Sherriff, B.L., Hartman, J.S. & White, W.B. 1990, "A high-resolution ^{27}Al and ^{29}Si NMR study of alkaline earth aluminosilicate glasses", *Journal of Non-crystalline solids,* vol. 124, pp. 194-206.

Mishulovich, A. & Hansen, E.R. 2000, "Manufactured supplementary cementitious materials", *World Cement,* , no. June, pp. 98-103.

Mishulovich, A. & Hansen, E.R. 1996, "Manufacture of supplementary cementitious materials from cement kiln dust", *World Cement Research and Development,* , no. March, pp. 116-120.

Muller, D., Gessner, W., Behrens, H.J. & Scheler, G. 1981, "Determination of the aluminum coordination in aluminum-oxygen compounds by solid-state high-resolution ^{27}Al NMR", *Chemical Physics Letters,* vol. 70, pp. 59-62.

Mysen, B.O. 1990, "Role of Al in depolymerized, peralkaline aluminosilicate melts in the systems Li2O-AlrO3-SiO2o NarO-AlrO3-SiO2, and K2O-AI2O3-SiO2", *American Mineralogist,* vol. 75, pp. 120.

Mysen, B.O. & Richet, P. 2005, *Silicate glasses and melts - properties and structure,* 1st edn, Elsevier B. V., Amsterdam.

Nepper-Christensen, P. 1985, "Cement" in *Beton-Bogen*, eds. A.G. Herholdt, C.F.P. Justesen, P. Nepper-Christensen & A. Nielsen, second edn, Aalborg Portland, Denmark, pp. 268-298.

Nielsen, E.P., Herfort, D. & Geiker, M.R. 2005, "Phase equilibria in hydrated Portland cement", *Cement and Concrete Research,* vol. 35, pp. 109-115.

Odler, I. 2007, "Hydration, Setting and Hardening of Portland Cement" in *Lea's Chemistry of Cement and Concrete*, ed. P.C. Hewlett, 4th edn, Elsevier, Oxford, UK, pp. 241-289.

Ossi, P.M. 2003, *Disordered Materials - An Introduction,* 1st edn, Springer.

Péra, J., Husson, S. & Guilhot, B. 1999, "Influence of finelu ground limestone on cement hydration", *Cement and Concrete Research,* vol. 21, pp. 99-105.

Poulsen, S.L., Jakobsen, H.J. & Skibsted, J. 2009, "Methodologies for measuring the degree of reaction in Portland cement blends with supplementary cementitious materials by 27Al and 29Si MAS NMR spectroscopy", *Proceedings of the 17th IBAUSIL - Internationale Baustofftagung,* vol. 1, pp. 177-188.

Price, D.L. 1996, "Intermediate-range order in glasses", *Current Opinion in Solid State & Materials Science,* vol. 1, pp. 572-577.

Ramachandran, V.S. 1988, "Thermal analysis of cement components hydrated in the presence of calcium carbonate", *Thermochimica Acta,* vol. 127, pp. 385-394.

Ramachandran, V.S. & Chun-mei, Z. 1986, "Influence of CaCO3 on hydration and microstructural characteristics of tricalcium silicate", *Il Cemento,* vol. 83, pp. 129-152.

Richardson, I.G. 1999, "The nature of C-S-H in hardened cement", *Cement and Concrete Research,* vol. 129, pp. 1131-1147.

Sardeshpande, V., Gaitonde, U.N. & Banerjee, R. 2007, "Model based benchmarking for glass furnace", *Energy Conservation and Management,* vol. 48, pp. 2718-2738.

Schwarz, N., Cam, H. & Neithalath, N. 2008, "Influence of a fine glass powder on the durability characteristics of concrete and its comparison to fly ash", *Cement and Concrete Research,* vol. 30, pp. 486-496.

Shayan, A. & Xu, A. 2006, "Performance of glass powder as pozzolanic material in concrete: A field trial on concrete slabs", *Cement and Concrete Research,* vol. 36, pp. 457-468.

Shelby, J.E. 2005, *Introduction to glass science and technology,* 2nd edn, The Royal Society of Chemistry, Cambridge, UK.

Shi, C., Wu., Y., Riefler, C. & Wang, H. 2005, "Characteristics and pozzolanic reactivity of glass powder", *Cement and Concrete Research,* vol. 35, pp. 987-993.

Shi, C. & Zheng, K. 2007, "A review on the use of waste glasses in the production of cement and concrete", *Resources, Conservation and Recycling,* vol. 52, pp. 234-247.

Širok, B., Blagojević, B. & Bullen, P. 2008, *Mineral Wool,* 1st edn, Woodhead Publishing, Cambridge, UK.

Stamboulis, A., Hill, R.G. & Law, R.V. 2004, "Characterization of the structure of calcium alumino-silicate and calcium fluoro-alumino-silicate glasses by magic angle spinning nuclear magnetic resonance (MAS-NMR)", *Journal of Non-crystalline solids,* vol. 333, pp. 101-107.

Taylor, H.F.W. 1997, *Cement Chemistry,* Academic Press, New York.

Thomas, N.L. & Double, D.D. 1981, "Calcium and silicon concentrations in solution during the early hydration of Portland cement and tricalcium silicate", *Cement and Concrete Research,* vol. 11, pp. 675-687.

Tsivilis, S., Chaniotakis, E., Badogiannis, E. & Pahoulas, G. 1999, "A study on the parameters affecting the properties of Portland limestone cements", *Cement and Concrete Research,* vol. 21, pp. 197-116.

Tsivilis, S., Tsantilas, J., Kakali, G., Chaniotakis, E. & Sakellariou, A. 2003, "The permeability of Portland limestone cement concrete", *Cement and Concrete Research,* vol. 33, pp. 1465-1471.

Varshneya, A.K. 1994, *Fundamentals of inorganic glasses,* 1st edn, Academic Press, CA, USA.

Vuk, T., Tinta, V., Gabrovsek, R. & Kaucic, V. 2001, "The effect of limestone addition, clinker type and fineness on properties of Portland cement", *Cement and Concrete Research,* vol. 31, pp. 135-139.

World Business Council for Sustainable Development 2009, *Cement Technology Roadmap 2009 - Carbon emissions reductions up to 2050,* OECD/IEA, World Business Council for Sustainable Development.

Worrel, W., Price, N., Martin, N., Hendriks, C. & Meida, L.O. 2001, "Carbon dioxide emisssion from the global cement industry", *Annual Review of energy and environment,* vol. 26, pp. 303-329.

Yue, Y.Z., Christiansen, J.d. & Jensen, S.L. 2002, "Determination of the fictive temperature for a hyperquenched glass", *Chemical Physics Letters,* vol. 357, pp. 20-24.

Yue, Y.Z., von der Ohe, R. & Jensen, S.L. 2004, "Fictive temperature, cooling rate, and viscosity of glasses", *Journal of Chemical Physics,* vol. 120, pp. 8053-8059.

Zelic, J., Krstulovic, R., Tkalcec, E. & Krolo, P. 1999, "Durability of the hydrated limestone-silica fume Portland cement mortars under sulphate attack", *Cement and Concrete Research,* vol. 29, pp. 819-826.

Zeng, Q. & Stebbins, J.F. 2000, "Fluoride sites in aluminosilicate glasses: High-resolution 19F NMR results", *American Mineralogist,* vol. 85, pp. 863-867.

A CaF$_2$-CaO-Al$_2$O$_3$-SiO$_2$ system

A.1 Introduction

Addition of fluorines to silicates and aluminosilicates is known to demonstrate fluxing behavior by means of lowering the viscosity (Zeng, Stebbins 2000, Stamboulis, Hill & Law 2004, Hill, Wood & Thomas 1999). Addition of fluorine in the form of CaF$_2$ is thus a method for lowering the practical melting temperature of silicate or aluminosilicate melts without the addition of alkali carbonates giving rise to increased CO$_2$ emission from the raw materials. Furthermore it is possible to reduce the amount of carbonates required to obtain a given calcium content substituting part of the CaCO$_3$ by CaF$_2$.

In general, the reduced viscosity is believed to be caused by replacement of bridging oxygens in the glassy network with non-bridging fluorines. Several studies have reported a preference of fluorine to be linked to aluminum instead of silicon in peralkaline aluminosilicates. This is of importance as a large part of the fluorine will be lost by volatilization of SiF$_4$ species causing corrosion and environmental problems. If fluorine is bound to Al a significantly smaller fraction is lost by evaporation than if considerable amounts of SiF$_4$ were formed. In addition to replacing bridging oxygens linked to the network forming species, F-Ca(n) species with n representing the number of Ca coordinated with the fluorine is reported to be formed in calcium aluminosilicate glasses (Zeng, Stebbins 2000, Stamboulis, Hill & Law 2004, Hill, Wood & Thomas 1999).

In this work, we test the effect of using CaF$_2$ as the raw materials source of part of the CaO in the three component CaO-Al$_2$O$_3$-SiO$_2$ system. Based on the basis composition of CAS1, i.e. the eutectic composition of anorthite-wollastonite-tridymite, three glasses containing varying fluorine contents (2, 4 and 8 mol% CaF$_2$) have been synthesized. To maintain constant calcium content for all glasses, CaO was substituted with the given amount of CaF$_2$ during glass preparation. The main interest is to investigate the effect of fluorine addition on the practical melting temperature. Preliminary investigations of the fluorine structural role within the glassy network are also performed by solid-state ^{19}F MAS NMR spectroscopy. These investigations are used to explain the effect of fluorine addition on viscosity.

A.2 Experimental

Table A.1 states the designed compositions of the four glasses. The glasses were synthesized by melting the batch in a Pt$_{90}$Rh$_{10}$ crucible in a box furnace (model SF6/17 Entech, Angelholm, Sweden) in atmospheric air. The analytical chemicals SiO$_2$, Al$_2$O$_3$, CaCO$_3$ and CaF$_2$ were used for batch preparation. To get homogenized glasses, a two-step melting process was carried out. First, two glasses containing either none (CAS1) or 8 mol% CaF$_2$

(CAS-F_8) were melted for 2 hours at 1550°C and 1510°C, respectively. To minimize evaporation an Al_2O_3 lid was used to cover the crucible. The glasses are quenched on a graphite plate and subsequently crashed. To obtain the glasses in Table A.1 the crashed pieces of CAS1 and CAS-F_8 were mixed in the right proportions and remelted for 2 hours at 1510-1550°C depending on the CaF_2 content. The glasses were annealed at temperatures in the range 750-800°C depending on the CaF_2 content.

Table A.1: Designed chemical composition (mol%) of the fluorine containing CAS glasses.

	SiO_2	Al_2O_3	CaO	CaF_2
CAS1	65	9	26	0
CAS1-F_2	65	9	24	2
CAS1-F_4	65	9	22	4
CAS1-F_8	65	9	18	8

The viscosity (η) was measured using concentric cylinder viscometry in the temperature range from 1050°C to 1550°C under atmospheric conditions. This temperature range corresponds to viscosities of approx. 10^0-10^3 Pa s. The furnace was a box furnace (model HT 7, Scandiaovnen A/S, Allerød, Denmark) and the viscometer head was a Physica Rheolab MC1 (Paar Physica, Stuttgart, Germany). The viscometer was calibrated using the NBS (National Bureau of Standards) 710A standard glass.

The glass transition temperature (T_g) was determined calorimetrically using a simultaneous thermal analyzer (NETZSCH STA 449C Jupiter, Selb, Germany). T_g was found from the second upscan curve as the onset temperature of the glass transition peak using a heating rate for the second upscan of 10 K/min. This is equal to the prior cooling rate. This method for determining T_g agrees with the standard method described by (Yue, Christiansen & Jensen 2002, Yue 2008). In this work it has been utilized that at T_g the viscosity is 10^{12} Pa s.

Solid-state ^{19}F MAS NMR spectra were recorded at 282.2 MHz on a Varian UNITY-300 (B_0 = 7.05 T) spectrometer using a 5 mm home-built CP/MAS probe for 5 mm o.d. rotors and a spin-echo pulse sequence to reduce spectral artefacts related to truncation of the FID. The experiments employed a spinning speed of 10.0 Hz, an echo delay of 100 μs, a 30 s relaxation delay and a ^{19}F rt field strength of $\gamma/2\pi$ = 60 kHz. The spectra are references to neat $CFCl_3$. NMR measurements were performed on the three fluorine containing glasses as well as on a pure CaF_2 sample.

Vickers hardness (H_v) was measured by micro indentation (Duramin, Struers, Denmark). Varying loads in the range 1.96 N to 9.81 N was applied for 5 s and 15 indentations were performed for each determination of H_v.

A.3 Results and discussion

Figure A.1 shows the viscosity-temperature relation for the four melts (Table A.1). As expected the viscosity drops as the fluorine content within the melt is increased. The effect is most pronounced in the high-viscosity range. The viscosity temperature relation is described by the MYEGA equation (Mauro et al. 2009). From this description the practical melting temperature (T_{pm}) is found as the isokom temperature corresponding to a viscosity of 10 Pa s. Figure A.2 visualizes how both T_{pm} and T_g decreases as a function of the fluorine content. This confirms that the network connectivity to some extent is broken as CaF_2 is introduced to the melt. Addition of a few percentages CaF_2 is observed to significantly reduce both T_{pm} and T_g with approx. 40°C.
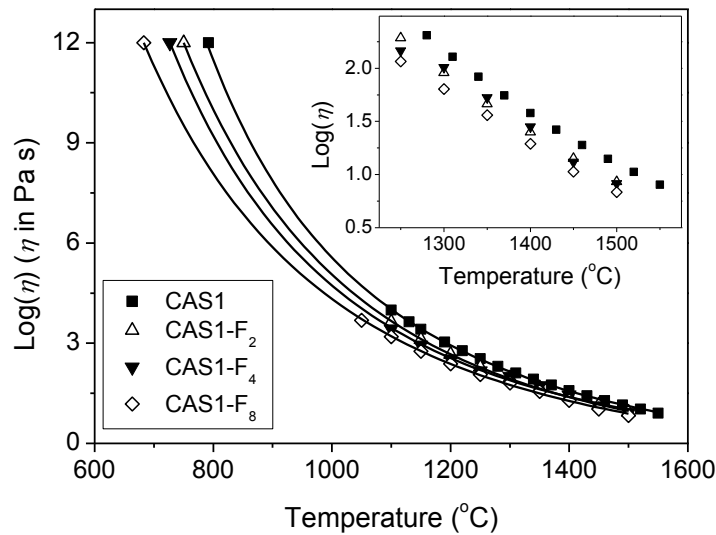

Figure A.1: Viscosity (η) given as log η as a function of temperature for the four glasses with varying fluorine content. The symbols represents the measured values and the solid lines are the fits of the MYEGA equation to the data. The inset shows a zoom on the low viscosity end of the plot.
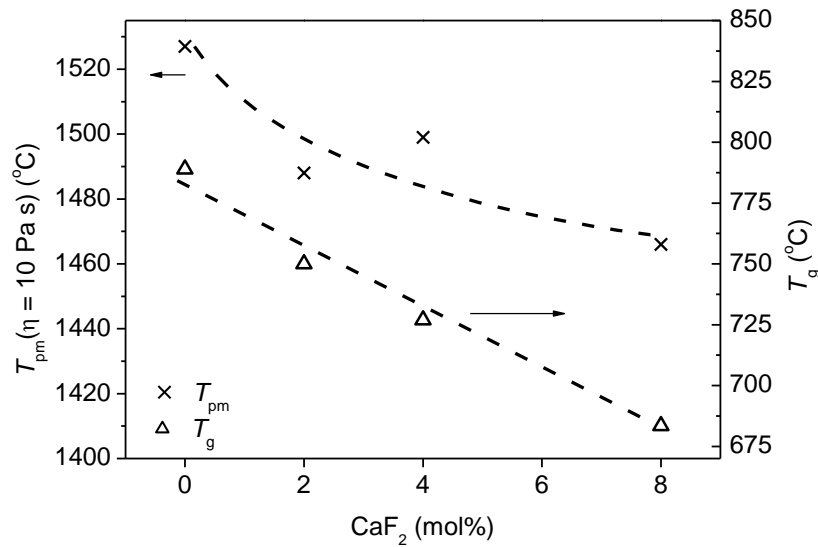
Figure A.2: Practical melting temperature (T_{pm}) and glass transition temperature (T_g) as a function of the CaF$_2$ content of the glasses. The dashed lines should be regarded as guides for the eye.
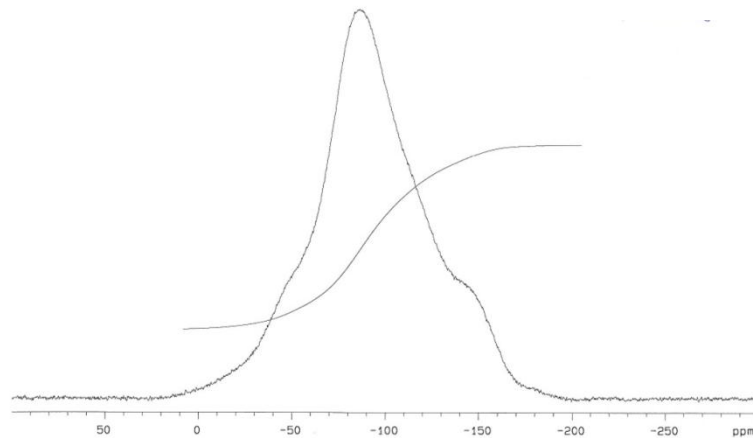

Figure A.3: ^{19}F NMR resonance of CAS-F$_4$. The s-shaped line represents the integration of the peak.

Similar ^{19}F MAS NMR resonances are obtained for all three fluorine containing CAS glasses. As expected the integral increases proportionally with increasing CaF$_2$ content. It has not been possible to determine the absolute fluorine content of the glasses as the signal intensity of the pure CaF$_2$ sample is significantly reduced due to strong homonuclear dipolar coupling between the ^{19}F nuclei. The resonance of CAS-F$_4$ is shown in Figure A.3. Broad peaks are observed at ~ -90ppm and ~ -140 ppm. A shoulder in the high frequency side of the largest resonances suggests a third peak to be present at ~ -50 ppm. Based on previous

^{19}F NMR investigations on aluminosilicates the peak at -90 ppm is identified as corresponding to F-Ca(n) units whereas the peak at -140 ppm has been proven to originate from Al-F-Ca(n) species (Zeng, Stebbins 2000, Stamboulis, Hill & Law 2004). The previous authors did not observe any peaks at approx. -50 ppm. The F-Ca(n) peak is significantly larger for all samples than the Al-F-Ca(n) peak, indicating that the majority of the fluorine is present in these sites. The ratio between the intensity of the Al-F-Ca(n) and the F-Ca(n) peaks is approximately constant (0.3-0.4) for all three samples. For the pure CaF_2 sample a sharp peak at -110 ppm is observed. This corresponds with previous observations (Zeng, Stebbins 2000, Stamboulis, Hill & Law 2004). That no peak is present at this chemical shift for the glass samples confirms that the fluorine is incorporated into the glass structure and not present as CaF_2 clusters. The incorporation of fluorine in Al-F-Ca(n) species, i.e., the replacement of bridging oxygens with fluorine, explains the reduction in characteristic temperature as shown in Figure A.2. Figure A.3 however reveals that the majority of the fluorine form complexes with Ca not breaking any bridging oxygen bonds. This might however also result in more network disruption as the ability of Ca^{2+} to crosslink two NBOs is lost.

Vickers hardness measurements show a vague tendency towards decreasing hardness as a function of fluorine content (Table A.2). A reduction in the network connectivity is expected to cause a reduced hardness. That only a vague tendency is observed might be linked to the fact that the majority of the fluorine is incorporated in F-Ca(n) units not breaking any bridging oxygen bonds.

Table A.2: Vickers hardness at different loads. The results are obtained as the average of 15 indentations.

Load (N)	0 mol% CaF_2	2 mol% CaF_2	4 mol% CaF_2	8 mol% CaF_2
1.96	6.40±0.12	6.41±0.12	6.51±0.12	5.76±0.39
2.94	6.37±0.14	6.34±0.11	6.40±0.15	6.32±0.12
4.91	6.38±0.09	6.32±0.06	6.34±0.18	6.28±0.13
9.81	6.25±0.10	6.20±0.11	6.20±0.17	6.15±0.14

A.4 Conclusions

The substitution of a few percentages CaO with CaF_2 is found to significantly reduce the practical melting temperature of the calcium aluminosilicate melt. The glass melting tank can thus be operated at a lower temperature by addition of fluorine to the melt resulting in a reduced energy consumption and thus CO_2 emission. ^{19}F MAS NMR reveals the fluorine to be incorporated in the glassy network within Al-F-Ca(n) and F-Ca(n) species.

A.5 References

Hill, R., Wood, D. & Thomas, M. 1999, "Trimethylsilylation analysis of the silicate structure of fluoro-alumino-silicate glasses and the structural role of fluorine", *Journal of Materials Science,* vol. 34, pp. 1767-1774.

Mauro, J.C., Yue, Y.Z., Ellison, A.J., Gupta, P.K. & Allan, D.C. 2009, "Viscosity of glass-forming liquids", *Proceedings of the national academy of sciences,* vol. 106, pp. 19780-19784.

Stamboulis, A., Hill, R.G. & Law, R.V. 2004, "Characterization of the structure of calcium alumino-silicate and calcium fluoro-alumino-silicate glasses by magic angle spinning nuclear magnetic resonance (MAS-NMR)", *Journal of Non-crystalline solids,* vol. 333, pp. 101-107.

Yue, Y.Z. 2008, "Characteristic temperatures of enthalpy relaxation in glass", *Journal of Non-crystalline solids,* vol. 354, pp. 1112-1118.

Yue, Y.Z., Christiansen, J.d. & Jensen, S.L. 2002, "Determination of the fictive temperature for a hyperquenched glass", *Chemical Physics Letters,* vol. 357, pp. 20-24.

Zeng, Q. & Stebbins, J.F. 2000, "Fluoride sites in aluminosilicate glasses: High-resolution 19F NMR results", *American Mineralogist,* vol. 85, pp. 863-867.

B Additional SEM-EDS results

This appendix presents additional SEM-EDS results referred to but not shown in the main thesis. All results are plotted as relative atomic percentages based on a total of ≈1200 spot analyses from three images for each sample. The experimental conditions are described in section 4.2.1.
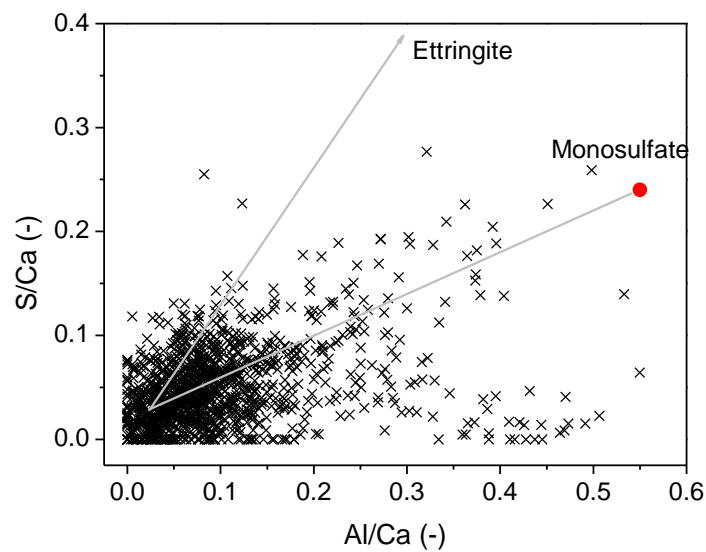

Figure B.1: S/Ca ratios as a function of Al/Ca ratios for EDS spot analyses based on spectral imaging of OPC paste hydrated 90 days.
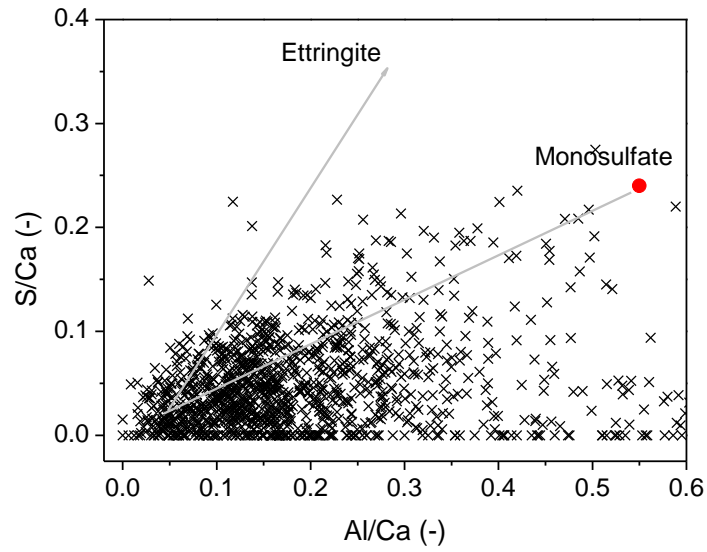
Figure B.2: S/Ca ratios as a function of Al/Ca ratios for EDS spot analyses based on spectral imaging of blended cement paste containing 30 wt% CLS$_{9N\ fine}$ hydrated 90 days.

Figure B.3: Al/Ca ratios as a function of Si/Ca ratios for EDS spot analyses based on spectral imaging of blended cement paste containing 30 wt% CLS$_{9N\ fine}$ hydrated 28 days.

Figure B.4: Al/Ca ratios as a function of Si/Ca ratios for EDS spot analyses based on spectra imaging of blended cement paste containing 30 wt% CLS$_{9N\ fine}$ hydrated 28 days. The figure shows a zoom on the region of low Al and Si contents.
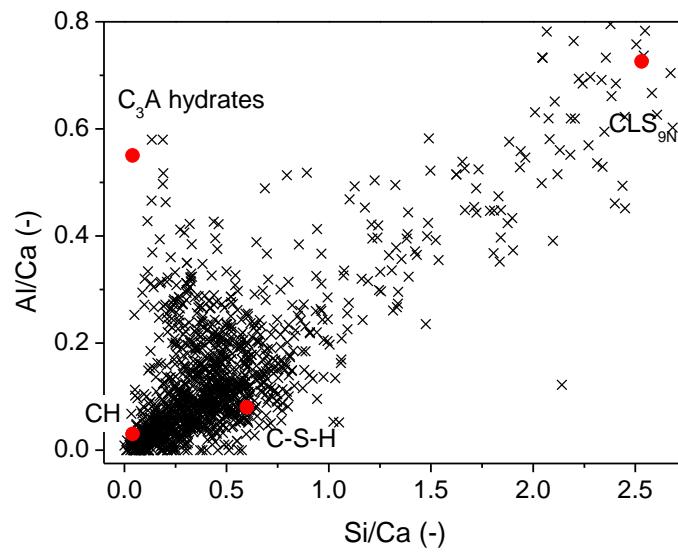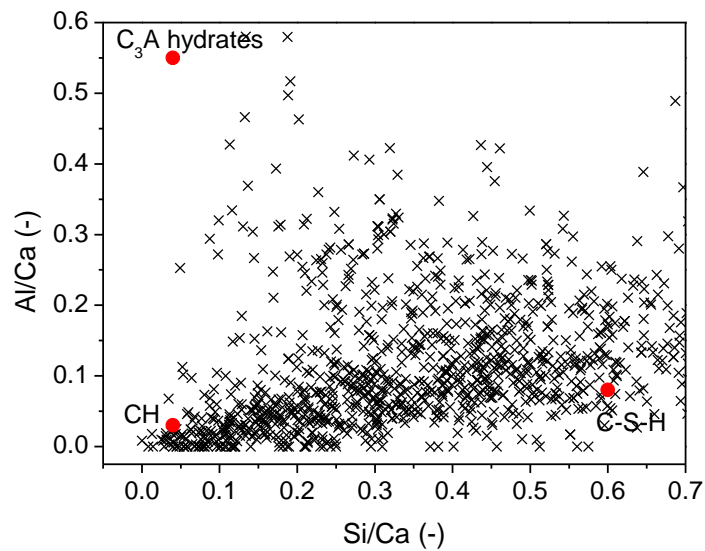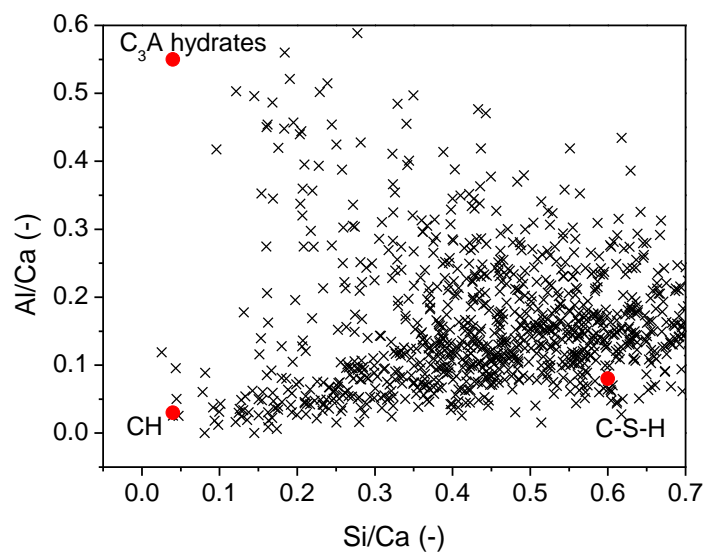

Figure B.5: Al/Ca ratios as a function of Si/Ca ratios for EDS spot analyses based on spectral imaging of blended cement paste containing 30 wt% CLS$_{9N\ fine}$ hydrated 90 days. The figure shows a zoom on the region of low Al and Si contents.
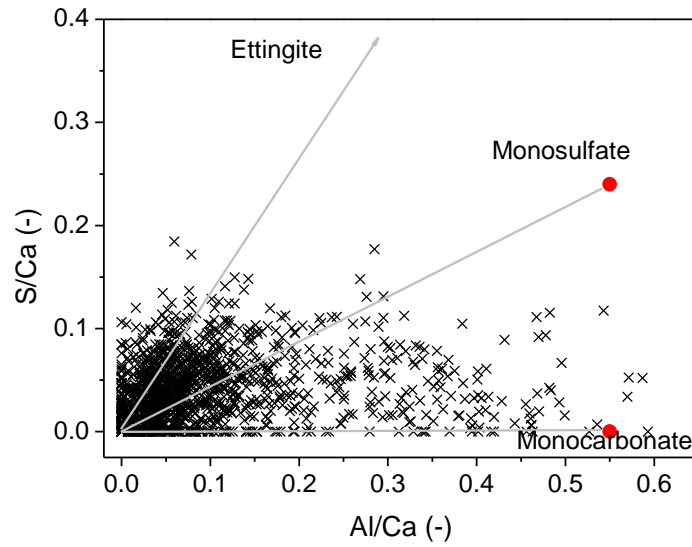
Figure B.6: S/Ca ratios as a function of Al/Ca ratios for EDS spot analyses based on spectral imaging of blended cement paste containing 30 wt% limestone hydrated 90 days.
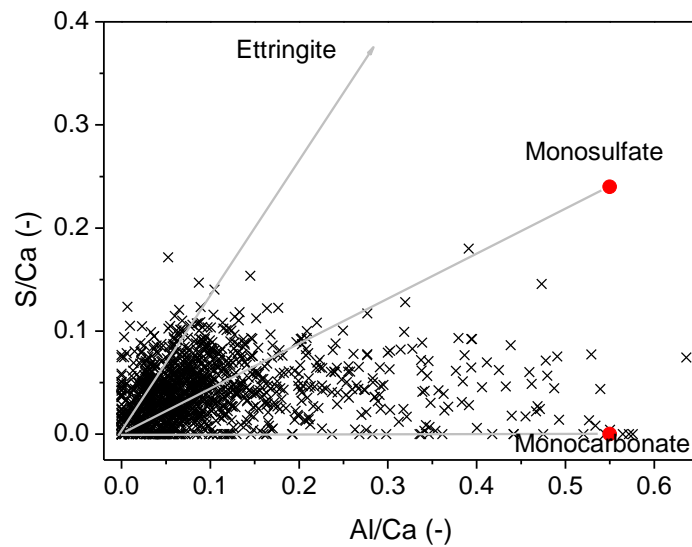

Figure B.7: S/Ca ratios as a function of Al/Ca ratios for EDS spot analyses based on spectral imaging of blended cement paste containing 20 wt% limestone and 10% CLS$_{9N\ fine}$ hydrated 90 days.

List of publications

I M. Moesgaard, Y. Z. Yue, Compositional dependence of fragility and glass forming ability of calcium aluminosilicate melts, *J. Non-cryst. Sol*, 355 (2009) 867-873.

II M. Moesgaard, D. Herfort, J. Skibsted, Y. Z. Yue, Calcium aluminosilicate glasses as supplementary cementitious materials, *Eur. J. Glass Sci. Technol. A.*, 51 (2010) 183-190..

III M. Moesgaard, R. Keding, J. Skibsted, Y. Z. Yue, Evidence of intermediate-range order heterogeneity in calcium aluminosilicate glasses, *Chem. Mater.*, 22 (2010) 4471-4483.

IV M. Moesgaard, D. Herfort, L. F. Kirkegaard, Y. Z. Yue, Optimal composition of calcium aluminosilicate glass particles used as supplementary cementitious materials, Proceedings of the 12th International Inorganic-Bonded Fiber Composites Conference (2010) 23-29.

V   M. Moesgaard, D. Herfort, M. Steenberg, L. F. Kirkegaard, Y. Z. Yue, Physical performances of blended cements containing calcium aluminosilicate glass powder and limestone, submitted to *Cem. Concr. Res.*, 41 (2011) 359-364.

VI M. Moesgaard, D. Herfort, M. Steenberg, Y. Z. Yue, Mechanical performances of blended Portland cements containing calciumaluminosilicate glass particles, 12th International Inorganic-Bonded Fiber Composites Conference (2010) 30-38.

VII M. Moesgaard, D. Herfort, S. L. Poulsen, J. Skibsted, Y. Z. Yue, Hydration of Blended Portland Cements Containing Calcium-Aluminosilicate Glass Powder and Limestone, *J. Am. Ceram. Soc.*, 95 (2012) 403-409.

Paper I

Compositional dependence of fragility and glass forming ability of calcium aluminosilicate melts

Mette Moesgaard, Yuanzheng Yue *

Section of Chemistry, Aalborg University, Sohngaardsholmsvej 57, 9000 Aalborg, Denmark

ABSTRACT

The compositional dependence of glass forming ability (GFA) of two series of calcium aluminosilicate melts is studied by measuring their viscous behavior and crystallization tendency. The first series consists of five compositions on the joining line between the eutectic point of anorthite–wollastonite–tridymite and that of anorthite–wollastonite–gehlenite. The series includes the eutectic compositions as end members. The second series consists of five compositions on a line parallel to the joining line on the alumina rich side. In the present work, GFA is described in terms of glass stability. The Hrubÿ parameter (K_H) [A. Hrubÿ, Czech. J. Phys. B 22 (1972) 1187] obtained from calorimetric data is used as a measure of glass stability. From the viscous behavior of the undercooled melts studied by viscometry the fragility (m) is derived. The results show that m is inversely proportional to K_H for the two series of melts, proposing m as an indirect measure of GFA. However, this proportionality is only valid for comparison of the glasses in the series of systematic substitutions of components. In general, the melts on the joining line between the two eutectic compositions are found to have superior GFA. Within each series GFA increases as a function of the network polymerization.

© 2009 Elsevier B.V. All rights reserved.

1. Introduction

Nowadays inorganic glasses can be made in many ways, e.g., by chemical vapor deposition, solid-state reactions and sol–gel methods [1,2]. However, the predominant way for producing inorganic glasses is still the melt-quench process. To optimize this process for producing high quality glasses and to design new glass systems for certain properties, it is essential to know the glass forming ability (GFA) of melts and to find its link to glass properties.

From a kinetic point of view, any melt can be made glassy if the quenching process is sufficiently fast to avoid crystallization. The critical cooling rate is the minimum cooling rate required to vitrify a melt, i.e., to get a glass with a crystal concentration lower than a certain standard value, e.g., 1 ppm. This rate can be considered as a direct measure of GFA [2–4]. As it is often difficult to determine the critical cooling rate it is of interest to find and use alternative methods for quantifying GFA.

The temperature (T) dependence of viscosity (η) of a melt plays a significant role in glass formation, since it determines the kinetic barrier for both nucleation and crystal growth. To describe this

dependence, scientists have proposed several semi-empirical models [5–7]. In this work, the Avramov–Milchev (AM) equation (Eq. (1)) is applied to express the temperature dependence of viscosity of the CaO–Al$_2$O$_3$–SiO$_2$ (CAS) system [5,8–10]. For the CAS system Ref. [11] has proven the AM equation to provide the best description of experimental data obtained in the entire temperature range.

The AM equation describes the kinetics of the molecular motion in undercooled melts based on the entropy concept [8]. The AM equation is often written in the following fashion:

$$\eta = \eta_\infty \exp\left[\varepsilon\left(\frac{T_r}{T}\right)^F\right]. \tag{1}$$

In Eq. (1) η_∞ is the viscosity at infinite high temperature, T_r is a reference temperature, ε is the dimensionless activation energy at the reference temperature, and F is the fragility index. It is convenient to choose as the reference state $T_r = T_g$ the glass transition temperature, at which the parameter ε is given as

$$\varepsilon = 2.3(\log\eta_{T_g} - \log\eta_\infty). \tag{2}$$

According to Ref. [11], $\log\eta_{T_g} = 12$, i.e., the viscosity at T_g is equal to 10^{12} Pa s. Thus, Eq. (1) can be expressed in the form:

$$\log \eta = \log \eta_\infty + (12 - \log \eta_\infty)\left(\frac{T_g}{T}\right)^F. \qquad (3)$$

Based on Arrhenius-type plots of the viscosity as a function of the T_g scaled inverse temperature (T_g/T) Angell has introduced the classification of strong and fragile melts [12,13]. A strong melt exhibit a near-Arrhenian behavior over the entire viscosity range whereas a fragile melt exhibits a non-Arrhenian behavior. If $F = 1$, the melt is the theoretically strongest system. SiO_2 ($F = 1.1$) and GeO_2 ($F = 1.4$) are the strongest melts known today, and possess the strongest GFA [5]. Fragility reflects the degree of order within a melt. In general a strong melt have a high degree of short range order, whereas a fragile melt often lacks directional bonds and thus does not have a well defined short range order. An inverse correlation between fragility and GFA has been found for various metallic glasses [14–16], and hence, fragility can be used as a quantitative measure of GFA for those systems. Whether this is the case for the CAS system will be demonstrated in this work.

The term glass stability refers to the ability of a glass to bypass crystallization upon heating. Generally, the glass stability can be evaluated from the correlation among the characteristic temperatures such as T_g, the onset temperature of crystallization (T_c), and the melting temperature (T_m) [17–22]. These characteristic temperatures are measured using differential scanning calorimetry (DSC). One of the glass stability indices is the Hrubÿ parameter (K_H) [17]:

$$K_H = \frac{T_c - T_g}{T_m - T_c}. \qquad (4)$$

The larger the parameter K_H, the higher is the glass stability. Since an inverse linear relation is found between K_H and the critical cooling rate, K_H may be used as a measure of GFA of a melt upon cooling [17,19–22].

The objectives of this work are to define and quantify GFA of ten CAS glass melts by finding their Hrubÿ parameter, and to explore the relationship between GFA and fragility for melts within the CAS system.
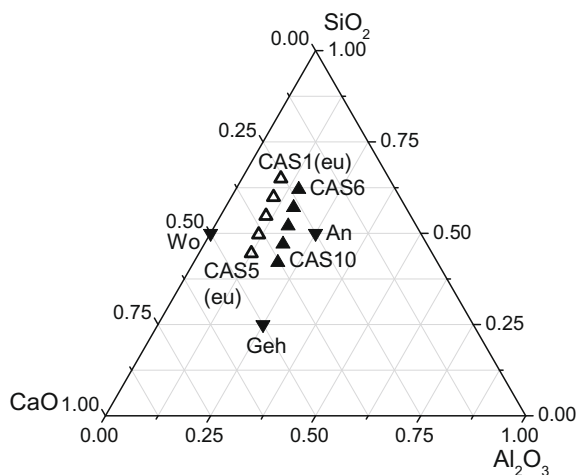

Fig. 1. The position of the 10 melts (upward triangles) within the CAS ternary phase diagram in mol%. The open triangles represent the eutectic series, i.e., CAS1 to −5, with the two end members being the eutectic compositions of An–Wo–Tri and An–Wo–Geh. The solid upward triangles represent the non-eutectic series, i.e., CAS6 to −10. The downward triangles state the position of the geological phases wollastonite, anorthite and gehlenite.

2. Experimental

Two series of five compositions each were synthesized and investigated in this work. In the ternary phase diagram of the CAS system the eutectic series (CAS1 to −5) is positioned on the joining line connecting the two eutectic compositions of anorthite–wollastonite–tridymite (An–Wo–Tri) and anorthite–wollastonite–gehlenite (An–Wo–Geh) with the two eutectic compositions being the end members. The non-eutectic series (CAS6 to −10) is positioned parallel to the eutectic series at larger alumina concentrations (Fig. 1). The chemical compositions are seen in Table 1.

The glasses were synthesized by melting the batch in a $Pt_{90}Rh_{10}$ crucible in a box furnace (model SF6/17 Entech, Ängelholm, Sweden) in atmospheric air. The batch was obtained by mixing the analytical chemicals SiO_2, Al_2O_3 and $CaCO_3$. To get a homogenized glass a two-step melting process was carried out. First, the batch was melted at 1823 K for 2 h. The melt was subsequently quenched in water to get crashed pieces. The crashed glass was remelted at 1823 K for another 2 h and cast on a graphite plate. The glasses were annealed at 1073 K and 1083 K for the eutectic and non-eutectic series, respectively. The chemical compositions were determined by means of wet chemistry (Aalborg Portland Group, Aalborg, Denmark).

In the low viscosity range (approximately 10^0–10^3 Pa s) the viscosity was measured by concentric cylinder viscometry in the temperature range from 1373 K to 1823 K under atmospheric conditions. The furnace was a box furnace (model HT 7, Scandiaovnen A/S, Allerød, Denmark) and the viscometer head was a Physica Rheolab MC1 (Paar Physica, Stuttgart, Germany). The viscometer was calibrated using the NBS (National Bureau of Standards) 710A standard glass.

In the high viscosity range (approximately 10^8–10^{13} Pa s) the viscosity was measured using micro-penetration viscometry using a vertical dilatometer (model 801L, Bähr-Termoanalyse, Hüllhorst, Germany). The precision of the equipment was tested using the DGG (Deutsche Glastechnische Gesellshaft) standard glass I and found to be within ±1% of the standard viscosities stated in [23]. The two methods for measuring the viscosity are described in more detail in [24–26].

T_g and T_c were measured using a simultaneous thermal analyzer (NETZSCH STA 449C Jupiter, Selb, Germany), from which both DSC and thermogravity signals were obtained simultaneously. For the DSC measurements monolithic glass samples of approximately 30–40 mg were grinded on side to ensure a better contact with the platinum crucible. The heat capacity curves were obtained using the evaluation method described in [27,28]. T_g is determined from the second upscan curve as the onset temperature of the glass transition peak using a heating rate for the second upscan of 10 K/min. This is equal to the prior cooling rate. This method for determining T_g agrees with the standard method described by [27,29] and is used in connection with the viscosity–temperature relation. For the stability investigations the samples were heated to 1723 K at a heating rate of 20 K/min to generate both an endothermic glass transition peak and an exothermic crystallization peak. From these investigations T_g' and T_c were found.

3. Results

Table 1 shows the compositions of the 10 CAS melts determined by means of wet chemistry. The results agree with the designed compositions. In addition, the number of non-bridging oxygen per tetrahedron (NBO/T) is given in Table 1. As ^{27}Al MAS solid-state NMR spectroscopy confirms that aluminum ions are only tetrahe-

Table 1
The compositions (in mol%) of the 10 CAS melts found by means of wet chemistry. CaO_{excess} is the amount of CaO not used for charge-balancing Al in tetrahedral coordination. NBO/T and CaO_{excess} are found using the classical approach assuming that each Ca^{2+} can charge compensate two aluminum–oxygen tetrahedra.

		SiO_2	Al_2O_3	CaO	NBO/T	CaO_{excess}
Eutectic series	CAS1	64.9	9.3	25.8	0.40	8.0
	CAS2	59.9	10.0	30.1	0.50	10.5
	CAS3	54.7	10.9	34.4	0.62	13.0
	CAS4	49.6	11.7	38.7	0.74	16.6
	CAS5	44.4	12.5	43.1	0.88	18.0
Non-eutectic series	CAS6	61.6	14.9	23.4	0.17	16.6
	CAS7	57.8	15.8	26.3	0.23	20.0
	CAS8	51.9	16.8	31.3	0.30	23.5
	CAS9	48.1	18.9	33.0	0.37	27.1
	CAS10	42.7	19.3	38.0	0.44	30.6

drally coordinated [30], the classical method described in [3,31] is applied for determining NBO/T. According to the method, each Ca^{2+} ion is coordinated to two AlO_4 tetrahedra to maintain charge balance.

Fig. 2(a) and (b) shows the viscosity data obtained from both micro-penetration and concentric cylinder viscometry. For both series of melts a decrease in viscosity in the low viscosity range
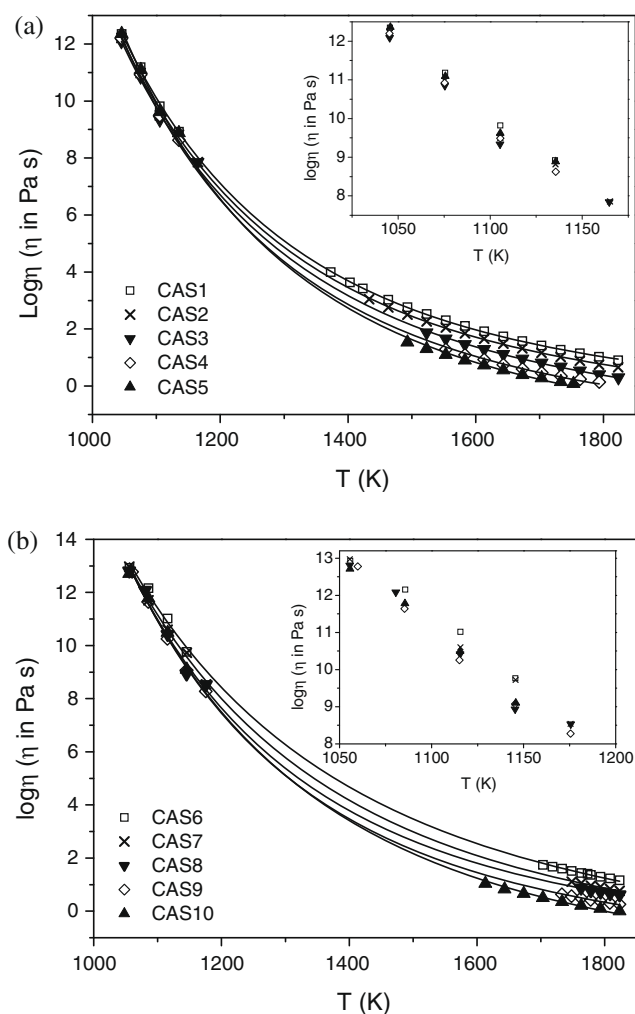
is observed as NBO/T increases, i.e., as the degree of polymerization of the three-dimensional network decreases. A similar behavior is not observed in the high viscosity range. In addition, Fig. 2(a) and (b) shows the fit of the AM equation (Eq. (3)) to the viscosity data using the Levenberg–Marquardt algorithm. From the figure it is observed that the AM equation provides a rather good description of the data, as the correlation coefficients of fit (R^2) is larger than 0.999. F can directly be obtained from the viscosity fit (see Table 2).

For silicate melts the fragility decreases as the degree of network polymerization increases. Pure SiO_2 glass has the lowest fragility parameter since its network is fully polymerized. Fig. 3 shows the dependence of F on NBO/T. For the non-eutectic series F increases with increasing NBO/T. A similar trend, however much less pronounced, is observed for the eutectic series.

To investigate the glass stability upon reheating, DSC upscans are performed at a heating rate of 20 K/min. Fig. 4(a) and (b) depict the temperature dependence of isobaric heat capacity (C_p) obtained for the glasses in the eutectic and non-eutectic series, respectively. For each glass an endothermic peak is observed around 1100 K, which is attributed to the glass transition. The T'_g values of the ten glasses are shown in Table 3. The usage of a heating rate of 20 K/min shifts T_g to larger values by approximately 10 K compared to the usage of 10 K/min (Table 3). In the temperature range 1350–1500 K, exothermic peaks are observed, which are attributed to crystallization of the glass. Both the width and the amplitude of the crystallization peaks vary, indicating that different crystal phases form in the different glasses. It is recognized that no crystallization peak occurs for the two glasses CAS1 and −2 during heating to 1723 K. This implies that both glasses have higher stability than the other glasses studied in this work. The endothermic peaks present in the high temperature range are attributed to melting of the crystalline phases.

Fig. 2. (a) Viscosity (η) given as log η as a function of temperature (T) for the melts in the eutectic series, CAS1 to −5. The symbols are the measured values and the lines are obtained by fitting the AM equation to the viscosity data. The inset shows a zoom on the data in the high viscosity range obtained by micro-penetration. (b) Viscosity (η) given as logη as a function of temperature (T) for the melts in the non-eutectic series, CAS6 to −10.

Table 2
Properties of the 10 CAS melts. F is obtained from the least square fit of the viscosity–temperature data using the AM equation. The fragility index m is obtained from Eq. (5).

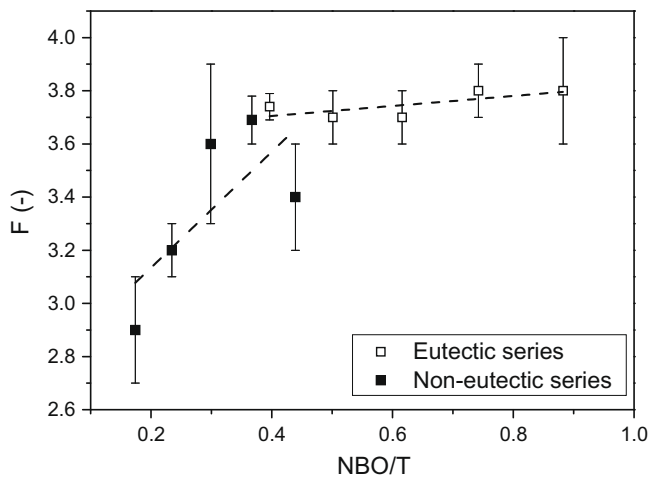|		F (–)	m (–)
Eutectic series	CAS1	3.74 ± 0.05	47.5 ± 0.6
	CAS2	3.7 ± 0.1	48 ± 1
	CAS3	3.7 ± 0.1	50 ± 1
	CAS4	3.8 ± 0.1	52 ± 1
	CAS5	3.8 ± 0.2	53 ± 3
Non-eutectic series	CAS6	2.9 ± 0.2	40 ± 3
	CAS7	3.2 ± 0.1	44 ± 1
	CAS8	3.6 ± 0.3	48 ± 4
	CAS9	3.69 ± 0.09	51 ± 1
	CAS10	3.4 ± 0.2	49 ± 3

Fig. 3. Fragility parameters (F) obtained from the fit of the AM equation to the viscosity–temperature data as a function of NBO/T for the two series of glass melts. The error bars are visualizing the standard deviation of the F values obtained from the non-linear regression. The straight dashed lines should be regarded as guides for the eyes.
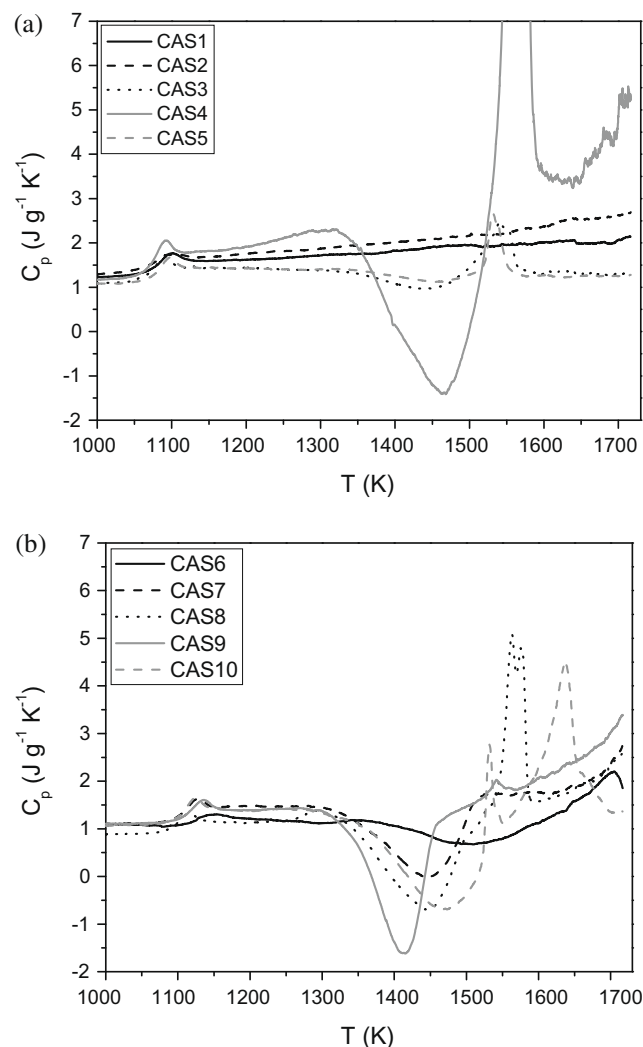
Table 3
Characteristic temperatures of the 10 CAS melts. T_g is from the DSC 2nd upscan curve using heating and cooling rates of 10 K/min. T_g' and T_c are found from the 1st DSC upscan curve using a heating rate of 20 K/min. T_m is found using the model proposed by [32] and K_H is the Hrubÿ parameter defined in Eq. (3).

		T_g (K)	T_g' (K)	T_c (K)	T_m (K)	K_H (−)
Eutectic series	CAS1	1062	1070	n/a	1443	∞
	CAS2	1054	1062	n/a	1543	∞
	CAS3	1051	1063	1344	1554	1.40
	CAS4	1054	1064	1336	1562	1.25
	CAS5	1062	1068	1341	1538	1.42
Non-eutectic series	CAS6	1094	1106	1379	1646	1.06
	CAS7	1086	1091	1330	1666	0.72
	CAS8	1072	1080	1320	1682	0.68
	CAS9	1087	1096	1332	1693	0.68
	CAS10	1078	1093	1347	1702	0.76

The melting temperature used to calculate K_H is estimated based on the model proposed in [32]. In the model it is assumed that T_m is close to the temperature of formation of the crystal phase formed at the highest temperature during cooling of a melt. This will be in equilibrium with the melt at the melting temperature. For the two eutectic compositions the liquidus temperature stated in the ternary CAS phase diagram is used for T_m as it is difficult to predict the liquidus for an eutectic composition [33]. The melting temperatures found using the model are relatively consistent with the temperature at the central position of the endothermic melting peaks observed in Fig. 4(a) and (b). The melting temperature and the Hrubÿ parameter are also stated in Table 3. As no crystallization is observed for CAS1 and −2 K_H in the table stated as equal to ∞. This applies for the specific heating rate used in these experiments, i.e., 20 K/min. It is observed that K_H in general is largest for the glasses in the eutectic series.

4. Discussion

4.1. Viscosity–temperature relation

The rheological properties of CAS melts are dependent on the structural arrangement within the melt. In contrast to silicon, tetrahedrally coordinated aluminum must be charge balanced by one positive charge. The existence of aluminum as a network former is thus dependent on the nearby presence of Ca^{2+} and the unit $Al^{3+} + 1/2Ca^{2+}$ can substitute for one Si^{4+}. If the content of Ca^{2+} is not sufficient to charge compensate the entire content of aluminum, the remaining part will be present as network modifying species. ^{27}Al MAS NMR analyses show no evidence for aluminum in octahedral coordination, reflecting that sufficient Ca^{2+} is present to charge balance all Al^{3+} ions in tetrahedral coordination. Thus steric hindrance does not prevent one Ca^{2+} from charge compensating two Al–O tetrahedra. The excess amount of CaO not used for charge compensation (CaO_{excess}) acts as network modifying oxides. The content of CaO_{excess} is given in Table 1 and is directly linked to NBO/T.

Viscosity is defined as the ratio between applied shear force and the rate of flow of a liquid. According to Ref. [34] NBO's provide the weakest connection within a CAS melt and are consequently decisive in determining dynamic properties, e.g., viscosity, as NBO's reduce the degree of polymerization of the network and create escape channels for the moving particle. This is clearly observed from Fig. 2(a) and (b) in the low viscosity range.

In the high viscosity range, i.e., at lower temperatures, the dependence of viscosity on composition is, however, much less pronounced (Fig. 2(a) and (b)). In this temperature range the divalent Ca^{2+} ions are due to the rather strong interaction with oxygen expected to attract nearby tetrahedra and to some extent thus strengthening the network structure [11,35,36].

Fig. 4. (a) Isobaric heat capacity (C_p) versus temperature (T) for the five glasses in the eutectic series (CAS1 to −5). (b) Isobaric heat capacity (C_p) versus temperature (T) for the five glasses in the non-eutectic series (CAS6 to −10). All measurements are carried out in atmospheric air using a heating rate of 20 K/min.
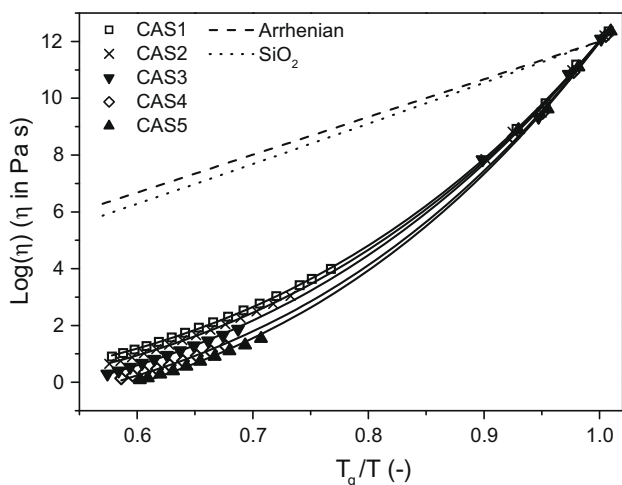
Fig. 5. Fragility plot visualizing $\log\eta$ versus the T_g scaled inverse temperature T_g/T. The plot includes the glasses in the eutectic series, pure SiO_2 glass [5] and a line representing Arrhenian behavior.

Fig. 6. The fragility or steepness index (m) obtained from the fragility plot versus NBO/T. The dashed lines should be regarded as guides for the eyes. The error bars represent the standard deviation of m derived from the standard deviation of F obtained from the non-linear regression of the AM equation.

4.2. Fragility

Despite the only minor dependence on F of NBO/T observed within the eutectic series (Fig. 3), the fragility plot in Fig. 5 indicates that the variation from Arrhenian behavior does increase when going from CAS1 to −5, i.e., with increasing values of NBO/T. In addition to the fragility parameter F derived from the AM equation Angell and co-workers [13,37] have proposed another fragility or steepness index (m) defined as the slope of the fragility plot in T_g, i.e., the $\log\eta$ versus T_g/T plot. m is thus in contrast to F directly linked to the fragility plot. Utilizing the results from the AM fits F can be converted to m as follows [38]:

$$m = (12 - \log\eta_\infty)F. \tag{5}$$

The values of m are given in Table 2 and Fig. 6 depicts m as a function of NBO/T. From the figure an obvious increase in m with NBO/T is observed for both series. This confirms that the vague increase in F observed from Fig. 3 is actually present despite the uncertainties associated with the values. The difference in the relation between fragility and NBO/T obtained as F is converted to m is believed to originate from the incorporation of the term $\log\eta_\infty$ in Eq. (5). In general $\log\eta_\infty$ is observed to decrease with increasing values of NBO/T.

The effect of CaO on the viscosity of the melt is also reflected in the fragility and [5,11,39] describe that the fragility increases linearly with increasing the CaO content independent of whether CaO is acting as a charge-balancing or network modifying compound. The results obtained in this work show agreement with the results reported in [5,39].

For each series it can thus be concluded that the glasses with the highest degree of network polymerization and the lowest content of CaO exhibit the lowest fragility.

4.3. Glass stability

A strong dependence of viscosity on temperature as observed for glasses formed from fragile melts causes a rapid increase of the diffusivity with raising temperature thus providing favorable conditions for crystallization of the glass resulting in a low stability [5]. Likewise, a glass undergoing polymorphic crystallization or even containing structural units similar to the crystalline material is expected to be less stable and crystallize at a lower temperature than a glass undergoing primary crystallization [40]. The temperature difference ($T_c - T_g$) is thus proportional to the glass stability.
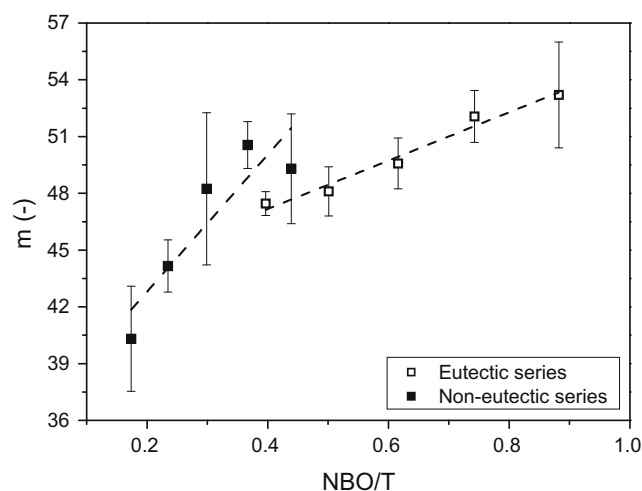
Contrary Hrubÿ [17] states that the temperature difference ($T_m - T_c$) is inversely proportional to the stability making this a good choice for the denominator of the Hrubÿ parameter.

That the stability towards crystallization upon reheating is related to the ease of crystallization avoidance during undercooling of a melt can be visualized by comparing Figs. 2 and 4. CAS1 and −2 show a large stability upon heating as no crystallization peak is observed. During the high temperature viscosity measurements it was also possible to obtain steady state measurements at significantly lower temperatures for these two compositions than for the other (Fig. 2(a) and (b)). This indicates the melts to be stable at large degrees of undercooling.

At temperatures below the temperature shown in Fig 2 stable viscosity measurements could not be obtained. The reason for this was sudden very drastic increases in viscosity due to crystallization of the melt. Especially the melts in the non-eutectic series show a reduced stability towards crystallization during undercooling. Fig. 7 illustrates how the viscosity for the melts in the non-eutectic series suddenly increases from a rather low level, indicating
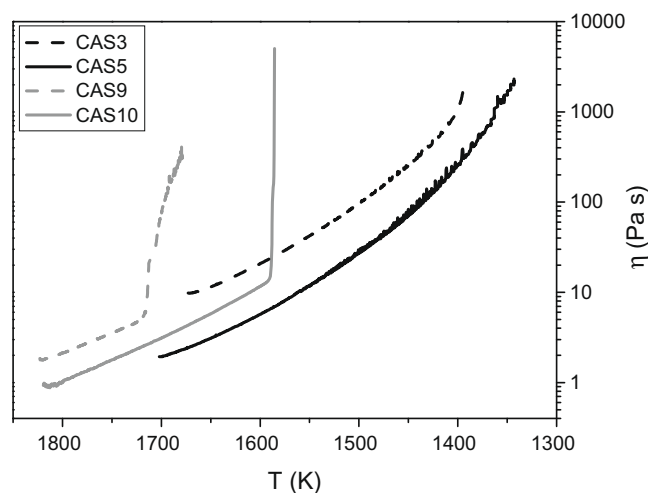

Fig. 7. Viscosity (η) change during continuous cooling of the melts in the low viscosity range. CAS3, −5 and −10 are cooled with 2 K/min and CAS9 is cooled with 1 K/min.

that crystallization occurs. The melts in the eutectic series on the other hand exhibit a continuous viscosity increase during cooling (Fig. 7).

As DSC is a dynamic method of analysis the position of the phase transitions is dependent on the heating rate employed during the measurement. Thus, the values obtained for K_H depend on the heating rate. This influence is particularly important for stable glasses not prone to crystallize, as the crystallization and melting processes might be bypassed when using a high heating rate. This behavior is observed for CAS1 and −2, and an absolute value of K_H is not obtained for these as the model does not apply to glasses for which T_c cannot be obtained. Thus, the usage of K_H as a measure of GFA shows limitations in its applicability. Ref. [17] refers to such stable glasses as being of a high-molecular polymer character and states that these can be prepared extremely easy. In general, the glasses in the eutectic series display the largest stability towards crystallization with CAS1 and −2 showing extreme stability. This indicates these to have the largest GFA as the two properties are proportional.

4.4. Relation between fragility and glass forming ability

It is generally known that SiO_2 possess a large GFA making it a commonly used glass former. In addition molten SiO_2 is the strongest liquid known [31]. This gives the first indication of an inverse correlation between fragility and GFA for silica melts. Contrary to fragile melts, strong melts have a high degree of short range order and a significant amount of directional bonds causing the strong melts to be more rigid. This rigidity is expected to create steric hindrance towards crystallization during cooling of the melt [3]. The improved short range order of strong melts might furthermore bring the melt thermodynamically closer to the crystalline ground state yielding a decreased thermodynamic driving force for crystallization [14]. Several theoretical concepts thus indicate a strong melt to have superior GFA to more fragile melts.

To test whether the inverse correlation is valid for the CAS melts examined in this work the obtained values of m and K_H are compared in Fig 8. From the figure a common trend cannot be observed for all ten compositions. Within each series, m is however observed to decrease as a function of K_H. This trend is most obvious for the non-eutectic series. For CAS1 and −2 K_H is set to 2 implying an extreme stability of these two glasses [17]. This be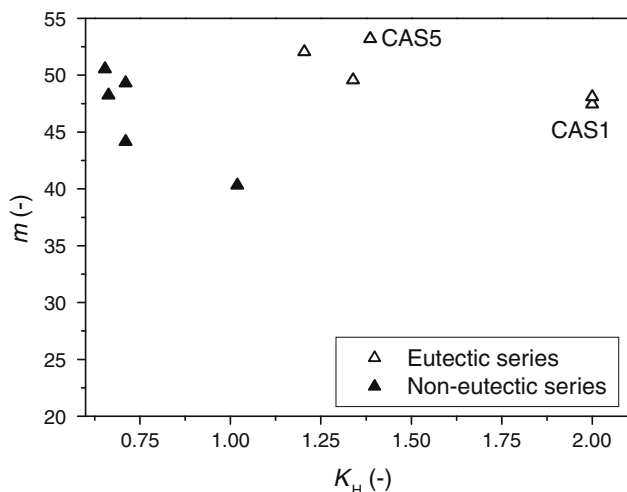havior suggests the expected inverse correlation between fragility and GFA to be valid within series of systematic variations of the chemical composition.

That the correlation is not valid for all ten compositions might also be caused by the difference in T_g observed between the two series. A linear correlation is reported in [37,41] between fragility and activation energy for viscous flow. This relation is however found to be valid only for materials with similar T_g. A similar effect of T_g on fragility could be expected in this work where the variation in T_g between the two series is more than three times as large as the variation within each series when comparing the results obtained from the AM equation. The difference in T_g might thus account for the behavior observed from Fig. 8. To finally confirm the inverse correlation between fragility and GFA for melts within the CAS system a larger amount of data would be an advantage.

The usage of the fragility as a measure of GFA suggests that within each series the melt with the highest degree of network polymerization and the lowest content of CaO possess the greatest GFA.

5. Conclusion

This work proposes alternative methods to the critical cooling rate for quantifying the GFA of inorganic oxide compositions within the CAS system. The glass stability upon reheating of the glass is quantified using the Hrubÿ parameter found by means of DSC. As generally accepted this parameter is used as a measure of GFA. By using this criterion it is found that the glasses within the eutectic series, especially CAS1 and −2 have the best GFA.

In addition, the fragility of the melts is determined by means of viscosity measurements by fitting the viscosity data with the AM equation. By relating the fragility to glass stability it is found that within each series of systematic compositional changes the fragility can be used as a measure of GFA. The fragility is found to be related to GFA by an inverse correlation. According to this criterion, the GFA is highest for the melts with the lowest content of NBO/T. Thus, CAS1, i.e., the eutectic composition of An–Wo–Tri, is the preferable choice for making a glass with high GFA.

Acknowledgements

References

[1] C.A. Angell, Science 267 (1995) 1924.
[2] A.K. Varshneya, Fundamentals of Inorganic Glasses, Academic, 1994.
[3] J.E. Shelby, Introduction to Glass Science and Technology, second Ed., The Royal Society of Chemistry, 2005.
[4] P.M. Ossi, Disordered Materials – An Introduction, Springer, 2003.
[5] I. Avramov, J. Non-Cryst. Solids 351 (2005) 3163.
[6] P. Richet, Y. Bottinga, Rev. Mineral. 32 (1995) 67.
[7] G.W. Scherer, J. Am. Ceram. Soc. 75 (1992) 1060.
[8] I. Avramov, J. Mater. Sci. Lett. 13 (1994) 1367.
[9] I. Avramov, Glass Sci. Technol. 71 C (1998) 198.
[10] I. Avramov, J. Non-Cryst. Solids 239 (1998) 6.
[11] M. Solvang, Y.Z. Yue, S.L. Jensen, D.B. Dingwell, J. Non-Cryst. Solids 336 (2004) 179.
[12] C.A. Angell, J. Non-Cryst. Solids 102 (1988) 205.
[13] C.A. Angell, J. Non-Cryst. Solids 131–133 (1991) 13.
[14] H. Tanaka, J. Non-Cryst. Solids 351 (2005) 678.
[15] R. Busch, E. Bakke, W.L. Johnson, Acta Mater. 46 (1998) 4725.
[16] Z.P. Lu, Y. Li, C.T. Liu, J. Appl. Phys. 93 (2003) 286.
[17] A. Hrubÿ, Czech. J. Phys. B 22 (1972) 1187.

Fig. 8. The fragility index (m) as a function of the Hrubÿ parameter (K_H) for the 10 compositions within the CAS system.

[18] Z.P. Lu, C.T. Liu, Phys. Rev. Lett. 91 (2003) 11505-1.
[19] A.A. Cabral Jr., C. Fredericci, E.D. Zanotto, J. Non-Cryst. Solids 219 (1997) 182.
[20] A.A. Cabral, A.A.D. Cardoso, E.D. Zanotto, J. Non-Cryst. Solids 320 (2003) 1.
[21] I. Avramov, E.D. Zanotto, M.O. Prado, J. Non-Cryst. Solids 320 (2003) 9.
[22] M.L.F. Nascimento, L.A. Souza, E.B. Ferreira, E.D. Zanotto, J. Non-Cryst. Solids 351 (2005) 3296.
[23] N. Böse, G. Klingenberg, G. Meerlender, Glass Sci. Technol. 74 (2001) 115.
[24] D.B. Dingwell, Geochim. Cosmochim. Acta 10 (1986) 1261.
[25] K.U. Hess, D.B. Dingwell, S.L. Webb, Am. Mineral. 80 (1995) 297.
[26] V.R. Brückner, G. Demharter, Glastechn. Ber. 48 (1975) 12.
[27] Y.Z. Yue, J. de C. Christiansen, S.L. Jensen, Chem. Phys. Lett. 357 (2002) 20.
[28] Y.Z. Yue, R. von der Ohe, S.L. Jensen, J. Chem. Phys. 120 (2004) 8053.
[29] Y.Z. Yue, J. Non-Cryst. Solids 354 (2008) 1112.
[30] M. Moesgaard, Y.Z. Yue, unpublished data.
[31] B.O. Mysen, P. Richet, Silicate Glasses and Melts – Properties and Structure, Elsevier, 2005.
[32] H.D. Nathan, C.K. Van Kirk, J. Petrol. 19 (1978) 66.
[33] P.C. Hewlett, Lea's Chemistry of Cement and Concrete, fourth Ed., Elsevier, 1988.
[34] J.F. Stebbins, Z. Xu, Nature 390 (1997) 60.
[35] J.F. Poggemann, G. Heide, G.H. Frischat, J. Non-Cryst. Solids 326&327 (2003) 15.
[36] H. Scholze, Glass – Nature, Structure and Properties, English Ed., Springer, 1990.
[37] R. Böhmer, K.L. Ngai, C.A. Angell, D.J. Plazez, J. Chem. Phys. 99 (1993) 4201.
[38] Y.Z. Yue, J. Non-Cryst. Solids 355 (2009) 737.
[39] M. Solvang, Y.Z. Yue, S.L. Jensen, D.B. Dingwell, J. Non-Cryst. Solids 351 (2005) 499.
[40] M. Moesgaard, H.D. Pedersen, Y.Z. Yue, E.R. Nielsen, J. Non-Cryst. Solids 353 (2007) 1101.
[41] I.M. Hodge, Macromolecules 16 (1983) 898.

Paper II

Calcium aluminosilicate glasses as supplementary cementitious materials

Mette Moesgaard,[a] *Duncan Herfort,*[b] *Jørgen Skibsted*[c] *& Yuanzheng Yue*[a1]

[a] *Section of Chemistry, Aalborg University, DK-9000 Aalborg, Denmark*
[b] *Aalborg Portland Group, DK-9000 Aalborg, Denmark*
[c] *Instrument Centre for Solid-State NMR Spectroscopy and Interdisciplinary Nanoscience Center (iNANO), Department of Chemistry, Aarhus University, DK-8000 Aarhus, Denmark*

The suitability of calcium aluminosilicate glass particles as a partial replacement for cement clinker has been investigated, both in terms of cement performance and for a potential reduction in CO_2 emission. The glasses studied were either from the pure $CaO–SiO_2–Al_2O_3$ system or contained impurities present in natural raw materials, i.e. clay, limestone and sand. In the present study the optimal composition of calcium aluminosilicate glasses suitable for this purpose is investigated by considering the consumption of limestone, melting temperature, glass forming ability, grindability and pozzolanity of the glasses. Since the investigation focuses on the low CaO region of the $CaO–SiO_2–Al_2O_3$ system, the CO_2 derived from limestone in the raw materials is significantly less than in the case of Portland cement. In addition, the glasses exhibit pozzolanic reactivity, thereby contributing to strength development and the overall cement performance.

---

1. Introduction

Today, global warming is considered by many to be the most serious threat to the natural environment and to human civilization. Most scientific studies agree that the current global warming anomaly is linked to the emission of greenhouse gases of which CO_2 is probably the most important. Considerable efforts are therefore being made, particularly in energy intensive industries such as Portland cement production, to reduce man made CO_2 emissions.[1–3] Portland cement (PC) is a hydraulic binder used in well over 90% of all concrete. The production of PC is a highly energy intensive process making it a significant contributor to the global CO_2 emission. It is estimated that the cement industry accounts for approximately 5% of the global man-made CO_2 emission.[1–3]

PC is produced by burning the raw materials consisting of 80–85 wt% limestone at high temperature, i.e. usually at ~1450°C. In fact, most of the CO_2 emission from cement production originates from the limestone with the so-called "raw materials CO_2" accounting for 500 to 550 kg CO_2 per tonne clinker. In an efficient cement kiln "fuel-derived CO_2" accounts for 250 to 300 kg CO_2 per tonne clinker. On average the production of 1 tonne of cement releases ~0·8 tonne CO_2.[1,2]

Different strategies are adopted by the PC industry to reduce the CO_2 emissions ranging from energy efficiency of cement plants and use of alternative fuels and raw materials to the development of blended cements. A blended cement (or composite cement) is an hydraulic cement consisting of PC and one or more inorganic materials that take part in the hydration reactions.[4] Thus, in blended cements, PC clinker is partially substituted by these inorganic materials, often denoted as supplementary cementitious materials (SCMs). The SCMs are either interground with the cement clinker after production of these, or the clinker and SCMs are ground separately and mixed as powders. Traditional SCMs such as fly ash, granulated blast furnace slag and micro silica, are all regarded as by-products from other industries and therefore do not contribute to the CO_2 emission associated with production of the cement. In practice, the utilization of these traditional SCMs is limited by their availability, transport cost and competition with other applications. In western Europe they are essentially fully utilized so that any further reduction in the clinker content in cement require new sources of alternative SCMs.[1,2]

A possible candidate for an alternative SCM is calcium aluminosilicate (CAS) glasses. CAS glasses are composed of the same oxides that also constitute PC and it is expected that the thermodynamic instability of glasses will provide hydraulic reactivity. When a PC is mixed with water, Ca^{2+}, Na^+ and K^+ ions are released into the pore solution resulting in a highly alkaline environment with pH values of 13·4~14·0.[4,5] Thus, when mixed with PC and water, the structural network of the glassy particles is expected to be depolymerized by OH^- ions in the high pH solution. This results in the release of Si- and Al-oxyhydroxides into the solution which then take part in the formation of hydration products similar to those formed during the hydration of PC. In this way the glass particles contribute to the strength development of the blended

Corresponding author. Email yy@bio.aau.dk

Table 1. Oxide compositions (mol%) for the Portland cement (PC) and the five glasses under investigations

	PC	$C_{26}A_9S_{65}$	$C_{43}A_{13}S_{44}$	CLS_{1N}	CLS_{5N}	CLS_{9N}
SiO_2	19·2	64·9	44·4	59·1	56·1	53·9
Al_2O_3	3·5	9·3	12·5	8·2	7·9	7·7
Fe_2O_3	1·5	-	-	3·0	2·9	2·8
CaO	70·8	25·8	43·1	22·1	21·2	21·3
MgO	1·5	-	-	4·2	3·9	3·9
K_2O	0·3	-	-	1·7	2·0	1·6
Na_2O	0·2	-	-	1·2	5·4	8·2
SO_3	2·8	-	-	<0·1	0·2	0·2
TiO_2	0·2	-	-	0·5	0·5	0·5

Table 2. Oxide composition (mol%) and loss on ignition (LOI) (wt%) for the minerals used as raw materials

	Clay	Limestone	Sand
LOI [a]	10·2	42·3	0·6
SiO_2	72·2	5·8	91·7
Al_2O_3	11·6	0·4	3·6
Fe_2O_3	4·2	0·1	0·3
CaO	1·4	92·3	1·2
MgO	5·7	1·1	0·7
K_2O	2·2	0·1	1·1
Na_2O	1·4	0·1	1·3
SO_3	0·6	<0·1	<0·1
TiO_2	0·8	<0·1	0·1
Mean particle diameter (µm) [b]	27·5	3·7	156·4

[a] LOI is determined at 950°C prior to determination of the chemical composition
[b] Determined by laser diffraction

cement. In recent years, utilization of waste glass as SCMs has been the focus of several studies, which have confirmed the hydraulic reactivity of glasses when mixed with cement.[6–9] As with other waste materials and byproducts, this is a limited resource, insufficient to meet the growing demand for SCMs.

In the present study we attempt to engineer and characterize CAS glass particles with a composition optimized specifically for their use as SCMs in PCs. To determine the optimal composition of the glass several factors must be balanced by considering the consumption of limestone, melting temperature, glass forming ability, grindability and pozzolanity. A pozzolan is defined as a silicate or aluminosilicate containing material that on its own does not possesses hydraulic reactivity but in the presence of calcium hydroxide and water at ordinary temperatures forms strength giving hydrate phases.[4]

2. Experimental

The glasses were synthesized by melting the batches of raw materials in a $Pt_{90}Rh_{10}$ crucible in atmospheric air (furnace: model SF6/17 Entech, Ängelholm, Sweden). The compositions of the five glasses produced are listed in Table 1. The model system glasses were obtained by mixing analytical chemicals of SiO_2, Al_2O_3 and $CaCO_3$, followed by a two-step melting process. First, the batches were melted at 1550°C for 2 h and subsequently quenched in water resulting in crushed fragments. Secondly, the crushed glass was remelted at 1550°C for another 2 h and cast on a graphite plate. Finally, the glasses were annealed at 800°C, i.e. approximately the glass transition temperature (T_g), for 10 min, and cooled slowly by switching off the furnace.

The raw material of clay (bentonite) was from Dantonit A/S, Odense, Denmark while the limestone and sand were provided by the Technical Centre at Aalborg Portland A/S, Aalborg, Denmark. The raw materials were used for preparation of the glasses and have the compositions and size characteristics given in Table 2. The loss on ignition (LOI) from the clay originates from water and some organic material, whereas CO_2 accounts for the LOI from limestone. Na_2CO_3 was added to the batches for glasses CLS_{5N} and CLS_{9N} to increase the Na_2O content. Prior to melt-

ing in the $Pt_{90}Rh_{10}$ crucible, the clay was heat treated at 900°C for 3 h (heating rate of 10°C/min) to remove the organic material. The batch was homogenized using a mortar and then melted at 1450°C for 3 h. The melt was cast on a graphite plate and annealed at 700 or 650°C for 10 min, and cooled inside the furnace by switching it off. The chemical compositions were determined by standard wet chemical analysis at the Technical Centre at Aalborg Portland A/S.

In the low viscosity range (approx. 10^0–10^3 Pa s), the viscosity (η) was measured using concentric cylinder viscometry. The furnace was a box furnace (model HT 7, Scandiaovnen A/S, Allerød, Denmark) and the viscometer head was a Physica Rheolab MC1 (Paar Physica, Stuttgart, Germany). In the high viscosity range (approx. 10^8–10^{13} Pa s) the viscosity was measured by means of micropenetration viscometry using a vertical dilatometer (model 801L, Bähr-Termoanalyse, Hüllhorst, Germany). The glass transition temperature was determined as the temperature corresponding to a viscosity of 10^{12} Pa s.[10]

Vickers hardness (H_v) was measured by micro indentation (Duramin, Struers, Denmark). A load of 0·96 N was applied for 5 s and 15 indentations were performed for each determination of H_v. The tendency of the glass to fracture was determined applying a load of 1·96 N for 5 s. At this load some indentations caused pure deformation whereas others caused both deformation and fracture to occur. Indentations were made until 15 indentations without crack formation were obtained and the tendency to fracture was found as the percentage of indentations causing fracture.

For tests of pozzolanity, the glass was ground to pass a 75 µm sieve. 1·00 g glass powder (~$1·5×10^{-2}$ mol) and 1·00 g $Ca(OH)_2$ ($1·3×10^{-2}$ mol) were mixed with 100 ml freshly boiled water and stored in a closed container for 7 days at 40°C. During storage the mixture was shaken with a horizontal rotary motion. The mixtures were filtered and the filtrates were stored for further analyses. For the solid state NMR investigations the collected solid was dried over silica gel in a desiccator. For determination of
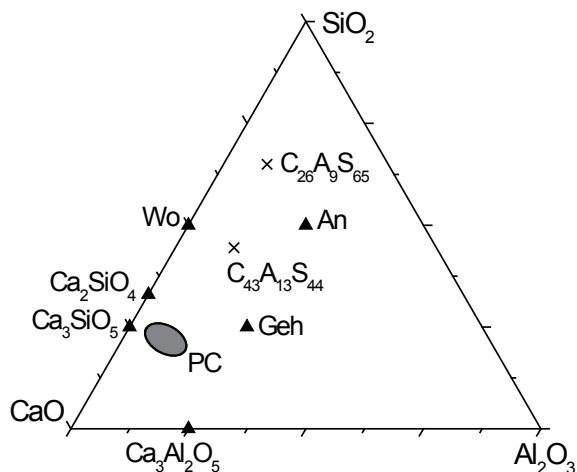
Figure 1. Molar ternary CaO–Al$_2$O$_3$–SiO$_2$ phase diagram. The compositional range of ordinary Portland cement (PC) is marked by the shaded area. Crosses mark the two eutectic compositions of anorthite (CaAl$_2$Si$_2$O$_8$)–wollastonite (CaSiO$_3$)–tridymite (SiO$_2$) (An-Wo-Tri) and anorthite–wollastonite–gehlenite (Ca$_2$Al$_2$SiO$_7$) (An-Wo-Geh). The binary phases important in PC, i.e. Ca$_3$SiO$_5$, Ca$_2$SiO$_4$ and Ca$_3$Al$_2$O$_5$ are marked by triangles

the mass of un-reacted glass the collected solids were washed with a weak solution of acetic acid to dissolve remaining Ca(OH)$_2$ and any hydration products formed. Finally, the washed glasses were dried over silica gel in a desiccator.

Solid state ^{29}Si MAS (magic angle spinning) NMR (nuclear magnetic resonance) spectra were recorded at 39·8 MHz on a Varian UNITY-200 (B_0=4·7 T) spectrometer, using a home built CP/MAS probe for 5 mm outer diameter rotors. The experiments employed a 45° excitation pulse for a radio frequency field strength of $\gamma B_1/2\pi\approx50$ kHz, a spinning speed of 10·0 kHz, a repetition delay of 30 s (CLS$_{9N}$) or 120 s (C$_{26}$A$_9$S$_{65}$), and 2000–7500 scans. The ^{27}Al MAS NMR spectra were recorded at 104·2 MHz on a Varian INOVA-400 (B_0=9·39 T) spectrometer using a home-built CP/MAS probe for 5 mm rotors. The spectra employed a spinning speed of 12·0 kHz, a 0·5 μs excitation pulse for $\gamma B_1/2\pi\approx60$ kHz, a 2 s relaxation delay, 1H decoupling during acquisition ($\gamma B_2/2\pi\approx55$ kHz) and typically 2000–5000 scans. ^{27}Al and ^{29}Si isotropic chemical shifts are given relative to a 1·0 M aqueous solution of AlCl$_3$.6H$_2$O and neat tetramethyl silane (TMS), respectively.

3. Results and discussion

To ensure the possibility of mass production, the glass particles must be made from low cost and locally available raw materials. Therefore, clay, limestone and sand, i.e. conventional raw materials for cement production, are chosen for the glass preparation. These materials are chosen since they are both locally available, i.e. in Denmark, and are composed of the

components required for production of CAS glasses. To reduce the "raw materials CO$_2$" the content of carbonates must be significantly lower than the carbonate content in the raw material mix for PC. The "fuel-derived CO$_2$" on the other hand can be reduced by choosing compositions with relatively low melting temperatures. In addition, it is essential for a glass melt to exhibit a good glass forming ability (GFA) which is often quantified by the critical cooling rate, i.e. the minimum cooling rate required to vitrify a melt.[11–13] A low critical cooling rate corresponds to a high GFA and thus melts with good GFA can be produced without forced cooling. During cement hydration, the reactions take place at the surface of the cement particles and thus the particle size needs to be fine enough to achieve an acceptable rate of hydration. To increase the ability of the glass to take part in the hydration reactions it must be crushed and ground to obtain a large surface area. Thus, the so-called "grindability" of the glass should also be considered since a significant amount of energy is also consumed during the crushing and grinding.

3. 1 Model system

The initial investigations were performed on the ternary CaO–Al$_2$O$_3$–SiO$_2$ model system. This is a representative system for cementitious materials, accounting for 90% of the oxides present in PC. Therefore, the model system can be used to investigate effects of variations in the contents of the three major components on glass properties.

The eutectic compositions of anorthite–wollastonite–tridymite (26CaO–9Al$_2$O$_3$–65SiO$_2$, mol%) (C$_{26}$A$_9$S$_{65}$) and anorthite–wollastonite–gehlenite (43CaO–13Al$_2$O$_3$–44SiO$_2$, mol%) (C$_{43}$A$_{13}$S$_{44}$) are chosen as the starting compositions. Figure 1 illustrates the compositional locations of the two glasses and PC in the ternary CaO–Al$_2$O$_3$–SiO$_2$ phase diagram. These glass compositions are chosen since the CaO contents are significantly less than in PC and because both compositions are eutectic compositions corresponding to minimum temperatures on the liquidus surface. This implies the possibility for the melts to be produced at relatively low temperatures compared to other compositions in the same compositional range. Furthermore, it is expected that C$_{26}$A$_9$S$_{65}$ and C$_{43}$A$_{13}$S$_{44}$ can be produced under normal cooling conditions without forced cooling.[14] This means that the glasses are expected to exhibit good GFA.

In PC, the "raw materials CO$_2$" originates from limestone consisting primarily of CaCO$_3$ but also small amounts of MgCO$_3$. The composition of PC slightly varies from one place to another, depending on the local raw material deposits. Based on the PC composition given in Table 1, the production of one tonne cement results in 516 kg of raw materials derived CO$_2$. In contrast, 180 kg and 300 kg CO$_2$ are
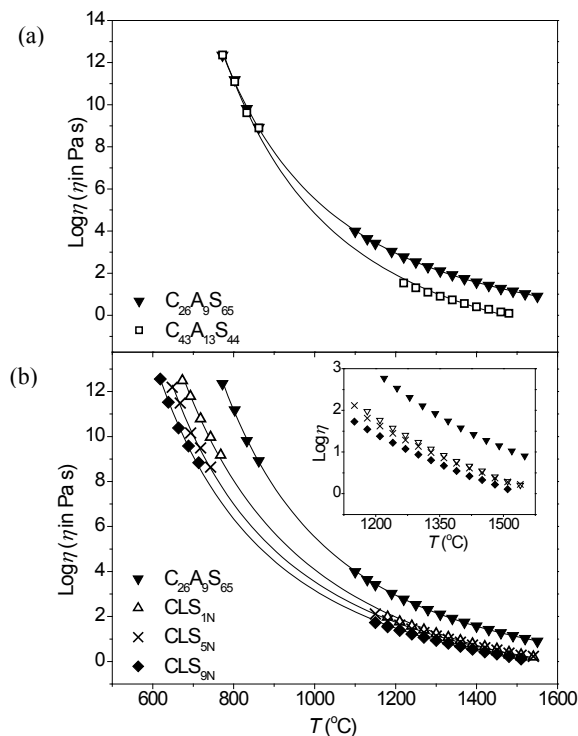
Figure 2. Viscosity (η), shown as log η, as a function of temperature (T). (a) Shows the results for the two model system glasses, $C_{26}A_9S_{65}$ and $C_{43}A_{12}S_{44}$, and (b) the glasses produced from natural raw materials. The inset shows an expansion of the high temperature range. The solid lines represent the fit of the MYEGA equation (Equation (1)) to the viscosity data

released from the raw materials needed to produce one tonne of $C_{26}A_9S_{65}$ and $C_{43}A_{13}S_{44}$, respectively.

The temperature required for melting, i.e. the practical melting temperature, affects the amount of "fuel-derived CO_2". For example, a reduction in the operating temperature of the melting furnace will lower the major energy losses caused by the flue gas, the furnace walls and openings. However, most often, part of the heat loss due to the flue gas is recovered, e.g. by heating of water used for household heating. For a modern continuous melting tank made of high temperature refractory, the furnace wall and opening losses account for approximately 15% of the energy input. This kind of heat loss can be significantly lowered by reduction of the practical melting temperature.[15–17] In this work, the practical melting temperature (T_{pm}) is defined as the isokom temperature corresponding to a viscosity of 10 Pa s. Figure 2(a) depicts the viscosity data obtained from both micropenetration and concentric cylinder viscometric measurements for the two model glasses. T_{pm} is determined by interpolation from these data, resulting in the values $T_{pm}(C_{26}A_9S_{65})$=1527°C and $T_{pm}(C_{43}A_{13}S_{44})$=1306°C. Thus, the increased content of modifying Ca^{2+} ions in $C_{43}A_{13}S_{44}$ has a significant impact on the melting temperature. Figure 2(a) also shows this impact in the low viscosity range. In contrast, there is only slight difference in viscosity between $C_{26}A_9S_{65}$ and $C_{43}A_{13}S_{44}$ in the high viscosity range.

The two model compositions, $C_{26}A_9S_{65}$ and $C_{43}A_{13}S_{44}$, both exhibit good GFA and the glasses are easily obtained by casting the melt on a graphite plate without any further quenching. Since it is difficult to determine the critical cooling rate, the GFA is often quantified by alternative means. The fragility of a melt is a measure of the degree of deviation from Arrhenian behavior of the viscosity–temperature relation.[18] According to our recent study,[19] the fragility can be used as an indirect measure of GFA for glasses in the CAS system. In this work, the fragility index *m* is found by modelling the viscosity data using the MYEGA Equation (1) where η_∞ is the viscosity at the high temperature limit[20]

$$\log \eta = \log \eta_\infty$$
$$+ (12 - \log \eta_\infty) \frac{T_g}{T} \exp\left[\left(\frac{m}{12 - \log \eta_\infty} - 1\right)\left(\frac{T_g}{T} - 1\right)\right]$$

(1)

The solid line in Figure 2 shows the fit of the MYEGA equation to the viscosity data. From the modelling it is found that $m(C_{26}A_9S_{65})$=49·6±0·4 and $m(C_{43}A_{13}S_{44})$=55·0±2·4. A comparison of the two fragility parameters indicates that $C_{26}A_9S_{65}$ should have a superior GFA.

In relation to the "raw materials CO_2 emission", $C_{26}A_9S_{65}$ has a considerable lower CaO content than $C_{43}A_{13}S_{44}$, whereas $C_{43}A_{13}S_{44}$ can be produced at a lower temperature and therefore results in the lower "fuel-derived CO_2 emission". The presence of minor components, especially alkali oxides, in the natural raw materials (Table 2) may lead to a pronounced reduction of the melting temperature. Thus, the low CaO content of $C_{26}A_9S_{65}$ is considered the most important factor for lowering the CO_2 emission, and hence, this composition is chosen to be the major constituent of the systems from natural raw materials for the study described below.

3.2 Glass system based on natural raw materials

The composition of $C_{26}A_9S_{65}$ is targeted using the natural raw materials (Table 2) by maintaining the ratios between the main oxides, i.e. CaO, Al_2O_3 and SiO_2. As the relative Al_2O_3 content in the clay is close to that in $C_{26}A_9S_{65}$, it is possible to obtain the target composition only by mixing the raw materials in the following proportions by weight: 63% clay, 31% limestone and 6% sand. This gives the glass composition shown in Table 1 for CLS_{1N} (the subscript indicates a Na_2O content of 1 mol%). From the compositions in Table 1, it is apparent that the natural minerals introduce ~10% minor components. In addition to alkali oxides, considerable amounts of MgO and

Fe_2O_3 are also introduced into the final glass composition where the presence of iron oxide gives the glass a dark green colour. CLS_{5N} and CLS_{9N}, containing 5 and 9 mol% Na_2O, respectively, are produced to investigate the effect of additional alkali oxide on the properties of the glass. In industrial scale production, additional alkali oxide can for example be introduced by recycling dust collected from the cement kiln or from albite or granite (syenite and alkali granite) high in alkali oxide, or directly as Na_2SO_4.

For the CLS glasses the limestone content is comparable to that of $C_{26}A_9S_{65}$. The production of 1 tonne CLS_{1N} glass results in ~175 kg CO_2 released from the limestone. For CLS_{5N} and CLS_{9N} the raw materials CO_2 emission is ~170 kg per tonne glass. This constitutes only approx. 30% of the CO_2 released from calcination during the PC production. The carbonate content affects both the "raw materials CO_2 emission" and the "fuel-derived CO_2 emission". As the carbonate content is reduced, the energy required to perform the calcination is also reduced. The enthalpy of calcination for the production of PC clinker is ~2100 kJ/kg.[4] From differential scanning calorimetric measurements on raw material batches of $C_{26}A_9S_{65}$ and CLS_{9N}, the enthalpy of calcination is found to be ~650 kJ/kg and ~325 kJ/kg, respectively. Thus, the "fuel-derived CO_2 emission" due to the calcination processes is significantly less for CAS glass production than for the PC production.

In Figure 2(b) it is shown how the viscosity–temperature relationship is affected by shifting from pure chemicals to natural raw materials. The viscosity drops dramatically over the entire temperature range from $C_{26}A_9S_{65}$ to CLS_{1N}. For instance, $\log\eta$ at 1000°C is reduced from $\log\eta=5\cdot5$ for $C_{26}A_9S_{65}$ to $\log\eta=4\cdot1$ for CLS_{1N}, i.e. more than an order of magnitude Additional Na_2O leads to a much larger decrease in viscosity in the low temperature range than in the high temperature range. However, the inset in Figure 2(b) shows that the viscosity does decrease as a function of the Na_2O content in this range despite a small extent. This decrease is reflected in the values of practical melting temperature listed in Table 3. As expected, the use of natural raw materials causes significant reductions in T_{pm} as compared to the model system glasses. $T_{pm}(CLS_{1N})$ and $T_{pm}(CLS_{9N})$ are ~12% and ~16% lower than $T_{pm}(C_{26}A_9S_{65})$, respectively, indicating that all glasses in the CLS series can be produced at reasonable temperatures.

As mentioned above, one of the major energy losses during glass production results from heat transfer through the furnace walls. This heat flux is proportional both to the difference between the inside temperature and the outside temperature of the furnace and to the thermal conductivity of the refractory (α). The proportional increase in α with temperature results in a similar increase in the heat loss. Based on the data of a common

Table 3. Characteristic temperatures and values of fragility (m) for the five compositions under investigation

	T_{pm} (°C) [a]	T_g (°C) [b]	m (-) [b]
$C_{26}A_9S_{65}$	1527	781·6±0·6	49·6±0·4
$C_{43}A_{13}S_{44}$	1306	782·9±2·0	55·0±2·4
CLS_{1N}	1346	688·6±1·4	43·2±1·2
CLS_{5N}	1329	654·3±0·9	44·0±0·8
CLS_{9N}	1285	629·7±0·8	43·7±0·7

[a] The practical melting temperature (T_{pm}) is given as the isokom temperature at $\eta=10$ Pa s.
[b] T_g and m are obtained from the fit of the viscosity–temperature data using the MYEGA equation.[20]

refractory material for high temperature furnaces (FIBROTHAL® F-14),[21] the heat loss is found to be reduced by about 35% by the use of natural raw materials (CLS_{1N}) for glass production instead of pure chemicals. Additional alkali oxide in CLS_{9N} further reduces the loss by ~5%. Thus, the energy loss can be reduced when the glasses are produced at significantly lower temperatures than used for the PC production. It should be noted that during glass production the energy for melting the raw materials must also be considered (~500 kJ/kg)[22] when evaluating the CO_2 emission. That said, the energy requirement for calcination is considerably lower for the glasses than for PC.

The MYEGA equation (Equation (1)) is used to fit the viscosity–temperature relation for the CLS glasses as shown by solid lines in Figure 2(b). From the fitting, the T_g and m values are obtained and listed in Table 3. The fragility index (m) is observed to decrease as minor components are incorporated into the glass system. This implies that the GFA is enhanced by using natural raw materials compared to the pure chemicals. No detectable effect on m and hence on GFA is seen when further additional Na_2O (e.g. from 1 to 5 or 9 mol%) is introduced.

In this work the grindability of the glasses is evaluated indirectly by measuring the hardness and the tendency of the glass to fracture at a given load. The Vickers hardness (H_v) data are measured at 0·96 N and shown in Table 4. When the natural raw materials are used, excess alkali oxide not used to charge balance Al^{3+} in tetrahedral coordination is introduced. The excess alkali oxide is expected to lower the hardness by the introduction of nonbridging oxygen. Despite the introduction of alkali oxides the hardness is observed to increase from $C_{26}A_9S_{65}$ to CLS_{1N}. The content of alkaline earth oxides is approximately constant for all glasses under investigation. The introduction of a third network former, i.e. Fe^{3+}

Table 4. Vickers hardness (H_v) measured at 0·96 N and fracture tendency found as the percentages of indentations causing fracture to occur at 1·96 N

	H_v (GPa)	Fracture tendency (%)
$C_{26}A_9S_{65}$	6·5±0·2	17
CLS_{1N}	7·1±0·2	35
CLS_{5N}	6·6±0·2	56
CLS_{9N}	6·6±0·2	69

ions, may explain the observed increase in H_v. As expected, the introduction of additional alkali oxide in CLS_{5N} leads to a reduced H_v compared to CLS_{1N}.

As the load exceeds the fracture strength, indentations cause fractures in the glasses. At a load of 1·96 N, the fracture tendency is found as the percentages of indentations causing fracture (Table 4). The fracture tendency is observed to increase from the ternary model system to the glasses produced from natural raw materials. A further increase in the tendency to fracture is observed as additional alkali oxide is introduced. Hence, qualitatively the brittleness of the glasses increases with the Na_2O content. Combining the results for H_v and fracture tendency, CLS_{9N} is found to have the best grindability. Thus, particle formation is expected to require the smallest energy consumption for this composition. Grinding of CLS_{1N} and CLS_{9N} in a porcelain mill confirms that particles of cement fineness are more easily obtained for CLS_{9N} than for CLS_{1N}. The duration of the grinding process can for CLS_{9N} be reduced by 6% compared to CLS_{1N}.

The shift from the model system to the glasses based on natural raw materials is observed to lower the practical melting temperature and improve the glass forming ability. The introduction of additional Na_2O causes a further reduction in the practical melting temperature. These changes will contribute to a reduction in the "fuel-derived CO_2". The evaluation of the grindability of the glasses shows that the use of natural raw materials results in an increase in both H_v and fracture tendency (Table 4). The introduction of extra alkali oxide is found to reduce the hardness and to increase the fracture tendency increases. Overall, the findings above indicate that the energy consumption is reduced in the production of glasses based on natural raw materials as compared to model system glasses, and that a further reduction may be achieved by the introduction of additional alkali oxide into the glass.

3.3 Pozzolanity

Partial substitution of PC with a SCM often reduces the compressive strength compared to pure cement. To minimize the reduction in strength, the SCM must be capable of contributing to the strength by pozzolanic reactions taking place during cement hydration. The pozzolanic reactivity of $C_{26}A_9S_{65}$ and the CLS glasses is tested as the reactivity of the glass powder in a saturated $Ca(OH)_2$ solution. The alkaline conditions of the saturated $Ca(OH)_2$ solution resembles the pore solution in cement pastes and mortars and the pozzolanic reactivity is quantified as the fraction of glass that has reacted with $Ca(OH)_2$ after a certain period of time.

The main hydration product resulting from PC hydration is the so-called calcium silicate hydrate (C-S-H) phase. The C-S-H phase is an amorphous or nearly amorphous calcium silicate hydrate with the general formula $xCaO–SiO_2–yH_2O$ where both x and y may vary over a wide range. The C-S-H phase is formed as the isolated SiO_4 tetrahedra (Q^0 units), of the calcium silicates in the cement clinker (Ca_3SiO_5 and Ca_2SiO_4, Figure 1) react with water and polymerize into dimers and chains of SiO_4 tetrahedra, i.e. Q^1 and Q^2 units.[4,5,23] The Q^n nomenclature refers to an SiO_4 or AlO_4 unit with n bridging oxygens and $(4–n)$ nonbridging oxygens.

During hydration the aluminate ions mainly form crystalline calcium aluminate hydrates, however, a small amount is also incorporated in the silicate chains of the C-S-H phase.[4,5,24,25] The hydration of the aluminate phases in anhydrous cement can be followed by the gradual conversion of tetrahedrally coordinated AlO_4 into octahedrally coordinated AlO_6 sites present in the calcium aluminate hydrates.[4,5,26] To investigate qualitatively if similar hydration products are formed by the reaction of the calcium aluminosilicate glasses with $Ca(OH)_2$ and water, ^{29}Si and ^{27}Al solid state MAS NMR spectra have been acquired for $C_{26}A_9S_{65}$ and CLS_{9N} before and after the reactivity test.

In ^{29}Si MAS NMR the chemical shift reflects the degree of polymerization (Q^n, n=0–4) of the SiO_4 tetrahedra with values in the range from −60 to −120 ppm for silicates and aluminosilicates relative to tetramethyl silane (TMS). An increasing degree of polymerization (n) results in a shift of approx. 8–10 ppm to lower frequency.[24–29] The ^{29}Si MAS NMR spectra for $C_{26}A_9S_{65}$ and CLS_{9N} before and after the pozzolanity test (Figure 3) exhibit broad resonances in the range from −75 ppm to −115 ppm, reflecting the amorphous nature of the glasses including different Q^n units. The resonances for the CLS_{9N} glass are somewhat broader than those observed for $C_{26}A_9S_{65}$, which arise from the paramagnetic impurities (Fe^{3+} ions) in the glass made from natural raw materials. Subtraction of the spectra before and after the reactivity test, using an appropriate scaling factor, reveals sub-spectra which only include resonances from the hydration products (Figure 3(c) and (f)). For both glasses these difference spectra show resonances in the range −75 to −90 ppm, where the distinct peaks at −80·5 ppm and −84·5 ppm may be assigned to Si in Q^1 and Q^2 units. This indicates that a chain-like silicate structure is formed during the reaction with $Ca(OH)_2$ and water, since the main resonances in the difference spectra resemble ^{29}Si MAS NMR spectra observed for the C-S-H phase formed by PC hydration.[24,25]

In ^{27}Al MAS NMR, resonances in the range 55 to 80 ppm are expected for AlO_4 units whereas AlO_6 octahedra result in resonances with chemical shifts from −15 to 20 ppm relative to an 1 M aqueous solution of $AlCl_3.6H_2O$.[30,31] The ^{27}Al MAS NMR spectrum of $C_{26}A_9S_{65}$ (Figure 4(b)) includes a broad resonance corresponding to Al in tetrahedral coordination where its asymmetric lineshape reflect the presence of a range
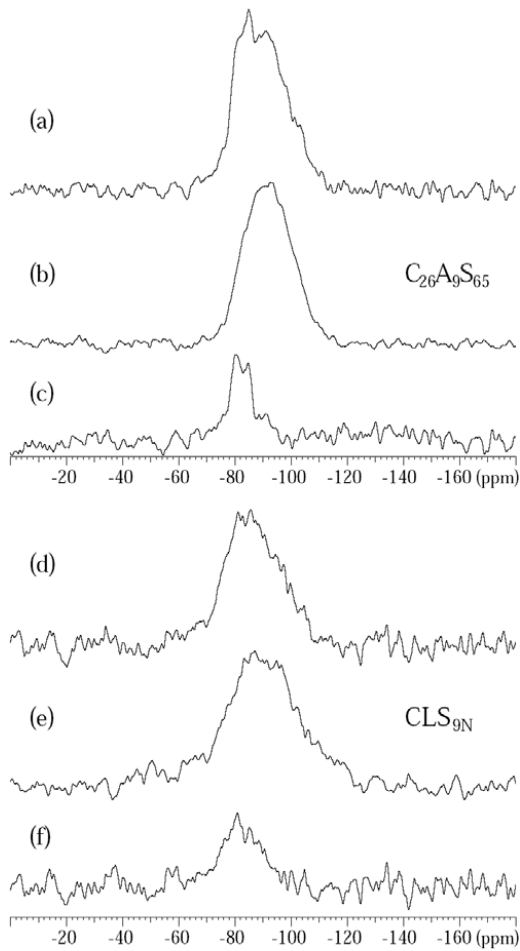
Figure 3. ^{29}Si MAS NMR spectra (4·7 T) of the $C_{26}A_9S_{65}$ (a)–(c) and CLS_{9N} (d)–(f) glasses following their reactivity with $Ca(OH)_2$ and water at 40°C for 7 days. Parts (b) and (e) show the spectra of the anhydrous materials while the spectra of the samples after the reactivity tests are shown in parts (a) and (d). Subtraction of the spectra before and after the reactivity test, using a optimized scaling factor for the spectra of the anhydrous materials, results in the difference plots illustrated in parts (c) and (f) which only include resonances from the hydration products

Figure 4. ^{27}Al MAS NMR spectra (9·4 T) of the $C_{26}A_9S_{65}$ (a)–(c) and CLS_{9N} (d)–(f) glasses before (b), (d) and after (a), (d) the reactivity tests. The difference spectra are shown in parts (c) and (d) and are obtained in a similar manner as those derived from the ^{29}Si MAS NMR spectra (Figure 3) for the same samples

of different AlO_4 sites as expected for an amorphous phase. In addition to tetrahedrally coordinated Al, the ^{27}Al MAS NMR spectrum of CLS_{9N} (Figure 4(e)) also includes a resonance with a centre of gravity at 14·3 ppm, reflecting a small fraction of Al in octahedral coordination in this sample. The corresponding spectra of the glasses after the pozzolanic reactivity test (Figure 4(a) and (d)) reveal a sharp peak at 8·5 ppm, reflecting that a hydration product including octahedrally coordinated Al in an ordered phase has formed.

Comparisons of the intensities in the spectra of the samples after the reactivity tests and in the difference spectra in Figure 3 and 4 reflect the degree of reaction for the glasses. Thus, for $C_{26}A_9S_{65}$ it is estimated that 18·6% and 19·6% of the material has reacted in the pozzolanity test from the intensities observed in the ^{29}Si and ^{27}Al MAS NMR spectra, respectively.
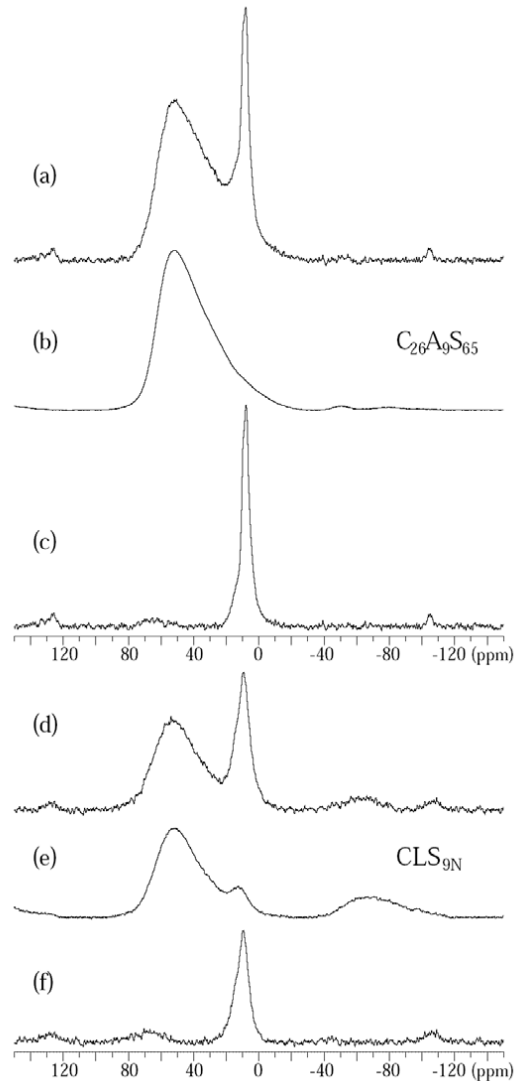
Similarly, for CLS_{9N} it is found that 32·2% (^{29}Si NMR, Figure 3) and 29·5% (^{27}Al NMR, Figure 4) of the glass has reacted with $Ca(OH)_2$ and water. The degrees of reaction, determined independently from the ^{29}Si and ^{27}Al MAS NMR spectra, agree very well, indicating that this is a valuable approach to estimate the degree of reaction for amorphous glass materials. Moreover, the results show that the two glasses to some extent are pozzolanic materials.

The degree of pozzolanic reactivity for the glasses has been estimated by a simple determination of the mass of un-reacted glass. Conversely, the pozzolanic reactivity is quantified as the amount of glass that reacts during the test. Figure 5 shows that the introduction of minor components to the glass from natural minerals enhances the pozzolanic reactivity from 11·7 to 14·1%. The introduction of additional
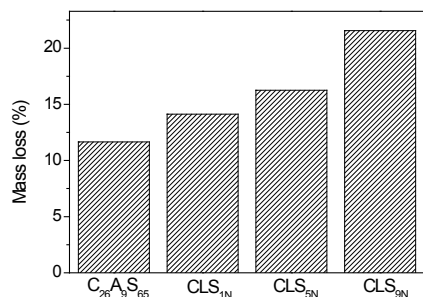
Figure 5. Degree of pozzolanic reactivity for the glasses given as the mass loss of glass during the reactivity test

alkali oxide in CLS$_{9N}$, i.e. as a network modifying component, further increases the reactivity to 21·6%. The degrees of reaction determined by this method are generally lower than the values obtained by ^{27}Al and ^{29}Si MAS NMR. This difference may reflect that the calcium aluminosilicate hydration products are not completely removed by washing with the weak solution of acetic acid, resulting in lower estimates for the degree of pozzolanic reactivity.

4. Conclusion

CaO–SiO$_2$–Al$_2$O$_3$ glasses have been produced both from pure chemicals and from natural raw materials for the potential use as supplementary cementitious materials (SCMs) in the Portland cement industry. The compositions of the glasses have been optimized for glass forming ability, minimum melting temperature, minimum limestone content in the batch, maximum grindability to cement fineness, and maximum pozzolanic reactivity for cement performance.

The results indicate that compared to conventional Portland cement, the glasses can be produced with slightly lower CO$_2$ emissions associated with fuels, but significantly lower CO$_2$ emissions from the raw materials. The NMR investigations have shown that the glasses exhibit some degree of pozzolanic activity, thus contributing to the development of strength during cement hydration. Thus, these CAS glasses may potentially be used as SCMs, resulting in both a reduced CO$_2$ emission from cement production and an acceptable cement performance.

Acknowledgements

References

1. Damtoft, J. S., Lukasik, J., Herfort, D., Sorrentino, D. & Gartner, E. M. Sustainable development and climate change initatives. *Cem. Concr. Res.*, 2005, **38**, 115–27.
2. Worrell, E., Price, L., Martin, N., Hendriks, C. & Meida, K. O. Carbon dioxide emission from the global cement industry. *Ann. Rev. Energy Environ.*, 2001, **26**, 303–29.
3. Rehan, R. & Nehdi, M. Carbon dioxide emissions and climate change: policy implications for the cement industry. *Environ. Sci. Pol.*, 2005, **8**, 105–114.
4. Taylor, H. F. W. *Cement chemistry*, Academic Press, Second edition, 1997.
5. Hewlett, P. C. *Lea's chemistry of cement and concrete*, Elsevier, Fourth edition, 2007.
6. Shi, C. & Zheng, K. A review on the use of waste glasses in the production of cement and concrete. *Resour. Conserv. Recy.*, 2007, **52**, 234–47.
7. Shayan, A. & Xu, A. Performance of glass powder as a pozzolanic material in concrete: A field trial on concrete slabs. *Cem. Concr. Res.*, 2006, **36**, 457–68.
8. Shi, C., Wu, Y., Riefler, C. & Wang, H. Characteristics and pozzolanic reactivity of glass powders. *Cem. Concr. Res.*, 2005, **35**, 987–93.
9. Schwarz, N., Cam, H. & Neithalath, N. Influence of a fine glass powder on the durability characteristics of concrete and its comparison to fly ash. *Cem. Concr. Res.*, 2008, **30**, 486–96.
10. Yue, Y. Z. Characteristic temperatures of enthalpy relaxation in glass. *J. Non-Cryst. Solids*, 2008, **354**, 1112–18.
11. Varshneya, A. K. *Fundamentals of Inorganic glasses*, Academic, 1994.
12. Shelby, J. E. *Introduction to Glass Science and Technology*, Second edition, The Royal Society of Chemistry, 2005.
13. Ossi, P. M. *Disordered Materials – An Introduction*, Springer, 2003.
14. Mysen, B. O. & Richet P. *Silicate glasses and melts – properties and structure, Developments in geochemistry* 10, Elsevier, 2005.
15. Sardeshpande, V., Gaitonde, U. N. & Banerjee, R. Model based energy benchmarking for glass furnace. *Energy Convers. Manage.*, 2007, **48**, 2718–38.
16. Conradt, R. A generic approach to the relation between pull rate and energy consumption of glass furnaces. *Glass. Sci. Technol. Glastech. Ber.*, 2000, **73**, 252–61.
17. Beerkens, R. Industrial glassmelting process analysis. *Am. Ceram. Soc. Bull.*, 2004, **83**, 28–32.
18. Angell, C. A. Relaxation in liquids, polymers and plastic crystals - strong/fragile patterns and problems. *J. Non-Cryst. Solids*, 1991, **131–133**, 13–31.
19. Moesgaard, M. & Yue, Y. Z. Compositional dependence of fragility and glass forming ability of calcium aluminosilicate melts. *J. Non-Cryst. Solids*, 2009, **355**, 867–73.
20. Mauro, J. C., Yue, Y. Z., Ellison, A. J., Gupta, P. K. & Allan, D. C. Viscosity of glass-forming liquids. *Proc. Natl. Acad. Sci. USA*, 2009, **106**, 19780–4.
21. Kantal A. B. FIBROTHAL® Handbook – Heating and Isulations Systems, Catalouge 8-A-1-3 04-08-3000, Kantal, Sweden.
22. Bouhifd, M. A., Besson, P., Courtial, P., Gérardin C., Navrotsky, A. & Richet, P. Thermochemistry and melting properties of basalt. *Contrib. Miner. Petrol.* 2007, **153**, 689–98.
23. Hjorth, J., Skibsted, J. & Jakobsen, H. J. ^{29}Si NMR studies of Portland cement components and effects of microsilica on the hydration reaction. *Cem. Concr. Res.*, 1988, **18**, 789–98.
24. Richardson, I. G. The nature of C-S-H in hardened cement. *Cem. Concr. Res.* 1999, **29**, 1131–1147.
25. Andersen, M. D., Jakobsen, H. J. & Skibsted, J. Incorporation of aluminum in the calcium silicate hydrate of hydrated Portland cements: A high-field ^{27}Al and ^{29}Si MAS NMR investigation. *Inorg. Chem.*, 2003, **42**, 2280–2287.
26. Skibsted, J. Henderson, E. & Jakobsen, H. J. Characterization of calcium aluminate phases in cements by ^{27}Al MAS NMR spectroscopy. *Inorg. Chem.*, 1993, **32**, 1013–1027.
27. Lippmaa, E., Mägi, M., Samoson, A. Engelhardt, G. & Grimmer, A. R. Structural Studies of Silicates by Solid-state High-Resolution ^{29}Si NMR, *J. Am. Chem. Soc.*, 1980, **102**, 4889–93.
28. Mägi, M., Lippmaa, E., Engelhardt, G. & Grimmer, A. R., Solid-state High-Resolution Silicon-29 Chemical Shifts in Silicates, *J. Phys. Chem.*, 1984, **88**, 1518–22.
29. Klinowski, J. Nuclear magnetic resonance studies of zeolites, *J. Progr. NMR Spectr.*, 1984, **16**, 237–309
30. Merzbacher, C. I., Sherriff, B. L., Hartman, J. S. & White, W. B. A high-resolution ^{27}Al and ^{29}Si NMR study of alkaline earth aluminosilicate glasses, *J. Non-Cryst. Solids*, 1990, **124**, 194–206.
31. Muller, D., Gessner, W., Behrens, H. J. & Scheler, G. Determination of the aluminum coordination in aluminum-oxygen compounds by solid-state high-resolution ^{27}Al NMR. *Chem. Phys. Lett.*, 1981, **70**, 59–62.

Paper III

Evidence of Intermediate-Range Order Heterogeneity in Calcium Aluminosilicate Glasses

Mette Moesgaard,[†] Ralf Keding,[†] Jørgen Skibsted,[‡] and Yuanzheng Yue*,[†]

[†]*Section of Chemistry, Aalborg University, DK-9000 Aalborg, Denmark, and* [‡]*Instrument Centre for Solid-State NMR spectroscopy and Interdisciplinary Nanoscience Center (iNANO), Department of Chemistry, Aarhus University, DK-8000 Aarhus, Denmark*

The intermediate-range order in peralkaline calcium aluminosilicate glasses is explored by two different models using solid-state ^{29}Si MAS NMR spectra as the main experimental basis. The two modeling approaches describe the spatial arrangement of the tetrahedral SiO_4 and AlO_4 units, that is, the intermediate-range order (IRO), assuming either a random distribution of structural units or a hierarchy in the IRO. The hierarchy creates a quasi-heterogeneous distribution of the structural units. Two series of calcium aluminosilicate glasses (five glasses for each) are chosen for the present study, compositions of which vary along the join between the anorthite-wollastonite-gehlenite eutectic point and anorthite-wollastonite-tridymite point, and parallel to the join. The validity of the two modeling approaches is examined by simulation of the frequency and intensity distributions observed in the ^{29}Si MAS NMR spectra of the 10 glasses using a sum of resonances predicted for the different types of structural units. The results clearly reveal that the ^{29}Si MAS NMR spectra support the quasi-heterogeneous IRO for the 10 glasses, since this approach gives a satisfactory fit to the experimental spectra. In contrast, simulations based on the model of random IRO cannot reproduce the ^{29}Si NMR spectra in a satisfactory manner. The observed hierarchy in the IRO may also explain the compositional dependence of both viscous behavior of the melts and the stability of the 10 glasses.

1. Introduction

The physical and chemical properties of a glass are determined mainly by its microstructure (hereafter called structure), which to a large extent depends on its chemical composition. In general, the characterization and understanding of the structure of crystalline materials have been established more thoroughly as compared to that of non-crystalline materials (i.e., glasses), reflecting the lack of long-range structural order in glasses which prevents the application of conventional structural tools such as X-ray diffraction techniques. Nevertheless, a substantial progress in our understanding of glass structures has been achieved in the past century[1–4] and in particular in recent years because of the rapid technical improvements of experimental tools such as EXAFS,[5,6] NMR spectroscopy,[5,7,8] and molecular dynamics simulations.[9] Using these tools, several aspects of both the short-range and the intermediate-range structure of silicate glasses have been clarified. However, some puzzles

still remain unsolved, especially, about the role of heterogeneity in the overall structural network.

Much effort has been devoted to determination of the topological arrangements of Al ions in aluminosilicate glasses, for example, the coordination number of Al, the bond-angle distribution, the linkage of AlO_x to alkali or alkaline earth ions, and the fulfillment of the aluminum avoidance principle.[7,9−15] Using different solid-state NMR techniques, Stebbins and co-workers[8,10−14] have investigated the structure of aluminosilicate glasses primarily along "charge compensated" joins, along which the total charge of the network modifying ions equals that of the AlO_2 units (e.g., $SiO_2-NaAlO_2$ and $SiO_2-CaAl_2O_4$ systems). Using Raman spectroscopy, Mysen and co-workers[16−18] have performed careful structural investigations of various "charge compensated" and peralkaline aluminosilicates. These results are the fundamental basis for the structural investigations of the calcium aluminosilicate (CAS) glasses presented in this work. However, the compositions of the

(1) Warren, B. E. *J. Am. Ceram. Soc.* **1934**, *17*, 249.
(2) Wright, A. C.; Leadbetter, A. J. *Phys. Chem. Glasses* **1976**, *17*, 122.
(3) Farnan, I.; Grandinetti, P. J.; Baltisberger, J. H.; Stebbins, J. F.; Werner, U.; Eastman, M. A.; Pines, A. *Nature* **1992**, *358*, 31.
(4) Gaskell, P. H. *J. Non-Cryst. Solids* **1997**, *222*, 1.
(5) Greaves, G. N.; Sen, S. *Adv. Phys.* **2007**, *56*, 1.
(6) Brown, G. E. J.; Farges, F.; Calas, G. *Rev. Miner.* **1995**, *32*, 317.
(7) Eckert, H. *Progr. NMR Spectrosc.* **1992**, *24*, 159.
(8) Lee, S. K.; Stebbins, J. F. *Am. Mineral.* **1999**, *84*, 937.
(9) Du, J.; Cormack, A. N. *J. Non-Cryst. Solids* **2004**, *349*, 66.

(10) Lee, S. K.; Stebbins, J. F. *J. Phys. Chem. B* **2000**, *104*, 4091.
(11) Stebbins, J. F.; Lee, S. K.; Oglesby, J. V. *Am. Mineral.* **1999**, *84*, 983.
(12) Lee, S. K.; Stebbins, J. F. *J. Non-Cryst. Solids* **2000**, *270*, 260.
(13) Murdoch, J. B.; Stebbins, J. F.; Carmichael, I. S. E. *Am. Mineral.* **1985**, *70*, 332.
(14) Stebbins, J. *Nature* **1987**, *330*, 13.
(15) De Jong, B. H. W. S.; Brown, G. E. *Geochim. Cosmochim. Acta* **1980**, *44*, 491.
(16) Mysen, B. *Contrib. Mineral. Petrol.* **1997**, *127*, 104.
(17) Mysen, B. O. *Am. Mineral.* **1990**, *75*, 120.
(18) Mysen, B. O.; Virgo, D.; Kushiro, I. *Am. Mineral.* **1981**, *66*, 678.

glasses in the present study deviate from those in previous investigations of aluminosilicate glasses as the glasses in this work generally possess relatively higher contents of both non-bridging oxygen (NBO) anions and Al^{3+} cations.

In this work we investigate the structure of peralkaline glasses within the CAS system. During the optimization of the chemical composition for a technical glass, with a similar composition as the CAS glasses investigated in this study, we found in a recent study a striking compositional dependence on both the glass forming ability and the melt fragility of the CAS melts.[19] To understand this behavior in more detail, it is necessary to characterize the structural changes that occur when the composition is modified, since the glass forming ability is dictated by the topological arrangement and the chemical bonding strength of glasses. In addition, investigations of the structure for the CAS system is particularly interesting since the majority of magmatic compositions and several technical glasses belong to aluminosilicate systems.[20,21]

In the present study we establish two different structural models for the intermediate-range order (IRO) and investigate their applicability to describe the distribution of structural units within two series of glasses, each including five different compositions. The IRO is defined as the structure extending beyond nearest neighbors (NN) within the glass. In one approach, a random spatial rearrangement of structural units is assumed, referred to as the "random IRO" (R-IRO) model. The other model employs a hierarchy in the intermediate-range order, resulting in a quasi-heterogeneous distribution of structural units and is thus denoted as the "quasi-heterogeneous IRO" (QH-IRO) model. The contents of the different structural units in the 10 glasses are derived from the two models using the chemical compositions of the glasses along with their solid-state ^{29}Si MAS NMR spectra. The validity of the models is evaluated by their ability to simulate the intensity and frequency distributions in the ^{29}Si MAS NMR spectra.

^{29}Si MAS NMR is a well-documented powerful tool for structural studies of aluminosilicates.[22−25] It is widely used as the isotropic ^{29}Si chemical shift ($\delta(^{29}Si)$) depends on both the degree of polymerization of SiO_4 tetrahedra and the presence of Al in the second coordination sphere to Si. However, simultaneous changes in the content of both the network modifying ions and the network forming Al ions may complicate the interpretation of single-pulse ^{29}Si NMR experiments. In such cases, supporting information may be obtained from two-dimensional ^{17}O and ^{27}Al triple-quantum (3Q) MAS NMR experiments, where ^{17}O requires the use of isotopically enriched samples.[10,12] In this work the structural modeling based on the chemical composition of

(19) Moesgaard, M.; Yue, Y. Z. *J. Non-Cryst. Solids* **2009**, *355*, 867.
(20) Mysen, B. O.; Richet, P. *Silicate glasses and melts properties and structure*; Elsevier B.V.: Amsterdam, 2005.
(21) Stebbins, J. F.; Xu, Z. *Nature* **1997**, *390*, 60.
(22) Lippmaa, E.; Mägi, M.; Samoson, A.; Engelhardt, G.; Grimmer, A. R. *J. Am. Chem. Soc.* **1980**, *102*, 4889.
(23) Mägi, M.; Lippmaa, E.; Engelhardt, G.; Grimmer, A. R. *J. Phys. Chem.* **1984**, *88*, 1518.
(24) Klinowski, J. *Progr. NMR Spectrosc.* **1984**, *16*, 237.
(25) Lippmaa, E.; Mägi, M.; Samoson, A.; Tarmak, M.; Engelhardt, G. *J. Am. Chem. Soc.* **1981**, *103*, 4992.

Table 1. Oxide Compositions (mol %) for the 10 CAS Glasses

	glass[a]	SiO_2	Al_2O_3	CaO	Ca_{excess}[b]
series 1	$C_{26}A_9S_{65}$	64.9	9.3	25.8	16.6
	$C_{30}A_{10}S_{60}$	59.9	10.0	30.1	20.0
	$C_{34}A_{11}S_{55}$	54.7	10.9	34.4	23.5
	$C_{39}A_{12}S_{49}$	49.6	11.7	38.7	27.1
	$C_{43}A_{13}S_{44}$	44.4	12.5	43.1	30.6
series 2	$C_{23}A_{15}S_{62}$	61.6	14.9	23.4	8.0
	$C_{26}A_{16}S_{58}$	57.8	15.8	26.3	10.5
	$C_{31}A_{17}S_{52}$	51.9	16.8	31.3	13.0
	$C_{33}A_{19}S_{48}$	48.1	18.9	33.0	15.5
	$C_{38}A_{19}S_{43}$	42.7	19.3	38.0	18.0

[a] The sample names refer to the actual molar compositions determined by wet chemical analysis. [b] Ca_{excess} is the amount of Ca^{2+} ions which is not used for charge balancing the Al^{3+} ions.
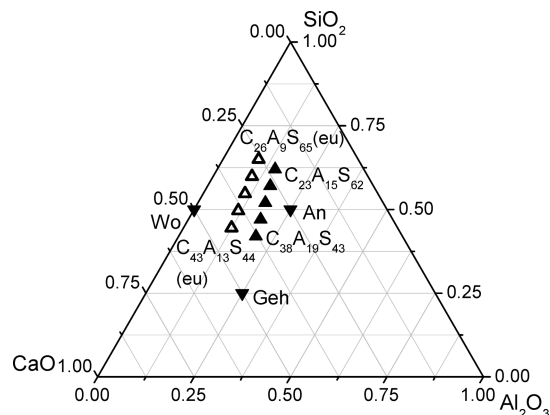

Figure 1. Graphical representation of the compositions for the 10 glasses (upward triangles) in the CAS ternary phase diagram (mol %). The open triangles represent series 1 (i.e., $C_{26}A_9S_{65}$ to $C_{43}A_{13}S_{44}$) with the two end members being the eutectic compositions of An-Wo-Geh and An-Wo-Tri, while series 2 ($C_{23}A_{15}S_{62}−C_{38}A_{19}S_{43}$) is illustrated by the solid upward triangles. The downward triangles correspond to the compositions for the mineral phases wollastonite, anorthite, and gehlenite.

the glasses allows extraction of new important information about the IRO from the single pulse ^{29}Si MAS NMR experiments.

2. Experimental Section

The glasses are divided into two series of systematic compositional variations and are placed in the vicinity of the eutectic compositions for anorthite-wollastonite-gehlenite (An-Wo-Geh) and anorthite-wollastonite-tridymite (An-Wo-Tri). The compositions of the 10 glasses are summarized in Table 1 while their location in the ternary CAS system is illustrated in Figure 1. The sample names of the glasses refer to the molar oxide composition determined from wet chemical analysis with C, A, and S representing CaO, Al_2O_3, and SiO_2, respectively

The glasses were synthesized by melting the batch in a $Pt_{90}Rh_{10}$ crucible in an electric furnace (model SF6/17 Entech, Ängelholm, Sweden) in atmospheric air. The individual compositions were obtained by mixing reagent-grade chemicals of SiO_2, Al_2O_3, and $CaCO_3$. A two-step melting process was carried out to obtain a homogenized glass. First, the batch was melted at 1823 K and kept at this temperature for 2 h. Subsequently, the melt was quenched in water to get shattered pieces. The shattered glass was melted again at 1823 K for 2 h and cast on a graphite plate. The chemical compositions of the resulting glasses (Table 1) were determined by standard wet chemical analysis at the Cement and Concrete Laboratory of the Aalborg Portland Group, Aalborg, Denmark.

The ^{29}Si MAS NMR spectra were recorded at 59.1 MHz on a Varian INOVA-300 (7.05 T) spectrometer, using a home-built CP/MAS probe for 7 mm outer diameter (o.d.) rotors. The powder samples, ground to a fineness below 75 μm, were packed in 7 mm partially sintered zirconia (PSZ) rotors (220 μL sample volume) and spun at 7.0 kHz. The experiments employed a radio frequency (rf) field strength of $\gamma B_1/2\pi \approx 40.0$ kHz, a pulse width of 3.0 μs (~45° flip angle), a 120 s repetition delay, and 1000−1400 scans. The ^{27}Al MAS NMR spectra were recorded at 104.2 and 156.3 MHz on Varian INOVA-400 (9.39 T) and INOVA-600 (14.09 T) spectrometers using home-built CP/MAS probes for 5 and 4 mm o.d. rotors, respectively. The 9.39 T spectra employed a spinning speed of 12.0 kHz, a 0.5 μs excitation pulse for $\gamma B_1/2\pi \approx 60.0$ kHz, a 2 s relaxation delay, and typically 6000 scans. The 14.09 T spectra used a spinning speed of 13.0 kHz, a 0.5 μs excitation pulse for $\gamma B_1/2\pi \approx 60.0$ kHz, a 2 s relaxation delay, and 1400−2100 scans. The [27]Al and [29]Si isotropic chemical shifts are reported relative to a 1.0 M aqueous solution of $AlCl_3 \cdot 6H_2O$ and neat tetramethyl silane (TMS), respectively.

The simulations and optimizations to the ^{29}Si MAS NMR spectra have been performed using the scaled Levenberg−Marquardt non-linear least-squares algorithm[26] included in the program QtiPlot 0.9.6.[27] A tolerance of 10^{-4} is used for the simulations.

3. Theoretical Approach

3.1. Distribution of Bridging and Non-Bridging Oxygen. A classical and commonly used model for silicate glass structures is the continuous random network (CRN) model proposed by Zachariasen.[28] The CRN model describes the glass structure as a three-dimensional network of corner-linked low-valence cation-oxygen polyhedra where the introduction of modifying oxides to the glass leads to the formation of NBOs randomly distributed within the three-dimensional network. On the basis of the CRN model, Greaves[29] has proposed the modified random network (MRN) model where different sizes of the network-forming and network-modifying polyhedra result in a micro segregation of the two structural units. This creates regions of modifier rich channels and other regions rich in more highly polymerized network-forming polyhedra.[5,9,30]

All glasses investigated in this work are peralkaline, in which both Si and Al act as network forming components. The excess Ca ions (Ca_{excess}), which are not involved in the charge balance of Al^{3+} ions, serve to charge balance the NBOs that are created by the presence of excess oxide ions. The first step in the description of the structure is to model the distribution of the various network forming $(Si,Al)O_4$ Q^n units (n is the number of bridging oxygens (BOs) linked to the network former). A preference of Al for fully polymerized Q^4 sites in

peralkaline aluminosilicates has been reported in several studies,[17,18,20,31−33] that is, no NBOs are linked directly to Al. This preference is found to increase with increasing Si/Al ratio, and for Si/Al > 1 the content of Al-NBO is reported to be insignificant.[31−33] For the samples studied in this work, the Si/Al ratio varies between 1.1 ($C_{38}A_{19}S_{43}$) and 3.5 ($C_{26}A_9S_{65}$), and Al is assigned solely to Q^4 units, implying that excess CaO will create NBOs associated with Si only.

Despite several investigations, inconsistencies in the description of the Q^n distribution of SiO_4 units in silicate glasses still remain within the glass community. Generally, two models are considered, that is, the binary model and the random model.[5,34−36] The former assumes the existence of only two different $Si(Q^n)$ units for a specific glass composition, the argument being that repulsive forces between the modifying ions prevent these ions from entering a site adjacent to Si in, for example, a Q^2 unit until no other Q^3 units are present. On the other hand, the random model assumes a statistical distribution of Q^n units for $n = 0-4$. The two models represent extreme situations and thus, Q^n distributions lying in between these two situations have been reported by several authors.[5,16,20,35,37,38] For example, ^{29}Si MAS NMR studies of binary alkali silicate systems have indicated the presence of three different Q^n units[34,37−39] and thereby that the randomness is larger than predicted by the binary model although still less than predicted by the random model. It has also been reported that a large field strength of the modifying ions increases the structural disorder.[13,20,31,35] From the relatively large field strength of calcium ions, the CAS glasses investigated in this work are expected to contain a certain degree of randomness deviating further from the binary model as compared to the alkali silicate systems as evidenced from investigations of such systems.[13,40] Hence, the random model is chosen to describe the distribution of Q^n units in the CAS glasses. In this model, the probability (p) that a randomly chosen Si−O bond includes a NBO is calculated as the ratio between the number of NBOs divided by the total number of bonds (NBO + BO):

$$p = \frac{\text{NBO}}{\text{NBO} + \text{BO}} = \frac{2Ca_{excess}}{Z \cdot \text{Si}} \qquad (1)$$

Here, Ca_{excess} and Si are the numbers of the excess calcium ions and the number of glass forming Si ions, respectively, while Z is the coordination number of the network former, that is, $Z = 4$. Using the p value obtained for the individual

(26) Marquardt, D. W. *J. Soc. Industr. Appl. Math.* **1963**, *11*, 31.
(27) *Qtiplot*; http://soft.proindependent.com/install.html.
(28) Zachariasen, W. H. *J. Am. Chem. Soc.* **1932**, *54*, 3841.
(29) Greaves, G. N. *J. Non-Cryst. Solids* **1985**, *71*, 203.
(30) Gedeon, O.; Liska, M.; Machacek, J. *J. Non-Cryst. Solids* **2008**, *354*, 1133.
(31) Merzbacher, C. I.; Sherriff, B. L.; Hartman, J. S.; White, W. B. *J. Non-Cryst. Solids* **1990**, *124*, 194.
(32) Allwardt, J. R.; Lee, S. K.; Stebbins, J. F. *Am. Mineral.* **2003**, *88*, 949.
(33) Lee, S. K.; Stebbins, J. F. *Geochim. Cosmochim. Acta* **2006**, *70*, 4275.

(34) Stebbins, J. F. *J. Non-Cryst. Solids* **1988**, *106*, 359.
(35) Buckermann, W. A.; Müller-Warmuth, W.; Frischat, G. H. *Glastech. Ber.* **1992**, *65*, 18.
(36) Avramov, I.; Rüssel, C.; Keding, R. *J. Non-Cryst. Solids* **2003**, *324*, 29.
(37) Emerson, J. F.; Stallworth, P. E.; Bray, P. J. *J. Non-Cryst. Solids* **1989**, *113*, 253.
(38) Maekawa, H.; Maekawa, T.; Kawamura, K.; Yokokawa, T. *J. Non-Cryst. Solids* **1991**, *127*, 53.
(39) Schramm, C. M.; De Jong, B. H. W. S.; Parziale, V. E. *J. Am. Chem. Soc.* **1984**, *106*, 4396.
(40) Schneider, E.; Stebbins, J. F.; Pines, A. *J. Non-Cryst. Solids* **1987**, *89*, 371.

Table 2. Calculated Distributions of Si(Q^n) Units for the 10 Glasses Assuming a Random Distribution of NBOs[a]

glass	Q^0	Q^1	Q^2	Q^3	Q^4
$C_{26}A_9S_{65}$	0	0	7.42	33.87	57.96
$C_{30}A_{10}S_{60}$	0	1.56	11.66	38.65	48.05
$C_{34}A_{11}S_{55}$	0	3.12	17.10	41.60	37.96
$C_{39}A_{12}S_{49}$	0	5.91	23.62	41.96	27.96
$C_{43}A_{13}S_{44}$	1.41	10.71	30.59	38.82	18.47
$C_{23}A_{15}S_{62}$	0	0	2.19	21.13	76.59
$C_{26}A_{16}S_{58}$	0	0	4.20	27.57	67.94
$C_{31}A_{17}S_{52}$	0	0	7.18	33.50	58.62
$C_{33}A_{19}S_{48}$	0	1.50	11.38	38.41	48.64
$C_{38}A_{19}S_{43}$	0	3.09	17.01	41.58	38.11

[a] The fractions are given as molar percents. "0" indicates that the unit accounts for less than 1% of the SiO_4 units in the sample. The distributions are calculated using eqs 1 and 2.

compositions, the molar fraction $x(Q^n)$ for each of the Si(Q^n) units can be calculated by combinatorics assuming a statistical distribution:

$$x(\text{Si}(Q^n)) = \frac{Z!}{n!(Z-n)!}(1-p)^n p^{Z-n}$$

$$= \frac{4!}{n!(4-n)!}(1-p)^n p^{4-n} \qquad (2)$$

Introduction of Al into a silicate glass enhances the structural disorder since the randomness is found to increase as the Si/Al ratio decreases.[10,16,34] This also means that use of the random model is reasonable for describing the distribution of different Q^n units in aluminosilicates. Table 2 lists the distributions of Si(Q^n) units for the 10 glasses obtained from eqs 1 and 2. The molar fraction of Si(Q^n) units of < 1% is neglected in the modeling of the ^{29}Si MAS NMR spectra, and thus, the presence of Q^0 units is neglected for all glasses except $C_{43}A_{13}S_{44}$ for which the fraction of Q^0 accounts for 1.41% of the structural units.

3.2. Al Avoidance Principle. The relative distribution of SiO_4 and AlO_4 units in the glass network is described in terms of the Si nuclei and the distribution of Al in the second coordination sphere of Si. Thus, the modeling approach provides no information on the identity of the network former linked to the AlO_4 tetrahedra in the following coordination spheres, that is, the Al avoidance principle[41] is not directly considered. The only assumption made is that all the Al ions are available for linking with SiO_4 tetrahedra, that is, no formation of large clusters of Al structural units is expected. The Al avoidance principle has previously been deduced from experimental observations,[13] and it is supported by theoretical calculations showing that the Al−O−Al linkages are energetically less favorable than Si−O−Si and Si−O−Al linkages.[15] However, it has also been reported that the Al avoidance principle is not fully obeyed within aluminosilicate glasses.[8,10−14] The degree of Al avoidance is derived from the equilibrium constant of the reaction, 2(Al−O−Si) ↔ (Si−O−Si) + (Al−O−Al),[11] and an Al avoidance degree of 1 corresponds to complete Al avoidance whereas a value of 0 denotes a random distribution of network forming Si and Al units. It is estimated

that the degree of Al avoidance for CAS glasses positioned on the meta-aluminous limit is about 0.85.[8,10−14]

The fulfillment of the Al avoidance principle in the present approach depends on the Si/Al ratio and the content of NBOs linked to Si. When the total number of BOs bound to Si is larger than the total number of BOs bound to Al, the Al avoidance principle can be fulfilled. This is the case for all glasses except $C_{38}A_{19}S_{43}$ for which at least 17% of Al is expected to be present in Al−O−Al linkages. The fulfillment of the Al avoidance principle in the two IRO modeling approaches is discussed later.

3.3. Random Intermediate-Range Order (R-IRO) Model. The first approach for modeling of the intermediate-range order is based on the principles of the CRN model. The structure beyond the nearest neighbors is thus described by a random distribution of Al around the SiO_4 tetrahedra. This distribution is assumed to follow similar statistical principles as for the NBOs around Si. The probability that a randomly picked Si-BO unit is linked to Al is initially calculated as the ratio between the content of Al and the total content of network forming cations (Si + Al) (Similar approach as eq 1). Using this probability, the fraction of each Si($Q^{ni}(m_i\text{Al})$) unit (m is the number of Al in the second coordination sphere to Si) is calculated as listed in Table 3 using the algorithm of eq 2. Again, structural units accounting for less than 1% of the sample are neglected. The number of non-negligible units increases within each series, when the content of both NBO and Al increases from $C_{26}A_9S_{65}$ to $C_{43}A_{13}S_{44}$ (series 1) and from $C_{23}A_{15}S_{62}$ to $C_{38}A_{19}S_{43}$ (series 2). For $C_{26}A_9S_{65}$, 9 different structural units exist whereas 13 non-negligible units are found for $C_{43}A_{13}S_{44}$. In the other series, $C_{23}A_{15}S_{62}$ has 7 non-negligible units while $C_{38}A_{19}S_{43}$ are found to include 14 different structural units.

3.4. Quasi-Heterogeneous Intermediate-Range Order (QH-IRO) Model. The QH-IRO model is based on the principles of the modified random network (MRN) model[29] which predicts clustering of NBOs within silicate glasses. For the glasses studied in the present work, clustering of NBOs results in highly polymerized regions of alternating SiO_4 and AlO_4 tetrahedra as well as highly depolymerized regions containing only a minor content of Al. This clustering creates concentration fluctuations within the glasses, which have been reported for several multicomponent oxide glasses[42−46] and is ascribed to the existence of chemical heterogeneities in the range of ∼1−3 nm. The existence of such an IRO hierarchy is supported by experimental observations from Raman spectroscopy, light scattering, and small-angle X-ray scattering studies.[43−45] Furthermore, a preferential bonding of Al to fully polymerized SiO_4 tetrahedra has been reported,[31,47,48] which supports the existence of nanometric spatial regions with different heterogeneities within the

(41) Loewenstein, W. *Am. Mineral.* **1954**, *39*, 92.

(42) Martinez, V.; Jurdyc, A. M.; Vouagner, D.; Martinet, C.; Champagnon, B. *J. Non-Cryst. Solids* **2005**, *351*, 2421.
(43) Conradt, R. *J. Non-Cryst. Solids* **2004**, *345&346*, 16.
(44) Mauro, J. C.; Uzun, S. S.; Bras, W.; Sen, S. *Phys. Rev. Lett.* **2009**, *102*, 155506.
(45) Moynihan, C. T.; Schroder, J. *J. Non-Cryst. Solids* **1993**, *160*, 52.
(46) Champagnon, B.; Wondraczek, L.; Deschamps, T. *J. Non-Cryst. Solids* **2009**, *355*, 712.
(47) Domine, F.; Piriou, B. *Am. Mineral.* **1986**, *71*, 38.
(48) Hess, P. C.; Wood, M. I. *Contrib. Mineral. Petrol.* **1982**, *81*, 103.

Table 3. Calculated Distributions of Si($Q^{ni}(m_i\text{Al})$) Units for the 10 Glasses Obtained by the R-IRO Model[a]

glass	Q^0	$Q^1(1\text{Al})$	$Q^1(0\text{Al})$	$Q^2(2\text{Al})$	$Q^2(1\text{Al})$	$Q^2(0\text{Al})$
$C_{26}A_9S_{65}$	0	0	0	0	2.56	4.49
$C_{30}A_{10}S_{60}$	0	0	1.17	0	4.39	6.53
$C_{34}A_{11}S_{55}$	0	0	2.24	1.38	6.95	8.77
$C_{39}A_{12}S_{49}$	0	1.89	4.02	2.42	10.28	10.93
$C_{43}A_{13}S_{44}$	1.41	3.85	6.86	3.95	14.09	12.55
$C_{23}A_{15}S_{62}$	0	0	0	0	0	0
$C_{26}A_{16}S_{58}$	0	0	0	0	1.94	1.70
$C_{31}A_{17}S_{52}$	0	0	0	1.16	3.45	2.56
$C_{33}A_{19}S_{48}$	0	0	0	2.24	5.62	3.52
$C_{38}A_{19}S_{43}$	0	1.51	1.58	4.05	8.50	4.46
i^b	1	2	3	4	5	6
n_i^b	0	1	1	2	2	2
m_i^b	0	1	0	2	1	0

glass	$Q^3(3\text{Al})$	$Q^3(2\text{Al})$	$Q^3(1\text{Al})$	$Q^3(0\text{Al})$	$Q^4(4\text{Al})$	$Q^4(3\text{Al})$	$Q^4(2\text{Al})$	$Q^4(1\text{Al})$	$Q^4(0\text{Al})$
$C_{26}A_9S_{65}$	0	3.89	13.65	15.96	0	1.97	10.37	24.24	21.25
$C_{30}A_{10}S_{60}$	0	5.49	16.34	16.21	0	2.29	10.22	20.27	15.08
$C_{34}A_{11}S_{55}$	0	7.21	18.17	15.27	0	2.49	9.42	15.83	9.98
$C_{39}A_{12}S_{49}$	1.37	8.76	18.63	13.21	0	2.49	7.94	11.25	5.98
$C_{43}A_{13}S_{44}$	1.80	9.64	17.18	10.20	0	2.20	5.88	6.98	3.11
$C_{23}A_{15}S_{62}$	0	4.54	9.39	6.47	0	7.16	22.19	30.57	15.80
$C_{26}A_{16}S_{58}$	1.32	6.95	12.18	7.12	1.18	8.29	21.80	25.49	11.18
$C_{31}A_{17}S_{52}$	2.18	9.72	14.44	7.15	1.54	9.12	20.34	20.14	7.48
$C_{33}A_{19}S_{48}$	3.36	12.62	15.82	6.61	1.89	9.46	17.78	14.86	4.66
$C_{38}A_{19}S_{43}$	4.83	15.20	15.96	5.59	2.16	9.06	14.27	9.99	2.62
i^b	7	8	9	10	11	12	13	14	15
n_i^b	3	3	3	3	4	4	4	4	4
m_i^b	3	2	1	0	4	3	2	1	0

[a] The contents are given as molar percentages where "0" indicates that the unit accounts for less than 1% of the sample. [b] Index numbers used for the different $\delta(Q^{ni}(m_i\text{Al}))$ units in eqs 3 and for the deconvolution of the ^{29}Si NMR resonances. The relative intensities for the individual resonances (a_i) are the molar fractions listed in the rows above for the different glasses.

Table 4. Calculated Distributions of Si($Q^{ni}(m_i\text{Al})$) Units Obtained by the HQ-IRO Model[a]

	Q^0	$Q^1(0\text{Al})$	$Q^2(2\text{Al})$	$Q^2(0\text{Al})$	$Q^3(3\text{Al})$	$Q^3(0\text{Al})$	$Q^4(4\text{Al})$	$Q^4(0\text{Al})$
$C_{26}A_9S_{65}$	0	0	0	7.42	0	33.87	28.51	29.45
$C_{30}A_{10}S_{60}$	0	1.56	0	11.66	0	38.65	33.60	14.45
$C_{34}A_{11}S_{55}$	0	3.12	0	17.10	1.70	39.90	37.96	0
$C_{39}A_{12}S_{49}$	0	5.91	0	23.62	19.06	22.90	27.96	0
$C_{43}A_{13}S_{44}$	1.41	10.71	0	30.59	37.65	1.17	18.47	0
$C_{23}A_{15}S_{62}$	0	0	0	2.19	0	21.13	48.39	28.20
$C_{26}A_{16}S_{58}$	0	0	0	4.20	0	27.57	57.02	10.93
$C_{31}A_{17}S_{52}$	0	0	0	7.18	8.69	24.81	58.62	0
$C_{33}A_{19}S_{48}$	0	1.50	0	11.38	31.15	7.26	48.64	0
$C_{38}A_{19}S_{43}$	0	3.09	15.55	1.46	41.58	0	38.11	0

[a] Quantities in molar percents. "0" indicates that the unit accounts for less than 1% of the sample.

glasses. This quasi-heterogeneous nature of the distribution of structural units is most likely found for network modifying ions with a low positive charge density as these ions have only a small stabilizing effect on NBOs and AlO$_4$ tetrahedra linked to the same SiO$_4$ tetradedron.[31,47]

For the fully polymerized regions, a structure of alternating SiO$_4$−AlO$_4$ units is assumed. For $C_{26}A_9S_{65}$, $C_{30}A_{10}S_{60}$, $C_{23}A_{15}S_{62}$, and $C_{26}A_{16}S_{58}$, the Al content is sufficiently low, that is, Al(Q^4) < Si(Q^4) (in molar fractions), to assign all Al to these fully polymerized regions, thus obeying the Al avoidance principle. For the other six glasses the remaining Al, which is not part of the fully polymerized regions, that is, Al(Q^4)−Si(Q^4) (in molar fractions), is assigned to Si(Q^3(3Al)) units, since a Si(Q^3) with a neighboring Al is more stable than a Si(Q^2) unit with an Al neighbor. Again a 1:1 ratio of Si and Al is assumed for the Si(Q^3(3Al)) units, resulting in the Al-avoidance principle being broken for these regions. For the glass with the highest Al content ($C_{38}A_{19}S_{43}$), Al must in addition be assigned to Si(Q^2) units. The distribution of Si($Q^{ni}(m_i\text{Al})$) units obtained from the HQ-IRO model is given in Table 4, which shows that the spatial intermediate-range arrangement of the glasses is described in terms of 4−6 different structural units. This contrasts the R-IRO model which predicts the presence of up to 14 different structural units (Table 3).

3.5. Comparison of the Models with ^{29}Si MAS NMR Spectra. The distribution of the Si($Q^{ni}(m_i\text{Al})$) units, predicted for the 10 glasses from the two different models,

is compared with experimental ^{29}Si MAS NMR spectra of the glasses, providing information on the validity of the two different models in the description of the intermediate-range structure of the CAS glasses. The observed chemical shifts, $\delta(^{29}\text{Si})$, for aluminosilicates depend on both the degree of polymerization of SiO$_4$ tetrahedra and the number of Al in their second coordination sphere. The ^{29}Si resonances observed experimentally are the sum of subpeaks originating from different SiO$_4$ environments where the subpeak area is proportional to the molar fraction of the individual Si(Q^{ni}-(m_iAl)) units. Thus, rather broad ^{29}Si resonances are expected since the models predict a range of different structural environments for each glass composition. The molar fractions for the individual Si($Q^{ni}(m_i$Al)) units are determined by the structural models and summarized in Tables 3 and 4. During the modeling process the intensities of the subpeaks are constrained to match the molar fraction predicted by models.

For tetrahedrally coordinated Si in crystalline as well as amorphous silicates and aluminosilicates $\delta(^{29}\text{Si})$ ranges from -60 to -120 ppm. This chemical shift region is split into smaller subregions, depending on the degree of polymerization of SiO$_4$ units. Fully polymerized Q^4 units exhibit chemical shifts in the range -100 to -120 ppm, and the introduction of a NBO lowers the shielding of the ^{29}Si nucleus by $5-10$ ppm for each NBO,[22-24] resulting in characteristic shifts toward higher frequency for Q^3, Q^2, Q^1, and Q^0 SiO$_4$ tetrahedra. Furthermore, the replacement of a Si−O−Si by a Si−O−Al bond results in a similar shift ($\sim$5 ppm) toward higher frequency,[8,22,24,25] preventing an unambiguous distinction of different Si($Q^{ni}(m_i$Al)) units from the chemical shifts alone, for example, a Si(Q^4(2Al)) unit may exhibit the same chemical shift as a Q^3(0Al) SiO$_4$ tetrahedron.

To test the validity of the R-IRO and HQ-IRO models, the ^{29}Si MAS NMR spectra are deconvolved using a sum of Gaussian shaped resonances corresponding to the different types of Si($Q^{ni}(m_i$Al)) units with relative intensities equal to the molar fractions predicted by the models (Tables 3 and 4).

$$f(x) = \sum_{i=1}^{15} \frac{a_i}{w \cdot \sqrt{\pi/2}} \exp\left[\frac{-2(x - x_{0i})^2}{w^2}\right]$$

$$= \sum_{i=1}^{15} \frac{a_i}{w \cdot \sqrt{\pi/2}} \exp\left[\frac{-2(x - \delta(Q^{n_i}(m_i\text{Al})))^2}{w^2}\right] \quad (3)$$

Thus, the ^{29}Si NMR resonances are described as a sum of Gaussian distributions (eq 3) where a_i is the relative area (i.e., the molar fraction) for a given structural unit and x_{0i} is the center of the resonance corresponding to the chemical shift $\delta(Q^{ni}(m_i$Al)). During the deconvolutions a_i is assumed to have a constant value, corresponding to the values listed in Tables 3 and 4. The relation between i, n_i, and m_i for the different $\delta(Q^{ni}(m_i$Al)) units are given by the last three rows in Table 3. The line width w is equal to 2σ, where σ is the standard deviation, and the relation between w and the full width at half-maximum (FWHM) is FWHM $= 2\sigma(2\ln 2)^{1/2} \approx 1.18w$.

FWHM is expected to be of the order of $\sim$10 ppm for glasses, which is approximately 1 order of magnitude larger than the line widths observed for crystalline samples with similar compositions.[8,49] The increased line width observed for amorphous samples is caused by the distribution of bond angles and atomic distances present in these materials. The line width is assumed to be constant for all samples in the deconvolutions, which is considered a reasonable approximation, taking into account that the different glasses are synthesized under nearly identical conditions, that is, similar cooling rates, using the same starting materials. Thus, all 10 glasses are expected to exhibit similar bond-angle and atomic distance distributions. The line width is additionally dependent on the chemical environment of the Si nuclei. However, the broadening caused by different atoms in the first and second coordination spheres to Si is expected to be of minor importance for the glasses as compared to similar crystalline materials. The reason for this is that the resonances are already broadened because of the bond angle and atomic distance distributions within the glass. Furthermore, line broadening from ^{29}Si−^{29}Si dipolar interactions is negligible because of the low ^{29}Si natural abundance while heteronuclear ^{27}Al−^{29}Si dipolar couplings and ^{29}Si chemical shift anisotropies are efficiently averaged out by magic-angle spinning. The usage of a constant line width within the modeling is discussed in greater detail later. The dependencies of chemical shift on the degree of polymerization of SiO$_4$ tetrahedra (n: the number of BO linked to Si) and on the incorporation of Al in the second coordination sphere (m: the number of Al) are assumed to be additive, that is, the chemical shift for a $Q^{ni}(m_i$Al) unit can be expressed by

$$x_{0i} = \delta(Q^{n_i}(m_i\text{Al}))$$

$$= \delta(Q^4(0\text{Al})) + (4 - n_i)A + m_i B \quad (4)$$

A deconvolution is performed for all 10 glasses simultaneously. A master spectrum is created combining all 10 ^{29}Si NMR resonances each shifted 60 ppm from the previous one in the direction of lower frequencies. Only signals in the range from -60 ppm to -120 ppm (original spectrum) are used. The deconvolution is then performed by subtracting the total ppm-shift from the $\delta(Q^4(0\text{Al}))$ value for each resonance, for example, 2×60 ppm is subtracted from $\delta(Q^4(0\text{Al}))$ of C$_{34}$A$_{11}$S$_{55}$, and 4×60 ppm is subtracted from $\delta(Q^4(0\text{Al}))$ of C$_{43}$A$_{13}$S$_{44}$. The fitting procedure is performed by the scaled Levenberg−Marquardt algorithm, using reasonable starting values for the four unknown parameters, that is, $w = 8.5$ ppm (corresponding to FWHM $= 10$ ppm), $\delta(Q^4(0\text{Al})) = -110$ ppm, $A = 7.5$ ppm, and $B = 5$ ppm. The validity of a model requires that the overall line shape of the ^{29}Si NMR resonance for each glass is matched by the deconvolution and that reasonable values for the four parameters are obtained.

(49) Greaves, G. N.; Meneau, F.; Kargl, F.; Wardi, D.; Holliman, P.; Albergamo, F. *J. Phys.: Condens. Matter* **2007**, *19*, 415102.
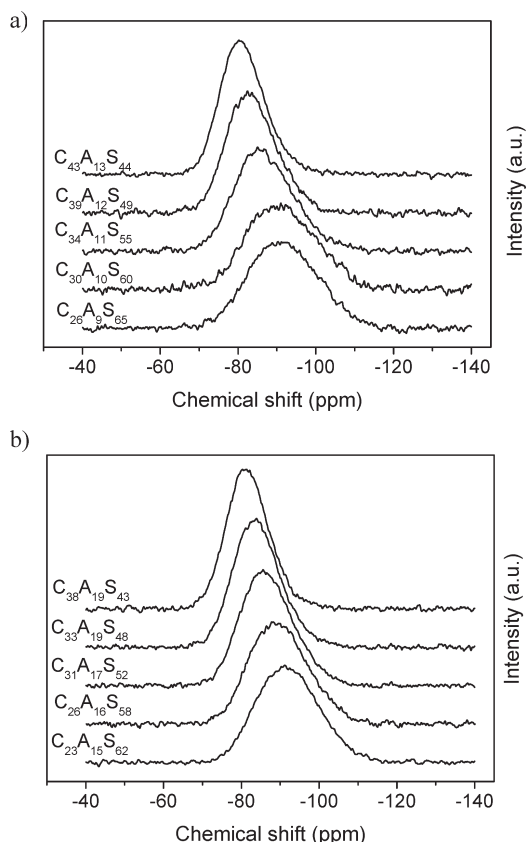
a)

b)

Figure 2. ^{29}Si MAS NMR spectra of the two series of calcium alumino-silicate glasses corresponding to the compositions (a) series 1, $C_{26}A_9S_{65}$ to $C_{43}A_{13}S_{44}$ and (b) series 2, $C_{23}A_{15}S_{62}$ to $C_{38}A_{19}S_{43}$. The spectra have been recorded under identical conditions at 7.05 T, using the spinning speed of $\nu_R = 7.0$ kHz and a 120 s relaxation delay.

4. Results

4.1. ^{29}Si MAS NMR. Figure 2 shows the ^{29}Si MAS NMR spectra for the 10 glasses, each including a broad resonance with a line width (FWHM) ranging from 12.7 ppm ($C_{38}A_{19}S_{43}$) to 22.3 ppm ($C_{26}A_9S_{65}$). The resonances shift toward higher frequencies within each series, that is, $C_{26}A_9S_{65}$ to $C_{43}A_{13}S_{44}$ and $C_{23}A_{15}S_{62}$ to $C_{38}A_{19}S_{43}$, which reflects the increase in the content of both Ca_{excess} and Al. The resonance lineshapes and widths of the individual spectra are simulated using the deconvolution procedure described in section 3.5, to evaluate the models for the intermediate-range order in the glasses.

4.2. R-IRO Model. The predicted intensity distributions for the ^{29}Si subpeaks, obtained with the random IRO model, cannot be validated from simulations of the ^{29}Si MAS NMR spectra constraining the intensity of each subpeak to match the molar contents predicted in Table 3. The simultaneous deconvolution of all 10 ^{29}Si resonances provides a poor fit to the experimental data with a correlation coefficient of $R^2 = 0.237$, as illustrated in Figure 3 for $C_{26}A_9S_{65}$ to $C_{43}A_{13}S_{44}$. In addition, the resulting values of the four unknown fitting parameters, $w = 29.5 \pm 0.2$ ppm, $\delta(Q^4(0Al)) = 33 \pm 1$ ppm, $A = -119 \pm 1$ ppm and $B = -60 \pm 1$ ppm, are far from the expected values discussed in section 3.5. Figure 4 shows the distribution of subpeaks for the individual $Si(Q^{ni}(m_iAl))$ units and the final description of the ^{29}Si resonances for
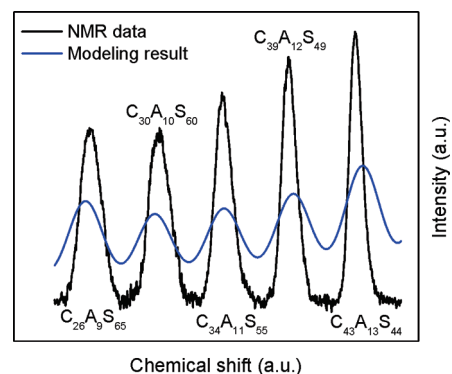

Figure 3. Result from simultaneous deconvolution of the resonances in all 10 ^{29}Si MAS NMR spectra using the R-IRO model, illustrated here for series 1, that is, $C_{26}A_9S_{65}-C_{43}A_{13}S_{44}$.

a)

b)
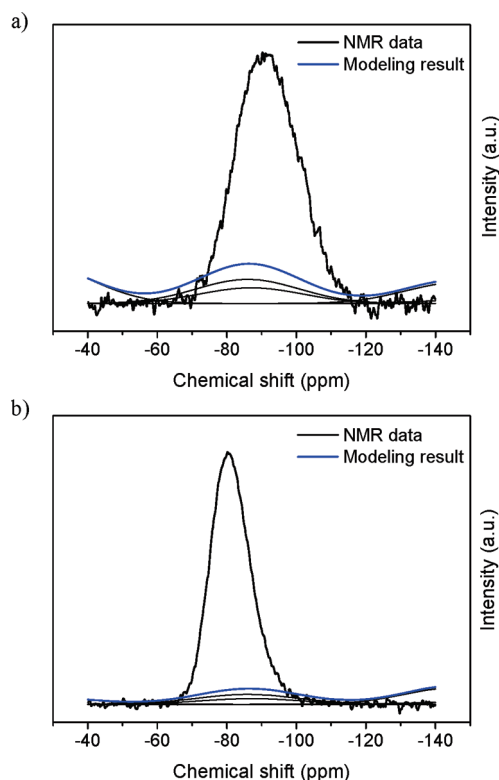
Figure 4. Deconvolution of the ^{29}Si NMR resonances for (a) $C_{26}A_9S_{65}$ and (b) $C_{43}A_{13}S_{44}$ using the R-IRO model. The experimental spectra are shown by thick black lines whereas the thin black lines illustrate the subpeaks originating from individual structural units. The sum of the deconvoluted resonances is shown by the blue line.

$C_{26}A_9S_{65}$ and $C_{43}A_{13}S_{44}$ from series 1. The difference between Figure 3 and 4 is because a large part of the intensity for the given sample is positioned outside the range of the experimental signal for that sample.

4.3. QH-IRO Model. When the intensities of the subpeaks are constrained to the contents of the different structural $Q^n(mAl)$ units predicted by the quasi-heterogeneous IRO model, convincing agreements are achieved between the deconvoluted and experimental ^{29}Si MAS NMR spectra for all 10 glasses. This is illustrated in Figure 5 while the optimized values of the four unknown parameters (w, $\delta(Q^4(0Al))$, A, and B) are summarized in Table 5. Reasonable values of the four unknown parameters from eqs 3 and 4 are

Table 5. Optimized Parameters, w, $\delta(Q^4(0Al))$, A, and B, from Deconvolutions of the ^{29}Si MAS NMR Spectra Using the QH-IRO Model[a]

w (ppm)	FWHM[b] (ppm)	$\delta(Q^4(0Al))$ (ppm)	A (ppm)	B (ppm)	R^2
10.71 ± 0.03	12.61 ± 0.04	-100.75 ± 0.06	8.61 ± 0.04	3.92 ± 0.01	0.964

[a] The uncertainties are given as the standard deviations obtained from the fitting procedure. [b] FWHM is the full width at half-maximum, FWHM $\approx 1.18w$.
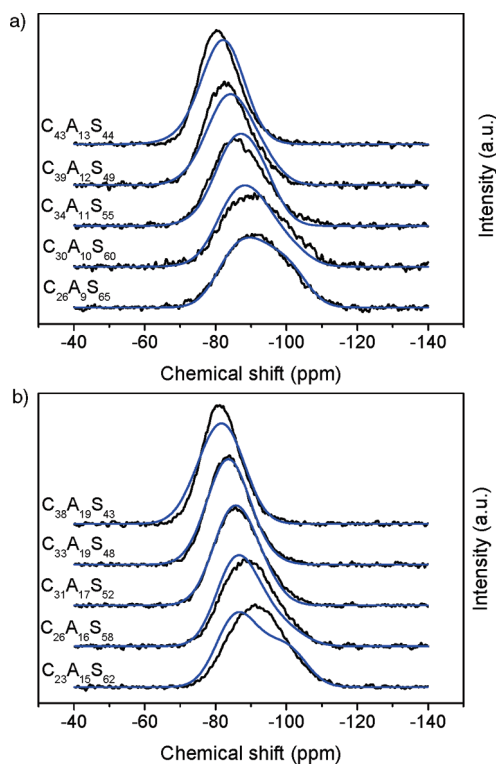
Figure 5. Deconvolutions of the ^{29}Si MAS NMR spectra for all glasses. The spectra are deconvoluted simultaneously using the QH-IRO model. The experimental spectra are shown by a black lines whereas the blue line illustrates the modeling result.

Figure 6. Deconvolution of the ^{29}Si NMR resonances for (a) $C_{26}A_9S_{65}$ and (b) $C_{43}A_{13}S_{44}$ using the QH-IRO model. The experimental spectra are shown by thick black lines whereas the thin black lines illustrate the subpeaks originating from individual structural units. The sum of the deconvoluted resonances is shown by the blue line.

obtained. The sum of the individual resonances provides an excellent fit to the experimental data, that is, $R^2 = 0.964$ for the simultaneous deconvolution of all 10 resonances.

The sensitivity of the optimized values for w, $\delta(Q^4(0Al))$, A, and B to the initial parameters used in the fitting procedure is tested. In this examination the starting values of w, A, and B are varied in the range $\pm 50\%$ of the original values, that is, $w = 8.5$ ppm, $A = 7.5$ ppm, and $B = 5$ ppm. The initial value for $\delta(Q^4(0Al))$ is varied in the range $\pm 10\%$ of the original shift, $\delta(Q^4(0Al)) = -110$ ppm. Different combinations of the starting values are used, for example, the largest value of $\delta(Q^4(0Al))$ ($\delta(Q^4(0Al)) = -120$ ppm) combined with the smallest values of A and B ($A = 3.75$ and $B = 2.5$) as the values of these parameters affect the result in opposite directions. The different combinations of starting values lead in all cases to values within the uncertainty limits of the parameters given in Table 5. Thus the parameters in Table 5 correspond to a strong local minimum obtained by the fitting procedure. In addition, the uncertainties associated with the four unknown parameters, given as the standard deviation obtained from the fitting procedure, are observed to be very small (i.e., $\sim 0.5\%$ for A which shows the largest relative uncertainty). Thus, the analysis above shows that it is possible to obtain an excellent description of all 10 ^{29}Si resonances
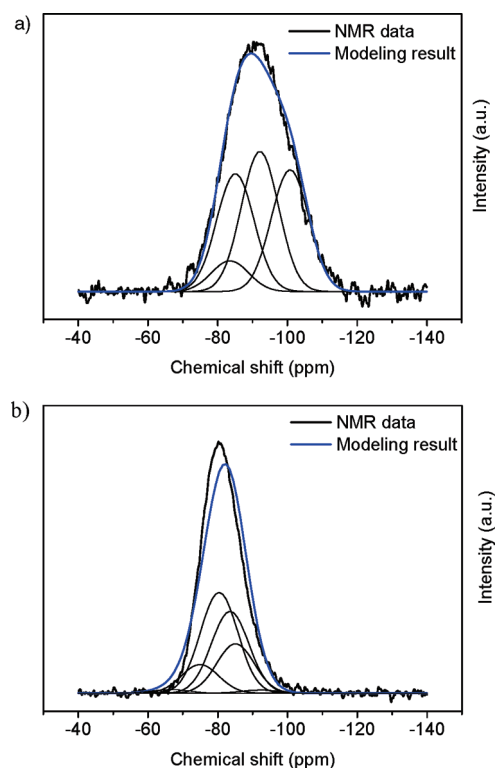
simultaneously, applying a structural model based on a quasi-heterogeneous IRO with just four unknown parameters which are determined with high precision (Table 5).

The individual descriptions of the resonances for each glass using the values of w, $\delta(Q^4(0Al))$, A, and B stated in Table 5 provide correlation coefficients (R^2) which range from 0.927 ($C_{23}A_{15}S_{62}$) to 0.996 ($C_{33}A_{19}S_{48}$) with an average of 0.970. Figure 6 shows the distribution of subpeaks for the individual Si($Q^{ni}(m_iAl)$) units along with the final simulation of the ^{29}Si resonances for $C_{26}A_9S_{65}$ and $C_{43}A_{13}S_{44}$.

4.4. ^{27}Al MAS NMR. The ^{27}Al MAS NMR spectra (9.39 T) of the 10 glasses strongly suggest that Al is only present in tetrahedral coordination and mainly involved in Al–O–Si linkages, since the centerband resonances mainly cover the spectral range of tetrahedrally coordinated Al[50] with centers of gravity ranging from 45–52 ppm (Table 6). In addition, the ^{27}Al MAS NMR spectra of $C_{23}A_{15}S_{62}$ and $C_{38}A_{19}S_{43}$ recorded at 14.09 T (Figure 7) support these findings, since these spectra include similar centerband resonances, however, with smaller line widths (FWHM = 22.3 ppm for $C_{23}A_{15}S_{62}$ and FWHM = 21.8 ppm for $C_{38}A_{19}S_{43}$)

(50) Müller, D.; Gessner, W.; Behrens, H. J.; Scheler, G. *Chem. Phys. Lett.* **1981**, *70*, 59.

Table 6. Centers of Gravity and Line Widths Observed in the ^{27}Al and ^{29}Si MAS NMR Spectra and in the Simulated ^{29}Si NMR Spectra Using the QH-IRO Model

	$\delta_{cg}(^{27}Al)^a$ (ppm)	FWHM$(^{27}Al)^a$ (ppm)	$\delta_{cg}(^{29}Si)^b$ (ppm)	FWHM(exp)^b (ppm)	δ_{cg}(QH-IRO)^c (ppm)	FWHM(QH-IRO)^c (ppm)
$C_{26}A_9S_{65}$	45.3	34.7	−92.4	22.3	−91.6	23.5
$C_{30}A_{10}S_{60}$	46.0	34.5	−90.9	23.1	−89.4	19.6
$C_{34}A_{11}S_{55}$	47.8	32.3	−87.4	17.7	−87.4	16.9
$C_{39}A_{12}S_{49}$	50.1	31.2	−84.0	15.4	−84.6	16.7
$C_{43}A_{13}S_{44}$	51.4	31.6	−81.6	13.3	−81.9	14.4
$C_{23}A_{15}S_{62}$	45.8	36.3	−91.8	19.2	−90.0	23.3
$C_{26}A_{16}S_{58}$	46.8	35.4	−89.5	18.4	−88.0	16.5
$C_{31}A_{17}S_{52}$	48.8	34.4	−86.6	15.9	−86.2	15.4
$C_{33}A_{19}S_{48}$	50.4	33.7	−84.0	13.9	−83.7	14.4
$C_{38}A_{19}S_{43}$	51.7	34.5	−81.6	12.7	−81.4	15.3

^{a} Center of gravity and line width of the centerband from the central transition observed in the ^{27}Al NMR spectra at 9.39 T. ^{b} Center of gravity and line width of the resonances observed in the ^{29}Si MAS NMR spectra (Figure 2). ^{c} Center of gravity and line width of the simulated ^{29}Si MAS NMR spectra obtained using the QH-IRO model (Figure 5).
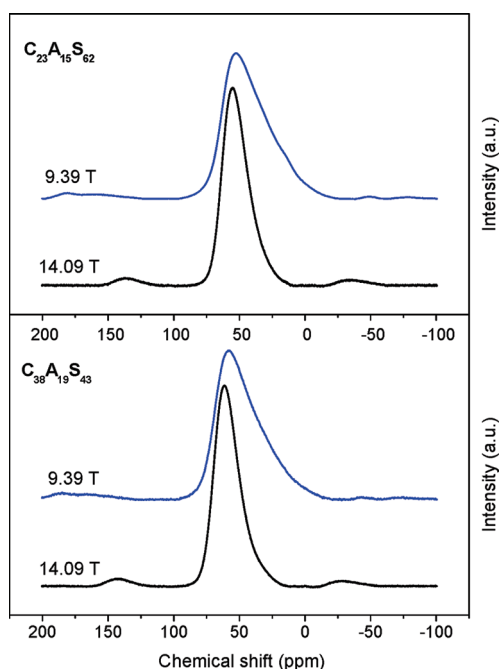

Figure 7. ^{27}Al MAS NMR spectra of $C_{23}A_{15}S_{62}$ and $C_{38}A_{19}S_{43}$ obtained at 9.39 and 14.09 T with spinning speeds of $\nu_R = 12.0$ kHz and $\nu_R = 13.0$ kHz, respectively.

and high-frequency shifts of the centers of gravity ($\delta_{cg} = 52.7$ ppm for $C_{23}A_{15}S_{62}$ and $\delta_{cg} = 59.2$ ppm for $C_{38}A_{19}S_{43}$) as compared to the resonances at 9.39 T. This reflects the inverse proportionality of the second-order quadrupolar broadening with the magnetic field strength. Isotropic chemical shifts from 55−65 ppm are characteristic for Al(OSi)$_4$ sites,[31,51,52] indicating that such sites are the dominant Al^{3+} environments in the glasses. Thus, these observations support the assumptions made in the modeling of the IRO of the calcium aluminosilicates.

For both series the centers of gravity for the ^{27}Al centerbands are observed to shift slightly toward higher frequency (Table 6 and Figure 7), indicating some changes in the local ^{27}Al environments. In analogy to

the ^{29}Si chemical shifts, it is expected that the introduction of a NBO linked directly to Al induces a displacement of the chemical shift toward larger frequencies.[53] A similar effect on the ^{27}Al chemical shift is expected if Al−O−Al bonds replace Al−O−Si linkages.[31]

^{27}Al MQMAS NMR investigations of peralkaline CAS glasses with similar compositions as the glasses studied in this work have shown the presence of minor contents of 5-fold coordinated Al in the glasses[54,55] by the observation of AlO$_5$ contents of up to 7%. Thus, minor contents of AlO$_5$ are likely to be present in the glasses investigated in this work, despite no clear observations of these sites from the ^{27}Al NMR spectra in Figure 7 (the effect of these sites on the modeling is discussed later). In agreement with the conclusions drawn from Figure 7, no 6-fold coordinated Al is observed in the previous 27Al MQMAS NMR investigation.[54]

5. Discussion

5.1. Nature of the IRO. The ^{29}Si NMR resonances change systematically within each series of glasses (Figure 2), since the centers of gravity shift toward higher frequency and the line width decreases for the samples $C_{26}A_9S_{65}$−$C_{43}A_{13}S_{44}$ and $C_{23}A_{15}S_{62}$−$C_{38}A_{19}S_{43}$, respectively (Table 6). Consequently, the low-frequency edge of the resonances shifts from about −115 ppm to −100 ppm in the two series, indicating that the glasses $C_{39}A_{12}S_{49}$, $C_{43}A_{13}S_{44}$ and $C_{33}A_{19}S_{48}$, $C_{38}A_{19}S_{43}$ essentially do not contain any Si(Q^4(0Al)) units, which are the most shielded structural components with chemical shifts in the range −100 to −120 ppm.[22−24] According to the R-IRO model, Si(Q^4(0Al)) units are present in all 10 glasses although their content decreases along each series from $C_{26}A_9S_{65}$ to $C_{43}A_{13}S_{44}$ and from $C_{23}A_{15}S_{62}$ to $C_{38}A_{19}S_{43}$. Thus, this model is in contrast to the observed high-frequency shifts of the resonances in the above-mentioned series. The corresponding decrease in the FWHM values, observed experimentally within each series (Table 6), conflicts also with the R-IRO

(51) Müller, D.; Gessner, W.; Samoson, A.; Lippmaa, E.; Scheler, G. *J. Chem. Soc., Dalton Trans.* **1986**, 1277.
(52) Lippmaa, E.; Samoson, A.; Mägi, M. *J. Am. Chem. Soc.* **1986**, *108*, 1730.
(53) Müller, D.; Hoebbel, D.; Gessner, W. *Chem. Phys. Lett.* **1981**, *84*, 25.
(54) Neuville, D. R.; Cormier, L.; Massiot, D. *Chem. Geol.* **2006**, *229*, 173.
(55) Neuville, D. R.; Cormier, L.; Montoullout, V.; Massiot, D. *J. Non-Cryst. Solids* **2007**, *353*, 180.

model, which predicts an increasing number of non-negligible types of structural units as the contents of NBO and Al increases. These discrepancies demonstrate that the R-IRO model cannot describe the ^{29}Si MAS NMR spectra in a satisfactory manner.

The QH-IRO model predicts the presence of detectable contents of Si(Q^4(0Al)) units only for $C_{26}A_9S_{65}$, $C_{30}A_{10}S_{60}$, $C_{23}A_{15}S_{62}$, and $C_{26}A_{16}S_{58}$ whereas Si(Q^3(0Al)) units are the most shielded entities for the remaining glasses (except $C_{38}A_{19}S_{43}$) with an estimated chemical shift of -92.1 ppm. These predictions are in good agreement with the ^{29}Si MAS NMR spectra (Figure 2). In addition, the IRO hierarchy is capable of reproducing the experimentally observed decrease in FWHM within each series as indicated by the data in Table 6. The high-frequency edge of the ^{29}Si NMR resonances (roughly from -74 ppm to -67 ppm, Figure 2) is only shifted slightly toward higher frequency in the series $C_{26}A_9S_{65}-C_{43}A_{13}S_{44}$ and $C_{23}A_{15}S_{62}-C_{38}A_{19}S_{43}$ which may reflect the increasing content of Q^1(0Al) units (and Q^0 for $C_{43}A_{13}S_{44}$) predicted by the QH-IRO model (Table 4). These are the most deshielded structural units, and these species are present in all samples. In general, the Q^n(mAl) units corresponding to a low degree of condensation exhibit somewhat higher intensities for series 1 than series 2 in the QH-IRO model (Table 4) which is in accordance with the slightly lower center-of-gravity frequencies ($\delta_{cg}(^{29}$Si)) observed for series 1 as compared to series 2 (Table 6). Thus, the distribution of structural units predicted from the QH-IRO model is found to approach the experimentally observed distribution and thereby, the QH-IRO model provides a suitable description of the intermediate range order in the CAS glasses, despite small variations between the predicted and the experimental results (Figure 5). The variations between the modeling results and the experimental ^{29}Si NMR resonances may be explained by the strict division between depolymerized calcium silicate regions and highly polymerized regions of alternating SiO$_4$-($^1/_2$Ca)AlO$_4$ units used within the modeling. This very strict division will most likely not be fully retained in the glasses. For example, minor contents of Al can be expected within the depolymerized regions and the 1:1 ratio between Si and Al in the highly polymerized regions is possibly violated to some extent.

Engelhardt et al[56] have investigated the structure of a wide range of CAS compositions, using a similar approach as employed in the present study, and described the structure in terms of a distribution of Si(Q^n(mAl)) structural units. In their work, the applicability of a model also assuming Al to be linked preferentially to the most polymerized Si(Q^n) units is tested and found to provide a reasonable description of the experimental data. This supports the quasi-heterogeneous distribution of Al in the second coordination sphere of Si found in the present study.

Figure 8 illustrates a schematic representation of the intermediate-range structure predicted from the two
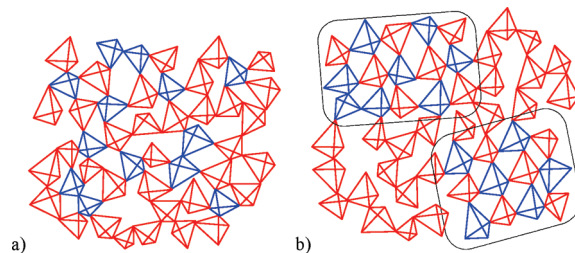
(56) Engelhardt, G.; Nofz, M.; Forkel, K.; Wihsmann, F. G.; Magi, M.; Samoson, A.; Lippmaa, E. *Phys. Chem. Glasses* **1985**, *26*, 157.

Figure 8. Schematic representations of the intermediate-range structure of the CAS glasses projected into two dimensions. Only the network forming tetrahedra are shown in the figure. Oxygen is located in the four corners of the tetrahedron surrounding the cation. The red tetrahedra indicate SiO$_4$ units and the blue tetrahedra represent the ($^1/_2$Ca)AlO$_4$ units. Part (a) illustrates a structural arrangement following the random IRO model while (b) visualizes the hierarchy in the IRO predicted by the quasi-heterogeneous IRO model. The highly polymerized regions of alternating SiO$_4$ and ($^1/_2$Ca)AlO$_4$ units are marked by squares.

modeling approaches. The content of intermediate-range clustering regions is expected to increase in each series as the contents of both Al and NBO increase. Thus, the hierarchy in the intermediate-range order and the degree of heterogeneity increases within each series of glasses, that is, $C_{26}A_9S_{65}$ to $C_{43}A_{13}S_{44}$ and from $C_{23}A_{15}S_{62}$ to $C_{38}A_{19}S_{43}$.

5.2. Structural Role of Al. Both theoretical models, describing the spatial arrangement of structural units in the intermediate range, are based on the distribution of Al around Si and focus only on the identity of the first and second nearest neighbors of Si. For these approaches the fulfillment of the Al avoidance principle within the framework depends on the Si/Al ratio and the content of NBOs bound to Si. It is possible to fulfill the Al avoidance principle for all glasses except $C_{38}A_{19}S_{43}$, if it is assumed that Al is only present as Al(Q^4) units. For $C_{38}A_{19}S_{43}$ at least 17% of Al is expected to be in Al$-$O$-$Al linkages.

The content of Al$-$O$-$Al linkages depends also on the specific model. For example, the random IRO model does not contain any assumption regarding the Al avoidance principle since it is only assumed that no clustering of Al occurs. In the R-IRO model (Table 3) the individual structural units must be accommodated into one continuous network to form the glass, which provides further limits on the Al avoidance as considerable contents of Si$-$O$-$Si bonds are predicted. Using the R-IRO model at least 32% of Al in $C_{26}A_9S_{65}$ take part in Al$-$O$-$Al linkages increasing to 58% for $C_{43}A_{13}S_{44}$. For series 2 the fraction of Al in Al$-$O$-$Al linkages is at least 42% for $C_{23}A_{15}S_{62}$ and 60% for $C_{38}A_{19}S_{43}$. Thus, about 50% of the Al is expected in Al$-$O$-$Al linkages, in agreement with the random nature of the modeling approach. However, these fractions of Al in Al$-$O$-$Al linkages appear unrealistically high since they are significantly larger than those reported for "charge compensated" CAS systems.[10,14]

In the QH-IRO model an alternating SiO$_4-$AlO$_4$ structure is assumed within the highly polymerized Al-containing regions, thus having a Si/Al ratio of 1:1. This means that the Al avoidance principle breaks down when Al is assigned to Si(Q^3), that is, Si associated with only 3 BO. For $C_{26}A_9S_{65}$, $C_{30}A_{10}S_{60}$, $C_{23}A_{15}S_{62}$, and $C_{26}A_{16}S_{58}$

no Al−O−Al linkages are expected since all Al sites are assigned to fully polymerized SiO_4 units. For $C_{34}A_{11}S_{55}$, $C_{39}A_{12}S_{49}$, and $C_{43}A_{13}S_{44}$, the expected fractions of Al in Al−O−Al linkages are 1%, 10%, and 17%, respectively. In series 2, the expected contents of Al in Al−O−Al linkages are 3%, 10%, 19% for $C_{31}A_{17}S_{52}$, $C_{33}A_{19}S_{48}$, and $C_{38}A_{19}S_{43}$, respectively. These degrees of Al avoidance are in the same range as those reported previously for the "charge compensated" CAS systems.[10,14]

As mentioned in section 4.4, the observed shifts in $\delta_{cg}(^{27}Al)$ (Table 6) indicate changes in the local ^{27}Al environment. The high-frequency shift of the resonances within each series may reflect an increase in the content of Al−O−Al linkages as predicted from both models.[31] However, the rather small displacements in centers of gravity (Table 6) seem not large enough to justify the presence of 50% Al in Al−O−Al linkages, which further supports the suitability of the quasi-heterogeneous model in the description of IRO in the CAS system.

The assumption that Al is solely present in tetrahedral coordination seems a good first approximation as this is clearly the dominant structural arrangement for the aluminate species. However, the presence of minor contents of 5-fold coordinated Al (< 7%) is expected to affect the modeling result. So far, the structural role of 5-fold coordinated Al is not fully understood, and it is unclear whether penta-coordinated Al can be regarded as a network former or as a modifying component.[54,55] To charge balance an AlO_5 units an additional positive charge is required as compared to Al in tetrahedral coordination. In this situation the actual content of Ca_{excess} will be lower than assumed in the modeling. This can possibly explain why the high-frequency edge for the majority of the modeling results in Figure 5 is positioned at slightly higher frequencies than the experimental data.

5.3. Variations of the Fitting Parameters. The fitting procedure employs a constant value to describe the dependence of $\delta(^{29}Si)$ on the introduction of NBO, that is, the fitting parameter A. Thus, the displacement of the chemical shift is the same for the introduction of the first NBO as, for example, for the third one. On the basis of comprehensive studies of silicate minerals with different degrees of polymerization, ^{29}Si chemical shift ranges for the different types of Q^n units have been reported.[22−24] Furthermore, from structural modeling of about 50 CAS glasses within a wide compositional range, chemical shifts for the Q^n units have been given by Engelhardt et al.[56] Considering the mean values of each interval combined with the results of Engelhardt et al., a linear regression of these data results in the value for A of 9.6 ± 0.9 ppm.

A similar approach is used to describe the dependency on $\delta(^{29}Si)$ on the replacement of a Si−O−Si by a Si−O−Al bond. From studies of aluminosilicate minerals with zeolite-like compositions, ranges of $\delta(^{29}Si)$ are obtained for the different $Q^4(mAl)$ units.[8,24] The reported ranges suggest that the introduction of one Al in the second coordination sphere results in a displacement of the chemical shift of (6.6 ± 0.3) ppm. Thus, the displacement can be regarded as independent of the number of Al

already introduced within the second coordination sphere of the $Si(Q^4)$ units. However, the absolute values for B found in the previous studies are larger than the B values obtained in this study. This reflects most likely the significant content of depolymerized structural units (Q^n with $n < 4$) present within the glasses of this work. This observation is consistent with the results obtained by spectral editing in ^{29}Si MAS NMR spectra of glasses with anorthite composition.[57] Likewise, variations in the Si/Al ratio are expected to affect the values of both A and B.

The line width of all subpeaks, originating from the different structural units, is during the modeling procedure regarded as a constant parameter. Of course, this is an assumption, as the width is known to depend on both the topological, that is, the distribution of bond angles and distances, and chemical environment of Si. The similar cooling rates, used during the preparation of all 10 glasses, ensure similar bond-angle and atomic distance distributions for all glasses. Thus, it is reasonable to assume that the broadening because of bond-angle and atomic distance disorder is constant for all samples. In a previous study of two series of aluminosilicates glasses on the meta-aluminous limit, the widths of the individual $Si(Q^4(mAl))$ resonances have been determined by modeling of ^{29}Si MAS NMR resonances.[8] For calcium aluminosilicates, FWHM is reported to vary in the range 0.8−1 ppm among the various $Si(Q^4(mAl))$ units, whereas for sodium aluminosilicates, the variation in FWHM is found to be ~2 ppm. The observed variations are not systematic which makes it difficult to incorporate them into the modeling procedure. In addition, the line broadening because of topological disorder diminishes the relative variation of FWHM. The absolute values for FWHM found in previous studies[8,57] (FWHM = 11−13 ppm) is comparable to the results obtained in the present work.

Further improvements of the description of the parameters A, B, and FWHM may, of course, provide more sophisticated modeling procedures and thereby potentially further improve the agreement with experimental data.

5.4. Impact of Structural Heterogeneity on Properties. The viscous behavior and crystallization tendency for the 10 CAS compositions studied in this work have been investigated recently[19] with the aim of finding the optimal composition of glass particles for the potential use as supplementary cementitious materials in blends with Portland cement. In that study it was found that both series only exhibit a weak dependence of the composition on the fragility but a strong compositional dependence of the stability of the glasses toward crystallization during reheating.[19] The melt workability and glass stability affect the applicability of the glasses in technical applications. Thus, it is of special interest to understand correlations between compositional changes and changes in structure and properties.

The observed intermediate-range quasi-heterogeneity, which is characterized by the clustering of highly

(57) Hiet, J.; Deschamps, M.; Pellerin, N.; Fayon, F. *Phys. Chem. Chem. Phys.* **2009**, *11*, 6935.

depolymerized SiO_4 units and highly polymerized AlO_4 and SiO_4 tetrahedra, is expected to influence the physical properties of the 10 CAS glasses and melts. In general, the glasses in series 1 show a larger stability toward crystallization upon reheating as compared to the glasses in series 2. In particular $C_{26}A_9S_{65}$ and $C_{30}A_{10}S_{60}$ exhibit superior stability[19] which may be explained by the observed hierarchy in IRO. The compositions in series 2 have the highest content of Al and for this reason the number of highly polymerized clusters of alternating $SiO_4-(^1/_2Ca)-AlO_4$ units is larger for series 2 as compared to series 1. These cluster regions in the IRO are expected to be frozen in at viscosities of $\eta \approx 10^4$ Pa·s.[39,43] Thus, they will remain in the glass structure during reheating until temperatures markedly above the glass transition are reached. These cluster regions constitute inhomogeneities capable of inducing heterogeneous nucleation. Large numbers of inhomogeneities create the largest reduction of the energy barrier toward crystallization. Another possibility is that clusters exceeding the critical sizes can act as nuclei for the crystallization process. The identity of the crystalline phases formed during heating of the glasses has been determined by powder X-ray diffraction for series 1.[58] Prior to these investigations, the glasses were subjected to a dynamic heating to 1523 at 20 K/min. No crystalline phases are observed in $C_{26}A_9S_{65}$ and $C_{30}A_{10}S_{60}$, whereas crystals are detected in the remaining glasses of series 1, the principal crystalline phases being anorthite, wollastonite, and pseudowollastonite. The composition of anorthite ($CaAl_2Si_2O_8$) corresponds to that expected for the highly polymerized regions of alternating SiO_4 and $(^1/_2Ca)AlO_4$ tetrahedra, whereas the composition of wollastonite and pseudowollastonite ($CaSiO_3$) corresponds to that expected for intermediate-range SiO_4 clusters rich in NBOs. For $C_{43}A_{13}S_{44}$, approximately 10% of the crystals are identified as gehlenite ($Ca_2Al[AlSiO_7]$). This phase is expected to be formed from clusters rich in Al. Thus, the formation of gehlenite in $C_{43}A_{13}S_{44}$ also indicates the breakdown of the Al avoidance principle. A study on the dependence of crystallization on the degree of undercooling for a series of calcium aluminosilicate liquids in the same compositional range as studied in this work also reveals the formation of non-isochemical crystal phases that reflects compositional fluctuations, and hence, structural heterogeneities in the melts. The phases reflecting compositional fluctuations form at low temperatures at which the mobility of the ions is restricted.[59]

Fragility is a measure of the deviation of the melt flow behavior from Arrhenian behavior.[60] A fragile melt exhibit non-Arrhenian behavior, whereas a strong melt has a near-Arrhenian behavior. The fragility reflects the degree of order in a melt where a strong melt generally has a high degree of short-range order while fragile melts do not have well-defined short-range order.[60] The strongest melt known today is pure SiO_2 and addition of a network modifying cation (e.g., Ca) into pure SiO_2 increases the disorder and thus the fragility. The fragility of aluminosilicates is also influenced by the Al content and it has been reported that the fragility of peralkaline CAS melts increases with a decreasing Si/Al ratio.[61] Thus, the fragility is expected to increase within each series of glasses from $C_{26}A_9S_{65}$ to $C_{43}A_{13}S_{44}$ and from $C_{23}A_{15}S_{62}$ to $C_{38}A_{19}S_{43}$, since both the content of NBO and Al increase in these series. However, only a minor compositional dependence of the melt fragility was observed in our recent study,[19] which may reflect the increasing degree of quasi-heterogeneity in the intermediate-range. This increase in IRO may counterbalance the expected increasing short-range disorder as the contents of NBO and Al increase. Thus, the quasi-heterogeneous nature of the IRO may in general account for the compositional dependence of stability of the glasses toward crystallization and fragility as observed for the 10 melts in the CAS system.

5.4. Perspective. As proved above, the nature of the intermediate-range order in CAS glasses is not random. Instead the appearance of the ^{29}Si MAS NMR resonances gives evidence of chemical fluctuations in the intermediate-range of the glass structure. These fluctuations can be described as clustering of highly depolymerized CaO-SiO_2 containing regions and highly polymerized regions of alternating SiO_4 and AlO_4 tetrahedra. Figure 5 shows the good agreement of this quasi-heterogeneous modeling with the experimental results obtained by ^{29}Si NMR. Although the modeling is found to provide a convincing description of the data, minor deviations between the simulated and experimental resonances are observed (Figure 5). To reduce these deviations, future models may consider the following refinements. (i) The content of five-coordinated Al may be probed by ^{27}Al MQMAS NMR and subsequently considered in the modeling approach. (ii) Ab initio calculations of the NMR parameters may be a promising approach, which can potentially be used to estimate influence of the fitting parameters, for example, the width, on variations in chemical and structural environments for the various structural units. (iii) The approach used in this work for obtaining structural information may potentially be combined with other methods, particularly, molecular dynamic simulations,[62] to provide new insight about the local structure of the glasses.

6. Conclusions

In this work, the intermediate-range order (IRO) for 10 peralkaline CAS glasses has been investigated by ^{29}Si MAS NMR in combination with structural modeling. Two approaches for the IRO have been established within the framework of the continuous random network and modified random network models, respectively. The first approach, that is, the R-IRO model, employs a random

(58) Moesgaard, M., unpublished data.
(59) Roskosz, M.; Toplis, M. T.; Richet, P. *J. Non-Cryst. Solids* **2006**, *352*, 180.
(60) Angell, A. *J. Non-Cryst. Solids* **1991**, *131−133*, 13.
(61) Solvang, M.; Yue, Y. Z.; Jensen, S. L.; Dingwell, D. B. *J. Non-Cryst. Solids* **2004**, *336*, 179.
(62) Vargheese, K. D.; Tandia, A.; Mauro, J. C. *J. Chem. Phys.* **2010**, *132*, 194501.

spatial arrangement of Al within the second coordination sphere to Si whereas the key factor of the second model, that is, the QH-IRO model, is the clustering of regions rich in highly polymerized AlO_4 and SiO_4 units and other regions rich in highly depolymerized SiO_4 units. This clustering is described as a hierarchy in the IRO. The applicability of the two modeling approaches to describe the structure of the peralkaline CAS glasses has been examined by deconvolution of experimental ^{29}Si MAS NMR spectra using subpeaks for the different structural units with relative intensities predicted from the models. The quasi-heterogeneous modeling approach, emphasizing a hierarchy in the IRO, results in good agreements between the simulated and experimental ^{29}Si MAS NMR spectra for all 10 glasses. In contrast, the random modeling approach is not capable of reproducing the ^{29}Si NMR resonances in a satisfactory manner. Thus, the structure of the glasses studied in the present work is dictated by a quasi-heterogonous IRO. Furthermore, the IRO hierarchy approach may explain the compositional dependences of the glass stability against crystallization, the glass forming ability and the fragility for the 10 glass systems.

Paper IV

OPTIMAL COMPOSITION OF CALCIUM ALUMINOSILICATE GLASS PARTICLES USED AS SUPPLEMENTARY CEMENTITIOUS MATERIALS

METTE MOESGAARD[*], DUNCAN HERFORT[**], LISE FRANK KIRKEGAARD[**], and

YUANZHENG YUE[*]

[*]*Section of Chemistry, Aalborg University, Sohngaardsholmsvej 57, 9000 Aalborg, Denmark*
[**]*Aalborg Portland, Rørdalsvej 44, 9220 Aalborg Øst, Denmark*

ABSTRACT

In this work, we investigate the potential use of CaO-Al_2O_3-SiO_2 glass particles as supplementary cementitious materials (SCM). A requirement for the glass as a useful candidate for SCMs is that the overall CO_2 emissions caused by cement production should be reduced significantly by replacing part of the cement with glass. This can be obtained by compositional modifications aiming at minimizing both the "process CO_2" and "fuel-derived CO_2" linked with glass production and maximizing the pozzolanic reactivity of the glass. A high pozzolanic reactivity ensures an acceptable performance of the final mortar or concrete. Based on the glass characteristics and testing of pozzolanic reactivity, we find that the glasses prepared from the naturally occurring minerals (clay, limestone and sand) are promising SCMs.

KEYWORDS:

CO_2 emission, Portland cement, supplementary cementitious materials, pozzolanity

INTRODUCTION

CO_2 emissions from human activity are widely recognized as the major cause of global warming observed over recent decades. Energy intensive industries are therefore making considerable efforts to reduce their CO_2 emissions. The production of Portland cement (PC) is one of these energy intensive industries, and it is estimated that the cement industry today accounts for approximately 5% of the global man-made CO_2 emissions (Damtoft, et al., 2005; Rehan & Nehdi 2005; Worrel, et al., 2001). Most of this CO_2 originates from the decarbonation of limestone which constitutes 80-85% of the raw materials for clinker production. This is referred to as "process CO_2". One strategy for reducing the CO_2 emissions from the cement industry is to reduce the clinker content in the cement. The clinker is partly substituted by alternative materials producing so-called composite cements. These alternative materials are referred to as supplementary cementitious materials (SCMs). It is important that the SCMs contribute positively to the final cement performance. Most SCMs are either latently hydraulic, such as granulated blast furnace slag, or pozzolanic, such as fly ash or silica fume. A pozzolan is defined as a silica or aluminosilica containing material that alone does not possess hydraulic reactivity but when mixed with calcium hydroxide and water reacts to form strength giving hydration products (Taylor, 1997). These materials are usually by-products from other industries and therefore do not contribute to the CO_2 emission of the cement production. In practice, the use of these materials is limited by their availability, transport costs and competition with other industries. At present they are almost fully utilized in Western Europe. Further reduction of the clinker content, therefore, requires new sources of alternative SCMs (Damtoft, et al., 2005; Rehan & Nehdi 2005; Worrel, et al., 2001). In addition, the demand for cement, especially in developing countries is expected to rise significantly over the coming decades placing even greater burden on the cement industry to reduce emissions (Damtoft, et al., 2005; Humphreys & Mahasenan 2002).

Possible candidates for alternative SCMs are calcium aluminosilicate (CAS) glass particles. CAS glass is composed of the same oxides found in Portland cement and the thermodynamic instability of glass is expected

to provide hydraulic reactivity. Hence the glass is expected to take part in the strength giving reactions occurring during cement hydration. In recent years, several studies have focused on the use of waste glass as SCMs. These studies have confirmed the hydraulic reactivity of the glass when mixed with cement. Glass can thus be considered as a pozzolan. Waste glass is however also a limited resource (Shi & Zheng 2007; Shayan & Xu 2006; Shi, et al., 2005; Schwarz, et al., 2008). In this work, we attempt to engineer CAS glass particles having a composition optimized for utilization as an SCM. This is done by considering both the extent to which the glass will take part in the hydration reactions and thus contribute to the strength of the composite cement, but also the amount of CO_2 released during glass production. In practice this is done by taking into account the consumption of limestone, practical melting temperature and pozzolanity of the glass. The first two characteristics are related to the energy and therefore CO_2 consumption during production.

For full scale production to be economically viable, the glass particles must be produced from low cost and locally available raw materials. Conventional raw materials i.e., clay, limestone and sand are therefore chosen. The raw materials are of course mixed in other proportions than for cement production. Investigations were first performed on a three component model system, i.e., the CaO-Al_2O_3-SiO_2 system (Moesgaard & Yue 2009; Moesgaard, et al., in press). These are the major oxides in the raw materials and account for 90% of the oxides in PC. Subsequently impurities present in naturally occurring minerals were introduced to test the effects on the characteristics of the glass. Four glass compositions were investigated in this work corresponding to the optimum composition found from investigations on the three component model system (Moesgaard & Yue 2009; Moesgaard, et al., in press) ($C_{26}A_9S_{65}$) and three compositions based on the naturally occurring minerals (referred to as the CLS glasses). The compositions of the glasses and that of ordinary PC are given in Table 1 and illustrated by the ternary CaO-Al_2O_3-SiO_2 phase diagram shown in Figure 1.

Table 1: Oxide compositions (mol%) of the five glasses investigated.

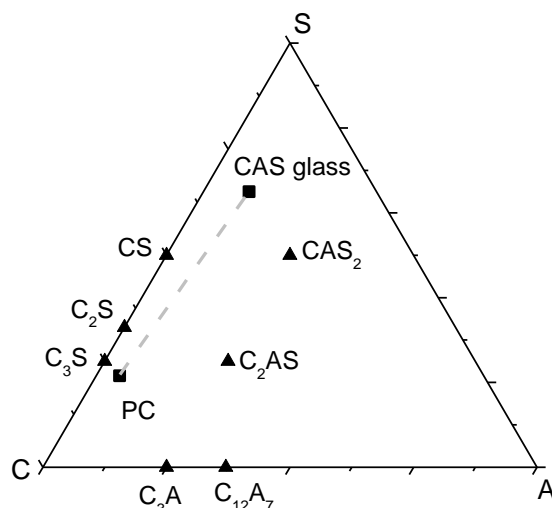|	PC cement	$C_{26}A_9S_{65}$	CLS_{1N}	CLS_{5N}	CLS_{9N}
SiO_2	19.2	64.9	59.1	56.1	53.9
Al_2O_3	3.5	9.3	8.2	7.9	7.7
Fe_2O_3	1.5	-	3.0	2.9	2.8
CaO	70.8	25.8	22.1	21.2	21.3
MgO	1.5	-	4.2	3.9	3.9
K_2O	0.3	-	1.7	2.0	1.6
Na_2O	0.2	-	1.2	5.4	8.2
SO_3	2.8	-	<0.1	0.2	0.2
TiO_2	0.2	-	0.5	0.5	0.5

Figure 1: Molar ternary CaO-Al$_2$O$_3$-SiO$_2$ phase diagram. Squares indicate the compositions of Portland cement (PC) and the CAS glasses under investigation (Table 1). Selected binary phases within the relevant compositional range are indicated by triangles. The traditional nomenclature with C, A and S representing CaO, SiO$_2$ and Al$_2$O$_3$, respectively, is used. Mixes of PC and the glass particles plot along the dashed line.

EXPERIMENTAL

The glasses were synthesized by melting the batch in a Pt$_{90}$Rh$_{10}$ crucible in air atmosphere (furnace: model SF6/17 Entech, Ängelholm, Sweden). For the model system glass, the batch was obtained by mixing the analytical chemicals SiO$_2$, Al$_2$O$_3$ and CaCO$_3$. A two-step melting process was carried out. First, the batch was melted at 1550°C for 2 hours. The melt was subsequently quenched in water to obtain crushed fragments. The crushed glass was remelted at 1550°C for another 2 hours and cast on a graphite plate. The glass was annealed at 800 °C, i.e. at approximately the glass transition temperature (T_g), for 10 minutes, and cooled slowly after switching off the furnace.

Clay (bentonite) for glass preparation was provided by Dantonit A/S Odense, Denmark. Sand and limestone were provided by Aalborg Portland A/S, Aalborg, Denmark. Analytical Na$_2$CO$_3$ was introduced to provide additional Na$_2$O. Prior to melting in the Pt$_{90}$Rh$_{10}$ crucible the clay was heat treated at 900°C for 3 hours (heating rate of 10°C /min) to remove any organic material. The batch was homogenized using a mortar and then melted at 1450°C for 3 hours. The melt was cast on a graphite plate and annealed at 700 °C or 650 °C for 10 minutes, and naturally cooled inside the furnace. The chemical compositions of the glasses were determined by standard wet chemical analysis at Aalborg Portland A/S.

In the low viscosity range (approx. 10^0-10^3 Pa·s), the viscosity (η) was measured using concentric cylinder viscometry. The furnace was a box furnace (model HT 7, Scandiaovnen A/S, Allerød, Denmark) and the viscometer head was a Physica Rheolab MC1 (Paar Physica, Stuttgart, Germany).

For tests of pozzolanity, the glass was ground to pass a 75 μm sieve. 1.00 g glass powder (1.5·10^{-2} mol) and 1.00 g Ca(OH)$_2$ (1.3·10^{-2} mol) were mixed with 100 mL freshly boiled water and stored in a closed container for 7 days at 40°C. During storage the mixture was shaken with a horizontal rotary motion. The mixture was filtered and the filtrate was stored for further analyses. For solid-state NMR investigations the collected solid was dried over silica gel in a desiccator. For determination of the mass of unreacted glass the collected solid

was washed with a weak acetic acid solution to dissolve remaining $Ca(OH)_2$ and any hydration products formed. The washed glass was dried over silica gel in a desiccator.

Solid-state [29]Si MAS (magic angle spinning) NMR (nuclear magnetic resonance) spectra were recorded at 39.8 MHz on a Varian INOVA-200 (4.7 T) spectrometer whereas the ^{27}Al MAS NMR spectra were recorded at 104.2MHz on Varian INOVA-400 (9.39 T) (14.09 T) spectrometers. The [27]Al and [29]Si isotropic chemical shifts were reported relative to a 1.0 M aqueous solution of $AlCl_3 \cdot 6H_2O$ and neat tetramethyl silane (TMS), respectively.

RESULTS AND DISCUSSION

The initial investigations on the three component $CaO\text{-}Al_2O_3\text{-}SiO_2$ system focused on the compositional range of the eutectic compositions of anorthite-wollastonite-tridymite and anorthite-wollastonite-gehlenite. This compositional range involves significantly lower CO_2 emission from decarbonation compared to Portland cement. Furthermore the eutectic compositions correspond to minimum temperature on the liquidus surface implying that the glasses can be produced at relatively low temperatures. Last but not least, it is expected that glasses within this compositional range can be produced without forced cooling (Mysen & Richet 2005). From these investigations we chose to focus on the eutectic composition of anorthite-wollastonite-tridymite, i.e. $C_{26}A_9S_{65}$ (Table 1) (Moesgaard & Yue 2009; Moesgaard, et al., in press). In this work this composition is targeted using the naturally occurring minerals. The target composition is obtained by mixing the raw materials in the following proportions by weight; 63% bentonite, 31% limestone, 6% quartz sand. This corresponds to the CLS_{1N} glass. The subscript indicates the molar content of Na_2O. The use of these minerals introduces approx. 10% impurities (Table 1). These are mainly MgO, Fe_2O_3 and alkali oxides. CLS_{5N} and CLS_{9N} containing 5 and 9 mol% Na_2O, respectively, is produced to investigate the effect on the characteristics of the glass of introducing additional alkali oxide. In an industrial scale production the alkali content could be increased e.g. by addition of cement kiln dust or Na_2SO_4.

CO_2 emissions from glass production

During cement production most of the CO_2 emission is caused by decarbonation of limestone, i.e., the so-called "process CO_2". As limestone is also used to provide the CaO in the glass this is also an important factor during glass production and the quantity of "process CO_2" released during production is directly linked to the CaO content of the material. Minor variations in the composition of PC are observed worldwide depending on the local raw materials deposits. PC of the composition given in Table 1 results in the release of 516 kg "process CO_2" per tonne cement produced. In contrast the production of the glasses $C_{26}A_9S_{65}$ and CLS_{1N} results in 180 and 175 kg "process CO_2" per tonne glass. This constitutes only approx. 30% of the CO_2 released from decarbonation during production of PC. Comparable quantities of "process CO_2" are released from the three CLS glasses.

The other major contributor to the CO_2 released from cement and glass production is the so-called "fuel-derived CO_2". This is derived from the burning of fossil fuels needed to obtain the high temperatures of production and can be reduced by choosing a composition with a relatively low melting temperature hereby reducing the operating temperature of the melting furnace (Beerkens, 2004; Conradt, 2000). The temperature of importance during glass production is the so-called practical melting temperature (T_{pm}) . In this work T_{pm} is defined as the isokom temperature corresponding to a viscosity of 10 Pa·s. This viscosity will ensure a reasonable flow and workability of the glass melt. T_{pm} is determined by interpolation from the viscosity-temperature data determined by viscometry (Table 2). From the table it is observed that $T_{pm}(C_{26}A_9S_{65})$ is even higher than the production temperature of PC (1450-1500°C). The introduction of approx. 10% minor components from the minerals has a pronounced effect on the melting temperature which is reduced by almost 200°C from $C_{26}A_9S_{65}$ to CLS_{1N}. The introduction of additional Na_2O further reduces the practical melting temperature.

Table 2: Practical melting temperature (T_{pm}) and degree of pozzolanic reactivity for the four compositions under investigation. T_{pm} is given as the isokom temperature at $\eta = 10$ Pa·s, and the degree of pozzolanic reactivity refers to the reactivity of the glass (wt%) with Ca(OH)$_2$ and water after 7 days.

	$C_{26}A_9S_{65}$	CLS_{1N}	CLS_{5N}	CLS_{9N}
T_{pm} (°C)	1527	1346	1329	1285
Degree of pozzolanic reactivity (%)	11.6	14.1	16.3	21.6

The CLS glasses can be produced at temperatures significantly lower than used for cement production. This is expected to have a pronounced effect on the "fuel-derived CO$_2$" especially by reduction of the major energy losses, i.e. the heat carried by the flue gas and the furnace wall and opening losses. Particularly the wall and opening losses are of importance as this energy normally cannot be recovered (Sardeshpande, et al,, 2007). Another parameter affecting the "fuel-derived CO$_2$" is the energy of reactions. During glass production the energy of fusion (~500 kJ/kg glass) (Bouhifd, et al., 2007) is of importance, whereas the energy of calcination (~1800 kJ/kg CaCO$_3$) is relevant for both glass and cement production. The reduced content of CaO in the CLS glasses relative to PC will therefore affect both the "process CO$_2$" but also the "fuel-derived CO$_2$".

Pozzolanity of glass

The SCMs are most often less reactive than PC. Therefore a partial substitution of PC with SCM will reduce the compressive strength compared to the pure cement. The most significant reductions are most often observed for the early strength (Shi & Zheng 2007; Massazza 2007). To ensure acceptable performance of the final mortar or concrete without being forced to increase the content of the composite cement it is of importance to minimize this reduction in compressive strength. This is possible if the SCM exhibits pozzolanity and therefore contributes to the strength giving reactions taking place during hydration. In this work the pozzolanic reactivity of the glasses is tested as the reactivity of glass particles in a saturated Ca(OH)$_2$ solution. The alkalinity of the Ca(OH)$_2$ solution resembles the pore solution of cement paste and mortar. The degree of pozzolanic reactivity is quantified as the fraction of glass that has reacted with Ca(OH)$_2$ and water after 7 days.

During cement hydration Si is mainly incorporated into the C-S-H phase. This is an amorphous calcium silicate hydrate. The C-S-H phase is formed as the isolated SiO$_4$ tetrahedra within alite and belite, i.e., Q^0 units, react with water to form polymerized chains consisting of Q^1 and Q^2 units. The formation of C-S-H can thus be followed by means of ^{29}Si solid state MAS NMR as this method allows one to distinguish between SiO$_4$ tetrahedra of different degrees of polymerization, i.e., Q^0, Q^1 etc (Taylor 1997; Odler 2007). The chemical shift of tetrahedrally coordinated Si in silicates and aluminosilicates is expected in the range -60 to -120 ppm. An increasing degree of polymerization results in resonances at lower ppm-values (Lippmaa, et al., 1980; Mägi, et al., 1984; Klinowski 1984). Figure 2 shows the ^{29}Si NMR spectra of $C_{26}A_9S_{65}$ and CLS_{9N}. Spectra are recorded before and after the reaction with Ca(OH)$_2$ and water. For both samples the broad resonances reveal the amorphous nature of the glass composed of various Q^n units giving rise to resonances in the entire range -60 to -120 ppm. In addition, Figure 2 illustrates the difference between the two which is obtained by subtracting the spectrum obtained before the pozzolanity test from the spectrum obtained after the test. To account for differences in the samples an appropriate scaling factor is used to ensure that the resonance from the original glass cancels out in the residual plot. For both samples the difference between the two is visualized as a resonance in the range -70 to -90 ppm. This corresponds to Si in Q^1 and Q^2 units indicating that a chain-like silicate structure forms during reaction with Ca(OH)$_2$ and water. A C-S-H like phase is thus formed. The presence of paramagnetic iron within CLS_{9N} causes the reduced signal-to-noise ratio observed for this glass compared to $C_{26}A_9S_{65}$.

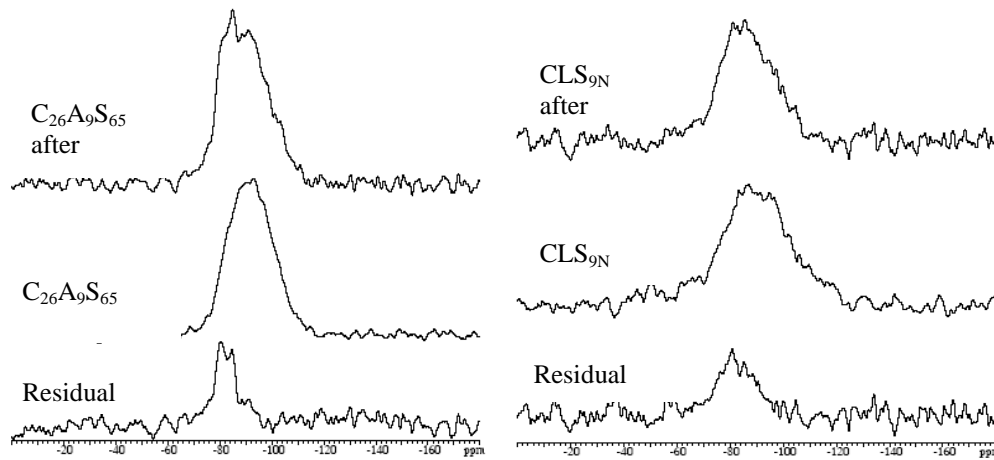**Figure 2** ^{29}**Si MAS NMR spectra of C$_{26}$A$_9$S$_{65}$ (left) and CLS$_{9N}$ (right). The "residual" spectra show the scaled resonance after the pozzolanity test minus the resonance before the pozzolanity test.**

Throughout the hydration of PC Al is primarily incorporated into crystalline calcium aluminate hydrates. The Al hydration can be followed as a gradual conversion of tetrahedrally coordinated monomeric AlO$_4$ units into octahedrally coordinated AlO$_6$ hydrates (Taylor 1997; Odler 2007). ^{27}Al MAS NMR can be used for this purpose as Al in tetrahedral coordination and in octahedral coordination give rise to signals in the range 55 to 80 ppm and -15 to 20 ppm, respectively (Merzbacher, et al., 1990; Muller, et al., 1981). Figure 3 shows the ^{27}Al NMR resonances of the two samples before and after the pozzolanity test as well as the residual spectrum. For C$_{26}$A$_9$S$_{65}$ (before the test) a broad resonance is observed, which corresponds to Al in tetrahedral coordination. Amorphous materials give broad peaks whereas crystalline phases cause narrow peaks. In addition to tetrahedrally coordinated Al, CLS$_{9N}$ (before the test) also contains a small fraction of Al in octahedral coordination.

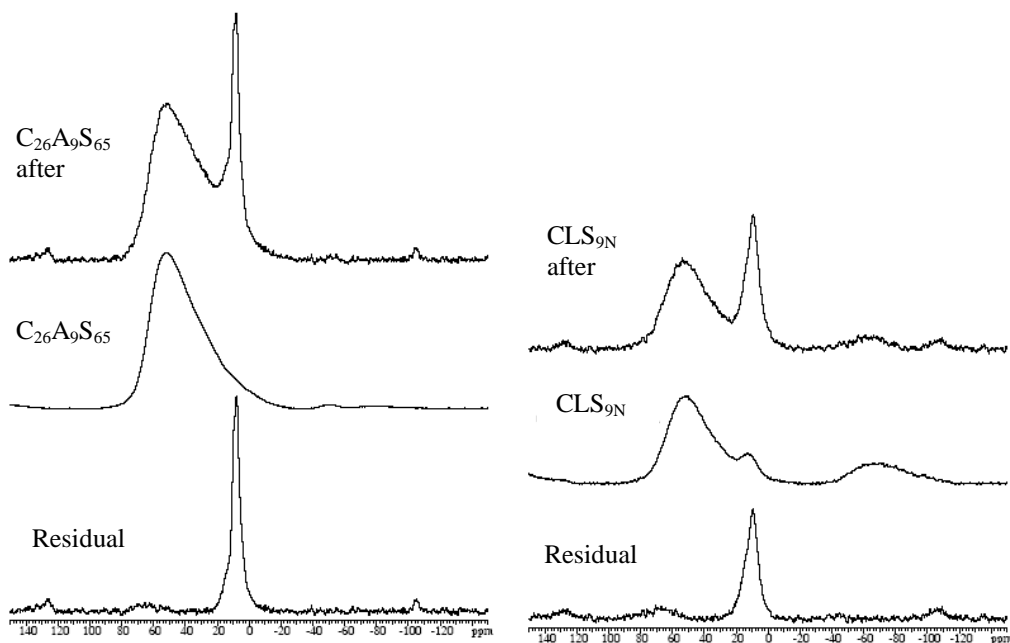**Figure 3:** ^{27}**Al MAS NMR spectra of C$_{26}$A$_9$S$_{65}$ (left) and CLS$_{9N}$ (right). The "residual" spectra show the scaled resonance after the pozzolanity test minus the resonance before the pozzolanity test.**

After the pozzolanity test, a sharp peak is observed for both samples in the range 0 – 20 ppm. Thus a crystalline phase containing Al in octahedral coordination forms as the amorphous calcium aluminosilica reacts with $Ca(OH)_2$ and water. This indicates the presence of a separate Al hydrate phase. This clearly shows that the glasses are reacting as pozzolanic materials.

The degree of pozzolanic reactivity is quantified as the fraction of glass that is reacting during the test (Table 2). The introduction of impurities from the natural minerals is observed to increase the reactivity and the introduction of additional Na_2O further increases the reactivity.

CONCLUSION

In this work, we tested the applicability of CAS glasses made from natural minerals as a partial replacement of cement clinker. The objective of the replacement is to reduce the CO_2 emissions from cement production. ~175 kg CO_2 is released from the decarbonation of the raw materials used to produce one tonne of glass, whereas ~516 kg "process CO_2" is released in the production of one tonne cement. The temperature of glass production affects the amount of "fuel-derived CO_2". The glasses based on naturally occurring minerals can be produced at temperatures that are 100-150°C lower than the temperature needed to produce Portland cement. Taking into account the energy of fusion for glass production, the "fuel-derived CO_2 emission" involved in the production of glass and Portland cement clinker is approximately equal. NMR investigations proved that the glasses are pozzolanically active. The pozzolanity is higher for the glass obtained using natural raw materials than the glass obtained using pure oxides. Introduction of additional Na_2O further increases the pozzolanity.

In general, the glasses show good potential as supplementary cementitious materials. The use of the glasses in composite cements is also expected to result in an overall CO_2 reduction in cement production. This is mainly due to the significantly lower raw material derived CO_2 emission from glass production process compared to production of Portland clinkers.

ACKNOWLEDGEMENTS

REFERENCES

Beerkens, R. 2004 "Industrial glassmelting process analysis". Am. Ceram. Soc. Bulletin 83, 28-32.

Bouhifd, M. A., Besson, P., Courtial, P., Gérardin C., Navrotsky, A., Richet, P. 2007. "Thermochemistry and melting properties of basalt". Contrib Mineral Petrol. 153, 689-698.

Conradt, R. 2000 "A generic approach to the relation between pul rate and energy consumption of glass furnaces". Glass Sci. Technol. Glastech. Ber. 73, 252-261.

Damtoft, J. S., Lukasik, J., Herfort, D., Sorrentino, D., Gartner, E. M. 2005. "Sustainable development and climate change initiatives". Cem. Concr. Res. 38, 115-127.

Humphreys, K., Mahasenan, M. 2002. "Toward a sustainable cement industry. Sub-study 8: climate change". An Independent Study Commissioned to Battelle by World Business Council for Sustainable Development.

Klinowski, J. 1984. " Nuclear magnetic resonance studies of zeolites". J. Progr. NMR Spectr. 16, 237-309.

Lippmaa, E., Mägi, M., Samoson, A. Engelhardt, G., Grimmer, A. R. 1980. "Structural Studies of Silicates by Solid-state High-Resolution 29Si NMR". J. Am. Chem. Soc. 02, 4889-4893.

Mägi, M., Lippmaa, E., Engelhardt, G., Grimmer, A. R. 1984. "Solid-state High-Resolution Silicon-29 Chemical Shifts in Silicates". J. Phys. Chem. 88, 1518-1522.

Massazza, F. 2007. "Pozzolana and Pozzolanic Cements" In Hewlett, P. C., ed. "Lea's chemistry of cement and concrete" Elsevier, 4th edition

Merzbacher, C. I., Sherriff, B. L., Hartman, J. S., White, W. B. 1990. "A high-resolution ^{27}Al and ^{29}Si NMR study of alkaline earth aluminosilicate glasses". J. Non-cryst. Sol. 124, 194-206

Moesgaard, M., Herfort, D., Skibsted, J., Yue, Y. Z. (in press) "Glass as a supplementary cementitious material" Submitted to Glass Technology – European Journal of Glass Science and Technology, Part A

Moesgaard, M., Yue, Y. Z. 2009. "Compositional dependence of fragility and glass forming ability of calcium aluminosilicate melts" J. Non. Cryst. Sol. 355, 867-873.

Muller, D. Gessner, W. Behrens, H. J., Scheler, G. 1981. "Determination of the aluminum coordination in aluminum-oxygen compounds by solid-state high-resolution 27Al NMR" Chem. Phys. Lett. 70, 59-62

Mysen, B. O., Richet, P. 2005. "Silicate glasses and melts – properties and structure, Developments in geochemistry 10", Elsevier, 1st edition

Odler, I 2007. "Hydration, Setting and Hardening of Portland Cement" In Hewlett, P. C., ed. "Lea's chemistry of cement and concrete" Elsevier, 4th edition

Rehan, R., Nehdi, M. 2005. "Carbon dioxide emissions and climate change: policy implications for the cement industry". Environ. Sci. Pol. 8, 105-114.

Sardeshpande, V., Gaitonde, U. N., Banerjee, R. 2007. "Model based energy benchmarking for glass furnace". Energ. Convers. Manage. 48, 2718-2738.

Schwarz, N., Cam, H., Neithalath, N. 2008. "Influence of a fine glass powder on the durability characteristics of concrete and its comparison to fly ash". Cem. Concr. Res. 30, 486-496

Shi, C., Wu, Y., Riefler, C., Wang, H. 2005. "Characteristics and pozzolanic reactivity of glass powders,". Cem. Concr. Res. 35, 987-993

Shi, C., Zheng, K. A. 2007. "Review on the use of waste glasses in the production of cement and concrete". Resour. Conserv. Recy. 52, 234-247

Shayan A., Xu, A. 2006. "Performance of glass powder as a pozzolanic material in concrete: A field trial on concrete slabs". Cem. Concr. Res. 36, 457-468

Taylor, H. F. W. 1997. "Cement chemistry", Academic Press, 2nd edition

Worrell, E., Price, L., Martin, N., Hendriks, C., Meida, K. O. 2001. "Carbon dioxide emission from the global cement industry". Annu. Rev. Energy Environ. 26, 303-329.

Paper V

Contents lists available at ScienceDirect

Cement and Concrete Research

Physical performances of blended cements containing calcium aluminosilicate glass powder and limestone

Mette Moesgaard [a], Duncan Herfort [b], Mette Steenberg [b], Lise Frank Kirkegaard [b], Yuanzheng Yue [a],*

[a] Section of Chemistry, Aalborg University, DK-9000 Aalborg, Denmark
[b] Aalborg Portland Group, DK-9000 Aalborg, Denmark

ARTICLE INFO

ABSTRACT

This work explores the suitability of calcium aluminosilicate (CAS) glass particles as an alternative to conventional supplementary cementitious materials (SCMs) such as fly ash and blast furnace slag. The reason for adding CAS glass particles to the cement blend is to reduce the CO_2 emission of cement production at the same level of performance. For this purpose, blended cement mortars containing 30 wt.% clinker replacement are characterized with respect to workability and mechanical performance. The results indicated that real emission reductions are possible, particularly for combinations of finely ground limestone and CAS glasses which resulted in significantly higher strengths than would be predicted from the individual contributions of each constituent.

© 2010 Elsevier Ltd. All rights reserved.

1. Introduction

The production of Portland cement accounts for approximately 5% of the global anthropogenic CO_2 emissions [1–4]. For an efficient process ~2/3 of the CO_2 emission comes from the calcination of limestone which makes up about 80% of the raw materials. This is referred to as the "raw materials CO_2 emission" and accounts for 500–550 kg CO_2 per ton of cement clinker. The other major contributor is the "fuel-derived CO_2 emission" constituting 250–300 kg CO_2 per ton of clinker for an efficient kiln. The demand for cement, especially in developing countries, is expected to at least double by 2050 [1,4,5]. Therefore, emissions per ton of cement must be halved just to maintain the status quo. Several levers have been identified for achieving this, such as improved process efficiency, increased use of supplementary cementitious materials (SCMs), increased use of biofuels, and carbon capture and storage [4]. This paper deals with innovative SCMs based on calcium aluminosilicate (CAS) glasses and limestone. The incentive for this is that traditional SCMs such as fly ash and granulated blast furnace slag are already in short supply in some parts of the world such as Europe [1,3,6]. An important consideration in developing these new SCMs is that they must make a significant contribution to standard, early or 28 day concrete strengths since it makes little sense to lower the clinker factor by e.g. 30% if correspondingly more cement is needed to achieve a given concrete strength. In addition, the use of the new SCMs must of course provide a significant reduction in the overall CO_2 emissions associated with production of the blended cements compared to ordinary Portland cement (OPC).

Previous work by the present authors showed that CAS glasses produced from natural sources of clay, limestone and sand (CAS_{1N} and CAS_{9N} in Table 1) are pozzolanically reactive in a $Ca(OH)_2$ solution [7]. A chain-like silicate structure consistent with the C–S–H phase is detected by means of the ^{29}Si NMR and an Al containing hydration product consistent with the calcium aluminate hydrate phases formed during OPC hydration is detected by ^{27}Al NMR. The introduction of additional Na_2O into CAS_{9N} reduces the melting temperature of the glass and enhances its glass forming ability on cooling, in addition to increasing its grindability and pozzolanic reactivity [7]. In this work, the physical performance of blended mortars containing 30 wt.% clinker replacement is investigated. Blended cements containing only the CAS glasses or a combination of both glass and limestone are examined.

2. Experimental procedures

Commercially available cement containing approximately 96% clinker and 4% gypsum was used to prepare mortars for physical tests. The mineralogical composition of the clinker (Bogue) and the chemical composition of the cement are given in Tables 1 and 2. The content of free lime was measured by titration in alcohol. The preparation and characterization of the CAS glasses are described in [7]. The chemical compositions of the glasses and other SCMs are given in Table 1. Clay, limestone and sand were used as raw materials for the glass preparation. The clay was provided by Dantonit A/S, Odense, Denmark and the limestone and quartz sand were provided by Aalborg Portland A/S, Aalborg, Denmark. The subscript of the CAS

Table 1
Chemical composition in wt.%. L.O.I. refers to the Loss On Ignition. For cement, limestone and fly ash XRF was used to determine the chemical composition. Atomic absorption spectrometry and spectrophotometry were used for the two glasses CAS_{1N} and CAS_{9N}. L.O.I. and the content of SO_3 were not determined for CAS_{1N} and CAS_{9N}.

Component	Cement	Limestone	CAS_{1N}	CAS_{9N}	Fly ash
SiO_2	19.0	4.4	53.0	51.0	55.2
Al_2O_3	5.8	0.4	13.4	12.4	24.7
Fe_2O_3	3.9	0.2	7.5	6.5	8.5
CaO	65.1	52.9	20.4	17.9	4.7
MgO	1.0	0.4	2.6	2.4	1.8
K_2O	0.4	0.1	2.1	2.0	1.6
Na_2O	0.3	<0.1	1.1	7.8	0.9
SO_3	3.7	0.1	–	–	0.6
L.O.I.	0.9	41.7	–	–	1.9

glasses refers to the molar content of Na_2O. In CAS_{9N} the Na_2O content has been increased by addition of Na_2CO_3. In industrial scale production additional alkali oxide can be introduced e.g. by recycling cement kiln dust or from albite or granite high in alkali oxide or directly as Na_2SO_4. CAS_{9N} was ground to two different finenesses and spun into fibers. For comparison the fibers were ground to the same fineness as one of the other CAS_{9N} samples (Table 3). Fibers are produced to compare the effect of using glasses with varying degrees of deviation from structural equilibrium conditions. The fibers were produced by Rockwool International A/S, Hedehusene, Denmark using the cascade spinning process, which is a type of centrifuge process drawing fibers by throwing out droplets of the melt [8].

Blended cement mortars containing 30 wt.% clinker replacement were prepared according to Table 4. For all mortars a water to cement ratio of $w/cm = 0.5$ was employed, where cm is the total content of cementitious materials including SCMs. In addition, the sand to cement ratio of the mortars was 1:3. The particle diameter of the sand in use was in the range of 0–2 mm.

The flow of the fresh mortar was measured using a flow table according to ASTM C230-80 (although tamped 20 rather than 25 times). The initial setting behavior was evaluated based on the heat of hydration during the first 18 h after preparation of the mortar using adiabatic calorimetry. Approximately 200 g of mortar was used for the measurement. Mortar prisms of $2 \times 2 \times 15$ cm^3 were made and stored in the molds for $24 \pm 1/2$ h at 20 ± 1 °C and a relative humidity of at least 95%. Hereafter the prisms were demolded and placed in water in the curing room (20 ± 1 °C) for a final hydration time of 2, 28 or 90 days. Each prism was cut in three for determination of compressive strength. The compressive strength was determined according to EN 196-1 except for the smaller prism size [9].

Thermogravimetric analyses of paste samples were performed using a simultaneous thermal analyzer (NETZSCH STA 449 C Jupiter, Selb, Germany). Three pastes were prepared: a reference containing 100% cement, a paste containing 30% limestone and a paste containing both 20% limestone and 10% CAS_{9N} fine (the sample with the largest surface area). For the pastes a water to cement ratio of $w/cm = 0.4$ was employed. For the thermal analyses 30–40 mg of ground paste was used. It was heated from 30 °C to 975 °C using a heating rate of 20 °C/min. The thermal analyses were performed immediately after the 90 days of hydration.

Powder X-ray diffraction patterns were obtained on a STOE diffractometer using capillary sample tubes. Cu–K_α radiation was employed in the range of $2\theta = 2$ to 127° with an interval of 0.015°. The

Table 2
Mineralogical composition (wt.%) of clinker.

Component	C_3S	C_2S	C_3A	C_4AF	Free lime[a]	LFS $(-)$[b]
Clinker	63.4	9.2	8.4	12.0	1.4	1.02

[a] The content of free lime is measured by titration in ethanol.
[b] LSF is the lime saturation factor.

Table 3
Characteristics of the replacement materials.

Material	Surface area (m^2/kg) [a]	Mean diameter (μm) [b]
Pure cement	575	7.7
CAS_{1N}	338	16.2
CAS_{9N}	371	14.4
$CAS_{9N-fine}$	629	6.0
$CAS_{9N-fiber}$	619	6.2
Fly ash	330	20.1
Inert filler (quartz)	Diameter <90 μm	
Limestone	1288	2.7

[a] Determined by air permeability using the Blaine method.
[b] Determined by laser diffraction.

generator conditions were 40 kV and 40 mA. The phases were identified by comparison with peaks from the reference samples of the International Centre for Diffraction Data database. Paste samples with $w/cm = 0.4$ were ground and investigated immediately after 90 days of hydration.

3. Results and discussion

3.1. Comparison of the supplementary cementitious materials

The performance of blended cements containing the two CAS glasses is compared to that of the blended cements containing finely ground quartz, i.e., an inert material not participating in the chemical reactions, and fly ash as a traditional SCM. The glasses and fly ash were ground to similar fineness.

For all the prepared mortars (Table 4), standard mortar workability is slightly improved with increased slump on the flow table of 2–8% compared to the pure cement mix. Thus the addition of CAS glass does not increase the water demand.

Calorimetric results are shown in Fig. 1. For all blended cements the heat of hydration is lower, indicating that the clinker is replaced by a material which is less reactive during the early stages of hydration. The two glasses appear to make little or no contribution to early hydration, as similar heat development patterns are observed for the blended cements containing glass and inert filler (quartz). On

Table 4
Composition of the prepared mortars.

Material	Composition (wt.%)				$P/(P+L)$[a]
	Cement	Pozzolan	Limestone	Inert filler	
Pure cement	100	0	0	0	–
CAS_{1N}	70	30	0	0	1.00
	70	20	10	0	0.67
	70	10	20	0	0.33
CAS_{9N}	70	30	0	0	1.00
	70	20	10	0	0.67
	70	10	20	0	0.33
$CAS_{9N-fine}$	70	30	0	0	1.00
	70	20	10	0	0.67
	70	10	20	0	0.33
$CAS_{9N-fiber}$	70	30	0	0	1.00
	70	10	20	0	0.33
Fly ash	70	30	0	0	1.00
	70	20	10	0	0.67
	70	10	20	0	0.33
Inert filler (quartz)	70	0	0	30	1.00
	70	0	10	20	0.67
	70	0	20	10	0.33
Limestone	70	0	30	0	0.00

[a] P includes both the pozzolans (CAS glass and fly ash) as well as the inert filler and L refers to limestone.

the other hand, the fly ash appears to make a significant contribution to the amount of early heat formation. The reason for this is believed to be that the finely ground fly ash acts as nucleation sites for the early alite hydration [10,11].

The strength development up to 90 days is shown in Fig. 2, normalized to the strength of the pure cement mortar (σ/σ_{rel}). The pozzolanic reactivity of the glass and fly ash is shown by the strengths of the mortars containing these materials which is significantly higher than that of the mortar containing quartz, i.e. relative strengths of 70 to 75% at 90 days compared to 55% for the quartz. The relative strength development of the quartz containing mortars reaches a plateau already after 28 days, whereas the strength of the remaining three blended cements continues to increase up to 90 days.

Fig. 3 shows the effect of grinding the glass to a higher surface area (over 600 m^2/kg as shown in Table 3), which as expected results in a significant acceleration of strength development. At 90 days the strength in increased from 73% to 93% by means of increasing the surface area.

The CAS glasses were obtained by cooling the glass melt fast enough to avoid crystallization. The degree of disorder in the glass depends on the cooling rate. The faster the cooling rate the higher the temperature at which the structure is frozen-in, and the higher the entropy and thus the degree of disorder of the final glass. A higher degree of disorder should result in a higher degree of reactivity in the blended cement. To test this hypothesis, two glasses with different degrees of structural disorder were produced at different cooling rates. High cooling rates can be achieved by drawing thin fibers from the glass melt. In this work, discontinuous fibers with diameters of 3–15 μm were produced from the CAS$_{9N}$ melt using the centrifugal spinning process [8] giving a cooling rate of about 10^6 K/s. In contrast, the glasses, which were cast onto a graphite plate, i.e., the normally cooled glasses, were cooled at about 10^3 K/s. The cooling rate is calculated using the procedure reported in ref. [12]. The excess energy stored in the structure of the fiber glass is about one order of magnitude larger than for the normally cooled glass ($\approx$80 J/g vs. $\approx$7 J/g) [12]. The fibers were ground to a surface area comparable to the surface of the fine CAS$_{9N}$ particles (629 m^2/kg) to compare the reactivity of the glasses. From Fig. 3, it is seen that the strength of the blended cement mortar containing the fast cooled fibers reaches 98% at 90 days compared to 93% obtained for the mortar containing normally cooled glass. The effect on reactivity of the degree of structural disorder within the glass is thus significantly less than the effect of the surface area.

4. Synergetic effect of limestone and pozzolan

In terms of volume, limestone is probably the most common clinker replacement material used today. Its role in accelerating
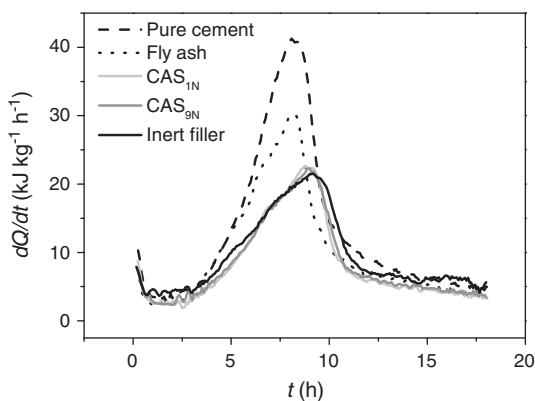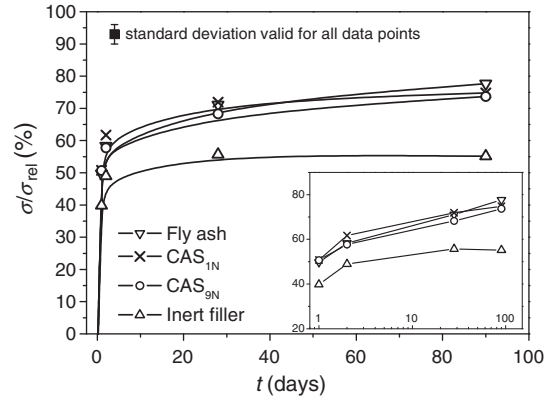

Fig. 2. Strength development of blended cement mortars containing different SCMs. The strength is given relative to the strength of pure Portland cement mortar (σ/σ_{rel}) as a function of hydration time (t). The uncertainty associated with the experimental error of the method is given as the single standard deviation error bar. The inset shows the strength development on a logarithmic time scale.

strengths is reported to be both physical and chemical as it reacts with available alumina to form the so-called CO$_2$–AFm phase [6,13–17]. The quantity of limestone taking part in these reactions is however limited and reported to be in the range of a few percent to about 10%, depending among other things on the C$_3$A content [6,16–18]. In addition, limestone is reported to accelerate the early alite hydration [17–21]. This might compensate the reduction in early strength caused by addition of the CAS glasses (Figs. 2 and 3).

Calorimetric results (Fig. 4) show that the early rate of heat development of the Portland limestone cement is intermediate between the pure cement reference and the sample containing 30% CAS glass. This could be due to the acceleration of C$_3$S hydration in the presence of CaCO$_3$. Heat development in the sample containing both limestone and glass is faster than the sample containing 30% glass, but slower than the sample containing 30% limestone. The total early heat formed in this blend is higher than in the limestone or glass blends on their own. We have no immediate explanation for this. Since it is unlikely that significant carboaluminate reaction would occur so early, increased alite hydration from heterogeneous nucleation must somehow be involved. It is however worthy noting that the heat of hydration for the ternary blend is higher than what would be expected from a simple sum according to the content of each component.
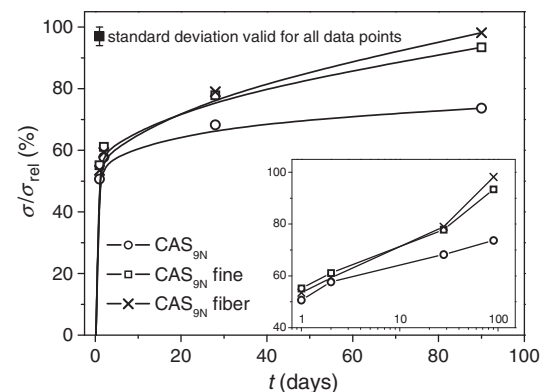

Fig. 1. The rate of heat evolution (dQ/dt) as a function of hydration time (t). The inert filler is quartz.

Fig. 3. Strength development of blended cement mortars containing CAS$_{9N}$ with varying surface area and excess internal energy. The strength is given relative to the strength of pure Portland cement mortar (σ/σ_{rel}) as a function of hydration time (t). The surface areas of the samples are: CAS$_{9N}$ (371 m^2/kg), CAS$_{9N}$ fine (629 m^2/kg) and CAS$_{9N}$ fiber (619 m^2/kg). The uncertainty associated with the experimental error of the method is given as the single standard deviation error bar. The inset shows the strength development on a logarithmic time scale.
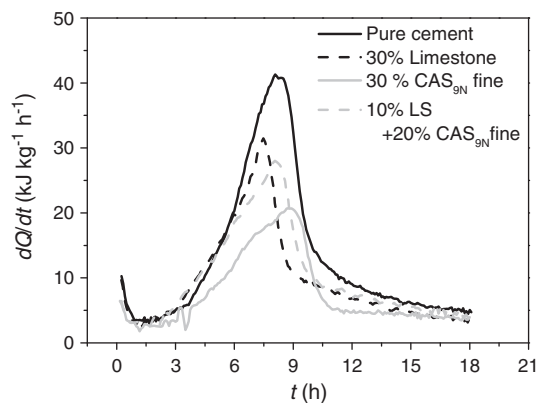
Fig. 4. The rate of heat evolution (dQ/dt) as a function of time (t) for the limestone containing mortars. LS refers to the limestone.

Fig. 5 shows the compressive strengths of the mortars as a function of the $P/(P+L)$ ratio. After 1 day hydration the strength of the limestone containing mortar has reached 66% relative to the pure cement reference. This is significantly higher than the 1 day strength obtained for blended cements containing either CAS glass or fly ash (Fig. 5). This is probably the result of increased hydration of the alite by heterogeneous nucleation of C–S–H on the fine limestone particles described in the literature [18,19,21]. For the ternary blends containing both pozzolan (fly ash or CAS glass) and limestone or inert filler and limestone the 1 day strengths can roughly be estimated from the content of each component. Thus, limestone can, to some extent, compensate for the reduced early strength of the blended cements containing CAS glass.

After 90 days hydration a significant synergetic effect is observed on the samples containing both limestone and CAS_{9N}, i.e., they exhibit significantly higher strengths than would be predicted from the individual contributions of each component (Fig. 5). Furthermore, the strength of the ternary blends exceeds that of the blended cements containing limestone as the only cement additive. Increased surface area significantly increases the strength development (Fig. 6) and for the mortars containing 20% $CAS_{9N-fine}$ and 10% limestone, the 90 days compressive strength even exceeds that of the pure cement. An effect of increasing the amount of energy stored in the glass during production is not observed for the blended cements containing both glass and limestone.

Fig. 7 shows the X-ray diffractograms of the three blended cements hydrated for 90 days. This validates the formation of monocarbonate in the samples containing limestone. Significant amounts of unreacted calcite are also indentified in these samples. This confirms that just a
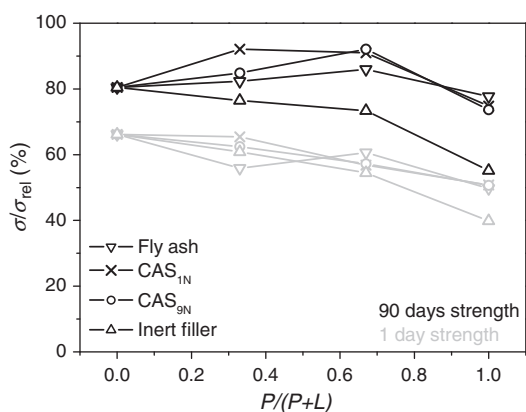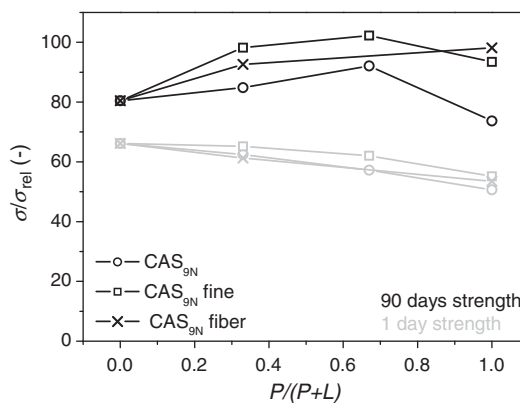

Fig. 6. Relative compressive strength of blended cement mortars containing CAS_{9N} with varying surface area and excess internal energy as a function of $P/(P+L)$. The strength is given in percentage relative to the strength of pure Portland cement mortar (σ/σ_{rel}). The surface areas of the samples are: CAS_{9N} (371 m^2/kg), CAS_{9N} fine (629 m^2/kg) and CAS_{9N} fiber (619 m^2/kg). P is the content of pozzolan (including the inert filler) and L is the content of limestone in wt.%.

fraction or the carbonate is reacting chemically with available alumina forming the calcium monocarboaluminate [17,18,21–23]. Portlandite, ettringite and C–S–H are furthermore identified in all samples and monosulfate is found in the two-component blends containing either 30% CAS glass or 30% limestone. Thus the addition of CAS glass does not alter the hydration phase assemblage relative to the assemblage normally formed during hydration of ordinary Portland cement [6].

The formation of hydration phases after 90 days is also investigated using thermal gravimetric analysis on paste samples (Fig. 8). The mass loss in the temperature range up to ~300 °C corresponds to the loss of water both from pore solution and from the different calcium silicate and calcium aluminate hydrate phases formed in the paste. In the temperature range of 440–540 °C Ca(OH)$_2$ is decomposed to CaO and water giving rise to the second mass loss. For the samples containing limestone a significant mass loss is furthermore observed in the temperature range of ~700–810 °C. This corresponds to the decarbonation of $CaCO_3$. From the observed mass loss the content of non-reacted $CaCO_3$ can be determined. The latter is used to calculate the degree of limestone reactivity. For the Portland limestone cement containing 30% limestone the degree of limestone reactivity is ~9%, whereas it is increases to ~16% as both limestone and CAS_{9N} is added to the same blended cement. The presence of the glass thus causes a larger fraction of the limestone to react chemically thus contributing to the formation of hydration phases. In that way, the combination of the physical filler effect of the limestone and the chemically cementitious reactivity of both limestone and fly ash or CAS glasses can be exploited to a greater extent.
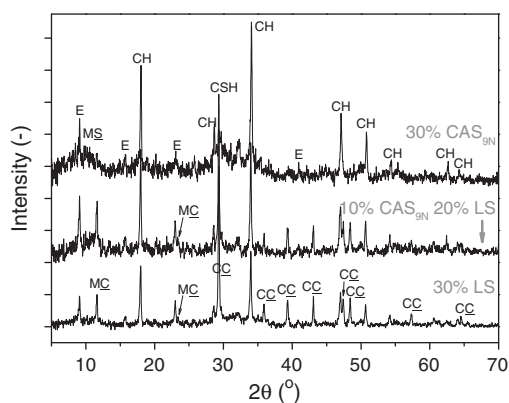

Fig. 5. Relative compressive strength (σ/σ_{rel}) of the mortars containing different SCMs as a function of $P/(P+L)$. P is the content of pozzolan (including the inert filler) and L is the content of limestone both in wt.%.

Fig. 7. X-ray diffractograms for the three blended cements. CH = portlandite, C$\underline{C}$ = calcite, E = ettringite, M$\underline{C}$ = monocarbonate, CSH = C-S-H and M$\underline{S}$ = monosulfate. LS: limestone.
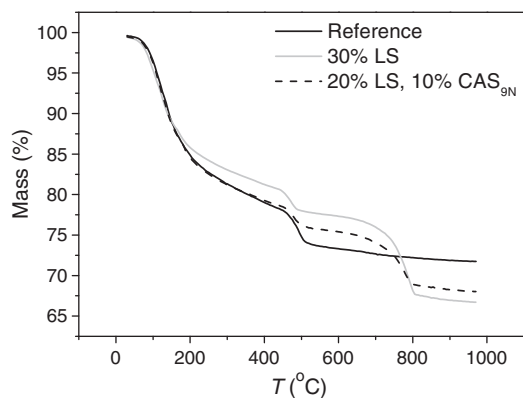
Fig. 8. Thermal gravimetric analyses of cement pastes hydrated for 90 days. LS refers to limestone.

Fig. 9. Relative raw materials CO_2 emission $(m_{CO2}/\sigma)_{rel}$ as a function of $P/(P+L)$. $(m_{CO2}/\sigma)_{rel}$ <1 indicates blended cements with a reduced CO_2 emission relative to the mechanical performance compared to pure cement. This limit is indicated by the dashed grey line. The CAS_{9N}, CAS_{9N} fine and CAS_{9N} fiber samples have surfaces areas of 371 m^2/kg, 629 m^2/kg and 619 m^2/kg, respectively.

The relatively high Al_2O_3 content of the glass compared to OPC is believed to be the reason of the increased reactivity. This is supported by previous studies indicating that a high C_3A content favors the consumption of carbonate in Portland limestone cements [14,16]. The conversion of monosulfate to monocarbonate releases sulfates resulting in the formation of ettringite. This is in agreement with the XRD analyses where no monosulfate was observed for the blended cement containing both limestone and CAS_{9N}. A larger AFt/AFm ratio is thus expected in the limestone containing cements. This will also contribute to a larger strength by an increase in the total volume of hydration products.

A similar synergetic effect in the late strength is reported previous on ternary blended cements containing both limestone and fly ash. In this study the degree of clinker substitution is 35 wt.% and the largest synergy effect is observed for small amounts of limestone (5 wt.%). This study confirms the conversion of monosulfate to monocarbonate and ettringite to be the reason for the enhanced late strength [24,25].

4.1. Evaluation of the raw materials CO_2 emission

In order for CAS glass particle to be useful SCMs less CO_2 must be released from the production of blended cements compared to pure cements for similar mortar or concrete performances. The production of blended cement includes both the production of cement clinker and that of CAS glass. To obtain a measure of the CO_2-release relative to the performance of the final concrete, the amount of CO_2 (given in kg) released during production of cement and SCM is normalized by the 90 days compressive strength (given in MPa) obtained for the given blended cement mortar. This is defined as the parameter m_{CO2}/σ.

The global average specific thermal energy consumption for production of PC is estimated to be 3.7 GJ/t clinker corresponding to the release of 250–300 kg fuel derived CO_2 per ton of clinker [4]. An efficient melting tank for glass production operating at a maximum temperature of 1600 °C has a thermal energy consumption of ~4 GJ/t [26,27]. The use of CAS glasses as SCMs sets no requirements to the homogeneity of the glass, and the glasses can thus be produced at considerably lower temperatures (1300–1350 °C) and with significantly reduced refining times than used for normal glass production [7]. These large continuous glass melting tanks producing up to several hundred tons of glass per days are often fired on fossil fuels with most new furnaces using natural gas where available. Therefore the fuel derived CO_2 emission is estimated to be comparable or slightly less for glass production than for production of Portland cement clinker. In the following calculations the fuel derived CO_2 release is approximated to 275 kg/t cement or glass. This corresponds to a glass melting tank fired on 100% natural gas or on a combination of coal and alternative fuels (often waste materials) in relative proportions corresponding to that used for cement production. No
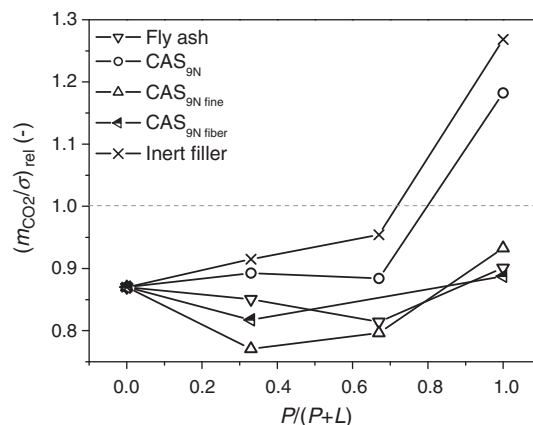
fuel derived CO_2 emission is linked to the use of fly ash, limestone and the inert filler.

Limestone is the major raw material used in the production of PC clinker accounting for 500–550 kg CO_2 per ton of clinker. For the production of the CAS glasses limestone accounts for approximately one third of the raw materials resulting in a raw materials CO_2 emission of approximately 175 kg CO_2 per ton of glass. When limestone is used as a clinker replacement, it is mixed with the cement after clinker burning, and hence, no CO_2 is released since calcination is avoided. The same goes for fly ash and the inert quartz as these will not contribute to any raw materials CO_2 emission neither to any fuel derived CO_2 emission associated with cement production.

The measure m_{CO2}/σ includes the CO_2 contributions from both fuel and raw materials. Fig. 9 compares m_{CO2}/σ for the different blended cements relative to that of pure cement as a function of the $P/(P+L)$ ratio. If $(m_{CO2}/\sigma)_{rel}$ <1 the CO_2 per mechanical performance is reduced for the blended cement compared to the pure cement. This is the case for all the blended cements except for those containing 30% inert filler and 30% of the coarse CAS_{9N}. If CAS glass is added as the only SCM, it must therefore be ground to a high surface area to effectively reduce CO_2 release relative to the mechanical performance. When both limestone and CAS glass are added, the relative CO_2 emission can be reduced by approximately 20% for the same 90 days compressive strength as obtained for OPC. CAS glasses can therefore be considered a good alternative to the limited resources of traditional SCMs especially when mixed with limestone.

Another alternative to the traditional by-product SCMs is clay mineral heat treated at 600–900 °C. This yields poorly crystalline or amorphous calcined clays exhibiting pozzolanity. The use of calcined clays in blended cements is however reported to increase the water demand significantly thus requiring addition of superplasticizer [28–30].

5. Conclusion

Calcium aluminosilicate glass has been shown to be a viable alternative to the traditional SCMs. The combination of limestone and CAS glass in the same blended cement provides higher late strengths than predicted from the individual contributions of each constituent. This is probably related to the rather high alumina content in the glass which causes a larger part of the limestone to participate in the hydration reactions. Combined with the pozzolanity of the CAS glasses this provides blended cements with late strengths even higher than obtained with the pure Portland cement. Real reductions in the CO_2 emission of ~20% are possible for the same cement strength and

performance compared to pure PC. This yields lower emission than achieved using fly ash or combinations of fly ash and limestone.

Acknowledgements

References

[1] J.S. Damtoft, J. Lukasik, D. Herfort, D. Sorrentino, E.M. Gartner, Sustainable development and climate change initiatives, Cem. Concr. Res. 38 (2008) 115–127.

[2] R. Rehan, M. Nehdi, Carbon dioxide emission and climate change: policy implications for the cement industry, Environ. Sci. Pol. 8 (2005) 105–114.

[3] E. Worrell, L. Price, N. Martin, C. Hendriks, L.O. Meida, Carbon dioxide emission from the global cement industry, Annu. Rev. Energy Environ. 26 (2001) 303–329.

[4] World Business Council for Sustainable Development, Cement Technology Roadmap 2009, Carbon emissions reductions up to 2050, OECD/IEA and the World Business Council for Sustainable Development, 2009.

[5] K. Humphreys, M. Mahasenan, Toward a sustainable cement industry, Sub-study 8: climate change, An Independent Study Commissioned to Battelle by World Business Council for Sustainable Development, March 2002.

[6] H.F.W. Taylor, Cement Chemistry, 2nd editionAcademic Press, New York, 1997.

[7] M. Moesgaard, D. Herfort, J. Skibsted, Y.Z. Yue, Calcium aluminosilicate glasses as supplementary cementitious material, Glass Technol.: Eur. J. Glass Sci. Technol. A 51 (2010) 183–190.

[8] B. Širok, B. Blagojević, P. Bullen, Mineral Wool, Woodhead Publishing, Cambridge, 2008.

[9] F.L. Smidth, Internal FLS standard — the Mini Rilem method of testing cement, Determination of strength and bulk density, internal report, F.L. Smidth, 1998.

[10] J. Hjort, J. Skibsted, H.J. Jakobsen, ^{29}Si MAS NMR studies of Portland cement components and the effects of microsilica on the hydration reaction, Cem. Concr. Res. 18 (1988) 789–798.

[11] H. Krøyer, H. Lindgreen, H.J. Jakobsen, J. Skibsted, Hydration of Portland cement in the presence of clay minerals studied by ^{29}Si and ^{27}Al MAS NMR sectroscopy, Adv. Cem. Res. 15 (2003) 103–112.

[12] Y.Z. Yue, R. von der Ohe, S.L. Jensen, Fictive temperature, cooling rate, and viscosity of glasses, J. Chem. Phys. 120 (2004) 8053–8059.

[13] T. Vuk, V. Tinta, R. Gabrovsek, V. Kaucic, The effects of limestone addition, clinker type and fineness on properties of Portland cement, Cem. Concr. Res. 31 (2001) 135–139.

[14] S. Tsivilis, E. Chaniotakis, E. Badogiannis, G. Pahoulas, A. Ilias, A study on the parameters affecting the properties of Portland limestone cements, Ceom. Concr. Res. 21 (1999) 107–116.

[15] S. Tsivilis, J. Tsantilas, G. Kakali, E. Chaniotakis, A. Sakellariou, The permeability of Portland limestone cement concrete, Cem. Concr. Res. 33 (2003) 1465–1471.

[16] J. Zelic, R. Krstulovic, E. Tkalcec, P. Krolo, Durability of the hydrated limestone–silica fume Portland cement mortars under sulphate attack, Cem. Concr. Res. 29 (1999) 819–826.

[17] V.S. Ramachandran, Thermal analysis of cement components hydrated in the presence of calcium carbonate, Thermochim. Acta 127 (1988) 385–394.

[18] W.A. Klemm, L.D. Adams, An investigation of the formation of carboaluminates, in: P. Klieger, R.D. Hooton (Eds.), Carbonate Additions to Cement, ASTM STP 1064, American Society for Testing and Materials, Philadelphia, PA, 1990, pp. 60–72.

[19] V.S. Ramachandran, Z. Chun-mei, Influence of CaCO$_3$ on hydration and microstructural characteristics of tricalcium silicate, Il Cem. 83 (1986) 129–152.

[20] V.S. Ramachandran, Thermal analysis of cement components hydrated in the presence of calcium carbonate, Thermochim. Acta 127 (1988) 385–394.

[21] J. Péra, S. Husson, B. Guilhot, Influence of finely ground limestone on cement hydration, Cem. Concr. Res. 21 (1999) 99–105.

[22] V.L. Bonavetti, V.F. Rahhal, E.F. Irassar, Studies on the carboaluminate formation in limestone filler-blended cements, Cem. Concr. Res. 31 (2001) 853–859.

[23] H.J. Kuzel, Initial hydration reactions and mechanisms of delayed ettringite formation in Portland cements, Cem. Concr. Comp. 18 (1996) 195–203.

[24] K. De Weerdt, H. Justnes, Microstructure of binder from the pozzolanic reaction between lime and siliceous fly ash, and the effect of limestone addition, Proceedings from the 1st International Conference on Microstructure Related Durability of Cementitious Composites, 2008, pp. 107–116.

[25] K. De Weert, H. Justnes, Synergetic reactions in triple blended cements, Proceedings of the 11th NCB International Seminar on Cement and Building Materials, 2009, pp. 257–261.

[26] V. Sardeshpande, U.N. Gaitonde, R. Banerjee, Model based energy benchmarking for glass furnace, Energ. Convers. Manage. 48 (2007) 2718–2738.

[27] Glass British, UK glass manufacture — a mass balance study 2008, Envirowise Sustainable Practices — Sustainable Profits, 2008.

[28] C. He, B. Osbæck, E. Makovicky, Pozzolanic reactions of six principal clay minerals: activation, reactivity assessments and technological effects, Cem. Concr. Res. 25 (1995) 1691–1702.

[29] B. Samet, T. Mnif, M. Chaabouni, Use of a kaolinitic clay as a pozzolanic material for cement: formulation of blended cement, Cem. Concr. Comp. 29 (2007) 741–749.

[30] B.B. Sabir, S. Wild, J. Bai, Metakaolin and calcined clays as pozzolans for concrete: a review, Cem. Concr. Comp. 23 (2001) 441–454.

Paper VI

MECHANICAL PERFORMANCES OF BLENDED PORTLAND CEMENTS CONTAINING OPTIMIZED CALCIUM ALUMINOSILICATE GLASS PARTICLES

METTE MOESGAARD[*], DUNCAN HERFORT[**], METTE STEENBERG[**] and YUANZHENG YUE[*]

[*]Section of Chemistry, Aalborg University, Sohngaardsholmsvej 57, 9000 Aalborg, Denmark
[**]Aalborg Portland, Rørdalsvej 44, 9220 Aalborg Øst, Denmark

ABSTRACT

In this work, we investigate the mechanical performance of blended Portland cements containing the optimized calcium aluminosilicate (CAS) glass described in Moesgaard, et al., 2010a. The glass is investigated in mortars with a water to cement ratio of 0.5, and both fibers and particles from molded glass, ground to different finenesses, are investigated. From strength development and workability of fresh mortar it is concluded that the glass shows promising results as a supplementary cementitious material (SCM), and even more promising results have been obtained with combinations of glass and finely ground limestone where significantly higher strengths are observed than would be predicted from the individual contributions of each constituent.

KEYWORDS:

CO_2 emission; Portland cement; supplementary cementitious materials (SCMs); pozzolanity.

INTRODUCTION

As already described in Moesgaard, et al., 2010a cement is a global growth industry and huge amounts are needed for infrastructure development, housing and industrial estates in the developing countries, and as 1 tonne of clinker is typically associated with 0.8 tonnes CO_2 emitted, new technologies are needed to de-couple the growth in cement production from a corresponding growth in CO_2 emissions. Several sources have already recognized this and a recent study (WBCSD-CSI & IEA, 2009) identified the increased use of SCMs as one of four necessary levers to achieve this goal. Substitution of clinker by SCMs is already increasing. This mainly involves the increased use of industrial by-products such as blast furnace slag and fly ash from coal fired power stations. However, as the processes for producing steel and electricity are replaced with new technology associated with less CO_2 emission, the availability of the traditional SCMs are diminishing. The amount of available conventional SCMs of 1.2 Gt/year forecasted by 2050 will therefore limit the reduction in clinker content to 73 %, if a global cement production of 4.4 billion tonnes per year is assumed; a reduction of only 6 % points compared to 2006 (WBCSD-CSI & IEA, 2009). Further reduction of the clinker content thus requires new sources of alternative SCMs (Damtoft, et al., 2005; Rehan & Nehdi 2005; Worrel, et al., 2001).

If the increased additions of SCMs are to make a real impact it is important that they do not result in a significant loss in the performance of the cement. Lower strengths for example mean that more cement is needed to achieve the same concrete strength resulting in little or no reductions in CO_2 per unit of concrete. In order to achieve a reasonable strength of the composite cement it is therefore important that the alternative material takes part in the hydration reactions contributing to the final strength.

Several potential calcium aluminosilicate (CAS) glasses have already been identified and the suitability of these glasses as SCMs has been confirmed from the measurement of pozzolanic reactivity using solid-state

[27]Al and ^{29}Si magic angle spinning NMR on glass samples submerged in a $Ca(OH)_2$ solution (Moesgaard, et al., 2010a). The hydraulic reactivity is assumed to derive from the structural disorder, i.e. thermodynamic instability, within the glassy materials. The Ca^{2+}, Na^+ and K^+ ions released into the pore solution, as Portland cement is mixed with water, will result in a highly alkaline environment with pH values of 13.4-14.0 (Lawrence, 2007). In the alkaline environment the glassy network will break down forming depolymerized Si- and Al-oxyhydroxides. As the CAS glasses are composed of the same oxides found in Portland cement these oxyhydroxides are expected to take part in the formation of hydration products similar to those formed during hydration of cement.

However, the strength contribution alone is not sufficient to provide a suitable SCM. The workability of the paste, mortar, or concrete also has to be acceptable. In this work, the cement clinker is partly substituted by CAS glass, or a combination of both glass and limestone. The composite cements are investigated in relation to workability of the fresh mortar, setting behavior and compressive strength of mortars at various periods of hydration. Finally, the effect of reduction of clinker content on the CO_2 emission linked with cement production is evaluated. Measurements on fly ash are used for comparison, and finely ground quartz is used as inert filler.

EXPERIMENTAL

The preparation and initial investigation of the CAS glass, CLS_{9N}, is described in Moesgaard et al. 2010a. The nomenclature refers to the raw materials, clay, limestone, and sand from which the glass is prepared by mixing in the proportions 63 wt% clay, 31 wt% limestone, and 6 wt% sand. The subscript indicates the molar content of Na_2O. Additional Na_2CO_3 is introduced to provide the rather high content of Na_2O. The glass has been ground to two different finenesses and spun into fibers, which have been subsequently ground to the same fineness as one of the CLS_{9N} samples (Table 1). The fibers are produced by Rockwool International A/S, Hedehusene, Denmark using the casade spinning process, which is a type of centrifuge process (Širok, et al., 2008).

Commercially available cement consisting of approximately 96% clinker and 4% gypsum was used to prepare mortars for physical tests. The mineralogical composition of the clinker (Bogue) and the chemical composition of the cement are given in Tables 2 and 3. The content of free lime was measured by wet chemistry. Composite cement mortars containing 30 wt% clinker replacements were prepared using the replacement materials stated in Table 1. In addition, composite cements containing both pozzolan (*P*), i.e. glass or fly ash (including the inert filler), and limestone (*L*) were prepared. *P/(P+L)* ratios of 0, 0.33, 0.67 and 1 were investigated. For all mortars a water to cement ratio of $w/c = 0.5$ by mass was employed, with *c* representing the total content of cement and replacement material. The cement to sand ratio of the mortars was 1:3 and the particle diameter of the sand in use was in the range 0-2 mm.

The flow of the fresh mortar was measured using a flow table according to ASTM C230-80 (although tamped 20 rather than 25 times). The initial setting behavior was investigated by measuring the heat of hydration during the first approximately 18 hours after preparation of the mortar using semi-adiabatic calorimetry. Approximately 20 g of mortar was used and the heat of hydration was determined from the temperature variations measured by the calorimeter. Mini-RILEM 2x2x15 cm^3 mortar prisms were made and stored in the molds for 24 ± ½ hours at 20 ± 1 °C and a relative humidity of at least 95%. Hereafter, the specimens were demoulded and placed in water in the curing room (20 ± 1 °C) for final hydration. Compressive strengths were measured directly after demoulding (1 day strengths) and after 2, 28 and 90 days of hydration in total, and each specimen was cut into three before measurement. The density of the prisms was determined by weighing.

Table 1: Characteristics of the Portland cement (PC) and replacement materials.

Material	PC	CLS_{9N}	CLS_{9N} fine	CLS_{9N} fibres	Fly ash	Inert filler (quartz)	Limestone
Surface area (m^2/kg) [a]	575	371	629	619	330	-	1288
Mean diameter (μm) [b]	7.7	14.4	6.0	6.2	20.1	$D_{max} < 90\ \mu m$	2.7

[a] Determined by air permeability using the Blaine method.

[b] Determined by PSD analysis

Table 2: Mineralogical composition (wt%) of clinker according to Bogue.

Component	C_3S	C_2S	C_3A	C_4AF	Free lime [a]	LFS (-) [b]
Clinker	63.4	9.2	8.4	12.0	1.4	1.02

[a] The content of free lime is measured by wet chemistry

[b] LSF is the lime saturation factor.

Table 3: Chemical composition in wt%. L.O.I. states the loss on ignition. For Portland cement (PC), limestone and fly ash XRF is used to determine the chemical composition, whereas wet chemistry is used for the glass CLS_{9N}. L.O.I. and the content of SO_3 are not determined for CLS_{9N}.

Component	PC	CLS_{9N}	Fly ash	Limestone
SiO_2	19.0	51.0	55.2	4.4
Al_2O_3	5.8	12.4	24.7	0.4
Fe_2O_3	3.9	6.5	8.5	0.2
CaO	65.1	17.9	4.7	52.9
MgO	1.0	2.4	1.8	0.4
K_2O	0.4	2.0	1.6	0.1
Na_2O	0.3	7.8	0.9	< 0.1
SO_3	3.7	-	0.6	0.1
L.O.I.	0.9	-	1.9	41.7

RESULTS AND DISCUSSION

Comparison of the different supplementary cementitious materials

The workability was evaluated based on the flow of the fresh mortars, and it was found that the flow of the mortars containing glass increased by 2-8 % compared to the flow of the mortars containing pure cement. Addition of 30 wt% SCMs does not increase the water demand and mortars can be produced under the same

conditions as pure cement. This is a major advantage compared to clay based SCMs for example, which invariably increases the water demand requiring additional water or super plasticizer to maintain sufficient workability (He, et al., 1994).
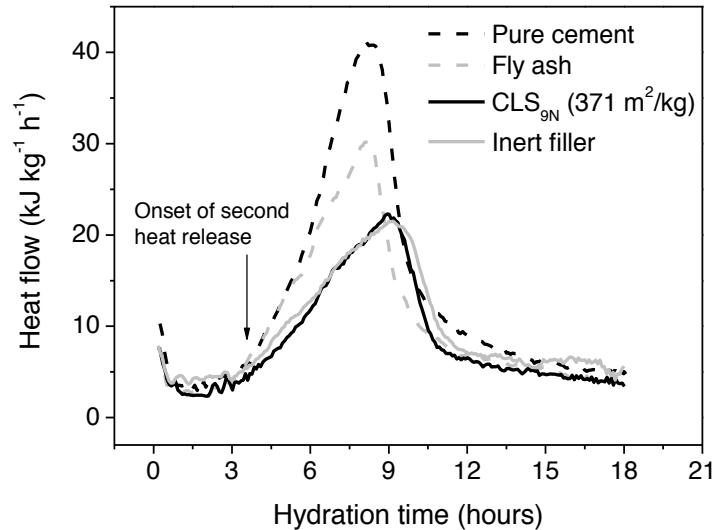

Figure 1: Setting behavior of mortar measured as the rate of heat evolution within the first 18 hours of hydration.

Figure 1 compares the heat flow within the first 18 hours of hydration for mortar containing pure cement, i.e., a reference sample, and the three different types of composite cements all containing 30 wt% of the SCMs or 30 wt% inert filler. It is observed, that the replacement of 30wt% of the cement with an alternative material changes the setting behavior. The total energy release is reduced indicating that the cement is replaced by a less reactive material. Similar heat flow patterns are observed for the composite cement containing the CAS glass and the cement containing the inert material indicating negligible early age pozzolanity of the CLS_{9N} glass. Fly ash on the other hand does react to some extent during these early stages as indicated by, more heat formation than the inert filler and glass. The onset of the second heat release can be used as a measure of the initial setting time. No significant changes in the onset are observed by the introduction of 30 wt% cement replacement. For the mortars containing CAS glass and quartz the rate of heat evolution observed for the main peak is however slower, and a slightly prolonged working period before the mortars solidifies (20-25%) is expected for these composite cements.

Figure 2 shows the development in compressive strength of the composite cement mortars which all contain 30 wt% cement replacement. The strength is given relative to the strength of the mortar containing pure cement, i.e. as σ/σ_{ref}. The pozzolanity of the glass and fly ash is apparent as the strength of the mortars containing these materials is significantly higher than the strength of the mortar containing 30wt% quartz. The strength of the sample containing quartz remains at 55% of the reference whilst, the mortars containing fly ash and glass continue to gain strength.
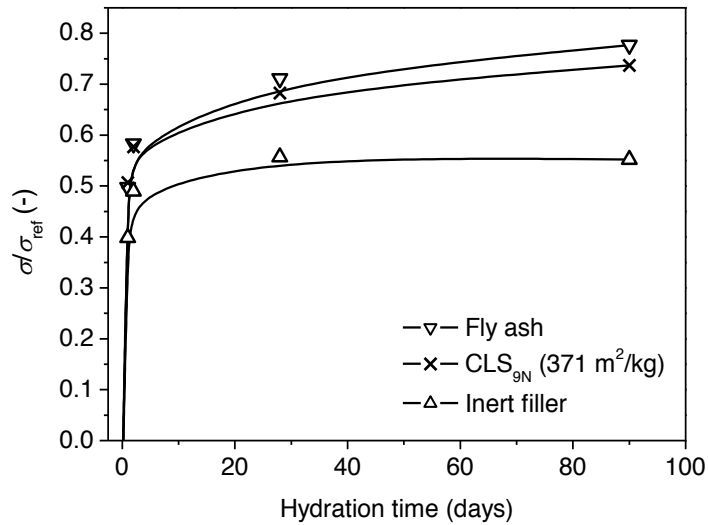
Figure 2: Strength development of composite cement mortars containing different clinker replacement materials. The strength (σ) is given as the relative strength to a pure Portland cement mortar (σ_{ref}). The solid lines should be regarded as guides for the eyes.

As expected from the results of the pozzolanity test (Moesgaard, et al., 2010a) the CAS glass contributes to the strength of the composite cements. Comparable performance is observed for the composite cements containing CAS glass and fly ash of similar fineness. A tendency of the fly ash to provide a slightly higher strength is however observed. A detailed discussion of the results can be found in Moesgaard, et al., 2010b.

Effect of particle size and cooling rate during glass production

During cement hydration, the reactions progress inwards from the surface of the particles. The particle size of the pozzolanic material is therefore expected to affect the rate of hydration and therefore the strength development. This phenomenon is evaluated from the results obtained on the three mortars containing different forms of CLS_{9N} (Table 1). The relative strength development is shown in Figure 3, and the increased surface area is observed to have significant impact on the strength over the course of hydration. The effect is most pronounced at longer hydration times.

The CLS_{9N} composition has also been used to draw thin glass fibers, and the cooling rate of this process is approximated to be in the range of 10^6 K/s, i.e., the glass is hyper-quenched. This is in contrast to the normally cooled glasses for which the cooling rate is approximated to be in the range of 10^3 K/s. The approximations of cooling rates are made according to the procedure of Yue, et al., 2004. The excess energy stored within the fiber glass is therefore significantly larger than for the normally cooled glass, proving a more disordered structure (Yue, et al., 2004). The fibers are ground to a surface area comparable to the CLS_{9N} (629 m²/kg) particles, and it is investigated (Figure 3) whether this increased energy stored within the fibers, i.e. the greater instability of the glass, has an effect on the reactivity of the glass. From Figure 3 the composite cement mortar containing the hyper-quenched glass has a slightly higher strength during late hydration than the mortar containing normally cooled glass, indicating that the glass with the highest thermodynamic instability has the greatest reactivity. Considering the uncertainty associated with the measurements, however, it is difficult to draw any firm conclusions.
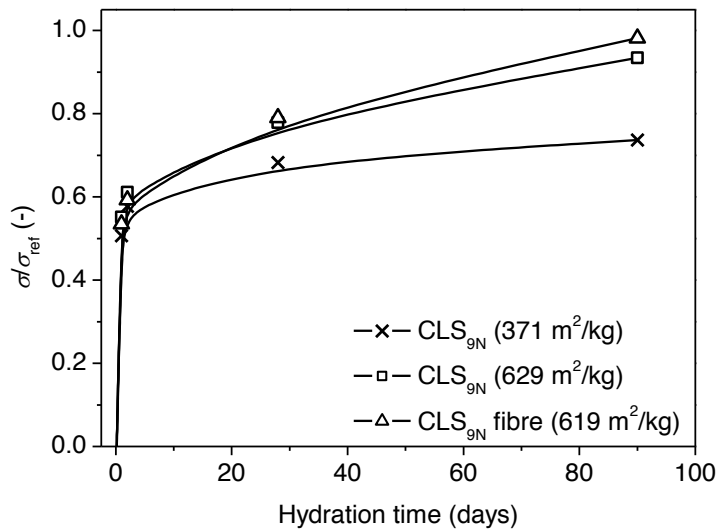
Figure 3: Strength development of composite cement mortars containing 30 wt% CLS$_{9N}$ with varying fineness and excess internal energy. The strength is given as σ/σ_{ref}. The solid lines should be regarded as guides for the eyes.

Composite cements containing both glass and limestone

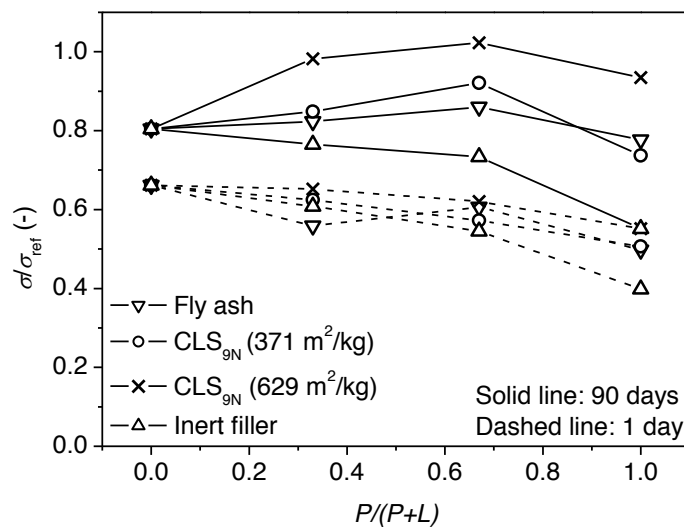**Figure 4: Relative compressive strength (σ/σ_{ref}) as a function of *P/(P+L)* for mortars with 30% cement replacement. *P* is the content of pozzolan (including the inert filler) and *L* is the content of limestone in wt%.**

The hydration of the mortars containing limestone was evaluated from the heat development. The degree of hydration of Portland limestone cement mortar with 30% cement replacement was midway between the pure cement reference and the sample containing 30% CLS$_{9N}$. The degree of hydration in the mortars containing both limestone and glass was higher approaching that of the reference cement without cement replacement (data not shown). This behavior is consistent with the measurements of early strength. In Figure 4 the

compressive strength of the mortar samples is plotted as a function of the $P/(P+L)$ ratio. Here P is the content of pozzolan also including the inert material and L is the limestone content. After 1 day's hydration the highest strength is observed for the composite cement mortars containing limestone as the only cement replacement material. The lowest strengths are observed for the samples containing 30% of the pozzolan (CLS_{9N}, fly ash or the inert material).

After 90 days of hydration the behavior is markedly changed for the mortars containing pozzolans participating in the strength giving reactions. At the early stage of hydration, mortars containing limestone as the sole replacement material exhibit still a slightly larger strength than the mortars containing only the fly ash or the coarse CLS glass. At the long duration of hydration however, a synergetic effect is observed between the limestone and the pozzolan and the samples containing both exhibit the highest strengths (Figure 4). It is presumed that the synergetic effect originates from a reaction between accessible aluminosilicates and limestone, forming the pore-filling phase, calcium monocarboaluminate hydrate. This is explained in greater detail in Moesgaard, et al., 2010b.

For the composite cements containing the fine CLS glass particles (CLS_{9N} 629 m^2/kg) the lowest strength is observed at $P/(P+L) = 0$, i.e. when no glass is present. For the sample containing 20% CLS_{9N} and 10% limestone the 90 days compressive strength even exceeds that of the pure cement. Increased thermodynamic instability (drawing of fibers) does not seem to have an effect on the compressive strength of the mortars containing both limestone and CLS_{9N} (data not shown).

CO_2 emission

For the CAS glass particles to be an effective solution towards reducing the CO_2 emission of cement production, reasonable mortar or concrete performances must be obtained per mass of CO_2 released for the composite cements including CAS glass as an SCM. To obtain a measure of the CO_2-release relative to the performance of the final concrete, the amount of CO_2 (given in kg) released from raw materials during production of cement and SCM is divided by the obtained compressive strength (given in MPa) of the given composite cement mortar. This is defined as the parameter m_{CO2}/σ. Limestone is the major raw material used in the production of PC clinker accounting for 500-550 kg CO_2 per tonne clinker (close to 1.2 tonnes limestone is needed to produce 1 tonne clinker). For the production of the CLS glasses limestone accounts for approximately one third of the raw materials resulting in a raw materials CO_2 emission of approximately 180 kg CO_2 per tonne glass. When limestone is used as a clinker replacement it is mixed with the cement after the burning, and therefore does involve any CO_2 emission. This is of course also the case with fly ash and the inert quartz. Figure 5 compares m_{CO2}/σ for the different composite cements relative to that of pure cement as a function of the $P/(P+L)$ ratio. Lower raw material CO_2 emissions, i.e., less than 1, are observed for all the composite cements except for the cement containing 30% inert filler and 30% of the coarse CLS_{9N}. If CLS glass is added as the only SCM it must therefore be ground to a high surface area to effectively reduce CO_2 emissions relative to the mechanical performance. When both limestone and CLS glass are added, the relative "raw materials CO_2 emission" can be reduced by 20-25%. CAS glasses, especially when mixed with limestone, can therefore be considered as a good alternative to the limited resources of conventional SCMs.
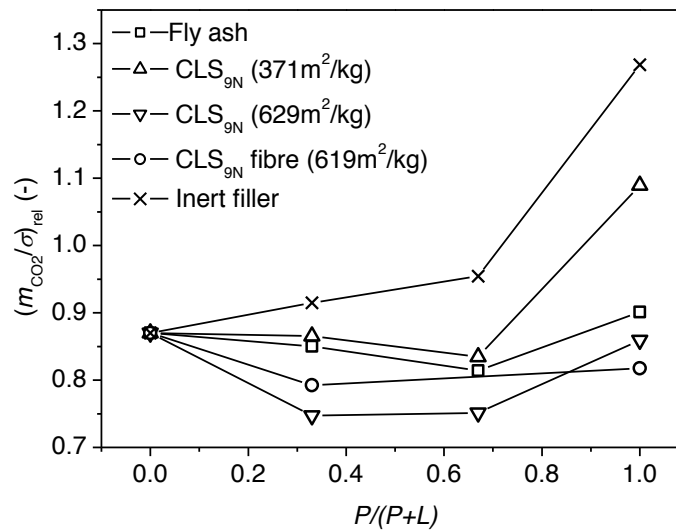
Figure 5. Relative raw materials CO₂ emission ((m_{CO2}/σ)$_{rel}$). The CO₂ emission (m_{CO2}) is given in kg of CO₂ released from raw materials during production of cement and alternative materials divided by the compressive strength (σ in MPa) of the composite cement mortars.

CONCLUSION

The goal of this investigation was to evaluate whether a refined calcium aluminosilicate glass, CLS_{9N}, which in earlier work was found to have pozzolanic properties (Moesgaard, et al., 2010a), can be used as an SCM. Mortars based on composite cements with 30% cement replacement were found to exhibit very promising flow behavior, and the water demand is unaffected by the addition of CAS glasses, which is a major advantage over natural pozzolans such as calcined clays. Initial setting behavior is found to be reasonable. Acceptable levels of late strength are also observed. The late strength of the composite cement mortars is in the range 70-90% of the strength of pure cement and is strongly dependent on particle size of the glass. The early strength, however, is only 50 to 60% of the early strength of mortars with pure cement. The pozzolanity of the CAS glasses is therefore most pronounced at longer periods of hydration.

The combination of limestone and CAS glass provides higher late strengths than would be predicted from the individual contributions from each constituent. The high alumina content of the glass is believed to result in a higher degree of reaction of the limestone compared to normal Portland limestone cements. In this way, the beneficial effects of limestone both as a filler material and as a reactive component can be exploited to a greater extent. Combined with the pozzolanity of the CAS glasses late strengths can be achieved which are even higher than the strengths of pure cement mortars. It is concluded that CAS glasses provide a promising alternative to traditional SCMs, achieving not just reduced emissions per tonne cement, but crucially real emissions reductions per unit of concrete produced to the same strength specification.

ACKNOWLEDGEMENTS

REFERENCES

Damtoft, J. S., Lukasik, J., Herfort, D., Sorrentino, D., Gartner, E. M. 2005. "Sustainable development and climate change initiatives". Cem. Concr. Res. 38, 115-127.

He, C., Makovicky, E., Osbæck, B. 1994. "Thermal stability and pozzolanic activity of calcined kaolin". Applied Clay Science 9, 165-187

Lawrence, C.D. 2007. "The Constitution and Specification of Portland Cement," in: P. C. Hewlett (Ed.), Lea's chemistry of cement and concrete, 4th Ed, Elsevier, Oxford, 2007, 131-194.

Moesgaard, M., Herfort, D., Kirkegaard, L.F., Yue, Y.Z. 2010a. "Optimal composition of calcium aluminosilicate glass particles used as supplementary cementitious materials"

Moesgaard, M., Herfort, D., Steenberg, M., Yue, Y. Z. 2010b. "Physical performance of composite cements containing calcium aluminosilicate glass powder and limestone" In preparation for Cem. Concr. Res.

Rehan, R., Nehdi, M. 2005. "Carbon dioxide emissions and climate change: policy implications for the cement industry". Environ. Sci. Pol. 8, 105-114.

Širok, B., Blagojević, B., Bullen, P 2008. "Mineral wool" Woodhead Publishing, Cambridge

World Business Council of Sustainable Development – Cement Sustainable Initiatives (WBCSD-CSI) & the International Energy Agency (IEA) 2009. "Cement technology Roadmap 2009 – Carbon emissions reductions up to 2050"

Worrell, E., Price, L., Martin, N., Hendriks, C., Meida, K. O. 2001. "Carbon dioxide emission from the global cement industry". Annu. Rev. Energy Environ. 26, 303-329.

Yue, Y.Z., von der Ohe, R., Jensen, S.L. 2004: "Fictive temperature, cooling rate, and viscosity of glasses". J. Chem. Phys., 120, 8053-8059.

Paper VII

journal

Hydration of Blended Portland Cements Containing Calcium-Aluminosilicate Glass Powder and Limestone

Mette Moesgaard,[‡] Søren L. Poulsen,[§] Duncan Herfort,[¶] Mette Steenberg,[¶]
Lise Frank Kirkegaard,[¶] Jørgen Skibsted,[§] and Yuanzheng Yue[‡,*,†]

[‡]Section of chemistry, Aalborg University, DK-9000, Aalborg, Denmark

[§]Instrument Centre for Solid-State NMR Spectroscopy, Department of Chemistry, and Interdisciplinary Nanoscience Center (iNANO), Aarhus University, DK-8000, Aarhus, Denmark

[¶]Aalborg Portland A/S, DK-9000, Aalborg, Denmark

This work investigates the hydration of blended Portland cement containing 30 wt% Na_2O–CaO–Al_2O_3–SiO_2 (NCAS) glass particles either as the only supplementary cementitious material (SCM) or in combination with limestone, using ^{29}Si MAS NMR, powder XRD, and thermal analyses. The NCAS glass represents a potential alternative to traditional SCMs, used for reduction of the CO_2 emission associated with cement production. It is found that the NCAS glass takes part in the hydration reactions after about 2 weeks of hydration and a degree of reaction of ~50% is observed after 90 days of hydration. The hydrated glass contributes to the formation of the calcium–silicate–hydrate (C–S–H) phase, consuming a part of the Portlandite ($Ca(OH)_2$) formed during hydration of the Portland cement. Furthermore, the presence of the glass and limestone particles, alone or in combination, results in an accelerated hydration for alite (Ca_3SiO_5), the main constituent of Portland cement. A higher degree of limestone reaction has been observed in the blend containing both limestone and NCAS glass as compared to the limestone–Portland mixture. This reflects that limestone reacts with a part of the alumina released from the hydrating glass, forming the calcium monocarboaluminate hydrate phase. Moreover, it may explain the synergy effect of using a combination of these two SCMs on the late compressive strength which is significantly higher compared to similar Portland cement blends using only NCAS glass or limestone as an SCM.

I. Introduction

GLOBAL warming, a manifestation of climate changes is considered a serious threat to our environment. Numerous scientific studies link climate changes to emissions of green house gasses, of which CO_2 is the major contributor. Thus, energy intensive industries are making considerable efforts to reduce their CO_2 emissions. Portland cement production is one of these industries and it is estimated that cement production accounts for about 5% of today's global man-made CO_2 emissions.[1–4] Roughly 60% of this emission is caused by calcination of the large amounts of limestone in the raw materials mix.[2–4] The demand for cement, especially in developing countries, is expected to rise significantly in the following years with a 50% increase likely in 2050.[3–5] Thus, to maintain the CO_2 emissions from cement production at the current level (in absolute terms), the specific CO_2 emission per ton cement produced must be reduced by one-third.

A well-known strategy to reduce the CO_2 emission is to decrease the Portland clinker content in the cement, as utilized in blended cements including one or more inorganic components referred to as supplementary cementitious materials (SCMs). Traditionally, materials such as silica fume, granulated blast furnace slag, and fly ash have been used as SCMs. These materials are amorphous or less crystalline silicates or aluminosilicates, and contribute to the formation of hydration products when mixed with cement either as pozzolans or as latent hydraulic materials. Numerous studies on the hydration of blended cements containing the traditional SCMs have shown that the principal hydration products are essentially similar to those formed in hydrated ordinary Portland cements (OPC).[6–10] However, the blended cements have generally lower contents of Portlandite ($Ca(OH)_2$) as a result of the dilution of the clinker and by the consumption of Portlandite as the SCMs participate in pozzolanic reactions. In general, blended cements show reduced early strength as compared to OPC, but an equal or increased strength after prolonged (e.g. 28 days) hydration.[6–13] The use of the traditional SCMs only results in small CO_2 emission associated with cement production as these are industrial by-products, however, their applicability may be limited by availability, transport costs, and competition with other industries. Today, these SCMs are essentially fully utilized in Western Europe and the supply of both fly ash and blast furnace slag is expected to be further reduced as coal fired power stations and blast furnace plants are replaced by more CO_2 efficient processes.[1,3] Thus, new and alternative sources of SCMs are required to further reduce the clinker content in cements on a global scale.

Another common clinker replacement material is limestone, often referred to as filler,[7,13–18] although it has both physical and chemical effects on the cement hydration. Limestone is a rather soft material and considerable fineness can thus be obtained by grinding. The high degree of fineness accounts for the improved physical properties of limestone–Portland cement blends such as a reduced water demand and increased durability.[7,14,15] In addition, limestone is partly consumed, contributing to the formation of hydration products, as it reacts with available alumina and forms the so-called CO_2-AFm phase, calcium monocarboaluminate hydrate. However, the quantity of chemically consumed limestone is limited and reported to be in the range from a few percent to about 10 wt%.[7,17–19]

In a recent study, we have investigated the physical performance of CaO–Al_2O_3–SiO_2 (CAS) and Na_2O–CaO–Al_2O_3–SiO_2 (NCAS) glass powders used as SCMs in combination with limestone.[20] The compositions of these glasses were

optimized toward a low energy consumption during production and at the same time a significant hydraulic reactivity in cement blends.[21] An economical production of glass on an industrial scale requires that the raw materials are locally available. These could be clay, limestone, and quartz sand, also used in the production of Portland cement clinker. The additional alkali oxide component in the glasses can be obtained from recycled kiln dust from cement production, from alkali feldspars present in granitic rocks or sedimentary equivalents, or directly as a mineral source of Na_2SO_4. The production of these CAS and NCAS glasses results in a CO_2 release from carbonates in the raw materials of about 175 kg per ton glass produced. This is significantly lower than the 550 kg CO_2 released per ton Portland cement clinker produced. Comparable amounts of CO_2 are expected to be released from the fuels used for production of both glasses and cement clinker. Thus, the production of the CAS and NCAS glasses may ideally emit less than 60% of the CO_2 emitted from Portland cement production. In our previous work, we investigated the physical performances of mortars containing both limestone and NCAS glass particles in the blended cement or blended cements containing only one of these components. The use of a single SCM (glass particles or limestone) made only small contributions to the early strength for the blended cements. However, the combined use of both SCMs resulted in a clear synergetic effect on the late strength development, which was significantly higher than that predicted from the individual contributions for each constituent.[20] In the present article, we characterize the hydration of the blended cements with the aim of obtaining an improved chemical insight into the observed synergetic effects on the physical performances for mortars containing both limestone and NCAS glass particles in the blended cement.

II. Experimental Procedure

The investigations were performed on cement pastes based on industrially produced CEM I Portland cement containing approximately 96% clinker and 4% gypsum. The Bouge mineralogical composition (wt%) of the clinker is 63.4% C_3S, 9.2% C_2S, 8.4% C_3A, and 12.0% C_4AF. This gives a lime saturation factor of LSF = 1.02. In addition, the clinker contains 1.4% free lime measured according to ASTM C 114-2009. Table I summarizes chemical compositions and specific surface areas for the Portland cement, the source of limestone, and the synthesized glass particles. The glass particles were prepared by melting natural minerals, i.e., clay, limestone, and quartz sand at 1350°C for 1 h, pouring the melt onto a brass mold, and subsequently crushing the cooled bulk glass. The clay was obtained from Dantonit A/S, Odense, Denmark while the sources of limestone and quartz were provided by Aalborg Portland A/S, Aalborg, Denmark. The glass preparation and its characteristics are described in detail elsewhere.[21] Three different blended cements, all with a clinker replacement level of 30 wt%, were prepared and compared to a pure cement reference. All pastes were hydrated at $20 \pm 1°C$ and a relative humidity of at least 95%. The compositions and abbreviated designations of the pastes are given in Table II.

The samples for the NMR analyses employed a water to cement ratio of $w/c = 0.5$ and the pastes were prepared, cured, and the hydration stopped using generally accepted procedures, as described recently.[24,25] The solid-state ^{29}Si MAS NMR spectra were recorded at 59.1 MHz on a Varian INOVA-300 (7.05 T) spectrometer, using a home-built CP/MAS probe for 7 mm o.d. rotors. The powder samples were packed in 7 mm partially sintered zirconia (PSZ) rotors (220 μL sample volume) and spun at $\nu_R = 7.0$ kHz. The experiments employed an rf field strength of $B_1/2\pi \approx 40$ kHz, a pulse width of 3.0 μs (~45° flip angle), a 30 s repetition delay, and 2500–3000 scans. The [29]Si isotropic

Table I. Chemical Composition (wt%) for the Portland Cement and the Two SCMs[†]

Component[†]	Cement	Limestone	CLS$_{9N}$
SiO_2	19.0	4.4	51.0
Al_2O_3	5.8	0.4	12.4
Fe_2O_3	3.9	0.2	6.5
CaO	65.1	52.9	17.9
MgO	1.0	0.4	2.4
K_2O	0.4	0.1	2.0
Na_2O	0.3	< 0.1	7.8
SO_3	3.7	0.1	–
Loss on ignition	0.9	41.7	–
Surface area (m^2/kg)[‡]	575	1288	629

[†]Data from XRF analysis (Portland cement and limestone) and atomic absorption spectrometry combined with spectrophotometry (CLS$_{9N}$ glass).
[‡]Surface area determined by air permeability using the Blaine method.

Table II. Compositions of the Studied Blended Cements

Sample	Composition (wt%)		
	Cement	Limestone	CLS$_{9N}$
Reference	100	0	0
LS30	70	30	0
LS20CLS10	70	20	10
CLS30	70	0	30

chemical shifts are reported relative to tetramethyl silane. The deconvolutions of the ^{29}Si MAS NMR were performed using the least-squares fitting program of the Varian Vnmr software and deconvolution approaches described elsewhere.[24,26–28]

The X-ray diffractometry (XRD) was conducted on paste samples in capillary sample tubes using a STOE powder diffraction system (701-0995) with CuK_α radiation (l = 1.54060 Å) and a nickel filter in the detector. The instrument was set up with a fixed PSD stage, operating at 40 kV and 40 mA in transmission mode, scanning the range $2\theta = 2°–127°$ at 0.015°/s. The phases were identified by comparison with patterns for the reference samples in the International Centre for Diffraction Data database. The XRD analysis included paste samples prepared with $w/c = 0.4$ and hydrated for 90 days, which were studied by XRD immediately after grinding the samples. Thermal analyses of the same paste samples ($w/c = 0.4$, hydration for 90 days) were performed on a thermal analyzer (NETZSCH STA 449C Jupiter, Selb, Germany), from which both differential scanning calorimetric (DSC) and thermogravimetry data were obtained simultaneously. For the thermal analyses, 30–40 mg of paste was heated from 30°C to 975°C at 20°C/min.

III. Results

Figure 1 shows the XRD patterns of the four pastes after 90 days hydration, while Table III displays the identified phases in these samples. As expected, a calcium monocarboaluminate hydrate phase (i.e., a CO_2-AFm phase) is identified for the blends containing limestone, in addition to a significant amount of calcite (Fig. 1). The sodium silicate hydrate ($Na_2SiO_3·9H_2O$) identified by XRD in the samples containing the CLS$_{9N}$ glass is ascribed to a small amount of this phase resulting from precipitation from the solution in the capillary pores during sample preparation. Figure 2 illustrates the phase diagram for the CLS30 blended cement assuming 100% reactivity for both the glass and cement after 90 days of hydration (CLS30$_{100\%\ reactivity}$). A glass reactivity of less than 100% will give a reactive mixture situated along the line connecting CLS30$_{100\%\ reactivity}$ and OPC.
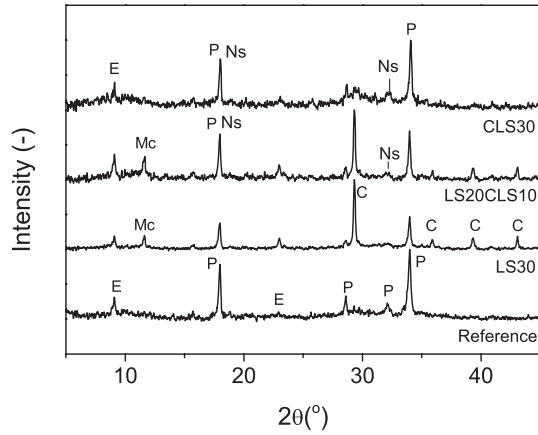
Fig. 1. Powder XRD patterns for the four pastes hydrated for 90 days. The identified phases are indicated by the following abbreviations: calcite (C), ettringite (E), calcium monocarboaluminate hydrate (Mc), monosulfate (Ms), sodium silicate hydrate (Ns), Portlandite (P).

Table III. Phases Identified by XRD after 90 Days Hydration

Hydrate phases	Reference	LS30	LS20CLS10	CLS30
Portlandite	X	X	X	X
C–S–H	X	X	X	X
Monosulfate	X	X		X
Ettringite	X	X	X	X
Monocarbonate		X	X	

Fig. 2. CAS (H) ternary phase diagram (mol%), illustrating the compositions for the ordinary Portland cement (OPC) and the three blended cements, taking into account the degree of reaction of the constituents after 90 days hydration. CLS_{9N} denotes the composition of the glass and CLS30(100% reactivity) refers to the chemical composition of the blended cement, assuming a 100% reactivity for the glass. For degrees of reaction of less than 100% for the glass, the compositions are situated on a line between CLS30(100% reactivity) and the OPC composition.

The results from thermal analyses of the samples hydrated for 90 days (Fig. 3) show a significant mass loss for temperatures up to 300°C, which is associated with a broad endothermic DSC peak. This loss can be attributed to the evaporation of water both from the pore solution and the removal of water molecules from the C–S–H and calcium aluminate hydrate phases. The DSC peak in this temperature range consists of several sub-peaks where the dominating peak (135°C–145°C) is ascribed to the loss of interlayer water
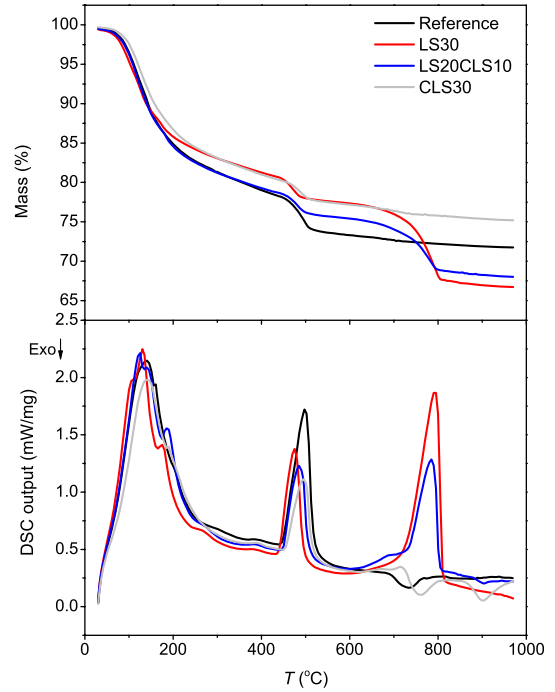

Fig. 3. Thermal analyses (DSC) for the pastes hydrated for 90 days. The upper graph shows thermogravimetric data plotted as the mass loss versus temperature while differential scanning calorimetric data (i.e., DSC output in mW/mg versus temperature) is illustrated in the lower graph.
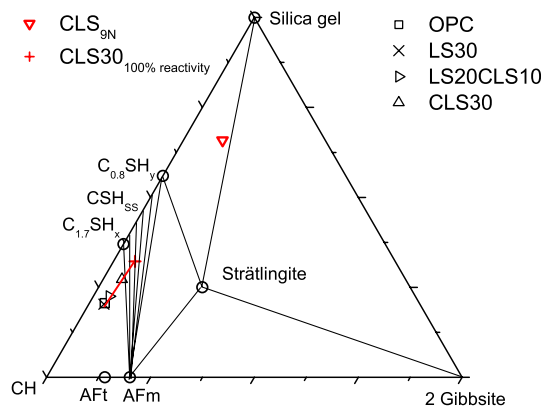
from the C–S–H phase. In the temperature range 440°C–540°C, Portlandite decomposes into CaO and water, resulting in the second mass loss associated with an endothermic DSC peak. For the pastes containing limestone an additional mass loss is observed in the range 700°C–820°C from decarbonation of limestone, which is also associated with an endothermic DSC peak. The small exothermic peak at 725°C–755°C may arise from recrystallization of calcium silicate phases formed during heating. We would expect this peak to occur in all samples but it is only visible for the samples without $CaCO_3$ decarbonation. For the glass-containing samples, a small exothermic peak is also observed in the range 870°C–880°C, which reflects devitrification of the glass, according to a similar DSC analysis of the pure CLS_{9N} glass.

The ^{29}Si MAS NMR spectra following the hydration for the blended cement containing 30% CLS_{9N} (CLS30) along with the spectra of the anhydrous mixture and the pure CLS_{9N} glass are shown in Fig. 4. The latter spectrum shows that the glass contains a range of different SiO_4 environments ($Q^n(mAl)$, $n = 0$–4, $m \leq n$) with a dominance of $Q^3(mAl)$ and $Q^4(mAl)$ sites. This implies that the resonances for the glass partly overlap with the Q^1, $Q^2(1Al)$, and Q^2 peaks at -79, -81.5, and -85 ppm, respectively, originating from the C–S–H phase. However, the resonances from the glass gives the only contribution to the spectral region from roughly -95 to -115 ppm, and thus, the relative intensity for the ^{29}Si sites in this phase is estimated from the deconvolutions, assuming that a subspectrum for the glass phase matches the spectrum of the anhydrous glass (Fig. 4). Thereby, it is assumed in our analysis that no preferential hydration occurs for any of the silicate species in the glass. The ^{29}Si MAS NMR spectra following the hydration of a 1:1 mixture (by weight) of the glass and $Ca(OH)_2$ indicate that this is an acceptable approximation. We note that preferential reaction for slag grains in a Portland cement-slag blend has been reported recently.[29] In that work, a subspectrum recorded for the partially reacted slag, isolated by selective dissolution, was used in the deconvolution of the ^{29}Si MAS NMR spectra
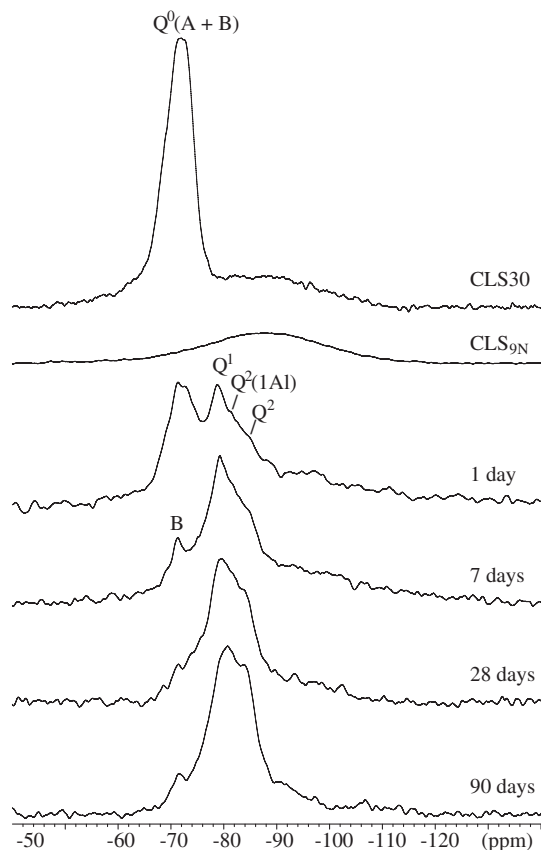
Fig. 4. ^{29}Si MAS NMR spectra of anhydrous and hydrated samples for the cement containing 30 wt% CLS_{9N} (CLS30), recorded at 7.05 T, using a spinning speed of 7.0 kHz and a 30 s relaxation delay. The second upper spectrum is obtained for a pure sample of the anhydrous glass, shown with a vertical scale that fits this component in the anhydrous blend (upper spectrum). The resonances from alite and belite are marked as $Q^0(A + B)$, where the narrow peak from belite at -71.3 ppm is most clearly observed after prolonged hydration, i.e., when nearly all alite is consumed. The Q^1, $Q^2(1Al)$ and Q^2 resonances from the C–S–H phase are also indicated.

to obtain the degree of slag reaction. For the OPC it is hard to distinguish the resonances from alite and belite before and after short hydration times. This reflects the small quantity of belite in the OPC combined with the presence of alite predominantly in its monoclinic M_I form which results in a lineshape where belite appears as a shoulder on the high-frequency part of the lineshape for alite. Deconvolution of the spectrum for the anhydrous OPC gives quantities of 72.1 wt% alite and 4.1 wt% belite, employing a subspectrum of the M_I form for alite[26] and the improved procedure for deconvolving ^{29}Si NMR spectra described recently.[25] The quantity of belite is somewhat lower than the amount of C_2S estimated by a standard Bogue calculation. However, the resonance from belite is more clearly observed after longer hydration times, reflecting the fact that alite is consumed and the reactivity for belite is much lower. Thus, it has been possible to estimate the quantities of alite and belite from deconvolutions of the ^{29}Si MAS NMR spectra, although the resulting uncertainties for the degrees of reaction for belite are high. The hydration for the other three cement blends (Table III) has been followed in a similar manner by ^{29}Si MAS NMR, as illustrated in Fig. 5 for the blend containing both limestone and CLS_{9N} (i.e., LS20CLS10).

The individual spectra for the anhydrous and hydrated samples of the four mixtures (Table II) have been deconvolved using subspectra of alite, belite, the Q^1, $Q^2(1Al)$, and Q^2 peaks of the C–S–H, and the CLS_{9N} glass. These intensi-

Table IV. Portlandite Contents for the Four Blends after 90 Days of Hydration Determined from Thermal Analysis

Sample	$m(Ca(OH)_2)/$ m(sample) (%)	$m(Ca(OH)_2)$ per cement fraction (%)[†]
Reference	19.1	19.1
LS30	12.6	18.0
LS20CLS10	12.3	17.6
CLS30	11.8	16.9

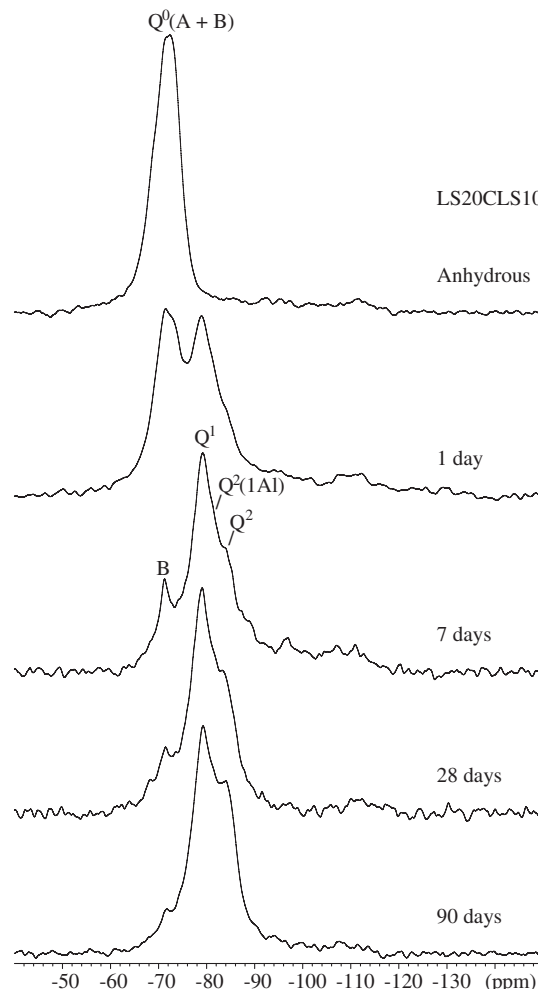[†]The Portlandite content is normalized to the fraction of cement in the blends.

Fig. 5. ^{29}Si MAS NMR spectra (7.05 T) following the hydration for the cement containing 20 wt% limestone and 10 wt% glass (i.e., LS20CLS10) obtained with a spinning speed of 7.0 kHz and a 30 s relaxation delay. The resonances can be assigned in a similar manner as indicated in Fig. 4.

ties allow calculation of the degrees of reaction for alite, belite, and the glass phase as illustrated in Fig. 6. As expected, alite reacts rapidly during the first few days of hydration, reaching a degree of reaction about 90% at 90 days for all mixtures. After ~1 week the first indication of belite hydration is observed and it reaches a degree of reaction of about 65–80% after 90 days. As a result of the large uncertainties of the intensities for belite in the deconvolutions, the degree of reaction for this phase can hardly be distinguished in the four blends. Most interestingly, a clear reaction of the glass phase is observed after 2 weeks of hydration [Fig. 6(b)] and it is seen that the reactivity of the glass in the two blends are quite similar during the first 28 days of hydration. After 90 days of hydration, the LS20CLS10 blend shows a lower
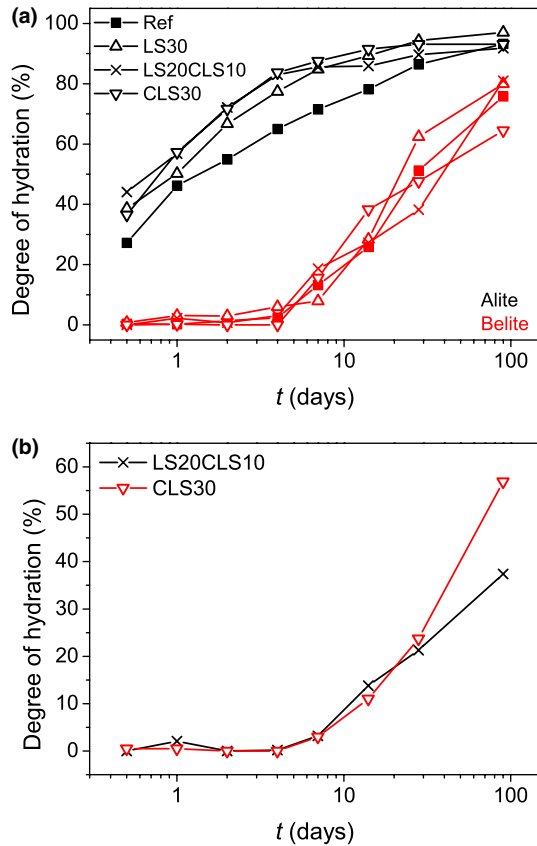
Fig. 6. Degrees of hydration from ^{29}Si MAS NMR for (a) alite and belite and (b) the CLS_{9N} glass powder as a function of the hydration time (t) for the four studied cement blends. The estimated uncertainties for the degrees of reaction for alite and belite are ±4% and ±20%, respectively, where the large uncertainty on the belite data reflects the low amount of this phase in the anhydrous cement. The estimated uncertainties for the degrees of glass reactions in part (b) are ±5% on the individual data points.

degree of reaction than CLS30. However, the determination of the degree of glass reaction for the LS20CLS10 blend is associated with a significant uncertainty, considering the low content of glass (10 wt%) in the anhydrous blend. Thus, we cannot exclude the fact that the degree of glass reaction is almost similar for the two blends and of the order of 40–55% after 90 days of hydration.

Figure 7 shows the compressive strengths for the three blended cements relative to the reference Portland cement after 90 days of hydration.[20] The strength of the cement containing both limestone and CLS_{9N} is higher than that
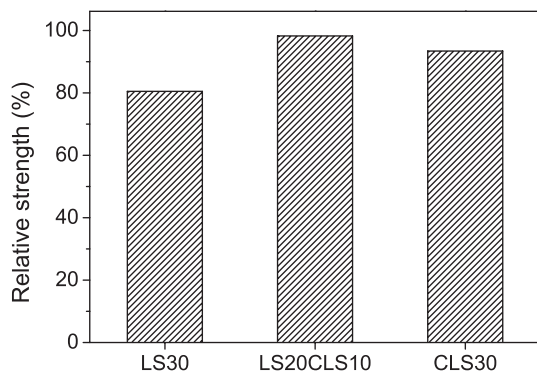

Fig. 7. Compressive strength normalized to the strength of the reference sample for the three blended cements. The data are adapted from Ref. 20.

predicted from the strengths of the cements containing only one of the SCMs, with the strength of LS20CLS10 approaching that of the pure cement reference.

IV. Discussion

(1) Reactivity of the Anhydrous Components

The studies of the hydrated pastes by XRD, thermal analyses, and ^{29}Si MAS NMR show that almost all of the Portland cement clinker has been consumed after 90 days for all cement blends under investigation. The degrees of alite hydration are above 90% for all blends, as revealed by ^{29}Si MAS NMR, and the XRD patterns (Fig. 1) indicating that only traces of the clinker minerals are present in the samples after 90 days.

The accelerated alite hydration observed for the three blended cements [Fig. 6(a)] has earlier been reported for blended cements containing finely ground SCMs and is associated with the fact that the SCMs act as nucleation sites for the C–S–H formation.[24,30–32] Despite the accelerated hydration for the blended systems, similar final degrees of alite hydration are observed for all the pastes, however, with an indication of a slightly higher degree of alite reaction for the LS30 blend as compared to the other samples. The rather low content of glass (CLS_{9N}) in the LS20CLS10 blend complicates the ^{29}Si MAS NMR quantification of the remaining glass phase after prolonged hydration. This may explain the lower degree of glass reaction for LS20CLS10 relative to the CLS30 blend after 90 days of hydration [Fig. 6(b)], since the limestone content is not expected to decrease the degree of reaction for the glass. Thus, a conservative estimate of the degree of glass is 40–55% for both samples after 90 days of hydration. Recently, Poulsen *et al.*[24] have performed ^{29}Si NMR analyses of an OPC of similar composition as used in this study and 30 wt% natural pozzolan or fly ash of comparable fineness as the CLS glass. In that work, the degree of hydration for the fly ash was approximately 20% after 90 days of hydration, whereas a slightly higher degree of hydration (~25%) was reported for the natural pozzolan. This indicates that the reactivity for the glass is slightly higher than that observed for the fly ash and natural pozzolan in cement blends with 30% replacement of the Portland cement.

The fraction of limestone consumed by the hydration reactions can be quantified from the thermogravimetric analyses (Fig. 3). If limestone is used as the only additive to Portland cement (30% replacement) the degree of reaction is about 9%, whereas it increases to ~16% when a combination of CLS glass and limestone is used as SCM. This may reflect that limestone reacts with Al_2O_3 from the glass and forms calcium monocarboaluminate hydrate (i.e., $C_4A\bar{C}H_{12}$). This phase forms in both blends containing limestone (Fig. 1 and Table III), however, with an increased amount in the LS20CLS10 blend as a result of the aluminate ions available from the hydrating glass. For example, a 50% degree of glass reaction results in an increase in available Al_2O_3 of ~0.3 wt% for LS20CLS10 as compared to the LS30 blend. Thus, the combined effect of limestone as both a physical filler and a reactive constituent is utilized to a greater extent in the cement blend containing both glass and limestone as SCMs. This may explain the synergetic effect observed in our recent study[20] where late (90 days) compressive strengths higher than those expected from the contributions from each constituent on their own were achieved for the blended cements containing both limestone and glass (Fig. 7). Furthermore, we note that a partial conversion of calcium monosulfoaluminate hydrate ($C_4A\bar{S}H_{12}$) into calcium monocarboaluminate hydrate results in a release of sulfate ions that leads to the formation of a larger amount of ettringite (i.e., $C_3A\bar{S}_3H_{32}$) thereby lowering the porosity of the hydrated material, contributing to an increase in strength. This effect has recently also been described by De

Weerdt *et al.*[30] for ternary Portland cements containing limestone and fly ash.

(2)　Identification of Hydration Products

Figure 2 shows the compositional plots in the CAS (H) subternary phase diagram for the materials that have taken part in the hydration reactions (i.e., bulk composition for the anhydrous constituents) to predict the relevant hydrate phase assemblages. In the blends without limestone the predicted phase assemblages are Portlandite, C–S–H, ettringite, monosulfate, iron oxide (e.g. an iron hydroxide phase), and the pore solution. When limestone is introduced into the blends, the predicted assemblages also include calcite in addition to Portlandite, C–S–H, ettringite, iron oxide, and the pore solution while monosulfate is replaced by calcium monocarboaluminate hydrate.

The higher silicate content in the glass-containing blends, as compared to the other blends, implies that the relative amount of C–S–H increases at the expense of Portlandite. Although the C–S–H can accommodate some alumina in the presence of excess Portlandite, the concentration of alumina in the C–S–H is expected to remain constant as CLS_{9N} is introduced. The introduction of CLS_{9N} increases the overall alumina content of the blended cement, however, the Al/Si molar ratio of the reactive part for the blended cement decreases when CLS_{9N} is introduced as a result of the relatively large silica content in the glass. Thus, the incorporation of Al into the C–S–H phase is not expected to increase,[33–35] which is confirmed by the ^{29}Si MAS NMR analysis that reveals Al/Si ratios for the C–S–H of Al/Si = 0.080, 0.077, 0.074, and 0.079 for the pure OPC, LS30, LS20CLS10, and CLS30 blends hydrated for 90 days. The uncertainty limits on the Al/Si ratios from ^{29}Si MAS NMR are estimated to ±0.05 and the ratios only account for tetrahedrally coordinated Al incorporated in the silicate chains of the C–S–H. The increased content of alumina from the glass will preferentially result in increased contents of ettringite and AFm phases (monosulfate and monocarbonate), depending on the availability of $CaSO_4$ and $CaCO_3$. The predictions are generally supported by the XRD data, except that no iron oxide phase has been identified in the hydrated blends. Moreover, the monocarbonate phase was identified by XRD, in agreement with recent results for limestone–Portland cements.[19,32,36–40]

In addition to a shift of the compositions toward higher Al_2O_3 and SiO_2 contents, the introduction of CLS_{9N} into the blended cements results in a significant increase in the content of alkali ions (mainly Na^+) into the system. The CLS30 blend contains 2.0 wt% $(Na_2O)_{eq}$ (i.e., $Na_2O + 0.658K_2O$), which is significantly higher than the quantity of 0.5 wt% $(Na_2O)_{eq}$ present in OPC (Table II). In general, fly ashes also contain relatively high alkali contents of about 5 wt% $(Na_2O)_{eq}$ which is comparable to the bulk content of 9 wt% $(Na_2O)_{eq}$ for CLS_{9N}. For cement-fly ash blends the ability of the C–S–H phase to incorporate alkali ions is observed to increase as the content of acidic oxides (i.e., SiO_2) increases in the C–S–H phase.[22,23,41] However, for the present glass containing blends, where the C/S ratio of the C–S–H phase is expected to be essentially constant at 1.7, the ability to bind alkali ions in the C–S–H phase may be limited.[41]

The content of Portlandite formed in each blend after 90 days of hydration is quantified (Table IV) from the mass loss in the range 440°C–540°C determined by thermal analyses (Fig. 3). As expected, the highest total amount of Portlandite forms in the pure cement sample and the lowest quantity is found in CLS30. The decrease in Portlandite contents in the blended samples is partly due to the dilution of the clinker. However, the dilution cannot fully account for the lower CH content in the blended cements (Table IV, second column). For the cement pastes containing CLS_{9N}, this reflects that Portlandite is partly consumed by the pozzolanic

reaction of CLS_{9N} to form a C–S–H phase with a C/S ratio that is higher than the corresponding ratio for the glass itself.

Both the OPC reference and the LS20CLS10 blend have significantly higher mass losses from dehydration of the calcium aluminate hydrates and C–S–H (Fig. 3, temperatures up to 300°C) than those in the blended cements containing only one SCM. The mass losses for LS30 and CLS30 over the temperature range up to 300°C account for about 90% of the mass loss of the reference cement for both blends. Moreover, the compressive strengths obtained after 90 days for these two blends become lower compared to the pure OPC (Fig. 7).

V.　Conclusions

The hydration of blended cement pastes containing Na_2O–CaO–Al_2O_3–SiO_2 (NCAS) glass particles, or combinations of NCAS glass and limestone, has been investigated by ^{29}Si MAS NMR, XRD, and thermal analyses. All blended cements show an accelerated alite hydration compared to the pure Portland cement. The NCAS glass takes part in the hydration reactions after about 2 weeks of hydration with a degree of reaction of ~50% after 90 days. A higher degree of reaction has been observed for limestone in the blend containing both limestone and the NCAS glass (16%) as SCMs as compared to the mixture including limestone only (9%). This may explain the synergetic effect between limestone and NCAS glass, which results in a higher compressive strength as compared to that in cement blends containing either limestone or NCAS glass at the same cement replacement level.

References

[1]E. Worrell, L. Price, N. Martin, C. Hendriks, and L. O. Meida, "Carbon Dioxide Emission from the Global Cement Industry," *Annu. Rev. Energy Environ.*, **26**, 303–29 (2001).
[2]R. Rehan and M. Nehdi, "Carbon Dioxide Emission and Climate Change: Policy Implications for the Cement Industry," *Environ. Sci. Poll.*, **8**, 105–14 (2005).
[3]J. S. Damtoft, J. Lukasik, D. Herfort, D. Sorrentino, and E. M. Gartner, "Sustainable Development and Climate Change Initiatives," *Cem. Concr. Res.*, **38**, 115–27 (2008).
[4]World Business Council for Sustainable Development, Cement Technology Roadmap 2009, *Carbon emissions reductions up to 2050, OECD/IEA and the World Business Council for Sustainable Development*, OECD Publishing, Bedfordshire, 2009.
[5]K. Humphreys and M. Mahasenan, *Toward a Sustainable Cement Industry. Sub-study 8: Climate Change, An Independent Study Commissioned to Battelle by World Business Council for Sustainable Development*, World Business Council for Sustainable Development, Geneva, March 2002.
[6]B. Lothenbach, K. Scrivener, and R. D. Hooton, "Supplementary Cementitious Materials," *Cem. Concr. Res.*, **41**, 217–29 (2011).
[7]H. F. W. Taylor, *Cement Chemistry*, Academic Press, New York, 2nd edition, 1997.
[8]M. Moranville-Regourd, "Cements Made from Blastfurnace Slag"; pp. 637–78 in *Lea's Chemistry of Cement and Concrete*, 4th edition, , Edited by P. C. Hewlett. Elsevier, Oxford, 2007.
[9]P. Fidjestøl and R. Lewis, "Microsilica as an Addition"; pp. 679–712 in *Lea's Chemistry of Cement and Concrete*, 4th edition, Edited by P. C. Hewlett. Elsevier, Oxford, 2007.
[10]C. D. Lawrence, "The Production of Low-Energy Cements"; pp. 422–70 in *Lea's Chemistry of Cement and Concrete*, 4th edition, Edited by P. C. Hewlett. Elsevier, Oxford, 2007.
[11]V. G. Papadakis, "Experimental Investigation and Theoretical Modeling of Silica Fume Activity in Concrete," *Cem. Concr. Res.*, **29**, 79–86 (1999).
[12]V. G. Papadakis, "Effect of Fly Ash on Portland Cement Systems – Part I. Low-calcium Fly Ash," *Cem. Concr. Res.*, **29**, 1727–36 (1999).

[13]N. Voglis, G. Kakali, E. Chaniotakis, and S. Tsivilis, "Portland-limestone Cements. Their Properties and Hydration Compated to Those of Other Composite Cements," *Cem. Concr. Comp.*, **27**, 191–6 (2005).

[14]T. Vuk, V. Tinta, R. Gabrovsek, and V. Kaucic, "The Effects of Limestone Addition, Clinker Type and Fineness on Properties of Portland Cement," *Cem. Concr. Res.*, **31**, 135–9 (2001).

[15]S. Tsivilis, E. Chaniotakis, E. Badogiannis, G. Pahoulas, and A. Ilias, "A Study on the Parameters Affecting the Properties of Portland Limestone Cements," *Ceom. Concr. Res.*, **21**, 107–16 (1999).

[16]S. Tsivilis, J. Tsantilas, G. Kakali, E. Chaniotakis, and A. Sakellariou, "The Permeability of Portland Limestone Cement Concrete," *Cem. Concr. Res.*, **33**, 1465–71 (2003).

[17]J. Zelic, R. Krstulovic, E. Tkalcec, and P. Krolo, "Durability of the Hydrated Limestone-Silica Fume Portland Cement mortars under Sulphate Attack," *Cem. Concr. Res.*, **29**, 819–26 (1999).

[18]V. S. Ramachandran, "Thermal Analysis of Cement Components Hydrated in the Presence of Calcium Carbonate," *Thermochim. Acta*, **127**, 385–94 (1988).

[19]W. A. Klemm and L. D. Adams, "An Investigation of the Formation of Carboaluminates"; pp. 60–72 in *Carbonate Additions to Cement, ASTM STP 1064*, Edited by P. Klieger and R. D. Hooton. American Society for Testing and Materials, Philadelphia, PA, 1990.

[20]M. Moesgaard, D. Herfort, M. Steenberg, L. F. Kirkegaard, and Y. Z. Yue, "Physical Performances of Composite Cements Containing Calcium Aluminosilicate Glass Powder and Limestone," *Cem. Concr. Res.*, **41**, 359–64 (2011).

[21]M. Moesgaard, D. Herfort, J. Skibsted, and Y. Z. Yue, "Calcium Aluminosilicate Glasses as Supplementary Cementitious Materials," *Glass Technol.: Eur. J. Glass Sci. Technol. A*, **51**, 183–90 (2010).

[22]J. Duchesne and M. A. Bérubé, "The Effectiveness of Supplementary Cementing Materials in Suppressing Expansion Due to ASR: Another Look at the Reaction Mechanisms Part 2: Pore Solution Chemistry," *Cem. Concr. Res.*, **24**, 221–30 (1994).

[23]C. X. Qian, H. D. Guo, X. G. Lan, and M. S. Tang, "Mechanism of Mineral Admixture Suppressing Alkali-Silica Reaction: Part II. Retardation of the Transport of Na, K and OH Ions in the Pore Structure Caused by Acidic Action of Mineral Admixture Particles in Matrix," *Cem. Concr. Res.*, **24**, 1327–34 (1994).

[24]S. L. Poulsen, H. J. Jakobsen, and J. Skibsted, "Methodologies for Measuring the Degree of Reaction in Portland Cement Blends with Supplementary Cementitious Materials by ^{27}Al and ^{29}Si MAS NMR Spectroscopy"; 177–88 in Proceedings of 17th IBAUSIL Inter. Baustofftagung, Vol. 1, Weimar, Germany, 2009.

[25]S. L. Poulsen, H. J. Jakobsen, and J. Skibsted, "Incorporation of Phosphorus Guest Ions in the Calcium Silicate Phases of Portland Cement from ^{31}P MAS NMR Spectroscopy," *Inorg. Chem.*, **49**, 5522–9 (2010).

[26]J. Skibsted, H. J. Jakobsen, and C. Hall, "Quantification of Calcium Silicate Phases in Portland Cements by ^{29}Si MAS NMR Spectroscopy," *J. Chem. Soc. Faraday Trans.*, **91**, 4423–30 (1995).

[27]M. D. Andersen, H. J. Jakobsen, and J. Skibsted, "Characterization of White Portland Cement Hydration and the C-S-H Structure in the Presence of Sodium Aluminate by ^{27}Al and ^{29}Si MAS NMR Spectroscopy," *Cem. Concr. Res.*, **34**, 857–68 (2004).

[28]S. L. Poulsen, V. Kocaba, G. L. Saoût, H. J. Jakobsen, K. L. Scrivener, and J. Skibsted, "Improved Quantification of Alite and Belite in Anhydrous Portland Cement by ^{29}Si MAS NMR: Effects of Paramagnetic Ions," *Solid State Nucl. Magn. Reson.*, **36**, 32–44 (2009).

[29]H. M. Dyson, I. G. Richardson, and A. R. Brough, "A Combined ^{29}Si MAS NMR and Selective Dissolution Technique for Quantitative Evaluation of Hydrated Blast Furnace Slag Cement Blends," *J. Am. Cer. Soc.*, **90**, 598–602 (2007).

[30]K. De Weerdt, M. Ben Haha, G. Le Saout, K. O. Kjellsen, H. Justnes, and B. Lothenbach, "Hydration Meachnisms of Thernary Portland Cement Containing Limestone Powder and Fly Ash," *Cem. Concr. Res.*, **41**, 279–91 (2011).

[31]V. S. Ramachandran and C. M. Zhang, "Dependence of Fineness of Calciumcarbonate on the Hydration Behavior of Tricalciumsilicate," *Durability Building Mater.*, **4**, 45–66 (1986).

[32]J. Péra, S. Husson, and B. Guilhot, "Influence of Finely Ground Limestone on Cement Hydration," *Cem. Concr. Res.*, **21**, 99–105 (1999).

[33]H. Krøyer, H. Lindgreen, H. J. Jakobsen, and J. Skibsted, "Hydration of Portland Cement in the Presence of Clay Minerals Studied by ^{29}Si and ^{27}Al MAS NMR Spectroscopy," *Adv. Cem. Res.*, **15**, 103–12 (2003).

[34]M. D. Andersen, H. J. Jakobsen, and J. Skibsted, "Incorporation of Aluminum in the Calcium Silicate Hydrate (C-S-H) of Hydrated Portland Cements: A High-field ^{27}Al and ^{29}Si MAS NMR Investigation," *Inorg. Chem.*, **42**, 2280–7 (2003).

[35]I. G. Richardson, J. Skibsted, L. Black, and R. J. Kirkpatrick, "Characterisation of Cement Hydrate Phases by TEM, NMR and Raman Spectroscopy," *Adv. Cem. Res.*, **22**, 233–48 (2010).

[36]V. L. Bonavetti, V. F. Rahhal, and E. F. Irassar, "Studies on the Carboaluminate Formation in Limestone Filler-blended Cements," *Cem. Concr. Res.*, **31**, 853–9 (2001).

[37]H. J. Kuzel, "Initial Hydration Reactions and Mechanisms of Delayed Ettringite Formation in Portland Cements," *Cem. Concr. Comp.*, **18**, 195–203 (1996).

[38]E. P. Nielsen, D. Herfort, and M. R. Geiker, "Phase Equilibra of Hydrated Portland Cement," *Cem. Concr. Res.*, **35**, 109–15 (2005).

[39]T. Matschei, B. Lothenbach, and F. P. Glasser, "The Role of Calcium Carbonate in Cement Hydration", *Cem. Concr. Res.*, **37**, 551–8 (2007).

[40]B. Lothenbach, G. Le Saout, E. Gallucci, and K. Scrivener, "Influence of Limestone on the Hydration of Portland Cement," *Cem. Concr. Res.*, **38**, 848–60 (2008).

[41]S. Y. Hong and F. P. Glasser, "Alkali Binding in Cement Pastes Part I. The C-S-H Phase," *Cem. Concr. Res.*, **29**, 1893–903 (1999).   □